Potential Seismogenic Faults in Norway

Master Thesis in Geodynamics

By
Kristina Smirnova

Department of Earth Science
University of Bergen

June 2019

Abstract

Identification of seismogenic potential of faults in an area is crucial in the assessment of earthquake hazard. One of the most challenging tasks in seismotectonic analysis that leads to the identification of the seismogenic potential of earthquake sources, is to correlate faults to seismicity. Significant number of studies are performed for areas experiencing high level of seismic activity, such as active plate boundaries. However, there are limited efforts in areas experiencing low level of seismic activity, such as intraplate settings, such as Norway. Therefore, analysis of seismogenic potential of faults is crucial and necessary, since large and destructive earthquakes have been documented in intraplate settings earlier. In Norway, there have been earthquakes of relatively large magnitudes (Lurøy earthquake of magnitude 5.8 in 1819, earthquake in Oslo region of magnitude 5.4 in 1904). One of the main concerns is that the recurrence interval for these earthquakes is unknown, due to limited observational period of earthquake records. Extending observational periods and studying reactivation potential of seismogenic faults is therefore the main objective of the following thesis. In total 56 significant faults (in total 184 segments) were identified and studied in six different zones in Norway and the adjacent offshore areas. A dedicated set of criteria are developed and adopted in assessing the reactivation potential of these faults and segments. Reactivation potential of 20 faults (including their segments) were found “possible”, in which only two were assigned “probable”.

Among those faults, where reactivation potential was found “possible”, only two faults were found to have a seismogenic potential assessed as “probable”. These are the Øygarden Fault Complex along the coast of Western Norway and the Stuoragurra Fault in Finnmark. Results will be submitted to the European Database for Seismogenic Faults (EDSF).

Acknowledgments

I would like to express my great thanks to Professor Dr. Kuvvet Atakan for providing an opportunity to study such an exciting topic. I am also thankful for his great assistance, expert advice and constructive suggestions during the development of this research work. I would also like to thank my co-supervisors, Mathilde Sørensen and Lars Ottemöller, for providing material required for the fast development of this thesis.

My grateful thanks are also extended to Jens Havskov who assisted with building the seismic catalogue and gave very valuable advices during thesis development. Also, I wish to appreciate Terje Utheim for assisting with GMT scripts. I would also like to express my thanks to Andreas Can Atakan for his assistance with D-Map interactive web-based Geographical Information System software. I would also like to thank engineering and scientific staff assisting in resolving minor issues along thesis development.

I would like to give special thanks to my boyfriend and parents who contributed to my emotional well-being throughout hard last weeks of thesis completion.

Table of contents

1 Introduction

Mapping active faults and understanding their seismogenic potential is critical in assessing seismic hazards in areas of low seismicity. In slowly deforming areas such as Norway it is essential to have long observational periods. Low to intermediate seismicity in these regions leads to low level of seismic hazards due to methodological constraints especially in Standard Probabilistic Seismic Hazard Assessment (PSHA) which is usually based on the observations for the last 40-50 years. Therefore, extending the observational periods to geological record is essential and hence identifying seismogenic faults and the associated slip rates, as well as maximum possible magnitudes becomes crucial.

In actively deforming plate boundaries due to high activity rates, the seismogenic faults are clearly identified based on the associated earthquake activity and the occurrence of large destructive earthquakes. However, in areas of low seismicity, identification of seismogenic faults is a difficult exercise, as the known earthquake records are usually much shorter in time than the earthquake cycles due to the low slip rates.

Norway and the adjacent offshore areas are located in such an area, a so-called “intraplate” setting, characterized by low seismicity. Stable Continental Regions (SCR) is a general term used to define the tectonic setting on mainland Norway. While this is true for the entire Scandinavia, we consider the tectonic setting for the study area as intraplate due to the adjacent offshore areas with rifting processes in the North Sea and passive margin development along the continental shelf in Norwegian and Barents Seas. As such the earthquake occurrence on mainland Norway and the adjacent offshore areas differ significantly.

Active faults in Norway are poorly known. Major challenge is to correlate mapped faults to seismicity. Focal mechanisms of earthquakes are reliable only for large seismic events which makes it difficult to cover the entire region. Lack of large earthquakes along with difficulties in quantifying earthquake parameters of various quality lead to inhomogeneous and incomplete seismic records. In addition, significant local variations in the stress orientation within the crust bring further complications. Therefore, identifying the seismogenic potential of previously mapped faults on both mainland Norway and in adjacent offshore areas is of key concern.

In Europe, mainly driven by the countries in the actively deforming plate boundary around Mediterranean and Alpine belt, an initiative to create a database for seismogenic faults have started a few decades ago. Through a systematic analysis of significant faults, the European Database for Seismogenic Faults (EDSF) (European Database for Seismogenic Faults, 2019), is now established as a thematic service in the scientific community. EDSF was compiled within the framework of the EU Project SHARE and is now included as a thematic service in the European Plate Observing System (EPOS) (European Plate Observing System, 2019). There are currently 21 countries providing data to EDSF at a national scale. These are, Albania, Algeria, Austria, Belgium, Bulgaria, Croatia, France, Germany, Greece, Italy, Macedonia, Montenegro, Morocco, Netherlands, Portugal, Serbia, Slovenia, Spain, Switzerland, Tunisia and Turkey.

In Norway, although there have been some national scale efforts to analyze the seismicity (e.g. Bungum et al., 1991; Hicks et al., 2000) and the neotectonics (Olesen et al., 2013), as well as a few dedicated studies on individual faults regarding their seismogenic potential (Olesen, 1988; Olesen et al., 1992; Dehls et al., 2002; Anda et al., 2002), until now there has not been a systematic study trying to identify the potential seismogenic faults in Norway and the adjacent offshore areas. The aim of this thesis is to address this issue through a systematic analysis of significant fault systems both inland and

offshore and quantify the earthquakes that could be related to these faults. In this study, all significant fault systems are identified in Norway and adjacent offshore areas including the Barents shelf (excluding Svalbard archipelago), using the available databases on geological, structural maps, and are quantified with respect to their location, length, geometry and kinematics. Earthquakes associated with each fault system are identified using criteria considering the uncertainties in the source parameters. Based on the geometry and kinematics of the faults with respect to the regional stress tensor orientation, reactivation potential of the identified fault systems and their segments are assessed. The faults are categorized into three main groups with regard to their reactivation potential; “not-possible”, “possible” and “probable”. Additional parameters such as the maximum possible earthquake magnitudes for each fault segment are calculated using empirical relations (Wells and Coppersmith, 1994).

Uncertainties in the input data for analyses of the identified fault systems and resulting interpretations are discussed in a separate chapter. In the conclusion chapter, only those faults and segments that are classified as “probable” with respect to their reactivation potential, are further considered for their seismogenic potential.

2 Background information

2.1 Tectonic and geological background

In this section the main goal is to compile main geological structures, major fault zones/complexes, zones of weakness, prevailing stress orientations in Norway and adjacent areas and their variations through geological time scale. In the following, short description of the main geological deformational processes is given in chronological order.

Baltica being an ancient paleocontinent formed in Paleoproterozoic presently represents the fundament for Scandinavia and most of the northern Europe (Torsvik and Cocks, 2005). Therefore, episodes of the main interest are confined to the events affecting Baltica, consequently Norway. These include interaction of Baltica with other continents, segregation of Baltica with its subsequent independence, Caledonian Orogeny – mountain-building era, opening of the Atlantic, separation of Norway and Greenland and development of Norwegian rifted continental margin.

Precambrian Eon (~4600 – 541 ± 1.0 Ma)

There were several significant geological processes taking place during Proterozoic Era that contributed to nowadays geological structures and stress orientations.

- Formation of a rift with Northwest-Southeast orientation

At a time range of 2500 to 1950 Ma the Archean continent (Finnmark and Troms) experienced stretching that led to the formation of several rift zones characterized by northwest-southeast orientation (Ramberg et al., 2007). Early stage of rift zones development led to the formation of layered mafic intrusions along with mafic swarms (dark, heavy igneous rocks) (Ramberg et al., 2007). Further development of rift zones was accompanied by the formation of volcanic and sedimentary stratigraphic sequences. At some places Fennoscandian shield was split that led to the opening of new sea (Kola Sea) along rift axis (Ramberg et al., 2007). However, ensuing tectonic changes caused closure of Kola Sea that entailed formation of a mountain belt due to collision of crustal blocks at around 1900 Ma (Ramberg et al., 2007).

- Formation of a Svecofennian mountain range

Formation of a Svecofennian mountain range took place at northern Fennoscandia at a period of 1960 – 1860 Ma (Ramberg et al., 2007). Folding and metamorphosis of deep igneous and sedimentary rocks occurred during formation of Svecofennian orogeny. Subsequently, around 1860 Ma newly created crust fragments have been welded to the older northeastern core (Ramberg et al., 2007). Metamorphosis and intrusions of large granites continued to about 1760 Ma (Ramberg et al., 2007).

- The Transscandinavian Igneous Belt (TIB)

Next stage of Scandinavian crust growth occurred due to intrusion of large volumes of granitic rocks at the western rim of Svecofennian mountain range during 1850 – 1650 Ma (Ramberg et al., 2007). These rocks stretched along 1500 km long area from Skåne at the south to Lofoten at the North. This belt of igneous rocks was named as The Transscandinavian Igneous Belt where the granitic rocks stick beneath the Caledonian rock pack (Ramberg et al., 2007).

- Crust development at the southern Scandinavia

Formation of Precambrian gneiss and granite makes up around 50 percent of Norway mainland. Referring to Myrvang (1996), Precambrian lithological units show high horizontal stresses. The following rocks have been created as a result of deformation and subsequent transformation of two mountain ranges. The oldest one is Gothic mountain range (1750 – 900 Ma) and the second one is Sveconorwegian orogeny (1130 – 900 Ma) (Ramberg et al., 2007). End of Sveconorwegian orogeny and the development of the Precambrian basement rocks in the southern Norway are marked by appearance of large granite bodies of 975 – 925 Ma age (Ramberg et al., 2007).

- Formation of supercontinent Rodinia

Several rifting events and intrusions of melt along with formations of mountain chains led Fennoscandian shield to become large and extensive. Series of Sveconorwegian plate collisions led to the formation of supercontinent Rodinia (Ramberg et al., 2007; Torsvik and Cocks, 2005).

- Break up of Rodinia

At around 850 – 750 Ma supercontinent Rodinia had been broken into several smaller parts. One of them, separated 850 Ma, was Baltica in composition with Fennoscandian shield and Norway (Ramberg et al., 2007). Rocks that formed at a time interval of 850 – 750 Ma bear characteristics of fragmentation and major climate change processes. One of the most important features is Trollfjord-Komagelva fault zone that is of early Precambrian origin and has been considered to represent zone of weakness during Rodinia break up (Ramberg et al., 2007). The following fault zone is of NW-SE orientation and cut eastern Finnmark into Tana fjord – Varanger fjord region on the southwestern side and Barents Sea region on the northeastern side (Ramberg et al., 2007).

Cambrian period (542 – 488 Ma)

- Opening of the Iapetus Ocean

Separation of Baltica and Laurentia led to the opening of Iapetus ocean that gradually expanded (Cocks and Torsvik, 2005). Successive seafloor spreading with rising mid-ocean ridge caused ocean water to flood over shallow parts of Baltica and other continents.

Ordovician – Silurian – Early Devonian period (488 – 405 Ma years)

- Closure of Iapetus ocean and formation of Caledonides

Late Ordovician – Silurian period is considered to be the stage in the tectonic history of Baltica that progressed the terrane's development accompanied by two major collisions. According to Torsvik and Rehnström (2003), the first collision took place during Ordovician – Silurian boundary (~ 443 Ma) and contributed to Baltica growth through its "soft oblique docking" with Avalonia. The second oblique collision between Baltica-Avalonia and Laurentia occurred at ~ 425 Ma (Scandinavian phase) (Cocks and Torsvik, 2005). The latest merge in contrast to the first one bore a different character. It is characterized by closure of Iapetus Ocean and the formation of thrust nappes known as Caledonian orogeny (Ramberg et al., 2007; Gee, 1975). Caledonian orogeny, in particularly Scandian orogeny, was a significant mountain-building episode in the tectonic history of Norway that affected at it most western part of former Baltica giving it mountain relief by several thrust and suturing episodes. Caledonian orogeny stretches from western parts of Europe at the south to Svalbard at the north. The best part that has been preserved extends along Norway.

Caledonian cover units have been transported from coastal and sea areas into the Baltica continent (Ramberg et al., 2007). When talking about the exact direction of movement one can find it quite difficult to determine. Lineaments can give an idea of the direction movements took place. Lineaments

are linear structures that form in deformed, mylonitic rocks (Ramberg et al., 2007). The shape of deformed minerals and conglomerate bodies reflects stretching direction and may also indicate the direction of units' transportation. Most of lineament patterns indicate thrust nappes have been transported in eastern and southeastern directions as shown in Figure 1 (Ramberg et al., 2007; Gabrielsen et al., 2002). The southernmost Caledonian cover units show slight changes in transportation direction. One can observe that lineament patterns shift from being easterly to southeasterly oriented with south-southeasterly orientation in the area of Oslo graben. Changes in lineaments orientation can reflect variations in the transportation across the mountain range. Central part of Caledonian orogeny shows lineaments that are parallel to the coast. One of the possible reasons can be oblique movement along the collision zone at the central part of the mountain range (Ramberg et al., 2007).

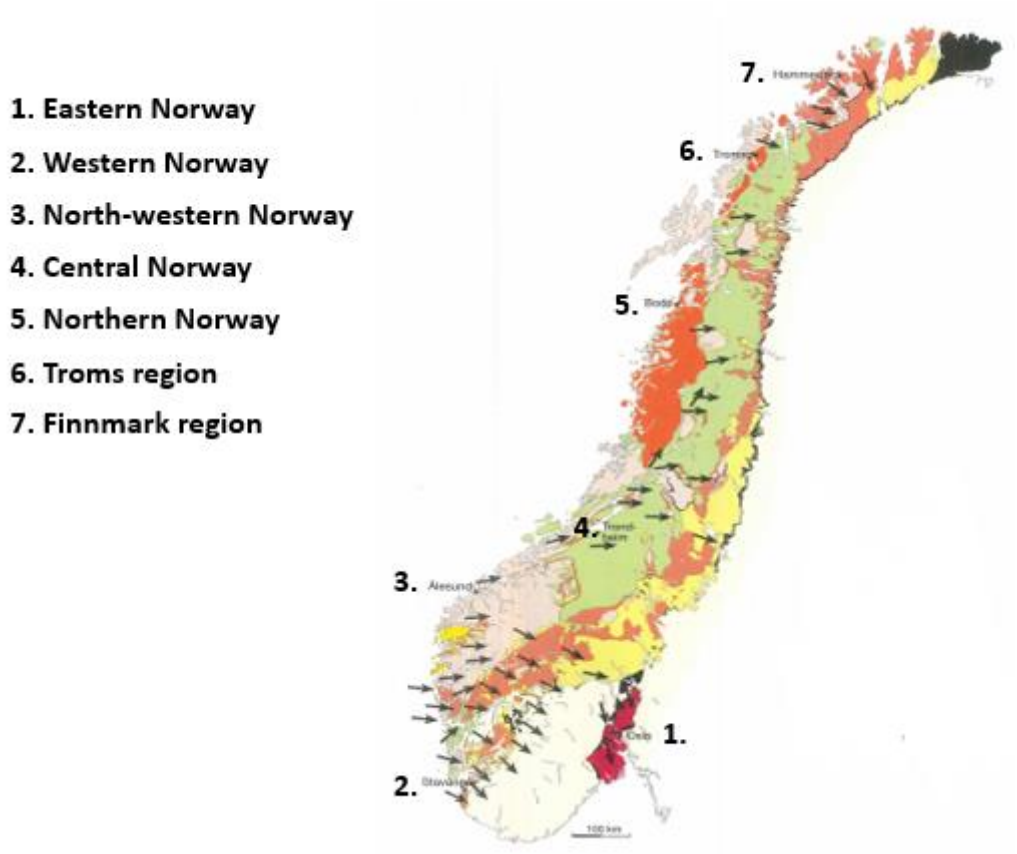

Figure 1: Arrows showing Caledonian thrust napes being transported to the east and southeast. (Modified picture, Ramberg et al., 2007).

Devonian period (416 – 359 Ma)

- Collapse of Caledonian mountain range

Thrusting was not the only mechanism affecting western Norwegian realm during Devonian. Kinematic indicators such as shear bands, asymmetric faults and boudins point out that in addition to top-to-the ESE shearing there have been top-to-the WNW shearing (Andersen, 1998; Braathen et al., 2000). Change of shearing direction happened due to plate backsliding – Mode I extension starting at around 408 Ma. Once thrusting episodes ceased, extensional mechanism shifted to its second Mode ensuing

crustal collapse (Braathen et al., 2000). This led to the thrust fault inversion, a process during which thrust faults inverted into normal faults (Ramberg et al., 2007). Consequences of the stretching caused decrease in thickness and height of the whole mountain range. Areas most affected by extension led to the formation of extensional shear zones. These Caledonian tectonic features, as shown in Figure 2, crop out along Caledonian mountain range, in particular from Stavanger in the south to Troms in the north with most of them having northeastern to northern orientation and dipping to the west (Ramberg et al., 2007). The remaining part of Baltica comprising newly-formed Laurussia was considered to be of flat character (Baarli et al., 2003).

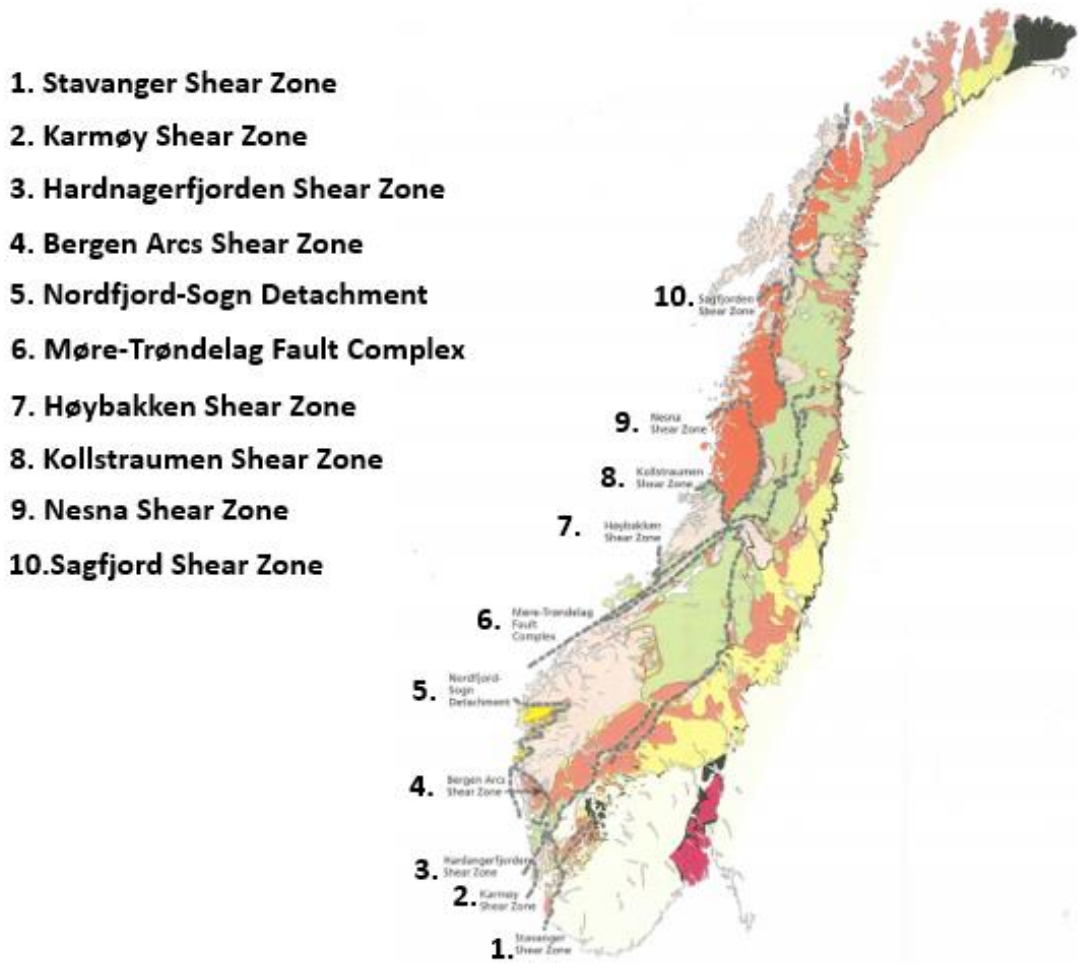

Figure 2: Major Shear Zones formed during Caledonian Orogeny. (Modified picture, Ramberg et al., 2007).

Carboniferous – Permian period (359 – 251 Ma)

During early and middle Carboniferous supercontinent Laurasia drifted towards the north. Laurasia drift accompanied by crustal movements led to the formation of numerous rift basins within mountain range predominantly of north-south orientation at Barents shelf and Svalbard area (Ramberg et al., 2007). Northwestern – southeastern stretching and sideways movements between Norway and Greenland led to the variety of shapes and structures of rift basins in Norway. Early Carboniferous had large rift basins with some of them subsided deep along the western coast of Svalbard and Bjørnøya whereas others characterized by deep depressions experienced little subsidence (Ramberg et al., 2007). Middle Carboniferous, on the other hand, characterized by narrow basins with small amount of subsidence. During late Carboniferous and Early Permian decrease in crustal motion and cease of rift

movements led to the formation of stable and continuous platform along large parts of Svalbard (Ramberg et al., 2007).

Early Permian is remarkable by collision of two supercontinents – Laurasia and Gondwana – led to the formation of supercontinent Pangea. As can be noticed geological processes for the time interval covering Late Silurian – late Carboniferous didn't leave any remarkable imprints on Oslo area meaning this geological time for Oslo area can be considered to be hiatus. However, geological processes taking place from the beginning of late Carboniferous (approx. 310 Ma) and for the next 70 years contributed to the formation and development of Oslo rift zone (Ramberg et al., 2007). Oslo rift zone formed as a consequence of crustal break up accompanied by severe volcanism in the area from Skagerrak to Østerdalen (Eastern Valley) and formation of large faults/fault complexes as shown in Figure 3 (Ramberg et al., 2007). Lithological units of Permian age formed as a result of intense volcanism were found to have high stresses (Myrvang, 1996).

Collision of Laurasia and Gondwana to form supercontinent Pangea entailed two other significant geological events: formation of mountain range known as Variscan (Hercynian) and fault line – Sorgenfrei-Tornquist zone (Ramberg et al., 2007). These structures gave a strong push to the development of Oslo rift further to the north (Ramberg et al., 2007). Orientation of Oslo rift longitudinal axis is mainly to north-south while stretching forces that cracked the crust is of east-west orientation (Ramberg et al., 2007). Movements along Sorgenfrei-Tornquist zone contributed to east-west stretching forces to develop further to the north (Ramberg et al., 2007).

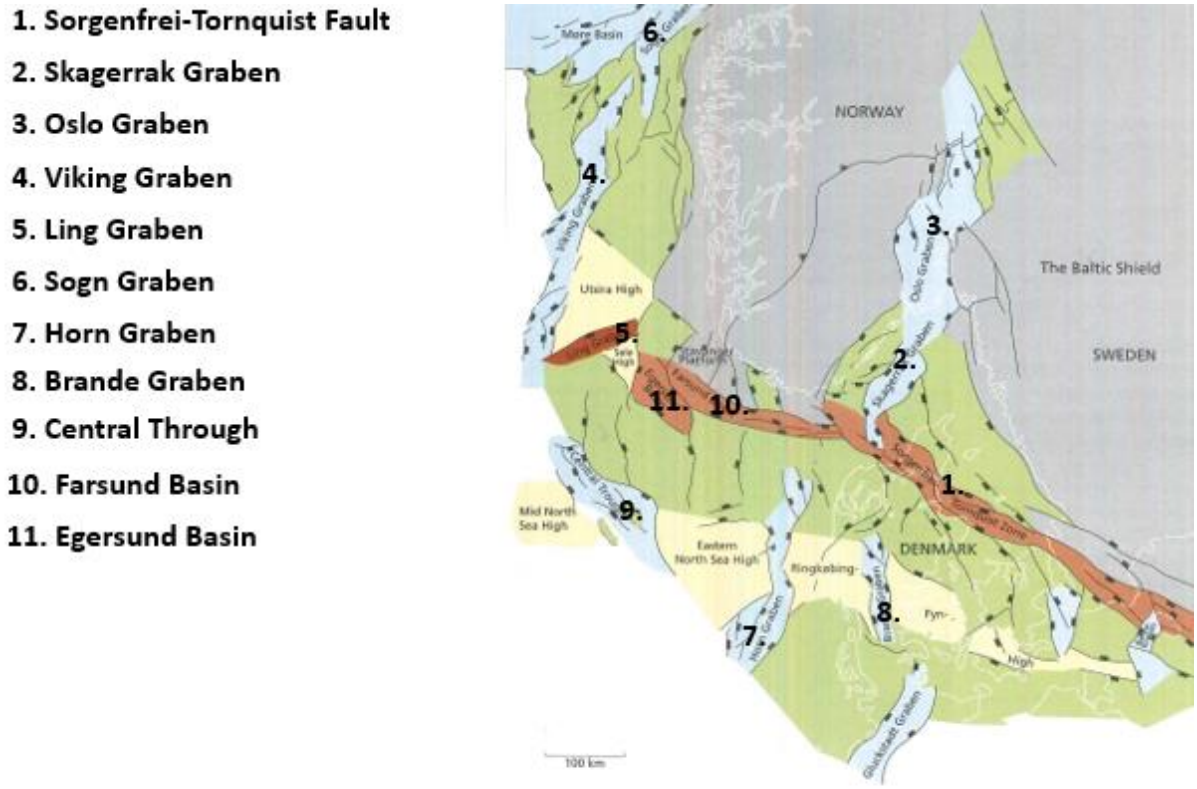

Figure 3: Major geological structures developed in the North Sea and Skagerrak strait during Permian. (Modified picture, Ramberg et al., 2007).

Ongoing Pangea breakup during late Permian – Cretaceous period gave a push to a major long-lasting polyphase rifting of the Norwegian continental shelf (Ramberg et al., 2007). An onset of rifting

commenced across nearshore areas with its further propagation towards the offshore realm. Initial extension between East Greenland and present-day Norwegian shelf took east – west direction (Torsvik and Cocks, 2005). That is oblique to the modern Norwegian coastline. As time was approaching late Cretaceous opening direction underwent changes and became a more northwest – southeast oriented (Torsvik and Cocks, 2005). That is perpendicular to the current Norwegian coastline.

Transition from late Permian to Triassic is tectonically remarkable by the end of volcanic and tectonic activity around Oslo area and its subsequent westwards shift. Several new rifts had been developed in the Northern Sea, Norwegian Sea and in Eastern Greenland (Ramberg et al., 2007).

Triassic Period (251 – 206 Ma)

In the beginning of Triassic supercontinent Pangea started to crack. Opening of the Tethys Ocean caused separation of new Europe from Africa. New rift basins and lowlands were formed between Norway and Greenland (Ramberg et al., 2007). Movements of the Earth crust in the North and Norwegian Seas continued in early Triassic. Large part of North Sea was land during most of the Triassic. The southern part of the Sea was gulf whereas the northern area was covered by several small rift basins (Ramberg et al., 2007). Despite most of Norway was land during Triassic its northern part for a long time was flooded by a large gulf known as Boreal Sea (Ramberg et al., 2007).

Jurassic Period (206 – 146 Ma)

Early and Middle Jurassic is tectonically remarkable by reorganization of continental plates and ongoing stretching of supercontinent Pangea. Stretching axis gradually shifted northwards to the central part of the Atlantic Ocean (Ramberg et al., 2007). Norway mainland and Norwegian continental shelf took their current shape. Dry climate prevailing during Triassic shifted to humid resulting in increased runoff and transportation of material from the mainland to continental shelf (Ramberg et al., 2007). Norwegian coastal areas took their shape after Permo-Triassic rift phase (Ramberg et al., 2007). Basins occupying North, Norwegian and Barents Seas were flooded. Norwegian Sea was relatively narrow sedimentation basin (Ramberg et al., 2007). Barents Sea was divided into southern and northern basin areas. Another significant event was a Middle Jurassic shift of fracturing/stretching direction in an ancient supercontinent Pangea. Spreading in the Atlantic Ocean forced its way towards the northeast fracturing into Norwegian sea and partly into the North Sea (Ramberg et al., 2007). This event entailed the formation of continuous elongated rift structure along the Norwegian shelf that followed Permo-Triassic rift and stretched from North to Barents Sea (Ramberg et al., 2007).

As late Jurassic rift developed several other tectonic structures formed. In the North Sea spreading took place in east-west direction (Ramberg et al., 2007). The resulting rift structures was named Viking graben at the north and Central graben at the south. Spreading in that area ceased at the transition to Cretaceous Era. Spreading continued and reached the Norwegian Sea in early Cretaceous. In that area spreading direction changed from the east-west to the northwest-southeast. The Norwegian structures formed include Halten terrace and Hammerfest basin (Ramberg et al., 2007)**.** Spreading pushed its way from Halten terrace to Møre and Vøring basins. Most of further successive rift movements in the southern part of the Barents Sea occurred during early Cretaceous. The structures formed include high altitude areas (Lopphøgda, Stappehøygda and Sentralbankhøgda) in the western and central part of the Barents Sea that at a later time were eroded (Ramberg et al., 2007). Northern part of the Barents Sea along with the mainland mostly were not influenced by late Jurassic rift development (Ramberg et al., 2007).

Formation of numerous complex structures during Jurassic rift contributed to the development of fault zones and fault complexes. Fault blocks from that time are characterized by steep sides, fault escarpments and inclination up to 60 degrees (Ramberg et al., 2007).

Another feature characteristic for the late Jurassic was volcanism. Intense vulcanism was observed in the middle of "three-armed" structure in between Moray Firth graben (southwestern arm), Viking graben (western arm) and Central graben (Ramberg et al., 2007). Smaller volcanos were detected in the southern Viking graben, Central graben, in the Egersund basin and along Norwegian coast (Ramberg et al., 2007).

Cretaceous Period (146 – 66 Ma)

At the beginning of Cretaceous period continent and lands were evenly distributed from pole to pole. However, seafloor spreading of ancient supercontinent Pangea caused continents to move away from each other. This event entailed opening of the Atlantic Ocean. Southern Atlantic Ocean was opened during early Cretaceous due to separation of southern America and southern (Ramberg et al., 2007). Northern Atlantic was opened as a result of Europe and northern America separation at a late Cretaceous (Ramberg et al., 2007).

Warm Cretaceous period characterized by volcanism and high level of CO2 emissions caused several large structural changes and flooding of low altitudes structures (Ramberg et al., 2007). Norwegian Sea accommodated deep regional basins such as Møre basin, Vøring basin, Harstad basin, Troms basin and Sørvestnaget basin. They were formed along main rift stretching axis and were subjected to stretching and thinning throughout late Jurassic and early Cretaceous (Ramberg et al., 2007). Barents shelf was a huge platform area during Cretaceous and represented northern boundary beyond which development of the Atlantic Ocean ceased (Ramberg et al., 2007). Stretching and rifting of the Atlantic Ocean took place along zones of weakness, in particular along the western side of Barents Sea, past Svalbard and then into Eurasia basin in Arctic Ocean (Ramberg et al., 2007).

Paleogene – Neogene (Cenozoic era) period (66 – 2.7 Ma)

Cenozoic era became a remarkable time when continents stopped to move and settled at places one can observe them today.

In Paleogene Norwegian Sea started to open whereas southern areas belonging to the Atlantic Ocean began to drift from each other ensuing onset of continental drift between Norway and Greenland at approx. 55 Ma (Ramberg et al., 2007). Development of the Norwegian Sea led to the formation of southeastern-northwestern fracture zones that were nearly perpendicular to the spreading ridge (Ramberg et al., 2007). One of the well-known fracture zones in the Norwegian Sea is Jan Mayen that borders with Vøring basin on the northern side of the fracture zone and Møre basin on the southern side. Opening of the Norwegian Sea influenced Barents Sea plates that became enclosed by two parallel transform faults. At northwest Barents Sea plates enclosed by Horsund fault zone whereas at the western part they are confined by Senja fault zone (Ramberg et al., 2007). Seafloor spreading of the Norwegian Sea is still active and is considered to belong to the group of slow spreading ridges (Ramberg et al., 2007).

In Paleogene Norwegian mainland began to rise. There are two main uplifts occurred in Cenozoic: uplift in southern Norway around Jotunheimen and in northern Norway around Lofoten fjord (Ramberg et al., 2007). There had been uplift around Trondheim fjord but at a lesser extent (Ramberg et al., 2007). North Sea had been shallow sea that periodically dried out whereas Norwegian Sea developed into a deep sea due to seafloor spreading between Norway and Greenland (Ramberg et al., 2007). North Sea

was relatively stable during Paleogene and Neogene periods but yet experienced small subsidence in particular along late Jurassic rift structures: Viking and Central grabens (Ramberg et al., 2007).

Late Pliocene – Pleistocene (Quaternary) epoch (2.7 Ma – 11500 years)

During last 2.7 Ma most of Norway, Svalbard and Barents Sea were periodically covered by glaciers. Uplift that took place during Cenozoic continued during ice ages. The largest uplift occurred at the west (Ramberg et al., 2007). Periodically coming ice ages reshaped earlier formed geological features by glacier erosion. Erosional products were further transported into the sea that led to the formation of continental shelf (Ramberg et al., 2007). Most of the time ice sheets of relatively small size formed. However, at about 900 000 years ago ice sheets started to grow. During great ice ages ice cap spread southwards to the continent. Sea level varied a lot by rising and falling between 100 and 150 meters depending on either ice sheets formed or melted (Ramberg et al., 2007).

One can distinguish four major ice periods occurring during the following time interval. The first one – Eem, the second – Elster, the third one – Saale and the fourth – Weichsel (Ramberg et al., 2007). Mostly records of the last ice age (Weichsel) can be observed in Norway since relicts of the earlier ice age deposits were removed by extensive inland ice cap (Ramberg et al., 2007). Large inland ice cap (Younger Dryas) in northern Europe and northern America grew to a large size at the end of the last ice age (Weichsel). It reached its maximum approx. in between 18 000 – 25 000 years ago (Ramberg et al., 2007). Western boundary of inland ice cap was represented by a shelf edge outside Norway whereas its southern side was restricted by Denmark and then the boundary went across northern Germany, Poland, Belarus and Russia (Ramberg et al., 2007). From around 18 000 years ago ice sheet balance changed from being positive to negative that caused inland ice cap to melt and calve (Ramberg et al., 2007).

Holocene epoch – 11 500 years – present

End of the last ice age entailed several significant changes in Norway. Melting of almost all glaciers caused global sea level change during which sea level rose 125 meters that contributed to a greater land uplift in Norway (Ramberg et al., 2007).

As glaciers melted many of steep mountain sides formed due to glacier erosion. Instability of eroded mountain sides was the main reason to cause numerous landslides and rockslides. These events triggered several natural disasters in Norway. Areas mostly affected by landslides are steep lands in western and northern Norway (Ramberg et al., 2007). Most well-known rockslides in western Norway are Loen slides (1905, 1936) and tsunami in Tafjord (1934) (Ramberg et al., 2007). In northern Norway the greatest concentration of rockslides is found in a zone extending from Balsfjord at the south to Reisadalen at the north (Ramberg et al., 2007). In addition, numerous of rockslides were taking place in Troms at the period of 11 500 – 10 500 years ago (Ramberg et al., 2007). In several cases landslides are triggered by earthquakes, such instances were also found in Norway. For example, it is assumed that tectonic fault in Kåfjord in Troms caused an earthquake that in turn triggered many rockslides in the area, young fault in Innfjorden in Romsdalen can be a reason of numerous rockslides at the inner fjords in Møre and Romsdal (Ramberg et al., 2007). Slides also occurred on the Norwegian continental slope. The largest submarine slides are Andøy slide (Troms), Trænadjup slide (west of Lofoten) and Storegga slide (outside Møre-Trøndelag coast) (Ramberg et al., 2007).

Short summary of significant events contributed to the development of Norway and formation of main geological structures are briefly listed and can be reviewed.

1) Crust (mainland) growth and development during Proterozoic era;
2) Formation of Caledonides due to collision of Baltica and Laurentia during Ordovician – Early Devonian that ensued development of fault zones and fault complexes;
3) Collapse of Caledonides in Devonian;
4) Formation of rift basins during Carboniferous – Permian;
5) Collision of Laurasia and Baltica that led to the formation of Pangea and formation of Oslo rift zone and numerous fault zones and fault complexes in the area; formation of Sorgenfrei-Tornquist fault zone that cause east-west oriented stretching (Carboniferous – Permian);
6) Jurassic rift development of the North and Norwegian Seas that led to the formation of Viking graben at the north and Central graben at the south and development of faults/fault complexes;
7) Jurassic intense vulcanism along Norwegian coast and in the area nearby Viking and Central grabens;
8) Further development of North, Norwegian and Barents Sea during Cretaceous. The deepest subsidence among them experienced Norwegian Sea during Cretaceous time;
9) Cenozoic Era: Mainland uplift, the largest uplift was observed at the west, opening of Norwegian Sea, opening of the Atlantic;
10) Late Pliocene – Pleistocene: Norway was covered by ice. Firstly by small ice sheets that started to increase and led to numerous ice ages. There had been assumed there were four major ice ages and only relicts of the last one can be found in Norway;
11) Late Pliocene – Pleistocene: formation of a Norwegian continental shelf out of glacial sediments that had been eroded down into the seas.
12) 11 500 – Holocene: Glaciers melted, large land uplift that led to the formation of numerous faults/fault complexes.

2.2 Seismicity in Norway and adjacent areas

Seismicity in Norway is higher than in other northwestern countries. Level of seismicity is relatively high from what can be expected in relatively stable tectonic environment, far from plate boundaries. Despite Norway locates in intraplate setting and experiences low to moderate level of seismicity, it borders with two major structures that are capable of causing earthquakes of large magnitudes within stable continental environments. These are the rifted passive continental margin and failed rift zones. Examples of large earthquakes along rifted passive continental margins in other regions include those in South Carolina in 1886 of magnitude 7.6, Exmouth Plateau in 1906 of magnitude 7.2, Taiwan Straits in 1604 of magnitude 7.7, Grand Banks in 1929 of magnitude 7.4 and Portugal in 1858 of magnitude 7.1 (Johnston and Kanter, 1990; Bakun and Hopper, 2004; Gomberg and Schweig, 2003; Bungum et al., 2005). Earthquakes along failed rifts in Basel in 1356 of magnitude 7.4, New Madrid in 1812 of magnitude 7.8, Hainan Island in 1605 of magnitude 7.3, New Madrid in 1811 of magnitude 7.6 and Kutch (Gujarat, Bhuj) in 2001 of magnitude 7.9 (Johnston and Kanter, 1990; Bakun and Hopper, 2004; Gomberg and Schweig, 2003; Bungum et al., 2005). In Norway historical records show that there have been 21 large earthquakes of magnitudes equal to 5.0 or large in the period 1759 – 2019 as listed in Table 1 and shown in Figure 4 (Husebye, 2005; Sellevoll and Sundvor, 2001; Earthquake track, 2019). Most of the them occurred along rifted passive continental margin with some seismic events registered also along the Viking Graben and the Oslo rift zone.

Table 1: Earthquakes of magnitude equal to 5.0 and larger that occurred in Norway (except Svalbard region) in the period 1759 – 2019.

Nr.	Year	Day	Month	North	East	Magnitude
1.	1759	12	22	57,70	11,10	5,70
2.	1819	31	8	66,40	14,40	5,80
3.	1866	9	3	65,20	6,00	5,70
4.	1904	11	23	59,20	10,50	5,40
5.	1907	14	1	66,60	9,50	5,00
6.	1907	27	1	66,20	8,60	5,30
7.	1913	19	7	64,30	6,30	5,00
8.	1927	24	1	59,90	1,80	5,30
9.	1931	6	7	54,10	1,50	5,30
10.	1935	17	7	65,90	7,20	5,00
11.	1937	27	11	71,00	10,20	5,10
12.	1955	3	6	61,90	4,10	5,20
13.	1958	23	1	65,20	6,50	5,00
14.	1959	29	1	70,87	7,45	5,90
15.	1969	29	9	65,10	6,50	5,00
16.	1977	4	6	61,61	2,47	5,00
17.	1982	7	29	60,12	2,15	5,00
18.	1984	7	27	65,98	13,07	5,40
19.	1986	2	5	62,78	4,81	5,00
20.	1988	8	8	63,68	2,44	5,30
21.	1989	23	1	61,97	4,42	5,10

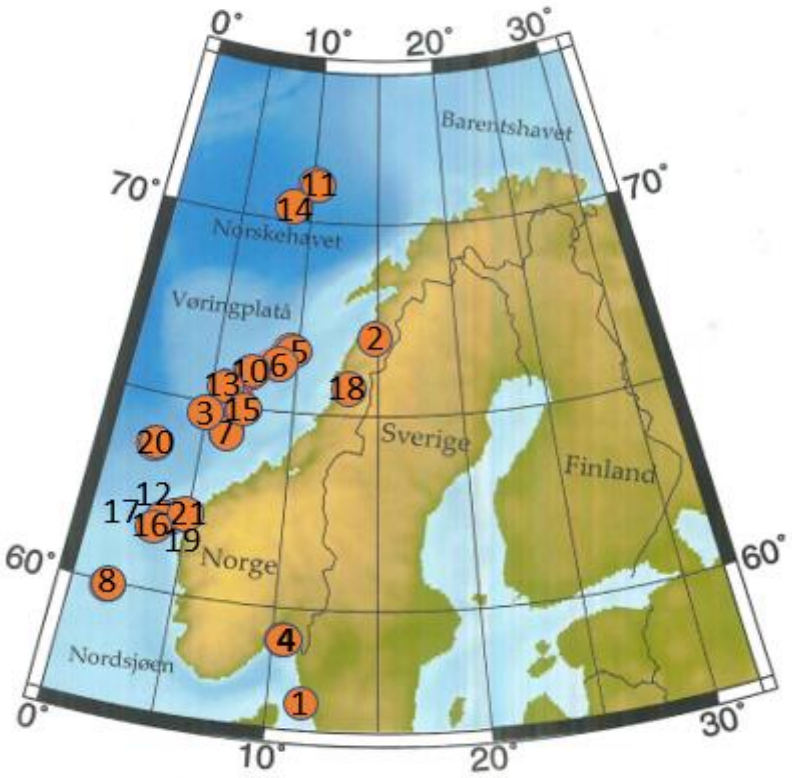

Figure 4: Earthquakes listed in Table 1 of magnitude equal to 5.0 and larger occurred in Norway in the period 1759 – 2019 (Modified picture, Sellevoll and Sundvor, 2001).

The main challenge related to seismic events occurring along such host structures is unknown recurrence interval. Seismic events of comparatively large magnitudes may repeat in several thousand years. Earthquakes of magnitude 5.0 and magnitude 7.0 may strike Norway every 10 and 1100 years respectively (Bungum et al., 2005).

Major driving mechanism that creates uniform stress distributed over large areas within most of continental regions is a “ridge-push” force (Bungum et al., 2005). A “ridge-push” force is a gravity-driven force that cause the plate to move away from the mid-ocean ridge. Studies done to investigate in situ stress and focal mechanisms in Norway by Simonsen (2018) and Hicks et al. (2000) respectively have shown that the maximum dominating compressive stress in Norway is caused by “ridge-push” force and it is of NW-SE orientation. Stress caused by “ridge-push” force in Norway is confined to areas nearby continental margin or lying at a short distance from it (Bungum et al., 1991). Other stress generating mechanisms typical in Norway are post-glacial rebound and lithospheric loading. Post-glacial rebound caused by recent deglaciation of Fennoscandia and subsequent isostatic adjustments generates stress along coastal areas. Lithospheric loading creates stress along oceanic crust and is caused by rapid deposition of glacial sediments (Bungum et al., 1991). Areas that are subjected to such stress are Lofoten and Norway Basins (Bungum et al., 1991). Another stress source that drawn attention of seismologists is anomalous elevation differences found in the southern and northern Norway (Fejerskov and Lindholm, 2000). In the southern Norway it is explained by Scandinavian mountains that generate gravitational stresses in adjacent offshore basins (Fejerskov and Lindholm, 2000). Referring to Fejerskov and Lindholm (2000) this may explain 90˚ stress rotation (from NW-SE to NE-SW) detected from the Norwegian margin to the northern North Sea. Similar NE-SW stress orientation justified by variations in gravitational stresses is observed southeast of the Møre-Trøndelag Fault Complex (Fejerskov and Lindholm, 2000). 90˚ stress inversion detected in northern Norway (Nordland) is explained by flexturing due to erosion and local uplift that in turn may be related to glacioisostatic adjustments (Fejerskov and Lindholm, 2000). The maximum horizontal stress axis in Oslo area is WNW-ESE orientated that is probably due to Neogene isostatic adjustments and structural complexity formed during Permian rifting and magmatic events (Fejerskov and Lindholm, 2000). As can be seen in Figure 5, stress regime in Norway is relatively complex and consists of several stress-generating mechanisms.

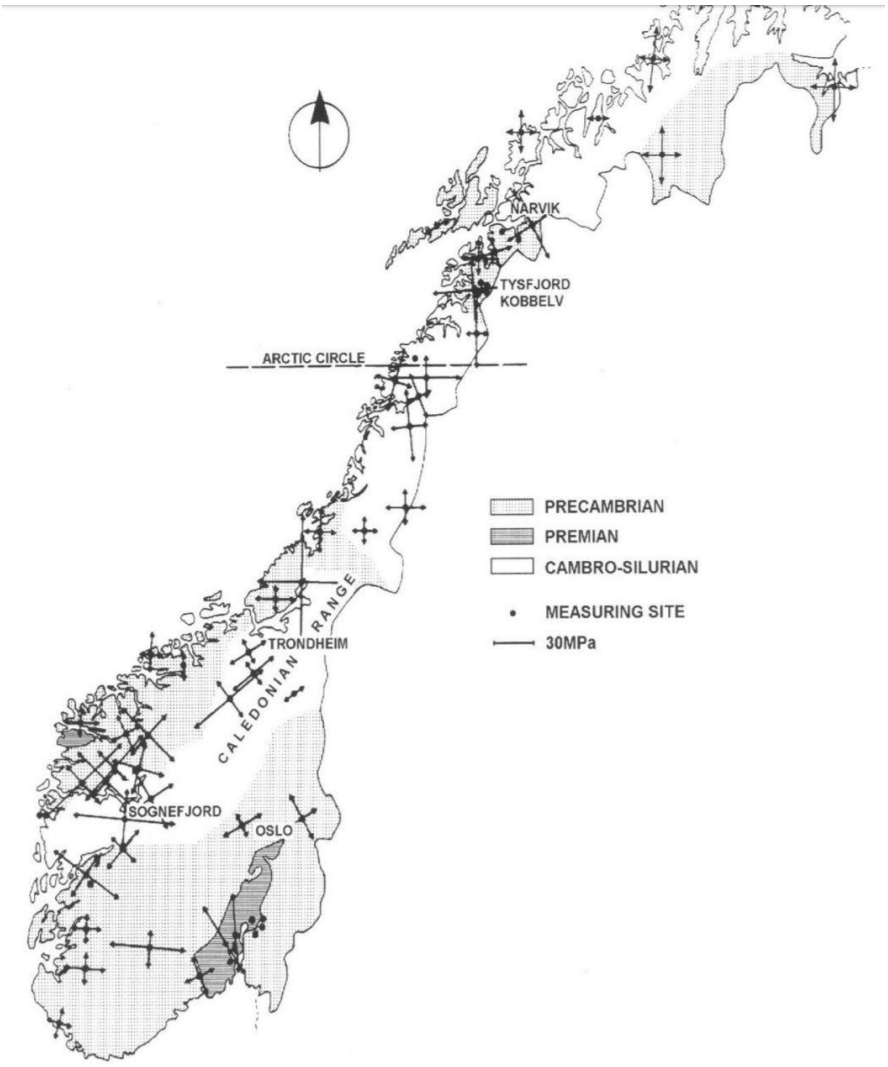

Figure 5: In situ stresses measured in Norway. (Modified picture, Myrvang, 1996).

Despite the stress regime in Norway is multifactorial normal faulting is found to be dominant onshore whereas reverse faulting is dominant offshore (Bungum et al., 1991). Strike-slip faulting also occur in Norway, in particularly it was found in the northern North Sea area with the anomalous 90˚ stress inversion. In that particular case, strike-slip is a transition faulting mechanism between onshore normal and offshore reverse faulting (Bungum et al., 1991). Majority of earthquakes in Norway occur at the brittle parts of the crust with many as well penetrating to relatively deep levels towards the Moho discontinuity (Bungum et al., 1991). Tendency of relatively (weak) character based on focal mechanisms revealed by Hicks et al. (1996) suggests that shallow seismic events (< 13 km) are mostly linked to normal faulting whereas seismic events with deep foci to reverse and strike-slip faulting.

Earthquakes usually occur along favorably oriented to the stress directions pre-existing zones of weakness such as grabens, fracture zones, fault complexes, fault zones, passive continental margins and failed rifts. Offshore concentration of seismicity in Norway localizes along Norwegian continental shelf that on the basis of tectonostratigraphy is subdivided into three distinct provinces (Ziegler et al., 1986). They are the “North Sea – intracratonic basin, the Norwegian Atlantic coast – a passive margin and the Barents Shelf – a sediment-covered intracratonic basin” (Bungum et al., 1991). High seismic activity in the North Sea is linked to the Viking Graben, western and southern coastal areas. Minor level of seismicity is observed along the Central Graben. Neighboring Skagerrak strait and offshore Oslo rift zone as well demonstrates high seismicity concentration. The Norwegian Atlantic coast shows

seismicity trend that stretches from the northern North Sea to the Western Barents Sea. Seismicity concentration in the area of the Barents Shelf is found to be confined to fault complexes and fault zones that are parallel to the Barents Shelf. Among them are well-known Senja fracture zone and Ringvassøy-Loppa Fault Complex. Offshore zones that appears to be relatively aseismic are Horda Platform, Shetland Platform, some areas in the Møre Basin and Trøndelag Platform enclosed by Rana Fault Complex at the east and Kristian-Bodø Fault Complex at the west (Bungum et al., 1991). Most prominent onshore seismicity concentration appears at the southwestern and southeastern Norway as well as northern Norway as shown in Figure 6.

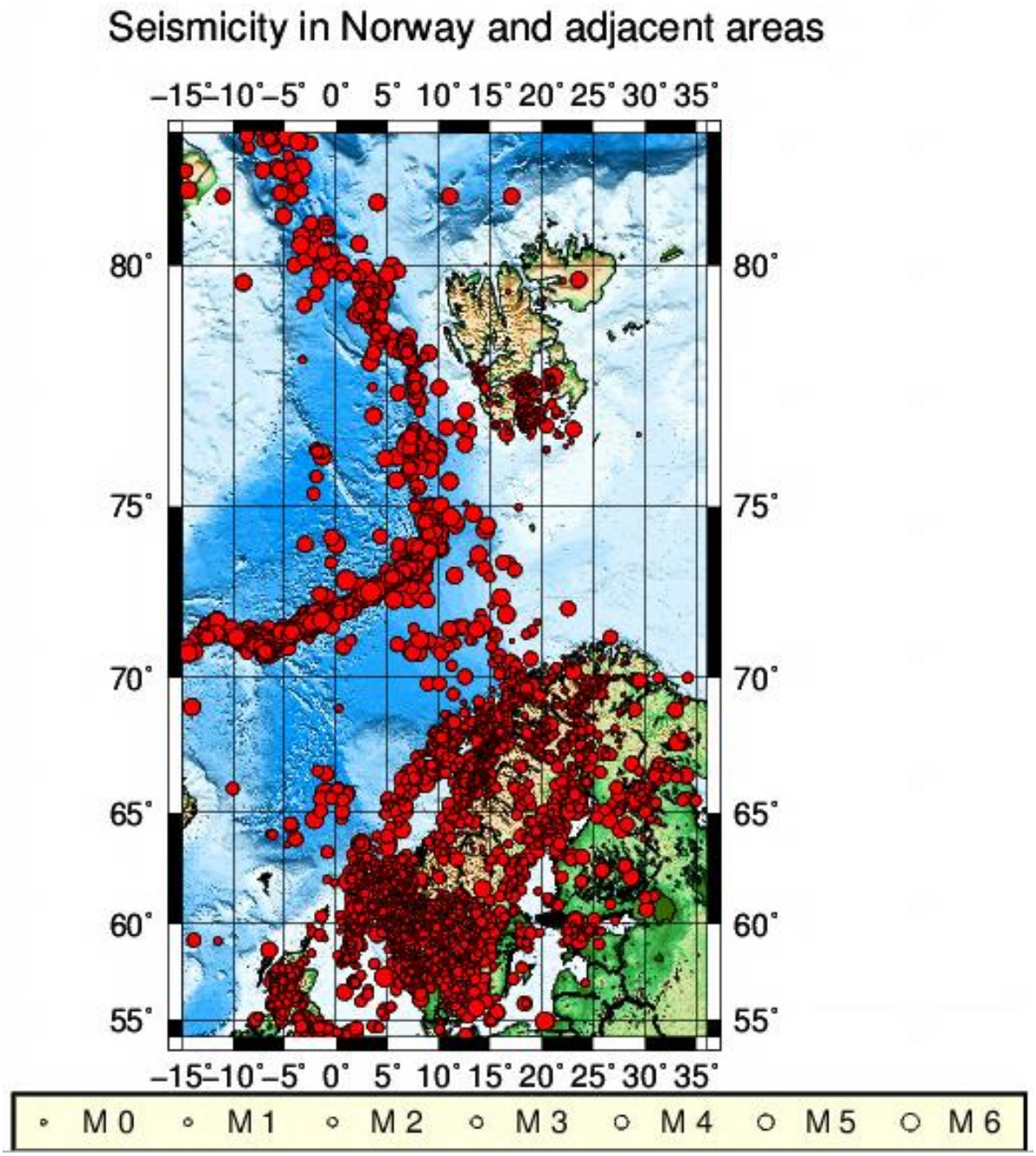

Figure 6: Earthquakes in Norway and adjacent areas for the time period 1900 – onwards. The red circles in the figure are seismic events. The size of a circle is proportional to the magnitude of the event.

The knowledge gathered about the seismicity in Norway, its adjacent areas and the stress orientations can be summarized and reviewed in Figure 7.

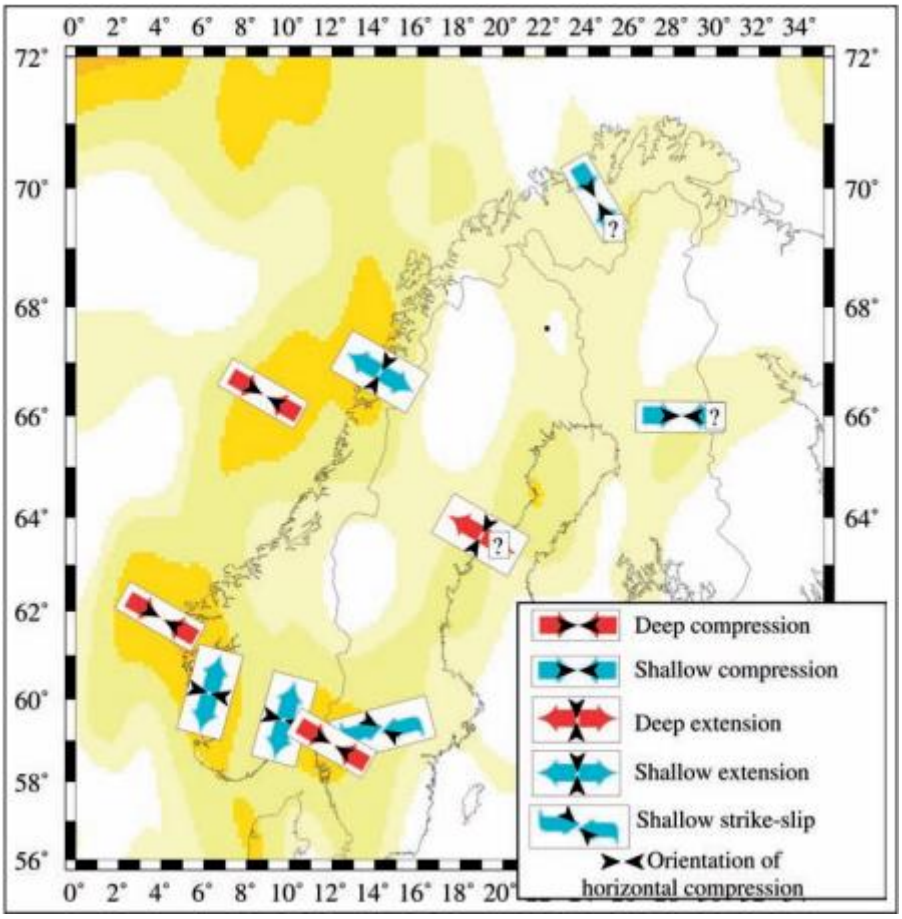

Figure 7: The data represented on the picture is synthesized from earthquake focal mechanisms and in situ stress measurements (Fjeldskaar et al., 2000). Seismic intensity is shown with the yellow color – the brighter the color the higher the seismicity of the area. Black arrows indicate orientation of horizontal compression. Red color indicates deep foci seismic events whereas blue color shallow foci earthquakes (Modified picture, Olesen et al., 2013).

From Figure 7 one can identify the most seismically active areas are southeastern, southwestern, northern Norway and partly the northern part of the Mid Norwegian margin. The dominant stress is NW-SE oriented that correlates well with the "ridge-push" force being prevailing stress generating mechanism. There are also some stress variations caused by other stress-generating mechanisms – glacioisostatic adjustment, lithospheric loading, gravitational differences or combination of them. At the areas along mid Norwegian continental margin, western offshore and northern Norway stress is NW-SE oriented whereas at the southwestern area the stress is NE-SW oriented. The stress in the eastern and southeastern Norway is of mixed character. Earthquakes with shallow foci is mostly observed onshore whereas seismic events with deep foci offshore. Strike-slip and reverse faulting is generally observed offshore whereas normal faulting onshore.

3 Methodology

The first step was to conduct literature survey to gather all necessary information about major deformational episodes in Norway and adjacent areas. It was important to identify major geological structures and significant fault systems associated with main tectonic episodes that have taken place in Norway and adjacent areas at various geological time periods. Also, it was necessary to gather knowledge about seismicity level at different parts (onshore as well as offshore) of Norway to reveal main seismicity trends. In addition, information related to stress generating mechanisms and stress field was also crucial for the purpose of the following study and hence was taken care of. The overall knowledge associated with tectonostratigraphy, seismicity and crustal stresses in Norway and adjacent offshore areas were obtained and analyzed at a large-scale.

The second step was to critically compile and sort the data required to perform the analyses and subsequent interpretation. Data necessary for the analyses include geological, geophysical and seismological data.

- Geological Data

Geological data compiled include major onshore and offshore faults, fault zones and complexes, lineaments, major structural elements, and bedrock geology. Faults, fault zones and complexes were compiled based on two criteria. These are:

- Faults, fault zones and complexes should be mapped on either bedrock geology map on land or offshore fault map or lineament map;
- Out of these faults only significant fault systems associated with each of the following deformational episode using the mapped main structural elements were chosen for the analyses.
  Deformational episodes:
  - Pre-Caledonian;
  - Caledonian;
  - Post-Caledonian;
  - Permian rifting in eastern Norway;
  - Jurassic rifting in the North Sea;
  - Cretaceous subsidence in Norwegian and Barents Seas;
  - Cenozoic uplift;
  - Quaternary glaciation;
  - Holocene post-glacial uplift.

Onshore faults, lineaments and bedrock geology were compiled from the Norwegian Geological Survey (NGU) (Norwegian Geological Survey, 2019), in particular from open-file maps “Berggrun raster” at a scale 1:250,000 and “Lineamenter satellittolket” at a scale 1:750,00. Offshore faults, fault zones and complexes along with major geological structural elements were mostly compiled from the Norwegian Petroleum Directorate (NPD) (Norwegian Petroleum Directorate, 2019), in particular from open-file maps “Faults and Boundaries” and “Structural Elements”. In addition, several significant faults, showing evidence of reactivation or causing concern among scientists, were compiled from the scientific literature. In total, 56 structural elements including onshore and offshore faults were compiled. Out of these 29 faults were identified on mainland Norway and 27 in the adjacent offshore areas.

- Geophysical Data

Geophysical data compiled include gravity data, magnetic data, Moho depth and crustal stress data.

- Gravity data compiled include gravity map that was extracted from the recent work "New aeromagnetic and gravity compilations from Norway and adjacent areas: methods and applications" (Olesen et al., 2010). Gravity map depicts residual gravity after isostatic corrections were applied to Bouguer gravity data.
- Magnetic data compiled include magnetic anomaly map that was extracted from the same source as gravity map (Olesen et al., 2010).
- Moho depths include compilation of two Moho maps. One of them is very detailed and was used to read onshore and offshore Moho depth. This was extracted from the work "New compilation of top basement and basement thickness for the Norwegian continental shelf reveals the segmentation of the passive margin system" (Ebbing and Olesen, 2010). Another one was used as a supplementary map to read depth to Moho for areas extending further Norwegian continental margin, in particular Jan Mayen region. This was extracted from the work done by Funck et al. (2017) "Moho and basement depth in the NE Atlantic Ocean based on seismic refraction data and receiver functions".
- Stress data include stress models generated based on the stress inversion of earthquake focal mechanism solutions from onshore and offshore Norway. In addition, in cases (Southern North and Western Barents Seas) when there were not enough focal mechanism solutions to generate stress model, direction of maximum horizontal compressive stress based on in situ measurements was used. Stress data was extracted from the work "Stress inversion of earthquake focal mechanism solutions from onshore and offshore Norway" (Hicks et al., 2000).

- Seismological Data

Seismological data compiled include two seismic catalogues and a compilation of focal mechanisms.

- First seismic catalogue was compiled based on events stored in the Norwegian National Seismic Network (NNSN). It consists of two parts. First part of seismic catalogue comprises seismic events before 1980. The only restrictions applied were latitude and longitude limits enclosing events within prime area (54.0 – 82.0˚ N, -15 – 36˚ E), and magnitudes limits (M > 3). Second part of seismic catalogue comprises seismic events from 1980 onwards. Restrictions applied were latitude and longitude limits enclosing events within prime area (54.0 – 82.0˚ N, -15 – 36˚ E), event ID (Q – earthquakes and P – probable earthquakes), threshold of the maximum root mean square (RMS) of the travel time residuals (RMS > 1.5), minimum number of stations (5 stations), depth limits (0 – 30 km), epicentral error limits (0 – 20 km). Figures representing seismicity were generated using Generic Mapping Tools to represent two sets of seismological data. Detailed GMT scripts are specified in appendix.
- Second catalogue was extracted from the work "Evaluation of seismicity in the area between the Troll field and the Øygarden fault" done by Tjåland and Ottemöller (2018). This catalogue was used in chapter 7 (discussion chapter) to compare whether earthquakes relocated using double-difference method enable to set better correlation between fault and seismicity and hence whether better estimation of reactivation potential of a fault can be done.
- Focal mechanisms were compiled from recent and revised works done by Tjåland and Ottemöller (2018); Sørensen (2002); and Michálek (2018). In addition, NNSN was searched from 2002 to 2019 for solutions with more than 10 polarities and not included in the above. The results of search were also included in the compilation of focal mechanisms.

The third step was to establish zones enclosing faults, fault zones and complexes. Zonation was made based on geological, geophysical and seismological features. In total, six zones were established. These are North Sea, Onshore Southern Norway, Norwegian Sea, Onshore Mid Norway, Barents Continental Shelf and Onshore Northern Norway. Afterwards, each fault element was assigned to one of six zones based on its geographical location.

The fourth step was to integrate faults and seismicity on one map. This was done using D-Map software (D-Map, 2019). All seismic records constituting catalogue were brought on one map to trace significant seismicity trends, in particularly alignment between seismicity and the faults. However, only seismic records with magnitude equal to 3.0 and larger were considered when correlating seismicity with the faults.

The fifth step was to perform analysis of each zone and faults (segments) contained therein. Method used for identifying reactivation potential of the faults is specified in the diagram below:

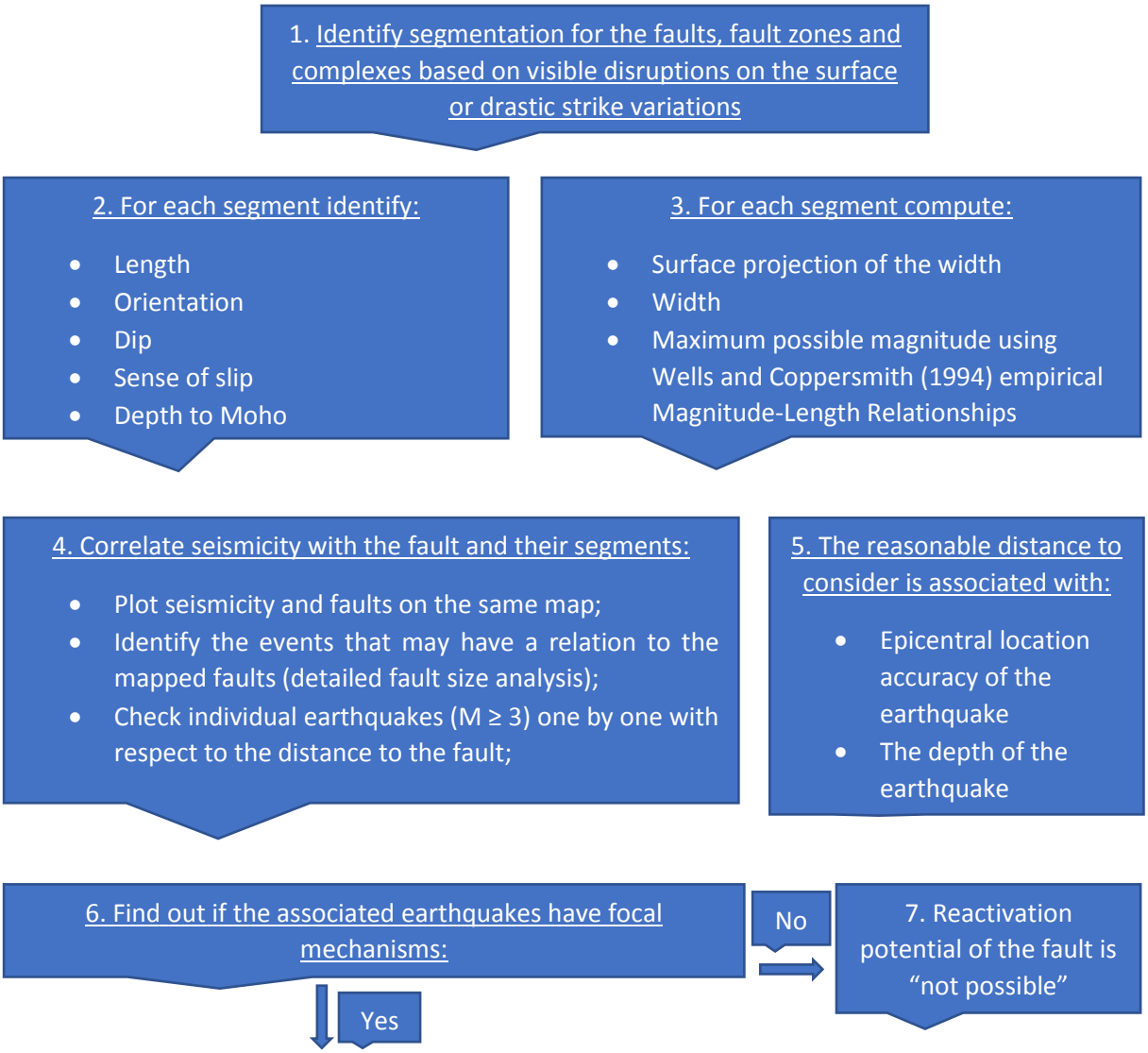

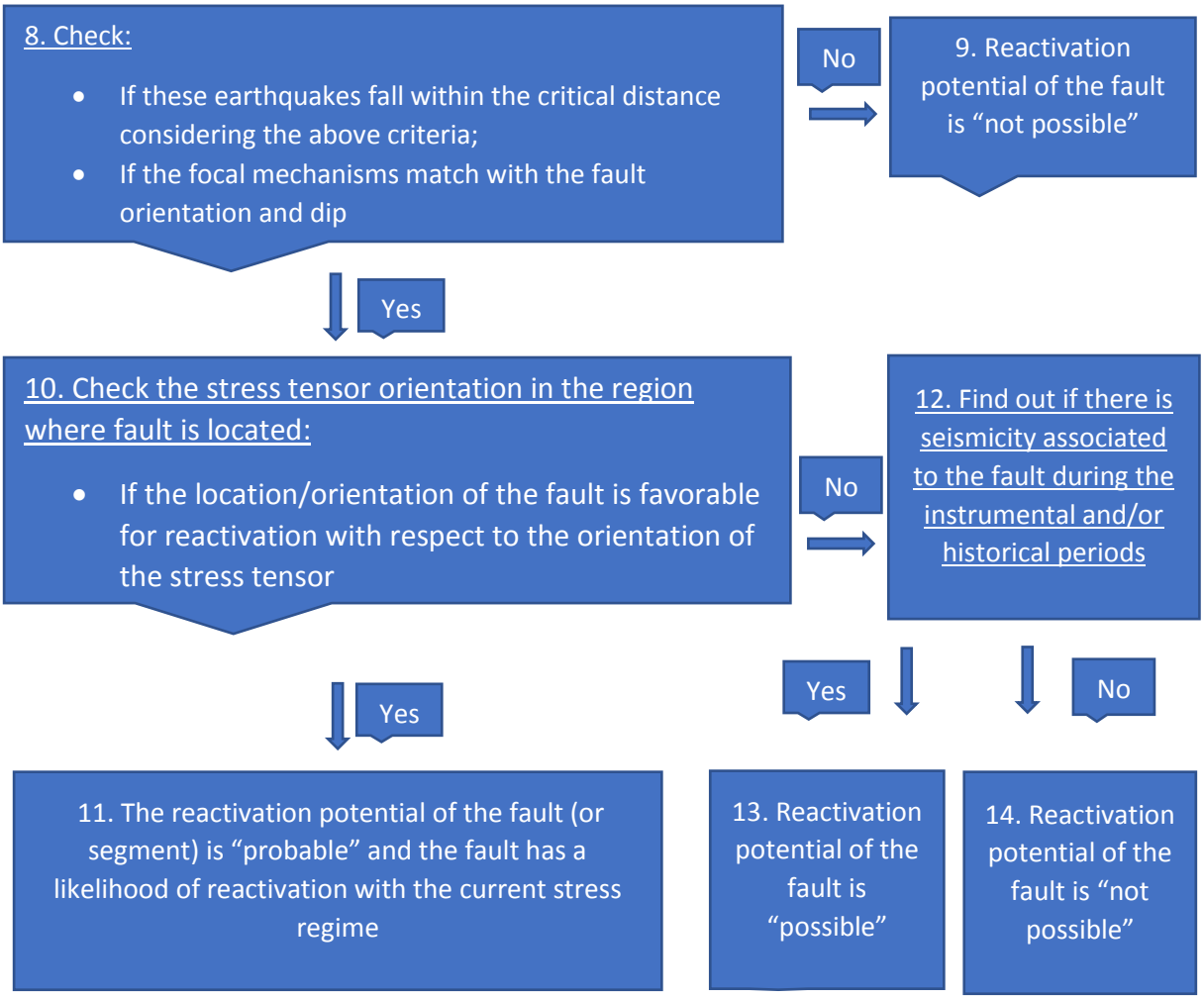

Comments on step 2 (diagram above)

- Length of the fault was measured using polyline tool in D-Map software (D-Map, 2019);
- Orientation of the fault was specified based on visualized fault(s)/segment(s) data;
- Dip for the offshore faults was specified using seismic cross-sections and for the onshore faults using the scientific literature;
- Sense of slip was specified using the scientific literature and for some offshore faults using the seismic profiles;
- Depth to Moho was specified based on Moho map.

Comments on step 3 (diagram above)

- Surface projection of the fault's (segment's) width was computed using the following mathematical relationship:

$$Surface\ projection\ of\ the\ width = \frac{tangent\ (90^{\circ} - dip\ of\ the\ segment)}{segment's\ depth\ to\ Moho} \quad (1)$$

- Width of the fault (segment) was computed using the following mathematical relationship:

$$Width\ of\ the\ fault\ (segment) = \frac{surface\ prjection\ of\ the\ width}{sinus\ (90^{\circ} - dip\ of\ the\ segment)}\ (2)$$

- Maximum possible magnitude was calculated using Wells and Coppersmith (1994) empirical Magnitude-Length relationships:

$Mag = 5.08 + 1.16 \times \log(Length)\ (3)$ – all rupture types;

$Mag = 5.16 + 1.12 \times \log(Length)(4)$ – strike-slip rupture;

$Mag = 5.00 + 1.22 \times \log(Length)(5)$ – reverse or thrust rupture;

$Mag = 4.86 + 1.32 \times \log(Length)\ (6)$ – normal rupture;

The sixth step was to perform further analyses and find out seismogenic potential of the faults (or segments). The way it was done is specified in the following diagram.

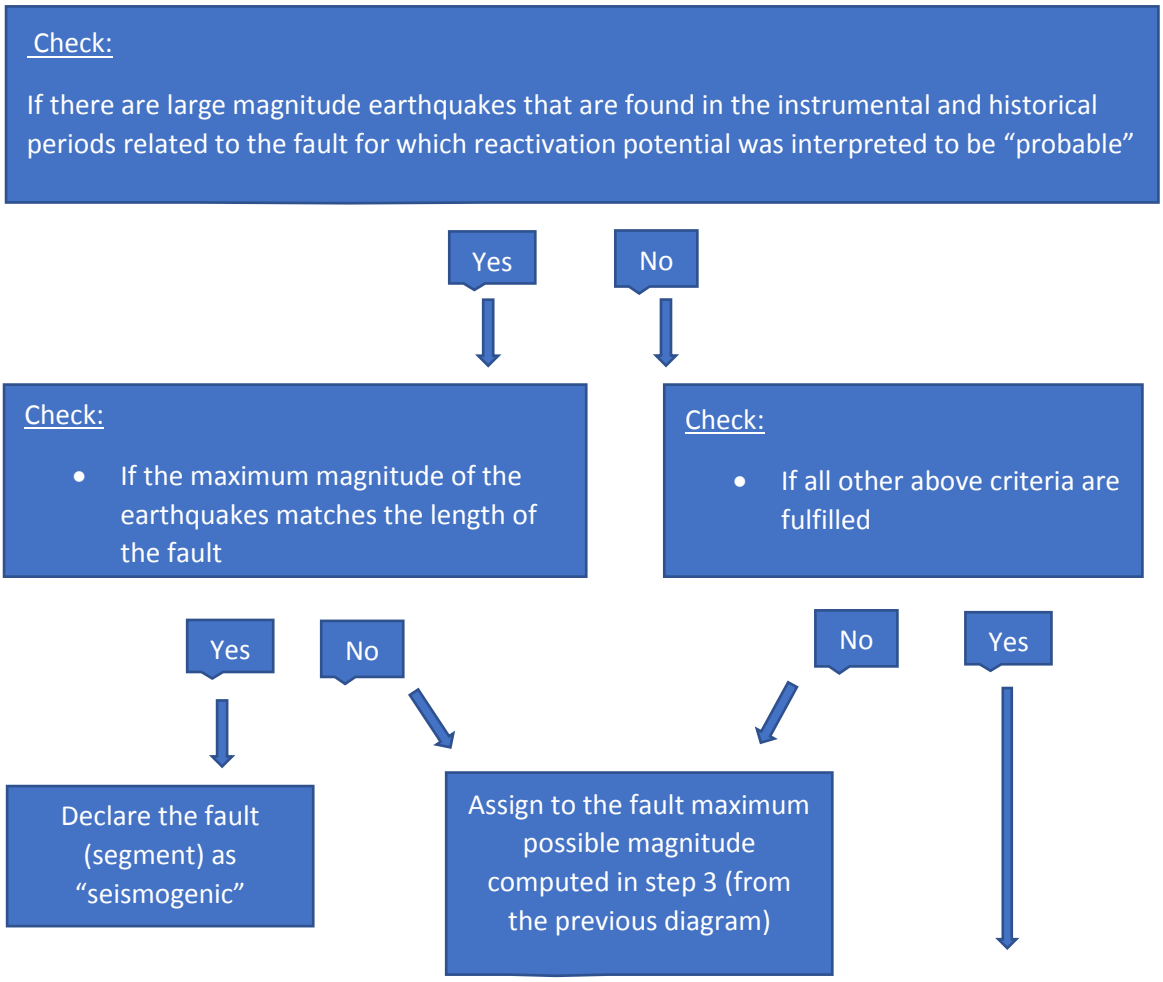

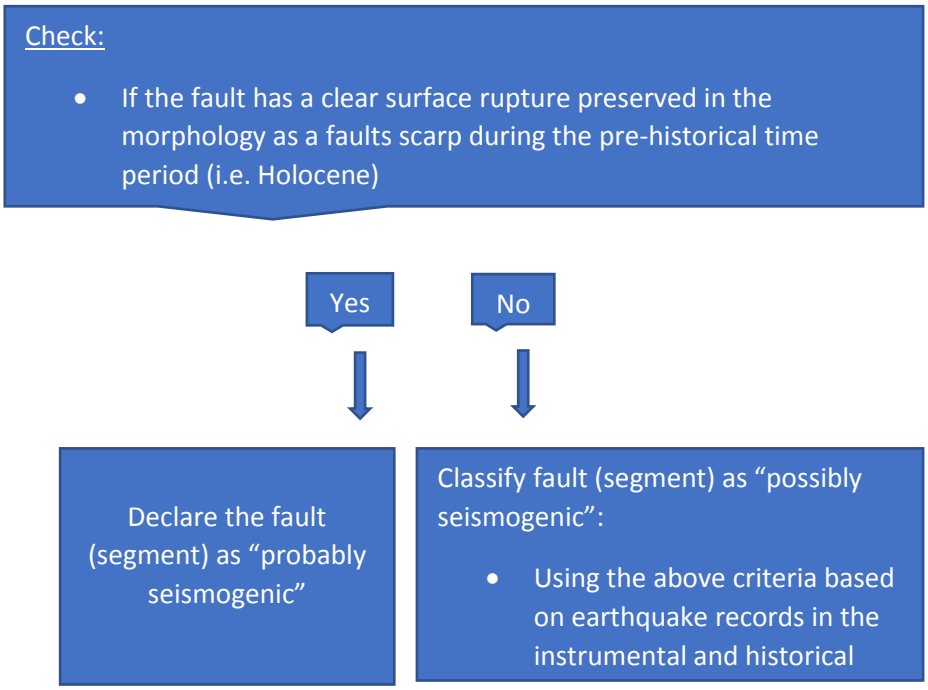

Following general analysis and knowledge are needed for adopting the above criteria:

- Identification of significant faults and their accuracy
- Earthquake location accuracy
- Focal mechanism determinations based on
    - first motion polarities;
    - moment tensor solutions.
- Statistical analyses of seismicity
    - temporal;
    - spatial.
- Active fault definitions
    - from literature;
    - European Database on Seismogenic Fault (EDSF).

4 Geological and geophysical data

4.1 Geological data

Geological data was primarily used to gather all necessary information regarding geological structures, major faults, fault zones, fault complexes and lineament trends. Geological data was gathered using several sources.

- Firstly, it is Norwegian Geological Survey (Norwegian Geological Survey, 2019), in particularly open-file maps "Berggrunn raster" at a scale 1:250,000 and "Lineamenter satellittolket" at a scale 1:750,000. This enabled to gather all necessary information about major onshore faults, fault zones, lineament trends and bedrock geology.
- Secondly, it is Norwegian Petroleum Directorate (Norwegian Petroleum Directorate, 2019), in particularly open-file maps "Faults and Boundaries" and "Structural elements" at a regional scale. This enabled to collect all necessary information about major offshore faults, fault complexes, zones and geological structures.
- Thirdly, it is scientific literature that discusses significance of certain onshore and offshore faults and fault zone/complexes that drew attention of many scientists and are important geological structures requiring further studies.

4.1.1 Onshore faults, fault zones and fault complexes

NGU bedrock geology map enables to reveal major geological units and structures formed during different tectonostratigraphic deformational episodes. This includes Caledonian episodes that led to the formation of extensive Caledonian mountain range stretching from the southern part of mainland Norway to Finnmark. Also, several large-scale faults, fault complexes and zones have been formed. Large-scale low-angle shear zones that formed during Mode II extension along west mainland Norway are:

- Hardangerfjord shear zone;
- Bergen Arc shear zone;
- Lærdal-Gjende fault complex;
- Røldal Shear Zone;
- Stord-Bømlo-Karmøy fault zone;
- Solund detachment fault;
- Kvamshesten detachment fault;
- Håsteinen detachment fault;
- Hornelen detachment fault.

Large-scale low-angle zones that formed along central and northern Norway are:

- Møre-Trøndelag fault zone;
- Nesna shear zone;
- Sagfjord shear zone.

Another important event that entailed development of the bedrock geology and geological structures along eastern mainland Norway is Permian rifting. This event led to the formation of Permian Oslo Igneous province and Oslo rift zone. Development of Oslo rift zone during Permian was driven by

stretching of the crust and formation of large-scale faults bounding Oslo graben and its offshore continuation, Skagerrak graben. Although Skagerrak graben is considered to be an offshore structure, in this thesis it is studied together with Oslo graben since they are both part of one large-scale Oslo rift structure. Faults bounding structures were named based on whether eastern or western side of the graben is bounded. In total four major faults were identified:

- Oslo Graben Eastern boundary fault;
- Oslo Graben Western boundary fault;
- Skagerrak Graben Eastern boundary fault;
- Skagerrak Graben Western boundary fault.

Other large-scale onshore structures that lie in the southern Norway are:

- Fedafjord fault that formed as a result of multiple faulting events (Gabrielsen et al., 2002);
- Porsgrunn-Kristiansand fault that is formed as a result of multiple faulting during Late Proterozoic to post-Permian times (Starmer, 1993);
- Mandal-Ustaoset newly discovered fault zone that separates Telemarkia into the Telemark sector to the east and the Hardangervidda sector to the west (Sigmond, 1985). The origin of the fault zone is uncertain. There are two theories one of which proposes that Mandal-Ustaoset fault zone is a suture developed as a result of a continent-continent collision, whereas another states it is a mega-fault zone (Sigmond, 1985).

Several faults stretching along northern Norway and Finnmark area as was revealed by Dehls et al. (2000) are prominent NE-SW lineaments. These are:

- Vestfjorden-Vanna fault of Upper Jurassic-Lower Cretaceous origin separating Precambrian terrain to the west and Caledonian nappe sequence to the east (Olesen et al., 1997);
- Kvaløysletta-Straumhella fault that is most probably of Permian age that has evidence of Tertiary recent reactivation (Olesen et al., 1997);
- Vargsund fault of uncertain origin that is related to reactivation of a major fault caused by either Devono-Carboniferous or Permo-Carboniferous rifting (Roberts and Lippard, 2005);
- Mierujavri-Sværholt shear zone of Palaeoproterozoic age with indications of post-glacial activity (Olesen et al., 1992a; Olesen et al., 1992b);
- Stuoragurra fault is a postglacial fault with a clear fault scarp preserved in the morphology and showing evidence of seismic activity (Olesen, 1988; Olesen at al., 1992a; Dehls et al., 2002).

A distinct fault zone lying at the northernmost mainland Norway is Trollfjorden-Komagelva fault zone. This is a complex fault zone of Neoproterozoic origin that experienced four deformational episodes. The first one is contractional deformation related to Timanian orogeny (~570 – 560 Ma) (Herrevold et al., 2009). The second one is contractional deformation associated with Caledonian orogeny (~470 – 460 Ma). The third one is extensional deformation related to regional extension (~ 375-370 Ma). The last one is extensional deformation associated with extensional faulting in either Mesozoic or late Paleozoic.

Northern Norway experiences high seismic activity mostly due to seismic swarms. The two well-known occurred in Meløy in 1978-1979 and in Steigen in 1992 (Bungum and Husebye, 1979; Atakan et al., 1994). However, there were not many faults in the area that have been reported in the literature. Therefore, four supplementary faults for the northern mainland Norway have been extracted from NGU open-file maps “Berggrunn raster” at a scale 1:250,000 (Norwegian Geological Survey, 2019). These faults are Værangfjord-Nordfjord, Meløyfjord, Meløy-Glomtfjorden and Skjærstadfjord faults. The faults are named based on the structures they cut, fjords.

4.1.2 Offshore faults, fault zones and fault complexes

Selection of offshore faults is made on the basis of prominent extensive structures depicted on offshore "Faults and Boundaries" NPD map (Norwegian Petroleum Directorate, 2019). In addition, "Structural elements" NPD map was used for identification of major structural units and important boundary zones and faults enclosing or separating them. Also, several significant offshore faults that were a subject of scientific discussions have been taken from the literature.

Norwegian continental shelf can be subdivided into three distinct provinces bearing various tectonic characteristics evolved during different rifting episodes. These are North Sea – intracratonic basin, Norwegian sea – deep Cretaceous basin and Barents shelf – sediment-covered intracratonic basin (Bungum et al., 1991). North and Western Barents Seas evolved as a result of post-Caledonian rifting episodes that lasted until early Cenozoic era (Bungum et al., 2005). Norwegian sea developed as a result of several extensional episodes during Late Devonian – Paleocene time (Norwegian Petroleum Directorate, 2019). Offshore faults are closely related to large-scale structures characteristic for each sea. Therefore, significant major faults, fault complexes and zones reflecting distinct features of each province have been identified and selected for further analysis.

Major faults and fault zones that belongs to the North Sea are:

- Sorgenfrei-Tornquist fault – large-scale structure that was reactivated several times during Triassic, Jurassic and early Cretaceous (Mogensen and Korstgård, 2003);
- Fjerritslev fault zone that was reactivated during Mesozoic time (Surlyk, 1980; Michelsen and Nielsen, 1993);
- Øygarden fault zone that marks the boundary between Horda Platform and western Norway crystalline massif and shows evidence of recent seismic activity (Bungum et al., 1991; Gabrielsen, 1989);
- Faults bounding Central Graben. These are Central Graben eastern boundary fault and Central Graben western boundary fault;
- Faults bounding Viking Graben. These are Viking Graben eastern boundary fault and Viking Graben western boundary fault;
- Faults bounding Horn Graben. These are Horn Graben eastern boundary fault and Horn Graben western boundary fault.

Major faults, fault zones and complexes that belongs to the Norwegian Sea are:

- Fles fault complex – extensive structure bounding Vøring Basin from the eastern side;
- Vesterdjupet fault zone – western boundary of the Ribban basin;
- Helland-Hansen Arch eastern boundary fault;
- Klakk fault complex separating Halten terrace and Rås basin;
- Ytreholmen fault zone – extensive structure bounding Dønna terrace from the western side;
- Revfallet fault complex – extensive structure bounding Dønna terrace from the eastern side;
- Faeroe-Shetland escarpment separating Møre marginal high from Møre basin;
- East Jan Mayen fracture zone separating ocean and continental crust of the Vøring basin (Bungum et al., 1991);
- Vøring plateau escarpment separating Vøring basin and the Vøring plateauø
- Lofoten-Vesterålen margin showing high seismic activity (Byrkjeland et al., 2000);
- Utrøst Ridge NW boundary fault;
- Bremstein-Vingleia fault complex bounding Halten terrace form the eastern side.

Major faults, fault zones and complexes that belongs to Barents Continental Shelf are:

- Senja fracture zone delineating southwestern boundary of Barents continental shelf;
- Troms-Finnmark fault complex delineating southeastern boundary of Barents continental shelf;
- Ringvassøy-Loppa fault complex separating Troms and Hammerfest basins;
- Bjørnøyrenna fault complex separating Bjørnøya basin at the west and Loppa high at the east;
- Leirdjupet fault separating Bjørnøya basin at the west and Fingerdjupet sub-basin at the east;
- Hornsund fault zone delineating northeastern boundary of Barents continental shelf.

Summarizing onshore and offshore faults, fault zones and complexes selected for the studies in the following thesis one ends up with compilation of 56 faults (29 – onshore; 27 – offshore) as listed in Table 2.

Table 2: Compilation of onshore and offshore significant fault systems.

Onshore Faults/Fault Zones/Fault Complexes	Offshore Faults/Fault Zones/Fault Complexes
	Sorgenfrei-Tornquist Fault
	Fjerritslev Fault Zone
	Central Graben Eastern Boundary Fault
	Central Graben Western Boundary Fault
	Øygarden Fault Zone
	Viking Graben Eastern Boundary Fault
	Viking Graben Western Boundary Fault
	Horn Graben Eastern Boundary Fault
	Horn Graben Western Boundary Fault
Oslo Graben Eastern boundary Fault	
Oslo Graben Western boundary Fault	
Skagerrak Graben Eastern boundary Fault	
Skagerrak Graben Western boundary Fault	
Fedafjord Fault	
Porsgrunn-Kristiansand Fault	
Mandal-Ustaoset Fault Zone	
Stord-Bømlo-Karmøy Fault Zone	
Røldal Shear Zone	
Hardangerfjord Shear Zone	
Lærdal-Gjende Fault Complex	
Bergen Arc Shear Zone	
Solund Detachment Fault	
Kvamshesten Detachment Fault	
Håsteinen Detachment Fault	
Hornelen Detachment Fault	
	Fles Fault Complex
	Vesterdjupet Fault Zone
	Helland-Hansen Arch Eastern Boundary Fault
	Klakk Fault Complex
	Ytreholmen Fault Zone
	Revfallet Fault Complex
	Faeroe-Shetland Escarpment
	East Jan Mayen Fracture Zone
	Vøring Plateau Escarpment
	Lofoten-Vesterålen Margin
	Utrøst Ridge NW Boundary Fault
	Bremstein – Vingleia Fault Complex
Møre-Trøndelag Fault Zone	
Nesna Shear Zone	
Værangfjord-Nordfjord Fault	
Meløyfjord Fault	
Meløy-Glomtfjorden Fault	
Skjærstadfjord Fault	
Sagfjord Shear Zone	
	Senja Fracture Zone
	Troms-Finnmark Fault Complex
	Ringvassøy-Loppa Fault Complex
	Bjørnøyrenna Fault Complex
	Leirdjupet fault
	Hornsund Fault Zone
Vestfjorden-Vanna Fault	
Kvaløysletta-Straumhella Fault	
Vargsund Fault	
Mierujavri-Sværholt Shear Zone	
Stuoragurra Fault	
Trollfjorden-Komagelva Fault Zone	

4.2 Geophysical data

Geophysical data compiled for the following study includes gravity data, magnetic data, Moho map and stress models generated based on stress inversion of earthquake focal mechanism solutions from onshore and offshore Norway.

4.2.1 Gravity data

Gravity data used for this study is a map depicting residual gravity after isostatic corrections were applied to Bouguer gravity data (Figure 8). Gravity map has been extracted from the recent work done by Olesen et al. (2010) “New aeromagnetic and gravity compilations from Norway and adjacent areas: methods and applications”.

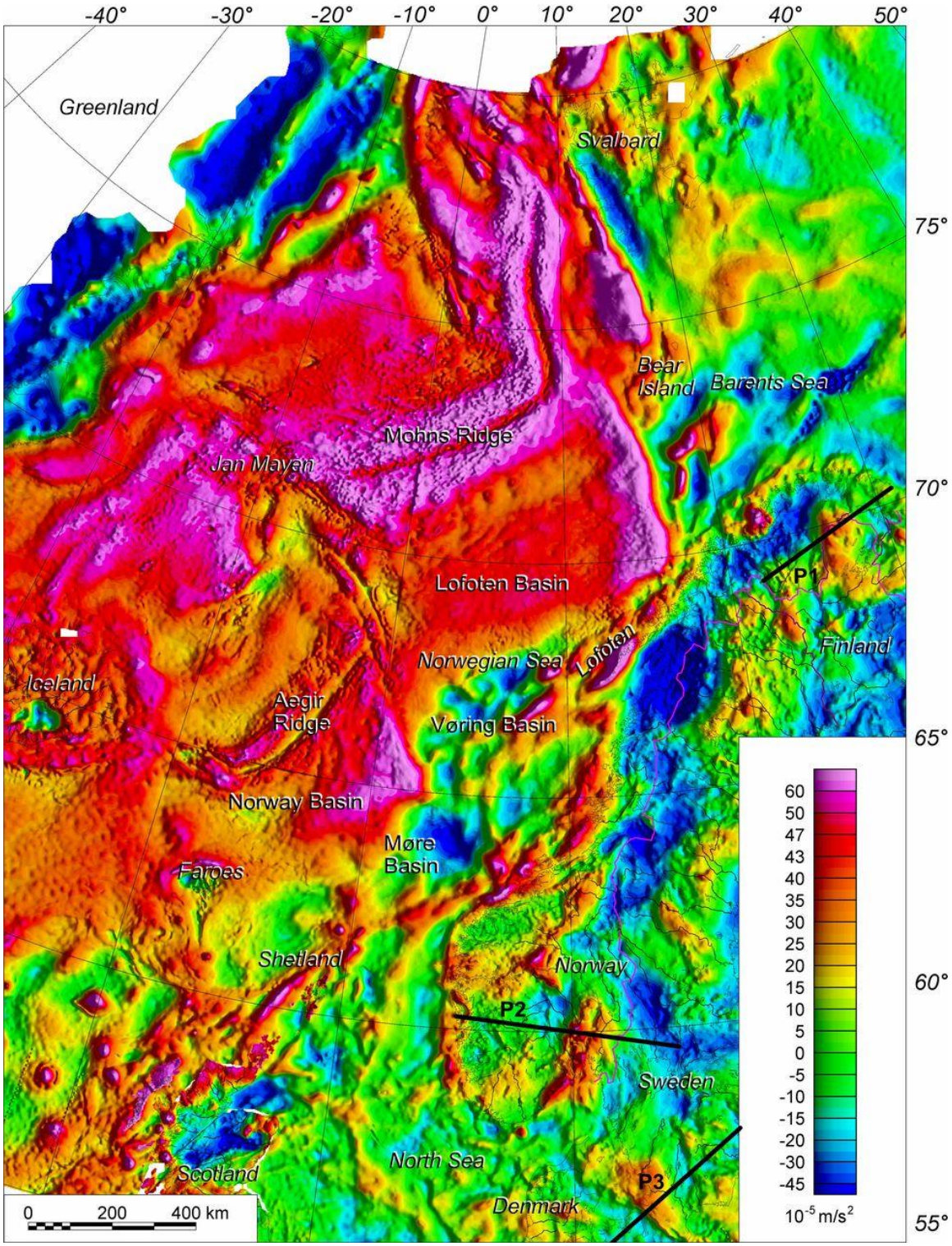

Figure 8: Residual gravity after isostatic corrections were applied to Bouguer gravity data. (Olesen et al., 2010). Black solid lines named P1, P2 and P3 should be disregarded in this study.

Gravity map gives insight into density contrasts and depicts geological units formed both at the surface and at the basement. Gravity anomalies enable to distinguish between oceanic and continental lithosphere, various geological structures (basins, platforms, highs, mountain ridges) and also trace

significant faults (faults, fault zones, fault complexes) that either merge, split or cut through various geological units.

Gravity map for Norway and adjacent area shows low gravity anomalies (blue color) that dominate onshore. This is explained by low-density Precambrian granites (Ramberg et al., 2007). Positive gravity anomaly is observed at the southern and western mainland Norway, Finnmark and along Norwegian continental shelf. Onshore positive gravity anomaly is explained by heavy Caledonian nappes (red, yellow colors) whereas offshore – mainly by topography. Offshore basement heights show positive anomalies and hence depicted with the red and yellow colors. These for example are offshore grabens, Central, Viking, Horn and Permian Oslo grabens. Platforms areas also show positive anomaly that is mostly represented by green color. Basins are usually low-topography structures and hence show low positive or negative anomalies represented with the green or blue colors. Other large-scale geological structures such as Barents continental shelf, Lofoten-Vesterålen margin, Jan Mayen fracture zone, Sorgenfrei-Tornquist fault, Øygarden and extensive Møre-Trøndelag fault zones are clearly depicted on the map showing positive anomaly.

4.2.2 Magnetic data

Magnetic data used for this study is a magnetic anomaly map of Norway and adjacent areas (Figure 9). Magnetic anomaly map has been extracted from the recent work done by Olesen et al. (2010) “New aeromagnetic and gravity compilations from Norway and adjacent areas: methods and applications”.

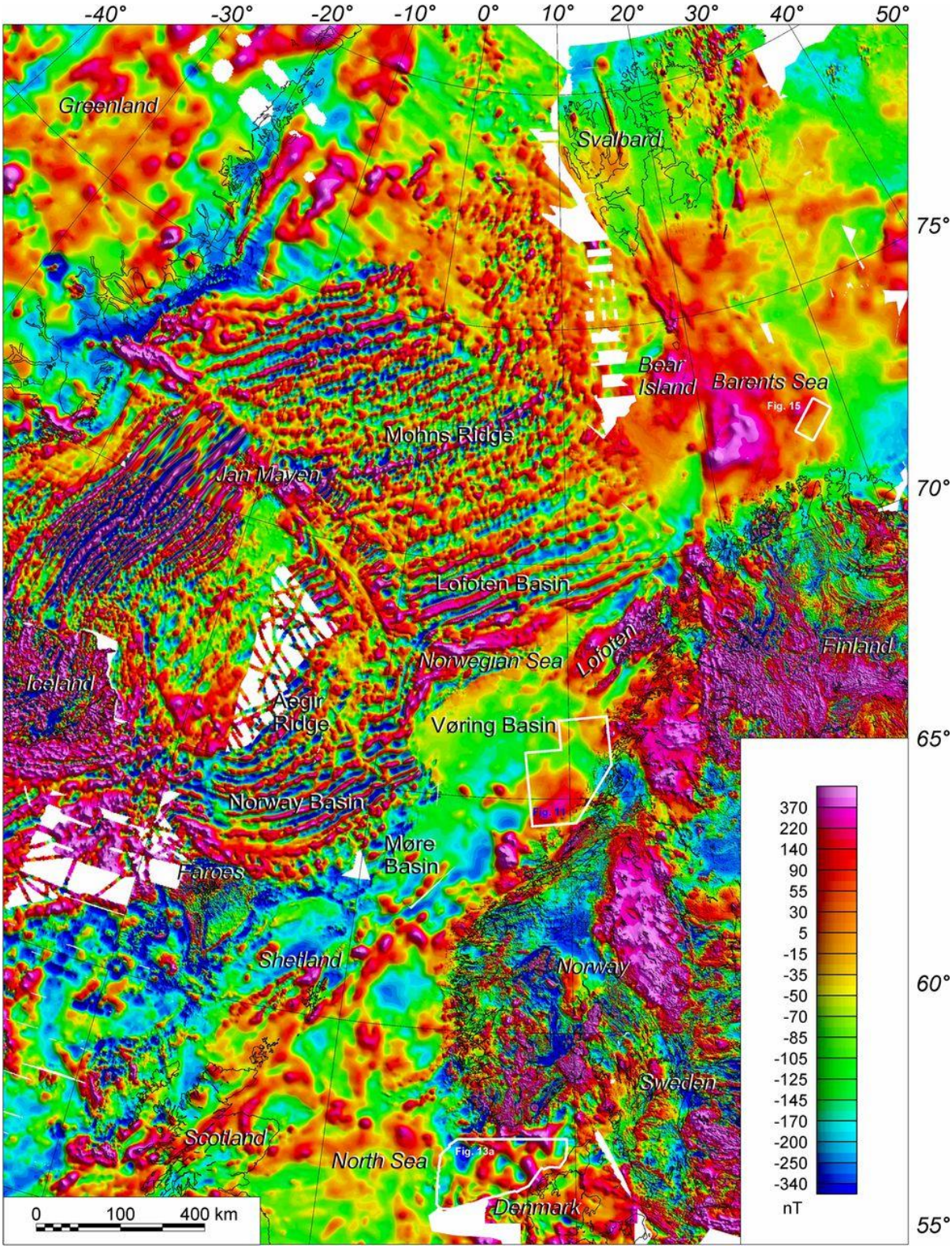

Figure 9: Magnetic anomaly map of Norway and adjacent areas (Olesen et al., 2010). White frames shown at the map should be disregarded in this study.

Magnetic anomaly map gives insight into rocks remnant magnetization and magnetic susceptibility of subsurface structures and basement units. Warm colors indicate rocks, structures, geological units that demonstrate high magnetic susceptibility. Cold colors, on the contrary, indicate structures with least

magnetic susceptibility. Magnetic anomaly map enables to trace significant magnetic geological structures and major faults and fracture zones. These are depicted with warm colors.

Major onshore magnetic structures traced using magnetic anomaly map are:

- Permian Oslo rift zone;
- Sorgenfrei-Tornquist fault;
- Newly discovered Mandal-Ustaoset fault zone;
- Shear structures formed during various Caledonian episodes;
- Devonian detachment structures at the western mainland Norway;
- Møre-Trøndelag fault zone;
- Northern mainland Norway;
- Finnmark.

Major offshore magnetic structures traced using magnetic anomaly map are:

- Barents continental shelf;
- Lofoten-Vesterålem margin;
- Vøring basin;
- Graben structures;
- Offshore part of Møre-Trøndelag fault zone;
- Trøndelag platfrom;
- Jan Mayen fracture zone;
- Offshore spreading ridges.

4.2.3 Moho maps

Moho map is used to read and collect depth to Moho data that is necessary for computations of two fault parameters, width of the fault and its surface projection. Moho map has been extracted from Ebbing and Olesen (2010) work “New compilation of top basement and basement thickness for the Norwegian continental shelf reveals the segmentation of the passive margin system” (Figure 10). In addition, supplementary Moho map extracted from the work “Moho and basement depth in the NE Atlantic Ocean based on seismic refraction data and receiver functions” done by Funck et al. (2017) is used for areas extending further Norwegian continental margin, in that particular case for the Jan Mayen region (Figure 11).

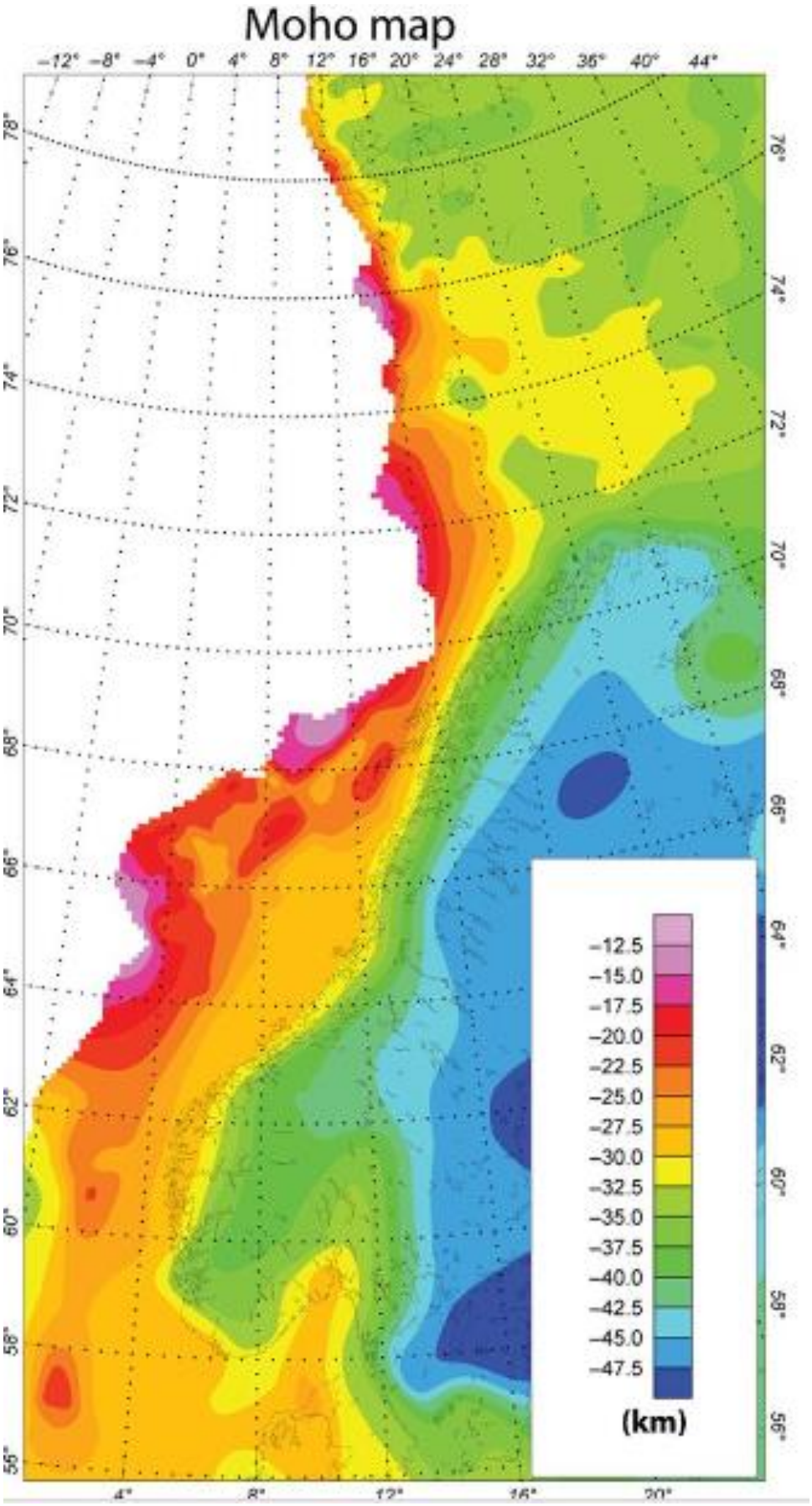

Figure 10: Modified Moho map (Ebbing and Olesen, 2010).

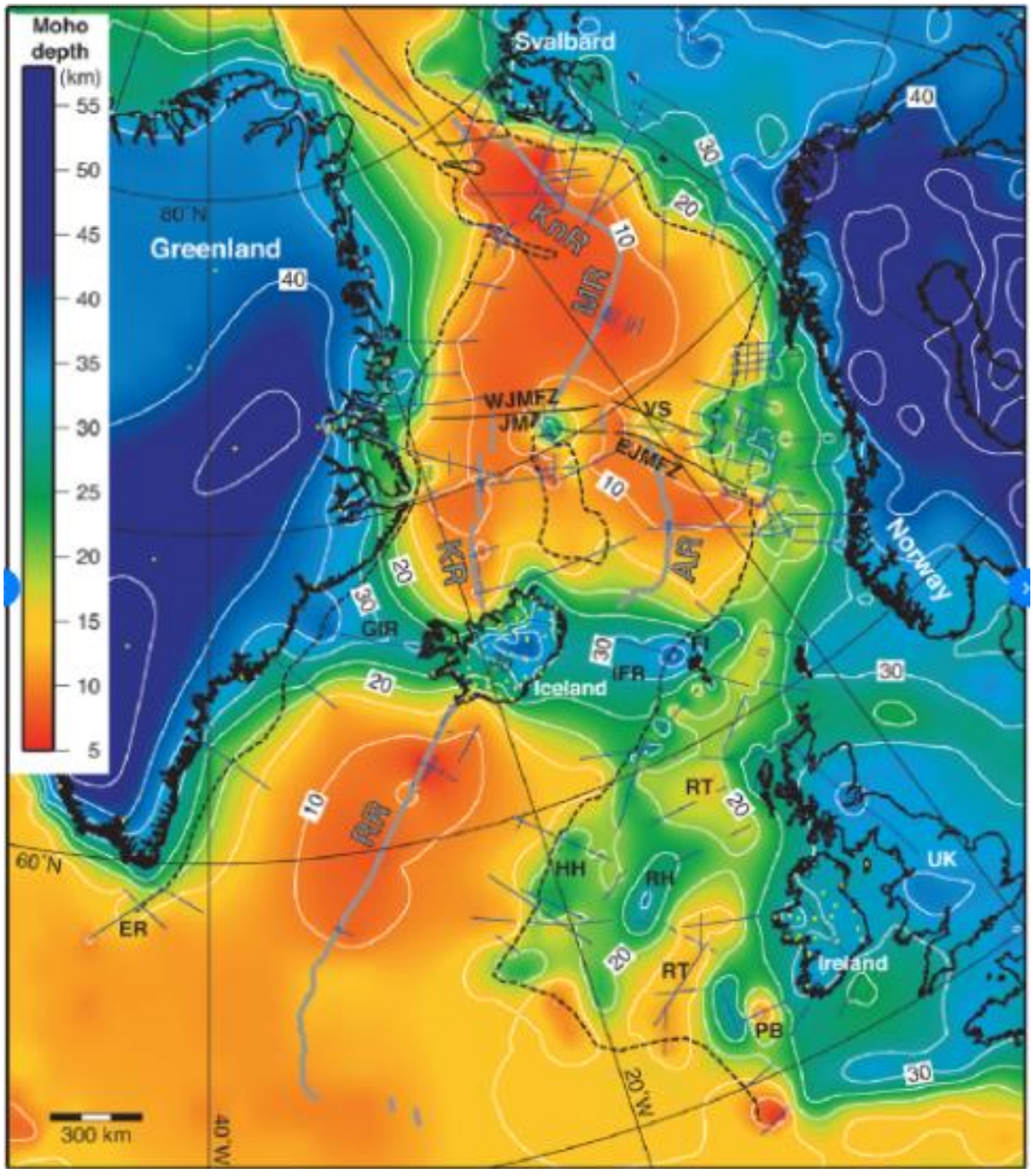

Figure 11: Supplementary Moho map used for areas extending further Norwegian Continental Margin (Funck et al., 2017).

4.2.4 Stress models

Stress models generated based on stress inversion of earthquake focal mechanism solutions from onshore and offshore Norway (Figure 13). These are used to compile information about regional stress tensor (Sigma 1, Sigma 2 and Sigma 3) for different onshore and offshore regions (Table 3). This information is critical since it enables to check on whether the orientation of a fault is favorable with respect to the orientation of the stress tensor or not. Stress models are extracted from the work "Stress inversion of earthquake focal mechanism solutions from onshore and offshore Norway" done by Hicks et al. (2000).

In total eight stress models were prepared for different regions. These are

- Oslo Rift area;
- Northern North Sea;

Northern North Sea is a complex area which experiences an influence of anomalous elevation differences in the southern Norway. This is explained by Scandinavian mountains that generate gravitational stresses in the adjacent offshore basins that may be the reason of 90˚ stress rotation detected from the Norwegian margin to the northern North Sea (Fejerskov and Lindholm, 2000). Therefore, three stress models were prepared based on 34 earthquake focal mechanism solutions for the Northern North Sea. First model reflects stress inversion of 26 nonrotated earthquake focal mechanisms. The second model reflect stress inversion of eight rotated earthquake focal mechanisms whereas the third one reflects composite stress inversion of 34 earthquake focal mechanisms.

- Southern North and Western Barents Seas;

For the Southern North and Western Barents seas there is not enough data available to get a stress model. However, there is borehole breakouts data that gives orientation of the maximum horizontal stress, that is ESE-WNW for the Southern North Sea and N-S for the Western Barents Sea as shown in Figure 12 (Hicks et al., 2000).

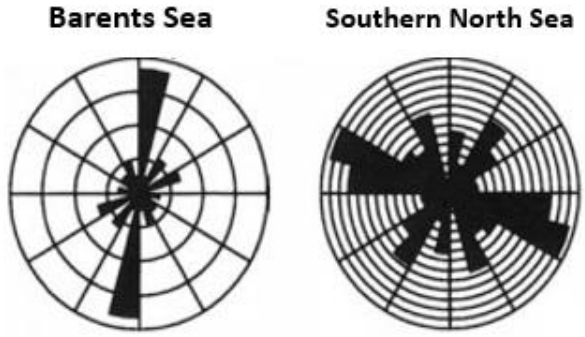

Figure 12: Orientations of the maximum horizontal compressive stress from in situ measurements (Hicks et al., 2000).

- Onshore West Norway;
- Offshore Mid Norway;
- Onshore Mid Norway;
- Finnmark.

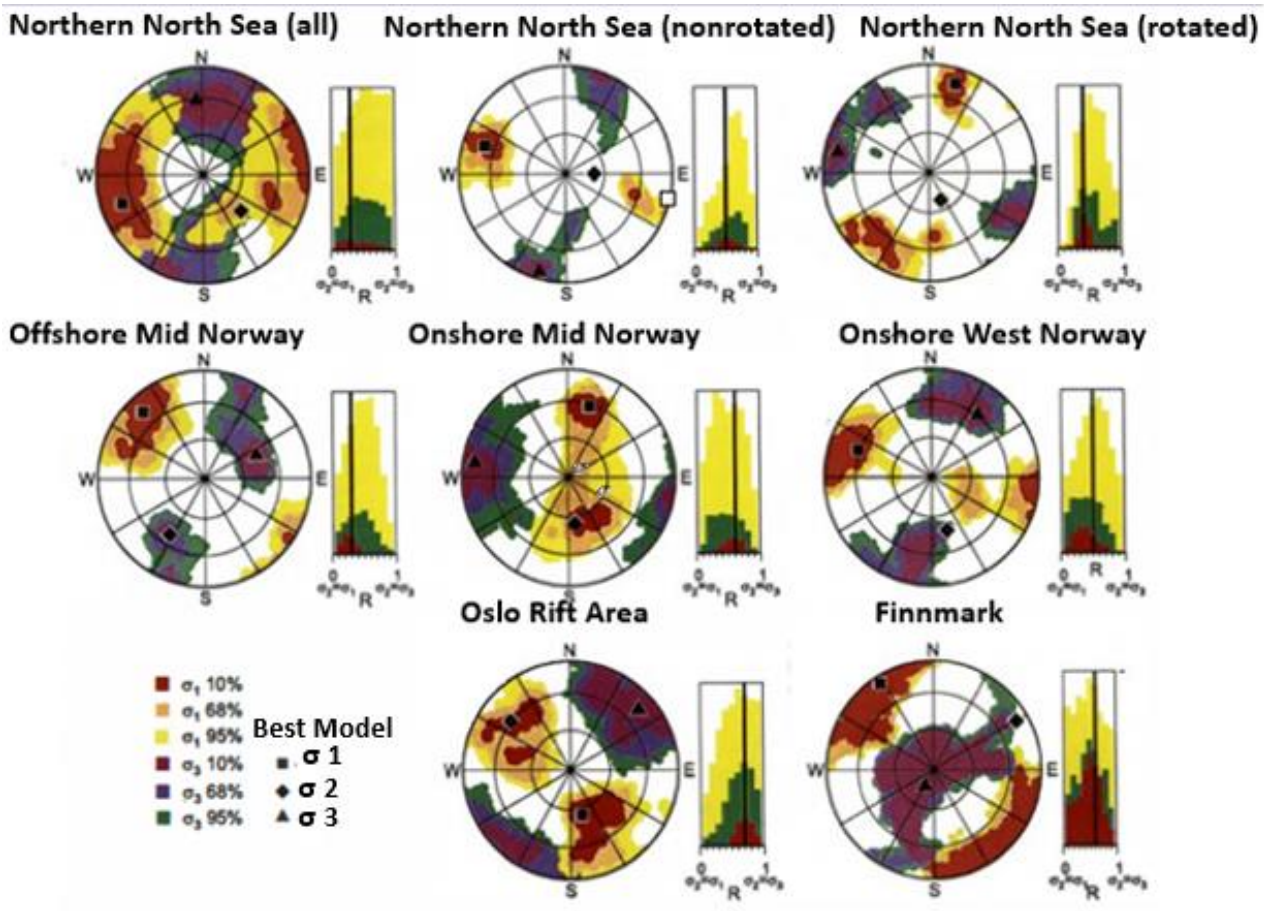

Figure 13: Hicks et al. (2000) results from the inversion of the earthquake focal mechanism solution. Red, green and yellow colors in the R-vale histogram represents 10%, 68% and 95% confidence limits, respectively. R-value is a relative magnitude of intermediate principal stress (sigma 2) with respect to maximum differential stress, R-value is defined as (sigma 1 – sigma 2)/ (sigma 1 – sigma 3) (Soh et al., 2018).

Table 3: Earthquake focal mechanism stress inversion results obtained for the six areas by Hicks et al. (2000).

	σ 1		σ 2		σ 3	
Area	**Trend**	**Plunge**	**Trend**	**Plunge**	**Trend**	**Plunge**
Northern North Sea (all)	251	21	133	50	355	31
Northern North Sea (nonrotated)	289	21	90	68	196	7
Northern North Sea (rotated)	17	17	157	68	283	13
Offshore Mid Norway	317	17	213	39	66	46
Onshore Mid Norway	17	32	172	55	279	12
Onshore West Norway	290	28	164	48	37	29
Oslo Rift Area	166	55	309	29	49	17
Finnmark	328	7	60	12	210	76

5 Seismological data

5.1 Background – development from macroseismic to instrumental data

Macroseismic data

First attempts to summarize seismicity in Norway was done by professor B. M. Keilhau and published in the journal of natural science "Efterretninger om Jordskjælv i Norge" in 1934. The first part of the study contains list of all earthquakes in Norway up to and including year of 1934. Lack of reliable and sufficient data at that time led to modest seismicity records for 1700's – seven earthquakes and 1800's 41 earthquakes. Another study summarizing seismic records for the time span of 1834 – 1887 "Berichte über die wesentlich seit 1834 in Norwegen eingtroffenen Erdbeben" was done by T. Ch. Thomassen. From the beginning of 1887 earthquake data has been collected systematically by Norwegian geological survey (NGU) (Norwegian geological survey, 2019) in Kristiania led by Dr. Hans Reusch. Since 1899 this task was taken over by Carl Fredrik Kolderup and redirected from Kristiania to Bergen Museum (Sellevoll and Sundvor, 2001). Systematic compilation of seismic records gathered on the basis of earthquake felt reports for the period 1887 – 1911 has been summarized in the Bergen Museum Yearbook (Figure 14).

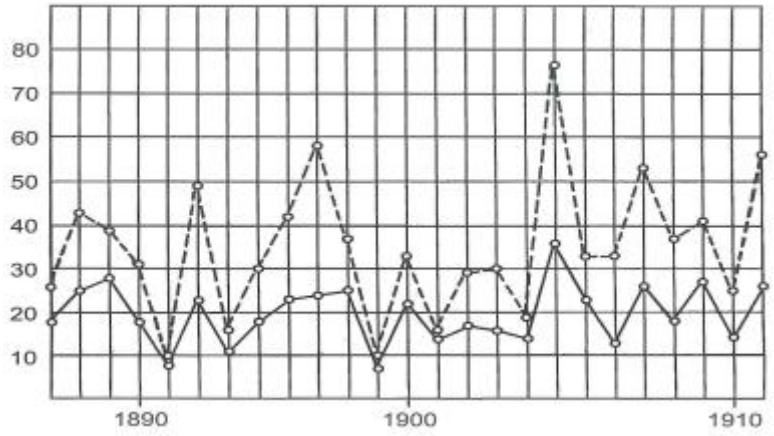

Figure 14: Number of seismic records for the period of 1887 – 1911. Dashed line shows number of earthquakes reported whereas solid line gives number of seismic events that was thought to happen. Later studies have shown that only 4 – 5 events were felt per year (Sellevoll and Sundvor, 2001).

From Figure 14, one can notice there was a huge difference between number of earthquakes reported and number of seismic events that was thought to happen. However, even at that time areas characterized by most seismicity in Norway and Sweden was identified (Figure 15).

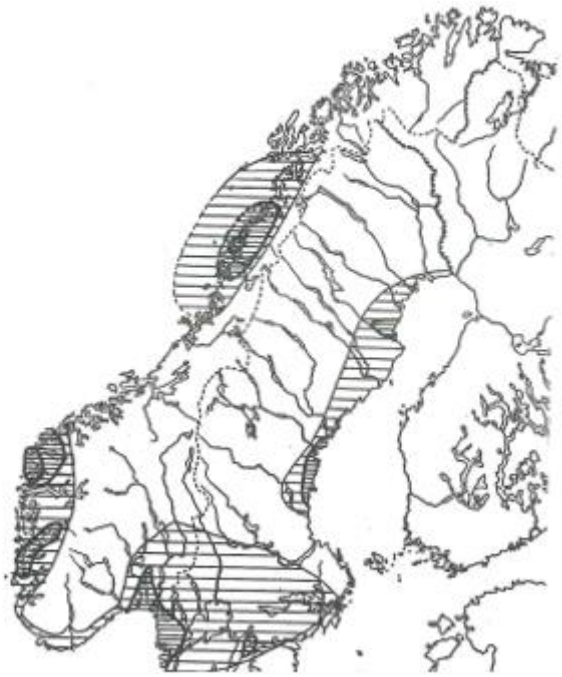

Figure 15: Seismicity in Norway and Sweden in the time period from 1887 – 1911. Hatched areas indicate zones of most seismic activity (Sellevoll and Sundvor, 2001).

From macroseismic to instrumental data

First seismograph – Bosch-Omori was installed in Bergen in 1905 and stayed operational until 1959 (Sellevoll and Sundvor, 2001). Another seismograph that was installed in Bergen is known as the Wiechert seismograph. Next modern seismograph – Willmore began to operate on Svalbard (Isfjord Radio) in 1958. In comparison to its precursor it registered as many as 70 earthquakes just in one month. With growing interest and aspiration to develop and establish seismological network in Norway in 1950's, the installation of seismographs in Norway and its adjacent areas became widespread. A seismograph was established on Jan Mayen in 1961 and was used to monitor volcanic activity. Later on, volcanic eruption at Beerenberg led to the establishment of a modern 3-station seismic network (Sellevoll and Sundvor, 2001). Subsequent seismographs/seismic stations became more modernized and were spread over extensive areas across Norway and its adjacent areas creating various seismic networks. Then, with time passed, number of seismic stations and seismic networks grew providing better seismicity estimates and quality of the data recorded due to gradual decrease of location uncertainties.

In that sense, one can distinguish three distinct periods in the development from macroseismic to instrumental data in Norway based on type of the data and location accuracy.

- First period lasted until 1960 and included macroseismic records. Macroseismic records were based on questionnaires and has been gathered systematically starting from 1887. Location of earthquake hypocenters could be hardly determined and gave huge location errors within 20 to 60 km interval. In special cases, one could end up with location error of 100 km (Sellevoll and Sundvor, 2001).
- Second period covered time span from 1960 to 1980 and included both macroseismic and instrumental data. Development of instrumental in addition to macroseismic data contributed

to the reduction of location errors to 15 – 20 km (Sellevoll and Sundvor, 2001). However, the majority of local events were not recorded instrumentally.

- Third period began starting from 1980 and lasts until today. Development of a network of stations and their extensive distribution along with modernized instruments allowed to register both local and regional seismicity. That significantly improved location accuracy. In special cases abundant number of seismic records gathered in areas of good station coverage allows to study seismicity applying even smaller location error threshold. Instrumental data in Norway and adjacent areas starting from 1970's is mostly collected by University of Bergen (UiB) and Norwegian Seismic Array Network (NORSAR). Although instrumental data became widely used, macroseismic records are still carried out showing average number of onshore felt earthquakes per year to be 4-5 (Sellevoll and Sundvor, 2001).

5.2 Instrumental seismological databases NNSN and ISC comparison

Norwegian National Seismic Network

First instrumental records in Norway appeared with installation of the first seismograph in 1905 in Bergen. Instrumental records for Norway and adjacent areas are stored in Norwegian local seismic database known as Norwegian National Seismic Network (NNSN) (Norwegian National Seismic Network, 2019). NNSN is mostly operated by UiB which has 35 seismic stations. Other agencies also contribute to the data collection (Figure 16, 17). Among them are:

- Norwegian Seismic Array (NORSAR) – 12 broadband stations;
- neighboring countries – Finland, Denmark, Sweden, Island and Great Britain;
- neighboring countries – Russia, Finland, Sweden;
- offshore seismic data provided by oil companies (Ekofisk field – Conoco Phillips, Grane – Equinor) (Annual report for the Norwegian National Seismic Network, 2018).

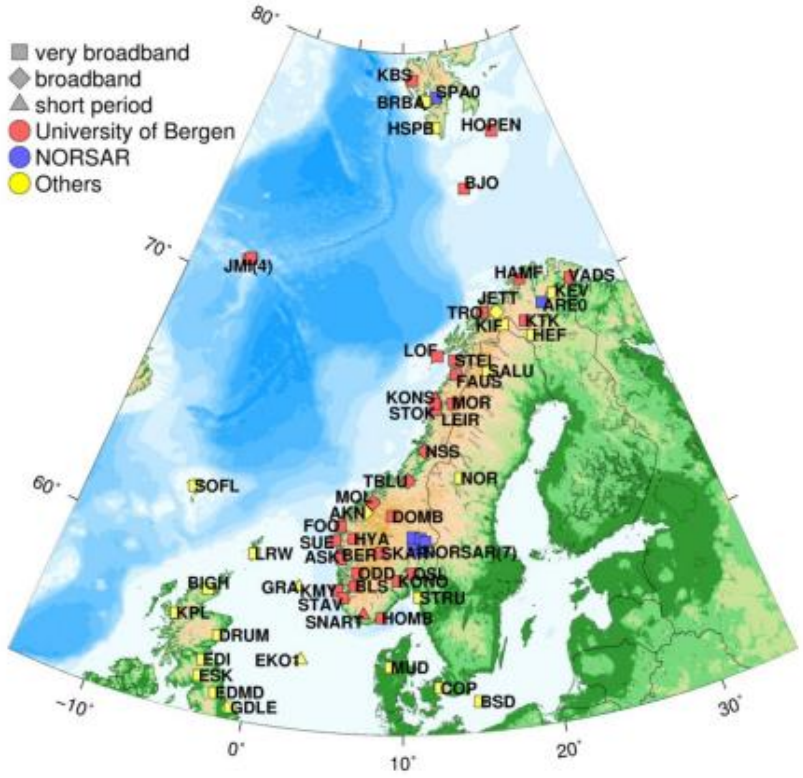

Figure 16: Stations running NNSN (Annual report for the Norwegian National Seismic Network, 2018).

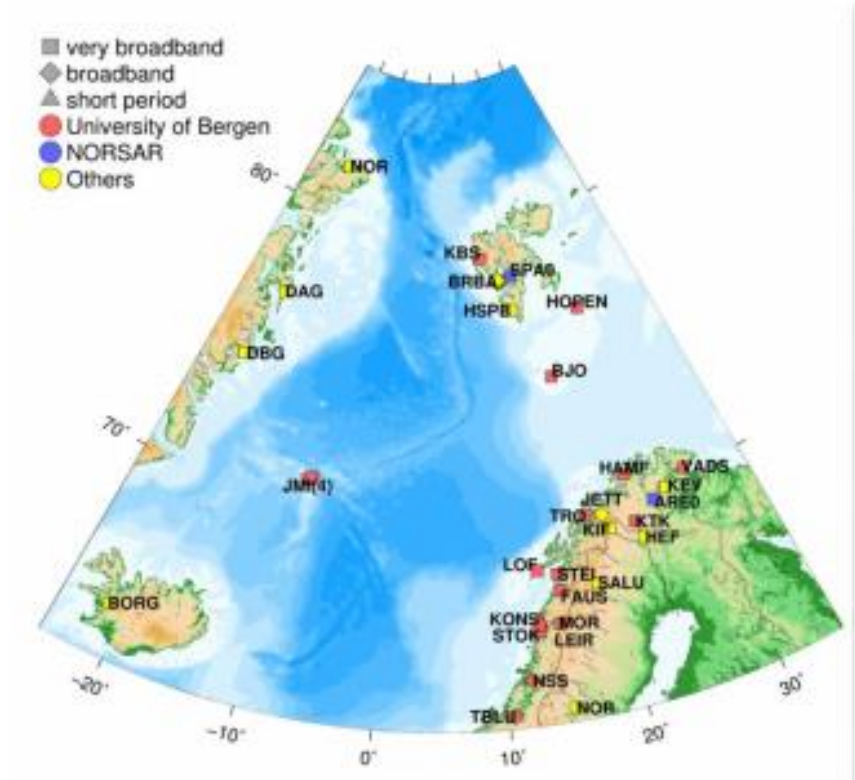

Figure 17: Stations operating in the Arctic contributing to NNSN (Annual report for the Norwegian National Seismic Network, 2018).

The amount of data stored in the NNSN database increased with increasing number of seismic stations installed across Norway and its adjacent areas. Establishment of Western Norway Network in 1984 and Northern Norway Network in 1988 contributed to data increase in the southern and northern Norway respectively. Seismicity in the Norwegian Sea was monitored by increased number of modernized seismic stations installed on Jan Mayen and Svalbard. Increased quantity of seismic data in the eastern Norway was provided by NORSAR arrays (Seismo Group, 2011). Increased number of seismic data gathered from unevenly distributed Norwegian seismic networks and other agencies covering different time periods led to heterogeneous database. This resulted in need to introduce new definition – prime area. Prime area for Norway and its adjacent areas is defined as an area enclosed by 54.0 – 82.0 ˚N in latitude and -15 – 36 ˚E in longitude and characterized by most complete seismic records (Seismo Group, 2011). From now and onwards only events within the prime area defined for Norway and its adjacent areas will be taken for further consideration in the following thesis.

Organization of the NNSN database

The aim was to make the NNSN database as complete as possible and data was collected from all available sources, for details see Seismo Group (2011). Majority of the data in the period before 1980's was provided by NORSAR and International Seismological Center (ISC) (International Seismological Centre, 2019a) that was established in 1964. Of particular importance is that ISC data with magnitude larger than or equal to 3.0 from 1964 until and including June 1982 was included in NNSN. From about 1982 and onwards it is considered that NNSN detects as many events as ISC and since then ISC was not included systematically. It is therefore considered that the NNSN database is the most complete available for our base area and particularly for Norway mainland.

Comparing NNSN and ISC databases

Although the NNSN database is considered the most complete, it can be useful to compare the ISC database with NNSN in order to spot irregularities and possible missing data. Before 1900, ISC has no data, so no comparison is possible. From 1900 until 1964, ISC data has not been systematically included in NNSN, so this is the first period to compare. For this purpose, one will generate plot for the 1900 – 1964 time interval where both NNSN and ISC seismicity records are shown (Figure 18). The only criteria that will be applied to both datasets are magnitude limits (aiming to get reliable results minimum magnitude threshold is set to 3.0) and latitude, longitude limits enclosing the prime area. Of particular importance is a magnitude type. When setting magnitude limits and not specifying the desired type of the magnitude, the programme always selects the largest magnitude that can be of any type.

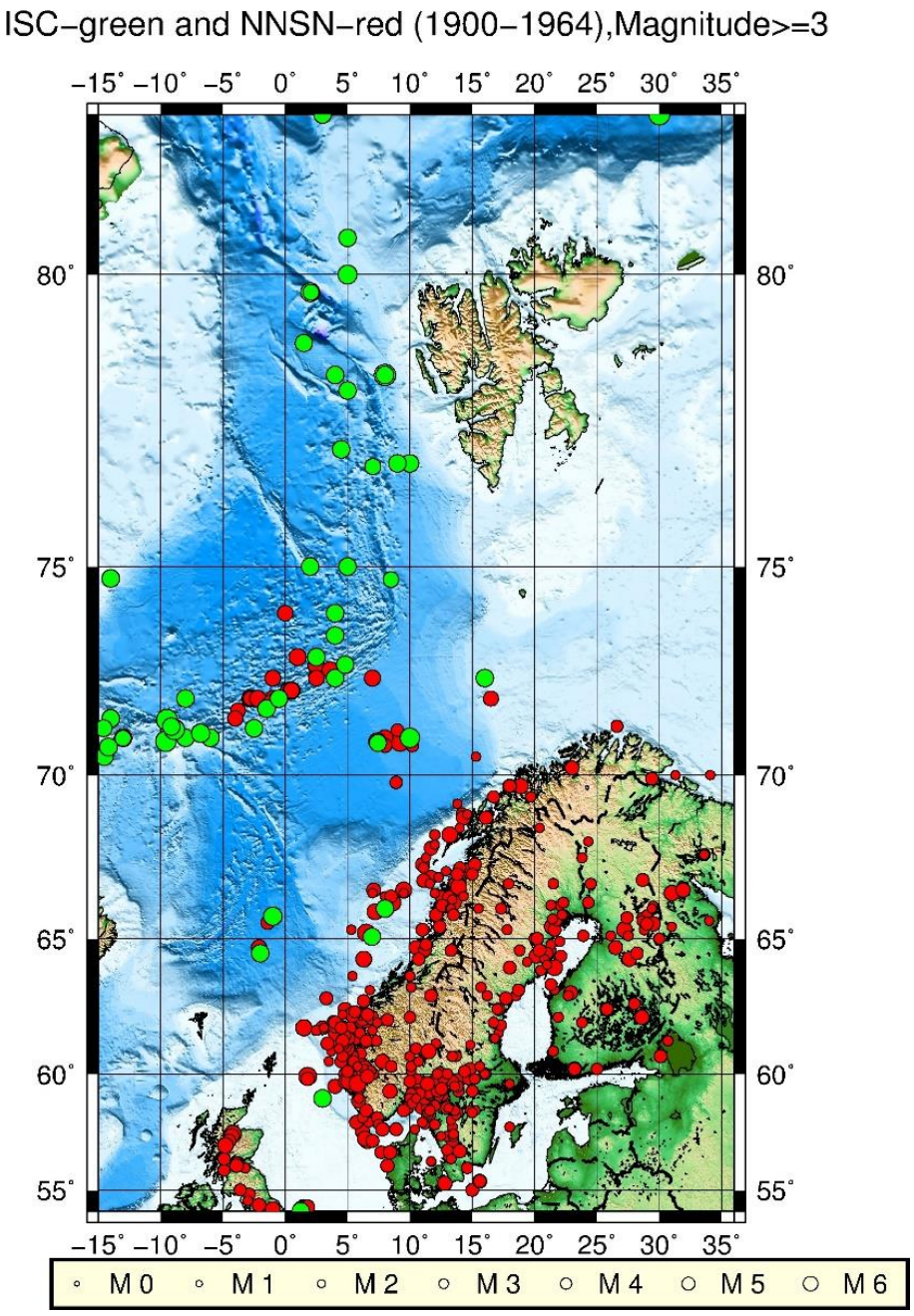

Figure 18: NNSN and reviewed ISC seismic records for the period 1900 – 1964. Only events with magnitude 3 and larger for both datasets have been selected. ISC seismicity is represented with the green color whereas NNSN seismicity with the red color. Total number of events obtained from ISC database being in prime area for the time period 1900 – 1964 are 52. Total number of events obtained from NNSN database being in prime area for the time period 1900 – 1964 are 481.

It is seen that NNSN has more events than ISC which is a good indication that NNSN is more complete for the southern and eastern part of the prime area than ISC. That is mostly due to NNSN has been revised with local and macroseismic data whereas ISC included just instrumental data gained from other seismological agencies and ISS (NORSAR and NGI, 1998). However, it is seen that NNSN lacks much of the data at the northwestern and northeastern part of the prime area. In particular a lot of data missed near Mohns and Knipovich ridges. But since the following thesis does not aim to study seismicity at and at close distances to the ridges the seismic data provided by ISC for the following area and time period can be disregarded. The same applies to the events to the northeast and northwest from Svalbard. Since these events are out of the limit of the study area, they can be disregarded.

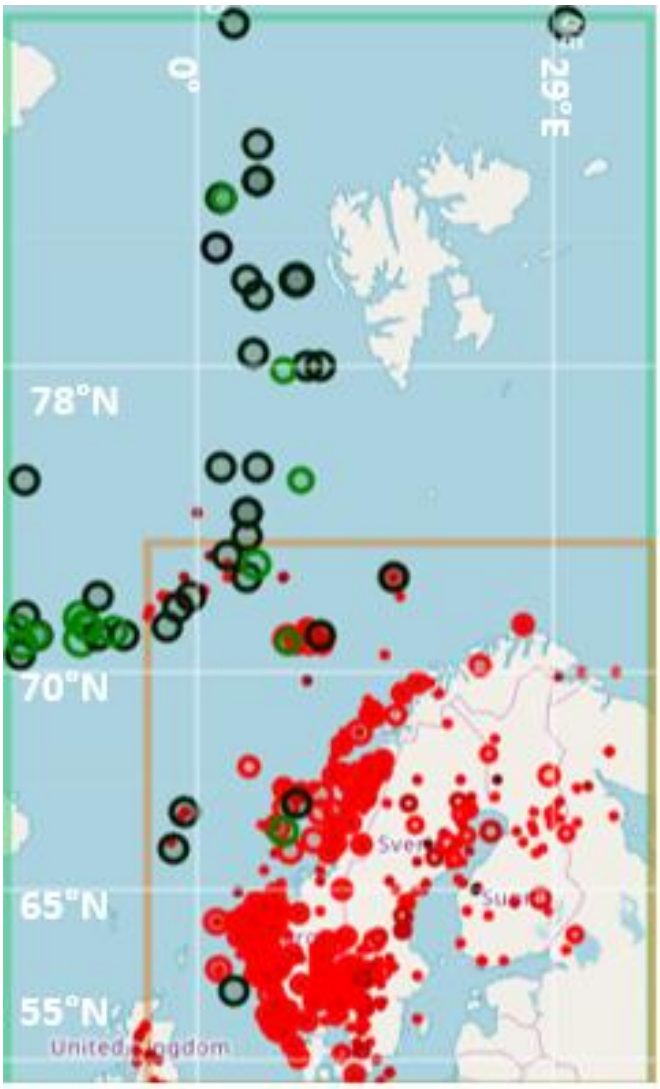

Figure 19: For the time period from 1900 – 1964; ISC seismic records are represented by green and dark green colors whereas NNSN seismic records are represented with red. ISC data in the prime area is enclosed by the green rectangle whereas NNSN data by orange rectangle.

In Figure 19, ISC data that is enclosed by the green rectangle is used to represent seismic activity for the time interval 1900 – 1964 but one cannot rely on it due to large location errors. Also, it is seen that NNSN data enclosed by the red rectangle has much more regional data available with the better locations meaning that NNSN seismic records are the only seismic records one can rely on for the time period 1900-1964 (Figure 19).

In order to stay convinced NNSN did not miss significant events ISC has in the NNSN rectangle, one can perform an illustrative check of seismic events that do not match up. The following check will be performed for two offshore events in the western Norway (Figure 20).

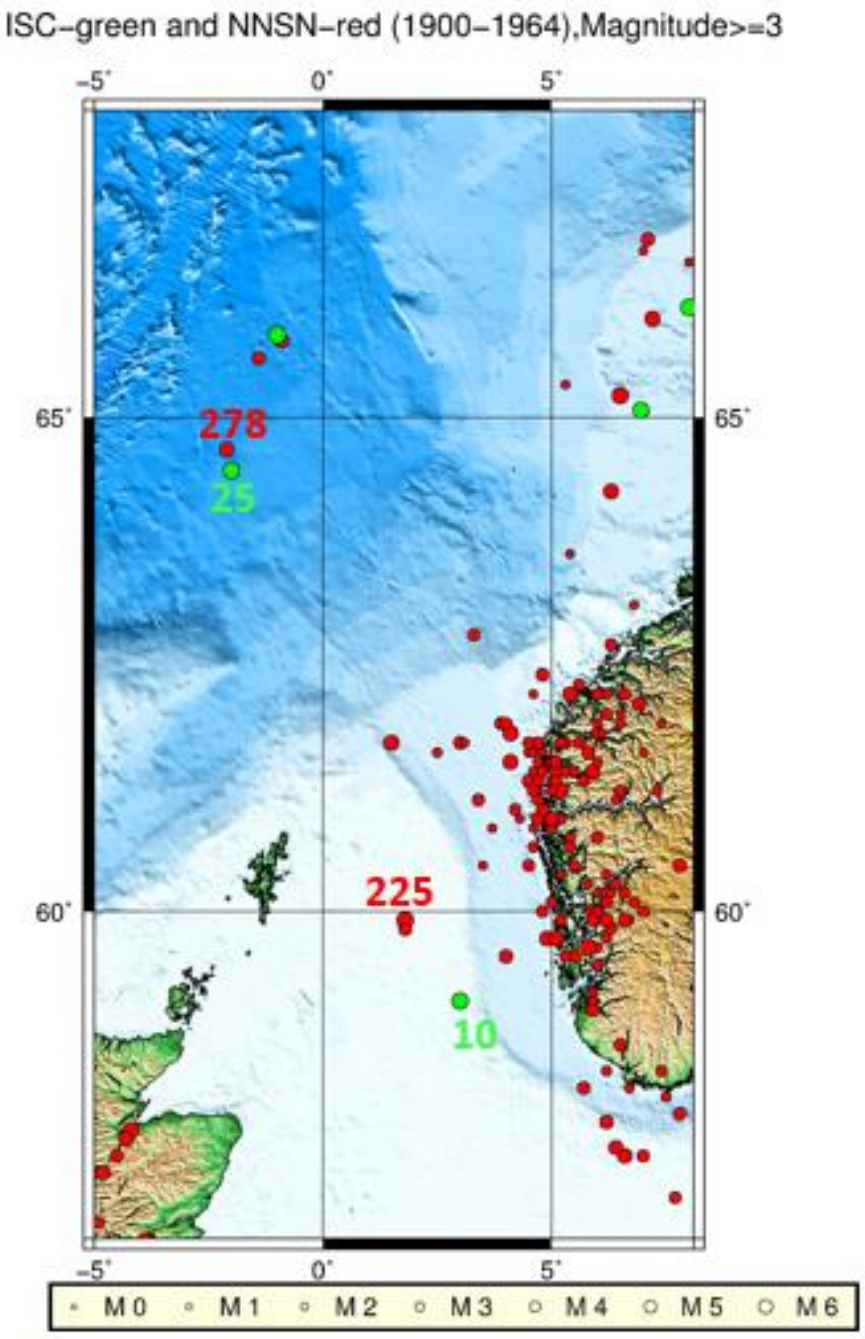

Figure 20: NNSN and reviewed ISC seismic records for the period 1900 – 1964. NNSN seismic records are red in colors whereas ISC are green. The check of seismic event coincidence in NNSN and ISC databases will be performed for the ISC events 10 and 25.

Table 4: Event №10 (ISC).

Database	Date	Time	Latitude	Longitude	Magnitude
ISC	1927.01.24	05.18	59.000	3.000	5.6
NNSN	1927.01.24	05.18	59.900	1.800	5.3
Shift (km)			50	67	

Event № 10 in ISC corresponds to the event № 225 in NNSN.

Table 5: Event №25 (ISC).

Database	Date	Time	Latitude	Longitude	Magnitude
ISC	1934.05.20	19.04	64.500	-2.000	5.6
NNSN	1934.05.20	19.04	64.700	-2.100	4.8
Shift (km)			11	6	

Event № 25 in ISC corresponds to the event № 278 in NNSN.

From Figure 20, it is seen that in both cases NNSN has events from ISC that show mismatches meaning that the epicenters in NNSN do not correspond to the ISC epicenters in the current ISC database (Tables 4; 5). That can be explained by the fact all Norwegian events have been revised independently of ISC and are therefore considered more reliable than the ISC locations (Muir Wood and Woo, 1987).

1964 – 1980

For the following time span, one has two sets of data from ISC and NNSN. According to Seismo Group (2011) report, starting from 1964 until and including June 1982 all ISC seismic data for events larger than 3.0 have been systematically included in NNSN database. Significant contribution was made for the arctic region and smaller seismic records were added. However, no attempts to relocate seismic events have been made hence it is important to check and compare events from both databases (Seismo Group, 2011). For that purpose, one will generate plot using the same method and criteria as were applied to the preceding time interval (Figure 21). Subsequent imposition of two sets of data allows to compare seismicity and identify mismatches if there are such.

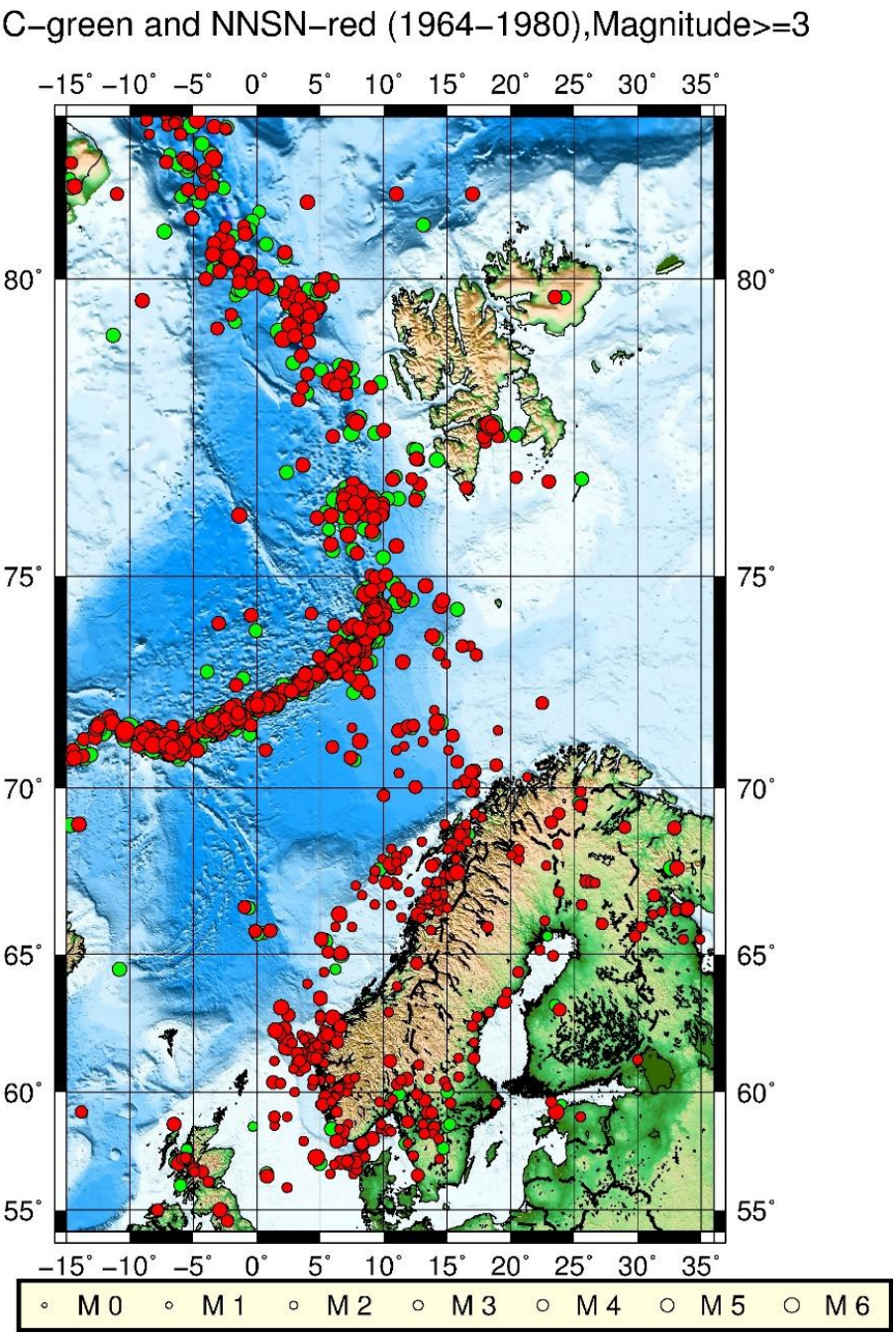

Figure 21: NNSN and reviewed ISC seismic records for the period 1964 – 1980. Only events with magnitude 3 and larger for both datasets have been selected. ISC seismicity is represented with green color whereas NNSN seismicity with red color. Total number of events obtained from ISC database being in prime area for the time period 1964 – 1980 are 444. Total number of events obtained from NNSN database being in prime area for the time period 1964 – 1980 are 749.

From Figure 21, it is seen that NNSN has more events than ISC that indicates NNSN is more complete for the prime area than ISC. That is due to inclusion of macroseismic data, revision of instrumental data and systematic inclusion of ISC data from 1964. Therefore, one can notice that NNSN seismic records now correspond to the ISC ones. In addition, NNSN seismicity is not that sparse in comparison with ISC records and clearly outlines most seismically active areas. Also, seismic event to the northeast from Svalbard that was seen on the plot for 1900 – 1964 time period disappeared in a plot for 1964 – 1980. That means there was no significant seismicity in that region indicating seismic activity to the northeast from Svalbard. Therefore, that seismic event is considered to be a mistake and is disregarded. It is also

seen that there is a slight difference between the ISC locations in the NNSN database and the ISC locations at ISC (Figures 21; 22). The integration of ISC data in NNSN was done around year 2000, however ISC has since changed its location model and location program and updated its database (International Seismological Centre, 2019b). This explains the shift in epicenters. In any case, the new ISC location does not change the basic seismicity pattern and no attempts will be made to update the NNSN database with the new ISC locations. However, it is seen that there are few ISC events that are either new or shifted a large amount (Figure 22). To be sure that NNSN has all significant seismic records one will perform an illustrative check for these four offshore events.

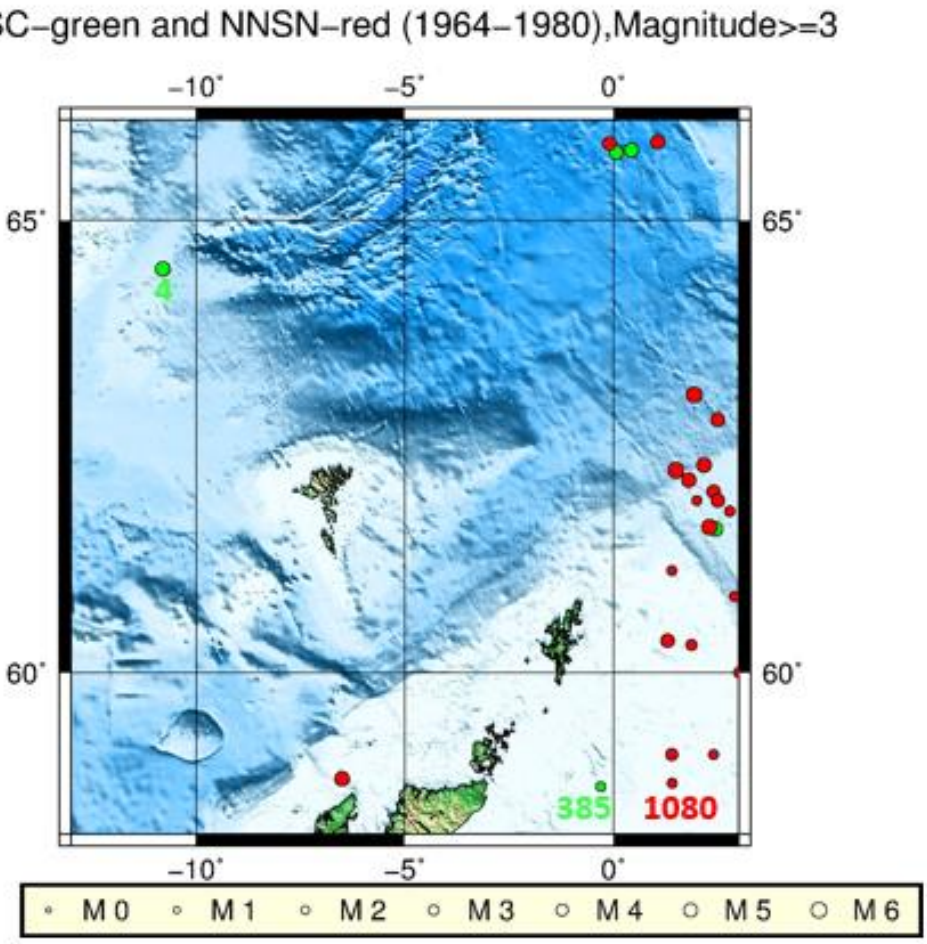

Figure 22: NNSN and reviewed ISC seismic records for the period 1964 – 1980. NNSN seismic records are red in colors whereas ISC are green. The check of seismic event coincidence in NNSN and ISC databases will be performed for the ISC events 4 and 385.

Table 6: Event №4 (ISC).

Database	Date	Time	Latitude	Longitude	Magnitude
ISC	1964.02.26	22.59	64.500	-10.800	4.4
Earlier ISC	1964.02.26	22.59	64.700	-17.300	4.4
Shift (km)			11	361	

Event № 4 is of concern since one identified it is not in NNSN database (Table 6). Comparison of information about the event provided by reviewed ISC bulletin search and by earlier ISC records stored in the local ISC database enables to decide which record should or should not be taken for further

consideration. Comparing latitude and longitude records of an event, one can notice a significant difference in longitude. The computed distance to which the event was relocated in latitude is 11.12 km whereas in longitude is 361.4 km. It is seen that the event has been relocated extremely in E-W direction after the ISC has been rebuilt for 1964 – 1984 (International Seismological Centre, 2019a). In that sense, one would expect large location errors for the event that will not give any reliable results anyway. Therefore, it would be sensible to not take it for further consideration.

Table 7: Event №385 (ISC).

Database	Date	Time	Latitude	Longitude	Magnitude
ISC	1977.11.09	03.37	58.600	-0.300	3.0
NNSN	1977.11.09	03.37	58.643	1.408	3.0
Shift (km)			2	95	

Event № 385 in ISC corresponds to the event № 1080 in NNSN (Table 7; Figure 22).

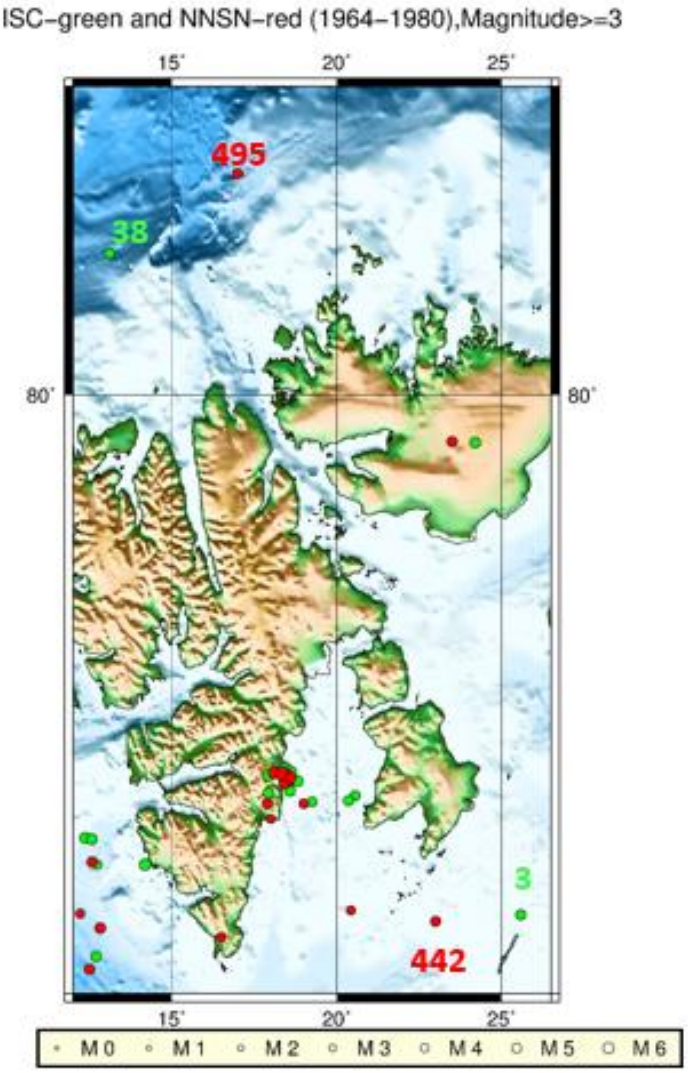

Figure 23: NNSN and reviewed ISC seismic records for the period 1960 – 1980. NNSN seismic records are red in colors whereas ISC are green. The check of seismic event coincidence in NNSN and ISC databases will be performed for the ISC events 38 and 3.

Table 8: Event №38 (ISC).

Database	Date	Time	Latitude	Longitude	Magnitude
ISC	1965.02.21	00.07	80.717	13.109	4.3
NNSN	1965.02.21	00.07	81.100	17.000	4.3
Shift (km)			21	216	

Event № 38 in ISC corresponds to the event № 495 in NNSN (Table 8; Figure 23).

Table 9: Event №3 (ISC).

Database	Date	Time	Latitude	Longitude	Magnitude
ISC	1964.02.26	07.31	76.855	25.584	4.3
NNSN	1964.02.26	07.31	76.810	23.000	4.2
Shift (km)			3	144	

Event № 3 in ISC corresponds to the event № 442 in NNSN (Table 9; Figure 23).

It can be concluded – latest ISC does not have any events in, particularly, outlying areas, that are not in NNSN and therefore, the NNSN database seems reliable for the time period considered.

1980 – 2016

For the following time interval there are two datasets available by both ISC and NNSN. Starting from 1980's seismic networks in Norway began to develop providing much more regional data to NNSN database. Consequently, from about 1980's (1982) and onwards it is considered that NNSN detects as many events as ISC, and ISC data was not included systematically. Subsequently, when comparing NNSN and ISC datasets, one can encounter with location mismatches. In order to check that, the plot of NNSN seismicity represented by red color and ISC seismicity represented by green colour for the events within the prime area with magnitude equal to 3.0 and larger is generated (Figure 24).

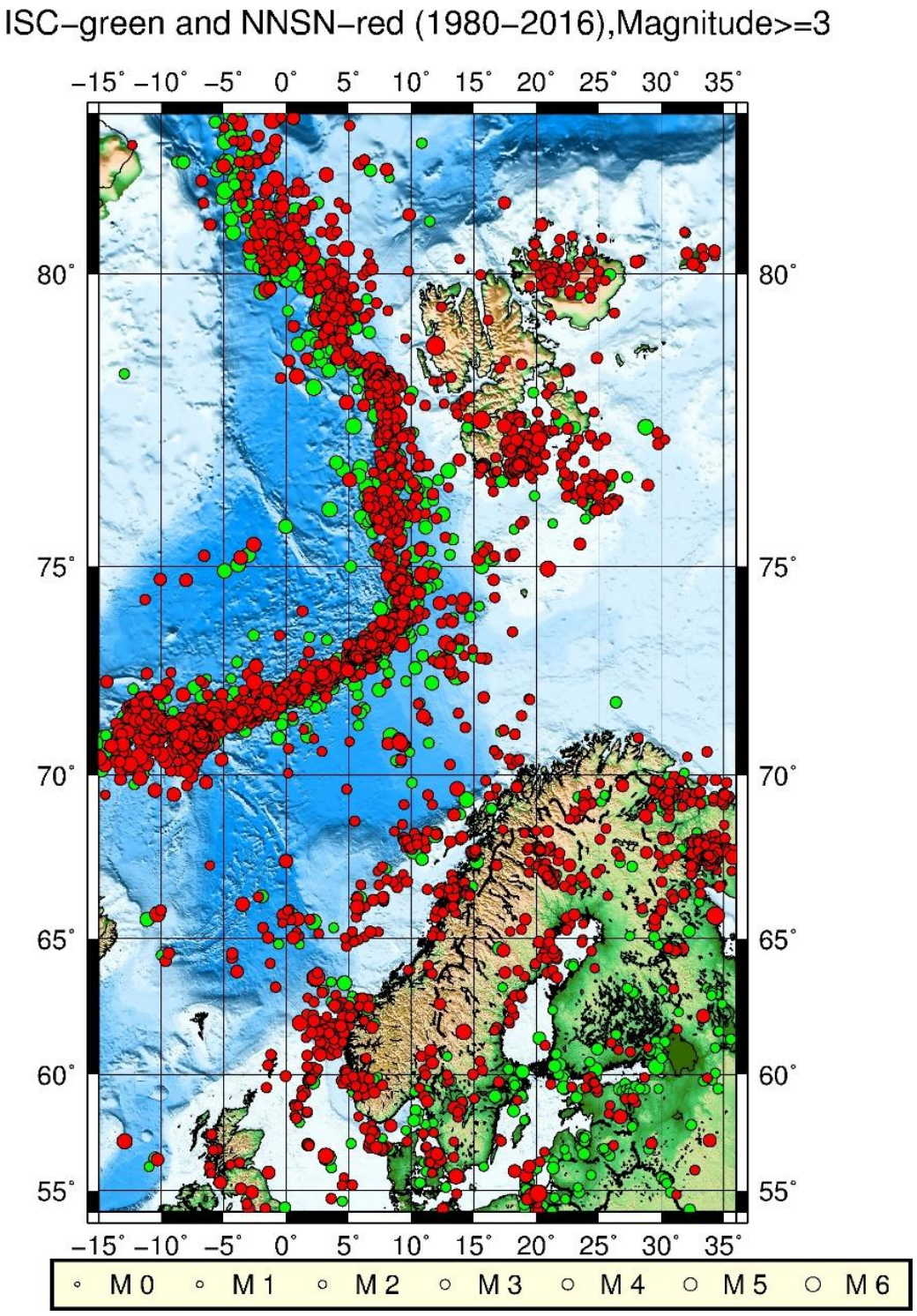

Figure 24: NNSN and reviewed ISC seismic records for the period 1980 – 2016. Only events with magnitude 3 and larger for both datasets have been selected. ISC seismicity is represented with green color whereas NNSN seismicity with red color. Total number of events processed from ISC database being in prime area for the time period 1980 – 2016 are 1688. Total number of events obtained from NNSN database being in prime area for the time period 1980 – 2016 are 3489.

From Figure 24, it is seen that NNSN has more events than ISC that is again due to the inclusion of macroseismic data, revision of instrumental data and systematic inclusion of ISC seismic records started in 1964. Also, one can notice that lots of ISC events that are located in the southeastern part of the prime area, in particularly outside Norway and its adjacent offshore areas. This means these

events are outside studying in the thesis area and hence they will not be taken for further consideration. In addition, from 1980's seismic networks in Norway began to develop that allowed to gather much more regional seismic data. Hence starting from 1980's NNSN seismic catalogue was mostly made by readings from BER stations (BER – name of agency for NNSN) and regional seismic networks. However, since development of seismic networks spread around Norway started at different time periods NNSN catalogue could not be fully completed at once for the whole prime area. Consequently, significant seismic events (those with magnitude large than 3.0) for the prime area from ISC database were merged with the BER catalogue (Seismo Group, 2011). Therefore, NNSN database for this time period is considered to be the most reliable and complete one. Again, from Figures 24, 25 it is seen that there are ISC events that do not match with NNSN. Therefore, in order to stay convinced NNSN has all significant events included, one can perform an illustrative check with three events in the same way as it was done for the two previous time periods. In cases if there will be such, the NNSN database would miss ISC seismic records one will give arguments why this is happened and then decide on whether it is worth to take ISC record for further consideration.

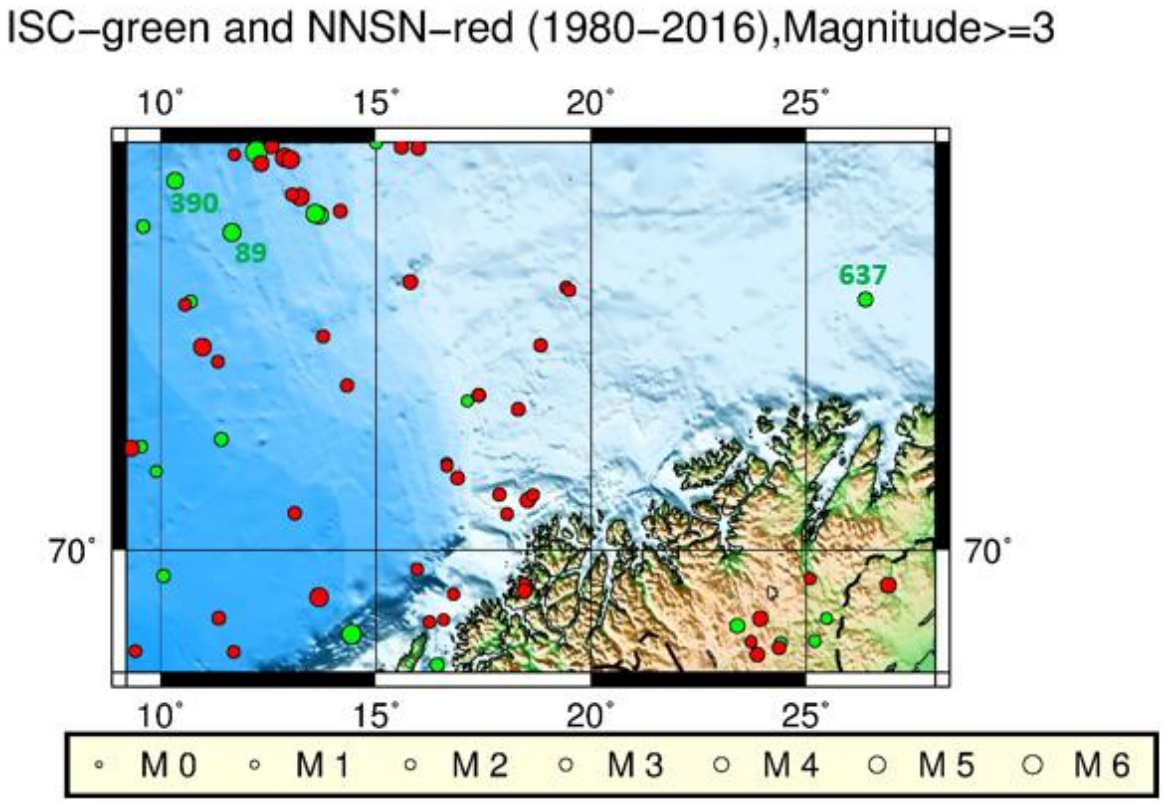

Figure 25: NNSN and reviewed ISC seismic records for the period 1980 – 2016. NNSN seismic records are red in colors whereas ISC are green. The check of seismic event coincidence in NNSN and ISC databases will be performed for the ISC events 637, 390 and 89.

Table 10: Event №637 (ISC).

Database	Date	Time	Latitude	Longitude	Magnitude
ISC	1996.01.01	02.10	71.900	26.380	3.6
Earlier ISC	1996.01.01	02.10	71.900	26.380	3.6
Shift (km)			-	-	

The event (№ 637) was not found in NNSN database and it had not been included from ISC since this was only done until 1982 (Table 10). The original observations were 5 P's and no back-azimuth from 5 arrays, so the location might be quite uncertain (International Seismological Centre, 2019a). In any case, it is just a single event in the area where it was observed meaning there is no significant seismicity ongoing in this region. Therefore, the event is disregarded.

Table 11: Event №390 (ISC).

Database	Date	Time	Latitude	Longitude	Magnitude
ISC	1992.08.24	21.21	72.738	10.334	4.1
NNSN	1992.08.24	21.21	72.929	8.634	2.8
Shift (km)			11	95	

Event № 390 does not have pair seen in the Figure 25. The reason for this is that after it was reconsidered by NNSN its magnitude changed from being 4.1 to 2.8 (Table 11). For pure comparison of NNSN and ISC databases, the same searching criteria were applied to both databases. They are latitude and longitude enclosing the prime area and minimum magnitude threshold equal to 3.0. Since magnitude of the event decreased to 2.8, it did no longer fall under searching criteria and hence NNSN event matching ISC event is not shown in Figure 25.

Table 12: Event №89 (ISC).

Database	Date	Time	Latitude	Longitude	Magnitude
ISC	1983.10.15	03.32	72.377	11.657	4.4
Earlier ISC	1983.10.15	03.32	72.311	10.886	4.3
Shift (km)			4	43	

Event № 89 is not in NNSN database (Table 12). It is far away from the network as it was in 1983, and it is near the ridge that is outside the studying area. However, this shows that for NNSN to be complete in its prime are, more ISC data should be included. Therefore, this event is disregarded.

2016 – onwards

For the last two years there is only one database – NNSN that provides seismic records. ISC requires 24 months to check and relocate all the data gained from other seismological agencies and hence recent seismic data is not available yet. Consequently, NNSN is the choice.

Concluding remarks

Comparing NNSN to ISC database, no significant evidence showing NNSN to be incomplete was found. From figures demonstrated in this section (section 5.2) for the different time periods and illustrative checks showing various cases of ISC events present, relocated and absent in NNSN, it was seen that NNSN has still all significant seismic trends characterized by more accurate locations than in ISC. Therefore, no attempts will be made to update the NNSN database with the events from ISC.

5.3 Earthquake location accuracy

Earthquakes are recorded by seismic stations that produce seismograms where information about seismic waves is reflected. Earthquakes generate body waves: P- and S-waves that are used to locate seismic events. Earthquake location is defined by four parameters. They are the hypocenter location defined by latitude, longitude and depth of a seismic event and its origin time which is the moment of rupture initiation. Hypocenter and origin time are in turn calculated using arrival time of seismic phases at different seismic stations. Difference in arrival time of two phases (P- and S-phases) and established seismic velocity model for the Earth are then used to calculate the distance (distance from seismic station to the hypocenter) (Havskov and Ottemöller, 2010).

Multiple station location

Using at least three seismic stations one can locate earthquakes. Intersection of three circles created through radii – distances from S-P arrival times gives the location of an epicenter (Figure 26). Assuming a surface focus, intersection of the circles does not give a point but rather an area of an epicenter location. This introduce the concept of errors in epicenter location.

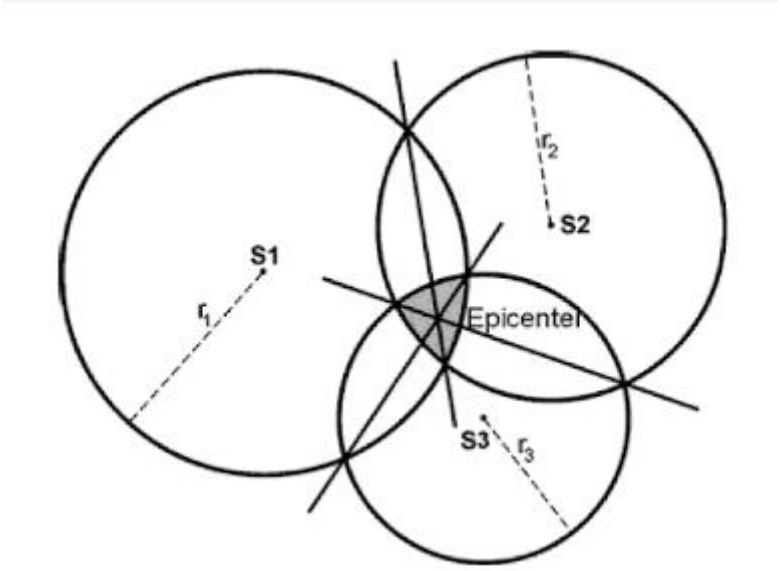

Figure 26: Simple manual location of an earthquake; r1, r2 and r3 are radii drawn from the center of seismic stations S1, S2 and S3 respectively. Shaded grey area is an area of circles' intersection – area of hypocenter location. Two intersection solid lines indicates the exact location of an epicenter (Modified picture from Havskov and Ottemöller, 2010).

There are methods that enable to determine the exact location of both epicenter (Havskov and Ottemöller, 2010) and hypocenter (Båth, 1979) in the area of circles' intersection.

Earthquake location using grid search

Manual location method was introduced to represent the concept of errors and challenges related to both epicenter and hypocenter location. However, nowadays earthquake location is determined through iterative methods by computers. The main idea of iterative methods is to find a solution with

the lowest possible difference (the residual) between the observed and calculated travel times. Residual is defined as “the difference between the observed and calculated arrival times, which is the same as the difference between the observed and the calculated travel times” (Havskov and Ottemöller, 2010). The overall error is calculated as the root mean square (RMS) of the residuals. RMS is the square root of the sum of the residuals squared divided by the number of observations (Havskov and Ottemöller, 2010). RMS is a parameter used to give an estimate of a location accuracy.

The simplest way to determine earthquake location is to do a grid search. This is to calculate RMS for each point in the model. The point with the lowest computed RMS is assumed to represent the location of a hypocenter (Havskov and Ottemöller, 2010). From Figure 27, it is seen that the RMS errors increase as one move away from the epicenter and the RMS contours form ellipses. We can consider this to be indications of the size of the location error in different directions. The shape of the ellipse represented on the left picture is given by RMS contours characterized by major axes in NW direction and minor axes in NE. This can be explained by elongated seismic network in NE direction that gives better seismic coverage and minor errors. On the contrary, one can observe poor station coverage in NW direction that leads to large errors and major axes in NW thereby determining orientation of the error ellipse (Figure 27). The greater the number of seismic stations locate nearby an earthquake epicenter, the smaller-size ellipse will be. In that sense, one has to control RMS value and number of stations when possessing to get reliable results.

The normal location programs calculate the so-called error ellipse which is defined a “calculated ellipsoid within which there is 67% probability equal to one standard deviation of finding hypocenter” (Havskov and Ottemöller, 2010). The shape and the size of error ellipse change depending of number and location of stations, network and the quality of the data.

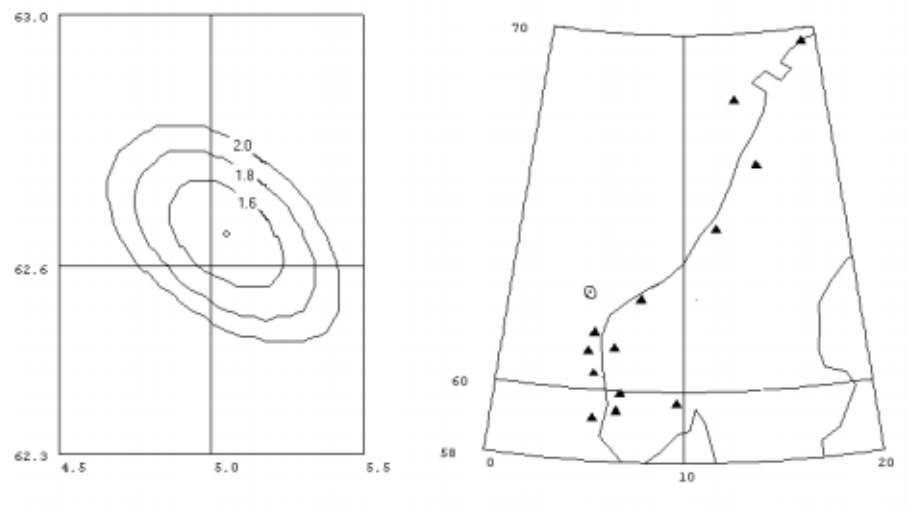

Figure 27: Looking at the right picture one can observe seismic event in the western Norway represented with a circle and seismic stations represented with triangles. The left picture shows RMS contours where the smallest one represents the lowest RMS value while subsequent ellipses grow outwards with increasing RMS value (Modified picture from Havskov and Ottemöller, 2010).

The minimum number of stations required to locate seismic event is four used to determine latitude, longitude, depth and origin time. Being critical to results obtained and keeping the right balance between data quality and quantity, a suggested number of stations to select when carrying out search

is five. The same rule applies to RMS selection criterion. An RMS value of 1.5 or smaller is considered a requirement to acceptable locations.

Hypocentral depth errors

Hypocentral depth is another parameter that requires thorough consideration. Hypocentral depth is determined by arrival times of phases (P- and S-phases) coming from an earthquake. Main challenge one encountered with is travel-time that does not show any variation with varying depth. Illustrative example of the issue can be seen in Figure 28.

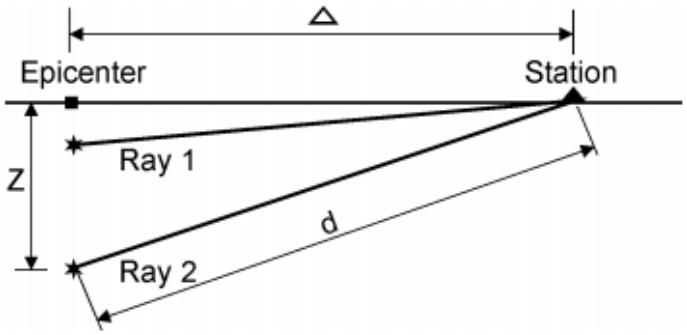

Figure 28: Figure representing travel-time-depth issue. Stars represent seismic events (Modified picture from Havskov and Ottemöller, 2010).

By looking at Figure 28, it can be seen that in spite of depth difference of seismic events, the length of Ray path 1 and 2 do not differ much meaning that they are almost of the same length (Ray path 2 is slightly longer than Ray path 1). This means that the calculated travel-time of P- and S- phases for a small depth variation for a shallow event will be small and therefore the depth is not sensitive to travel times. For a deeper event, at the same distance, the sensitivity of the travel time to the depth will be significant and the depth estimates for deep earthquakes would therefore be better than for shallow one. Therefore, a rule of thumb states that in order to get reliable depth estimates at least several close stations should have shorter path to the event than twice paths to its depth (Havskov and Ottemöller, 2010).

In order to establish depth range characteristic for Norway, one can refer to Janutyte et al. (2017) recent studies done for one of the most seismically active area – Nordland (Northern Norway). One of the conclusions reached states that shallow onshore seismic activity is in the range of 3 – 10 km whereas deeper offshore seismicity constraint is in the range of 15 to 25 km depth. Relying on the studies done, one can set hypocentral depth prevailing for Norway to be in a range of 0 – 30 km. This means that in Norway and its adjacent areas the condition of a distance of maximum twice the depth is usually hardly fulfilled. In addition, it is important to be aware of possible observational errors in arrival time as well as keep in mind that for the sake of simplification established homogeneous model of the earth is used instead of the real one. These can also result in misleading hypocenter error estimates. In that sense, there is no point in using hypocenter depth error limits for Norway and its adjacent areas since they are very uncertain and hypocenter depth will be set to limited range (0 – 30 km) anyway.

5.4 Catalogue compilation

5.4.1 Catalogue description

For seismic catalogue compilation one will use NNSN database based on the conclusion made on the database choice and cover time span starting from the time the first seismic reading was registered until the present time. When building seismic catalogue covering long time period, as it is the case, it is important to differentiate data on the basis of its quality and quantity.

Until 1980

Starting from the first macroseismic record stored in NNSN database until 1980, the quality of the data was not reliable enough. NNSN includes both macroseismic and instrumental data. Macroseismic records are based on felt reports and questionnaires and as was noted earlier provided overestimated magnitudes. Instrumental data for the following time interval was characterized by large location errors. For the time period before 1960 location errors are in the interval from 20 to 60 km whereas from 1960 – 1980 from 15 to 20 km (Sellevoll and Sundvor,2001). In addition, quantity of the data stored is not extensive and hence every seismic record is valuable. Therefore, for the time span until 1980 there will be no selection criteria set for the location accuracy. In that sense, it is important to focus on seismic records of relatively trustworthy readings that are usually provided for events of large magnitudes. Consequently, only events in Norway and its offshore adjacent areas of interest being in prime area with magnitude equal to 3.0 and large will be taken for further consideration and make the first part of a seismic catalogue. After searching criteria have been applied to NNSN database one ends up with 1231 events.

1980 – onwards

Starting from 1980's seismic stations in Norway became growing into seismic networks providing much more regional data. From that time, it is considered that NNSN is the most reliable and complete regional database that detects most seismic events in Norway and its adjacent offshore areas. Therefore, aiming to get most accurate and reliable results stricter conditions can be applied to the data selection process.

- In particular, it is important to perform search within the prime area and hence latitude and longitude limits will be set.
- Since data is more accurate and reliable, one can differentiate between various events causing any seismic activity. Events that are of interest for the following thesis are earthquakes and probable earthquakes. Therefore, selection criterion will be set to pick up just events of these types.
- To comply right balance between quality and quantity of the data, it is of significance to set maximum RMS threshold to be 1.5 with the minimum number of stations equal to five. In cases where one deal with abundant amount of data stricter requirements can be applied.
- The depth limits characteristic for Norway and its adjacent areas are set to be within 0 – 30 km interval.
- Hypocentral depth error limits is a parameter that will not be used in selecting process since travel-times do not change much with varying depth.

- Epicentral error limits (latitude and longitude error limits) is the parameter that can be used to clean the data and increase the level of reliability providing events with reasonable errors. To decide on which epicentral error limits will keep reasonable agreement between quantity and quality of the data one can perform several tests.

5.4.2 Location accuracy

Applying all aforementioned criteria to the time period from 1980 and onwards, one will start with the smallest epicentral error limit and then gradually increase it observing changes of overall seismicity pattern. Of particular importance are active areas with known seismicity of magnitude equal to 3.0 or larger. At a point of when seismicity pattern will no longer show large variations one will stop testing epicentral error limits and accept the one that has the best agreement between quality and quantity of the data.

Epicentral error limits

Epicentral Error Limits: 0 – 10 and 0 – 15 km

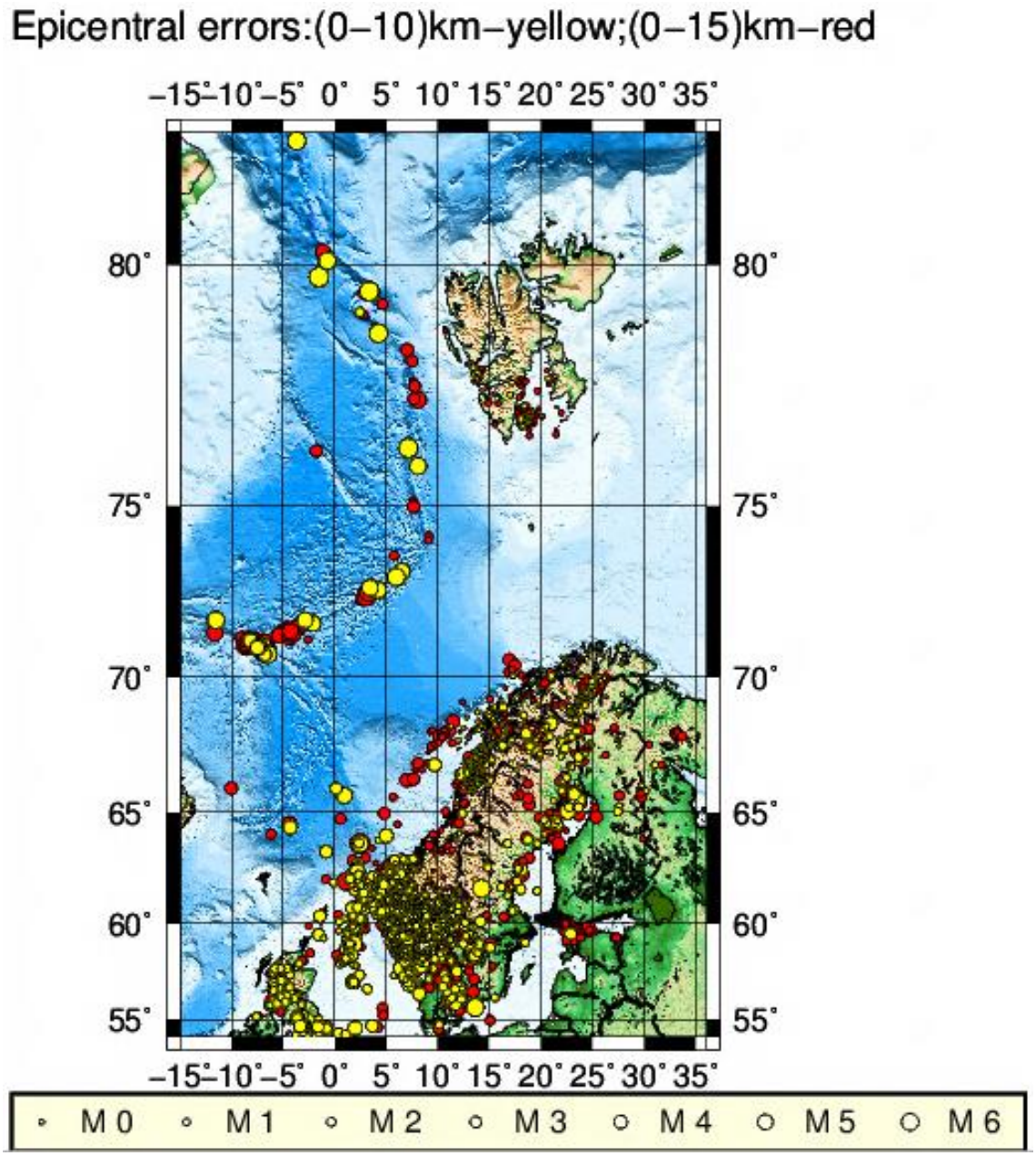

Figure 29: Seismic events with epicentral errors in the interval 0 – 10 km are represented with the yellow color for the time period from 1980 and onwards. Seismic events with epicentral errors in the interval 0 – 15 km are represented with the red color for the time period from 1980 and onwards.

From Figure 29, one can notice that there are large discrepancies between yellow (0 – 10 km epicentral error limit) and red (0 – 15 km epicentral error limit) seismicity represented meaning that epicentral error limit of 0 – 10 km is not reasonable. It can be seen that with larger epicentral errors limits, in particularly 0 – 15 km overall seismicity pattern (represented with the red color) looks to be more complete than the one (represented by yellow color) generated applying 0 – 10 km epicentral error limit (Figure 29). By applying larger epicentral error limit to the data, one got significant seismic trends that are not present when using 0 – 10 km epicentral error limit. This includes the shape of Mohns and Knipovich ridges that are more definite when using 0 – 15 km epicentral error limit. Of particular

importance are seismicity appeared on and nearby Svalbard and northern Norway areas and seismic trend that started taking shape along mid-Norwegian coast. In spite of some missing seismic trends began to take definite shape when using 0 – 15 km epicentral error limit, the reasonable agreement between quality and quantity of the data is still not reached. That is due to insufficient number of seismic events present on Svalbard and northern Norway areas that disturb clear picture of seismicity trends. In addition, no seismic events are present in the western Barents Sea and seismic trend along mid-Norwegian coast is still not clearly defined.

Epicentral Error Limits: 0 – 15 and 0 – 20 km

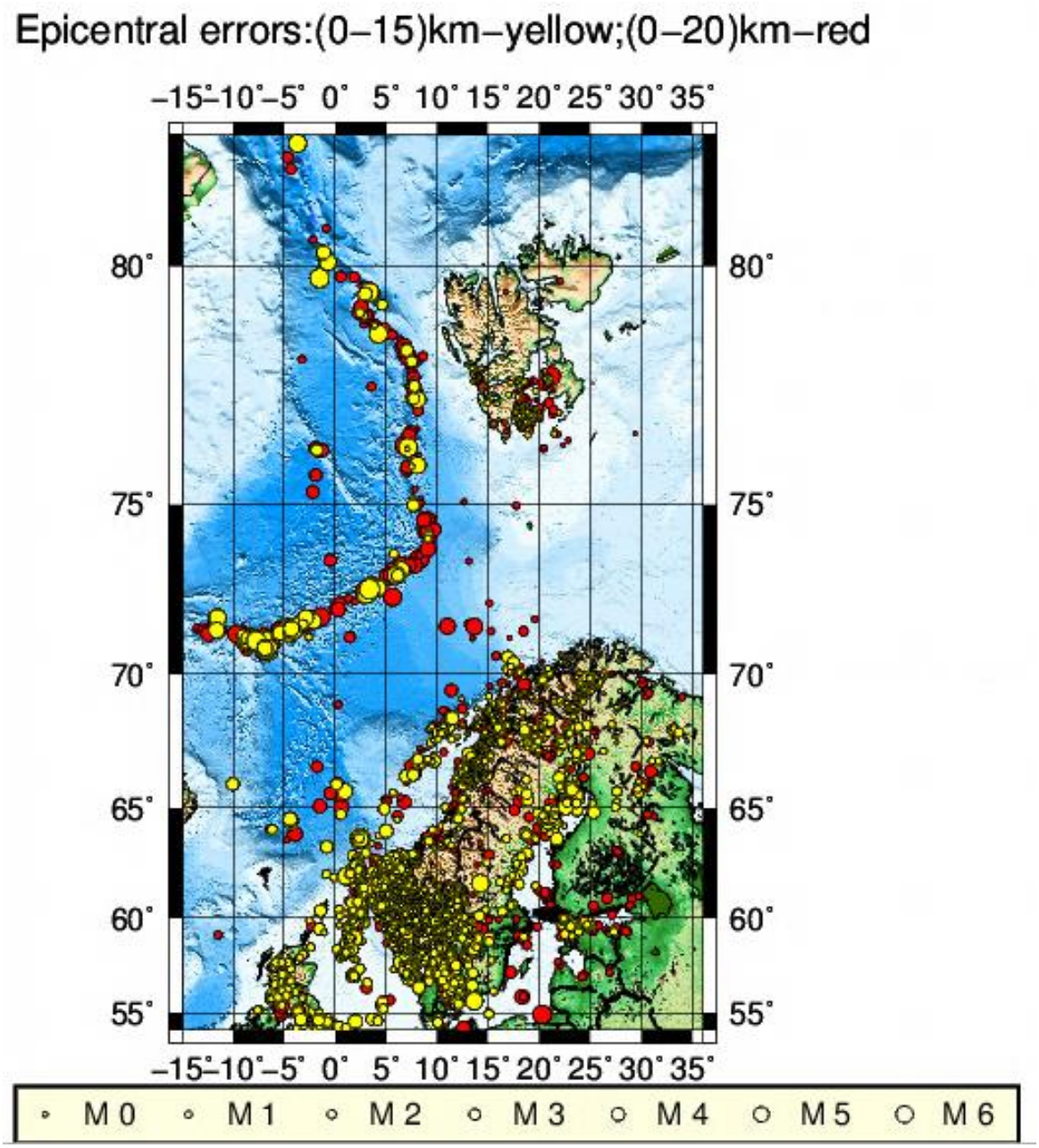

Figure 30: Seismic events with epicentral errors in the interval 0 – 15 km are represented with the yellow color for the time period from 1980 and onwards. Seismic events with epicentral errors in the interval 0 – 20 km are represented with the red color for the time period from 1980 and onwards.

From Figure 30, one can notice that there are still substantial discrepancies between yellow (0 – 15 km epicentral error limit) and red (0 – 20 km epicentral error limit) seismicity represented meaning that epicentral error limit of 0 – 15 km is not reasonable. It can be seen that when applying 0 – 20 km error limit one gets all significant seismicity trends outlined (Figure 30). They are seismicity along and nearby mid-Norwegian coast, seismicity at and nearby northern Norway, Svalbard and Western Barents Sea. This means 0 – 20 km epicentral error limit gives reasonable agreement between quality and quantity of the data and can be used when selecting events for seismic catalogue compilation. However, in

order to be convinced that this epicentral error limit is the most suitable to comply balance between quality and quantity of the data, it is important to compare it with the next one.

Epicentral Error Limits: 0 – 20 and 0 – 25 km

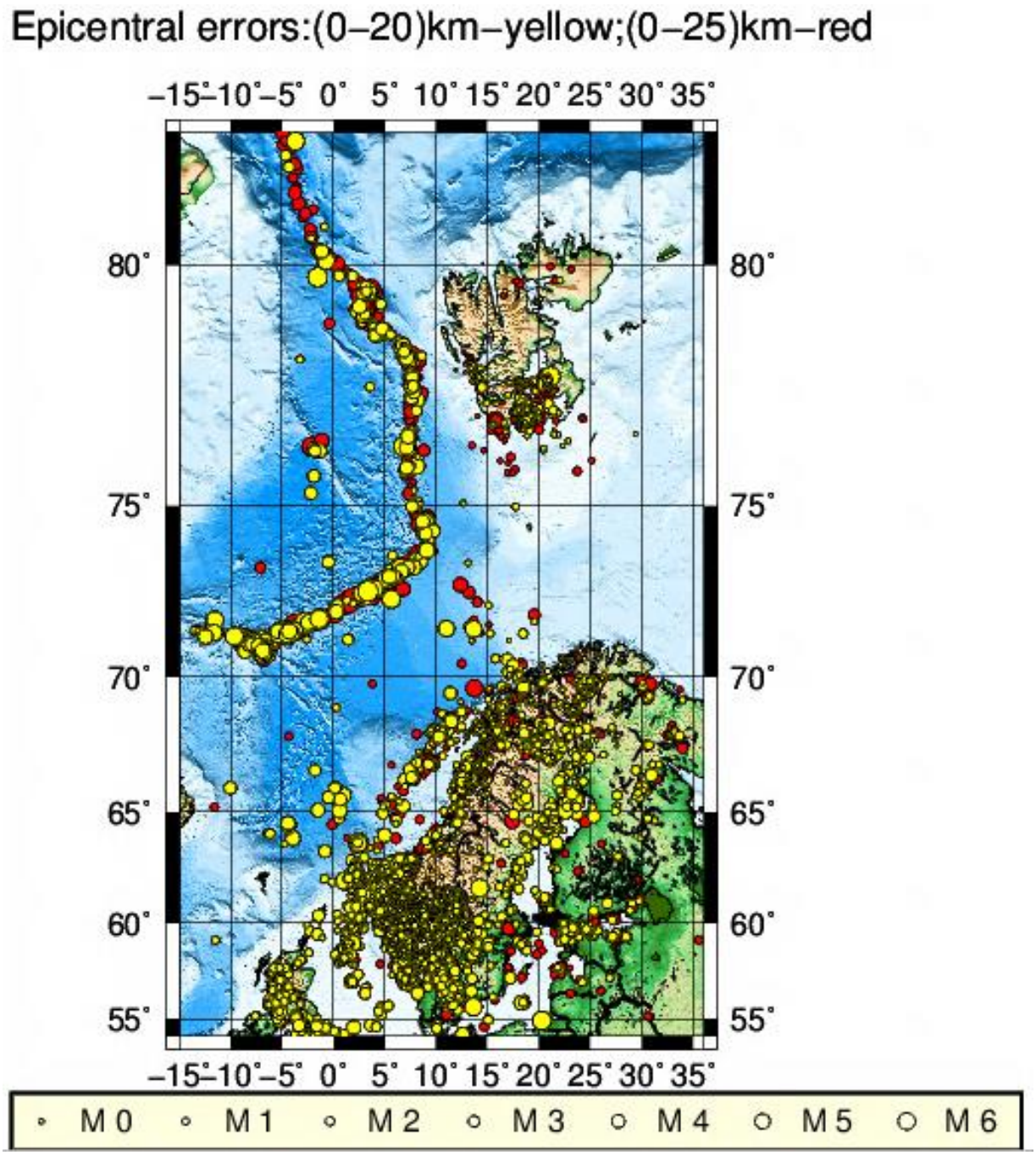

Figure 31: Seismic events with epicentral errors in the interval 0 – 20 km are represented with the yellow color for the time period from 1980 and onwards. Seismic events with epicentral errors in the interval 0 – 25 km are represented with the red color for the time period from 1980 and onwards. Number of events picked when using 0 – 25 km epicentral error limit is 12504.

From Figure 31, it can be seen that when using epicentral error limit of 0 – 25 km the overall seismicity pattern does not change. Moreover, one can notice that seismicity trends are almost identical when

using 0 – 20 km and 0 – 25 km epicentral error limits. That means the best possible agreement between quality and quantity of the data is reached when using 0 – 20 km epicentral error limit.

Since the criteria for the second part of the seismic catalogue are discussed, the last step is to control that the data covering period from 1980 and onwards is not contaminated by confirmed (E) and probable explosions (P) (SEISAN Earthquake Analysis Software for Windows, Solaris, Linux and Macosx, 2018). This can be done by using EXFILTER programme. This programme searches probable and confirmed explosions in certain time period, certain areas and with certain magnitudes that are then extracted from the seismic catalogue. Cleaned part of the second part constituting the seismic catalogue can be reviewed in Figure 32.

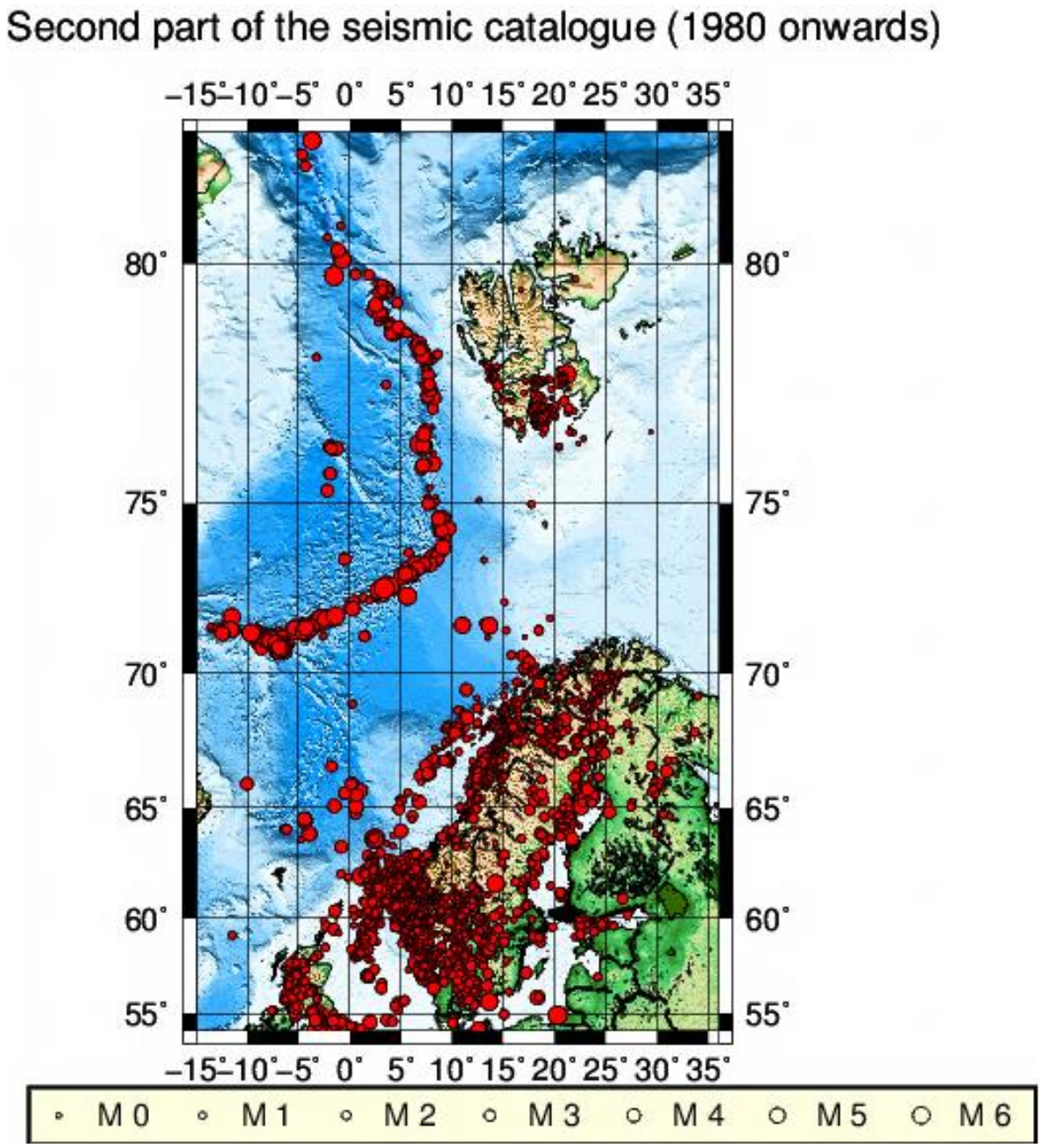

Figure 32: Seismicity is represented with the red color for the time period from 1980 and onwards. The seismicity that is represented is cleaned from probable explosions and one ends up with 6586 events.

Since the data constituting the second part (from 1980 and onwards) of the seismic catalogue is cleaned and prepared, one ends up having all parts of seismic catalogue. In that sense, compiled seismic catalogue consists of two parts:

- Seismic events within the prime area until 1980 with the minimum magnitude limit equal to 3.0 and larger;
- Seismic events within the prime area from 1980 and onwards with all aforementioned criteria applied.

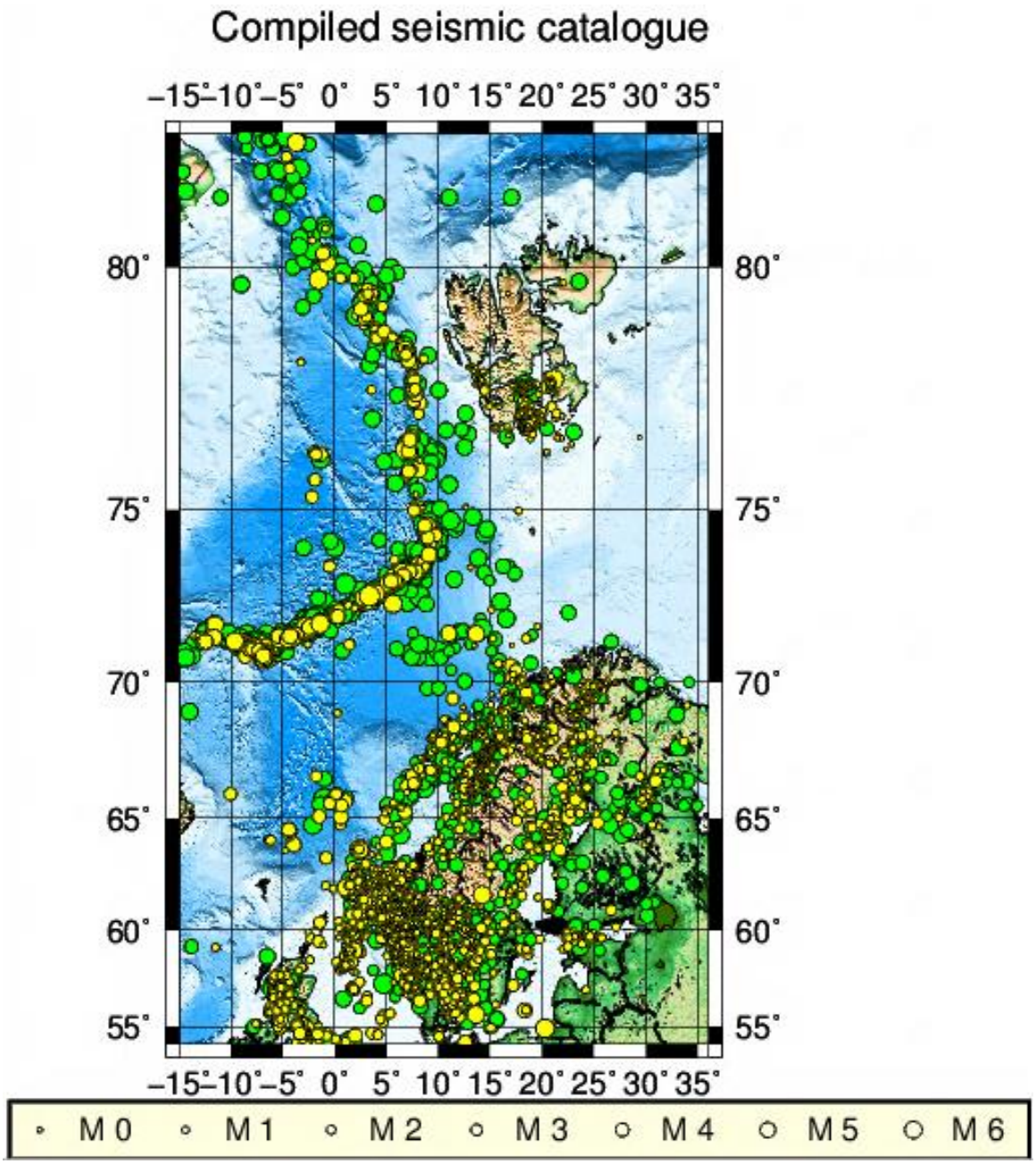

Figure 33: Compiled seismic catalogue with green color representing seismic data (first part of the catalogue) before 1980 and yellow color representing seismic data (second part of the catalogue) from 1980 and onwards.

After seismic catalogue was compiled and both parts of the catalogue were brought on Figures 33, one can see which seismic trend is represented by which color. Seismicity that is given by yellow color is more accurate meaning that one can rely on it. On the other hand, seismicity represented by green color does not have any restrictions, except the minimum magnitude that is equal to 3.0. Therefore, one should treat the data carefully considering reasonable range of inaccuracy. Total number of events compiling seismic catalogue is 7816. Final seismicity catalogue covering the periods before (green circles) and after 1980 (red circles) for Southern and Northern Norway (M>3) together with the faults (black) from Norwegian Petroleum Directorate are shown in Figures 34, 35.

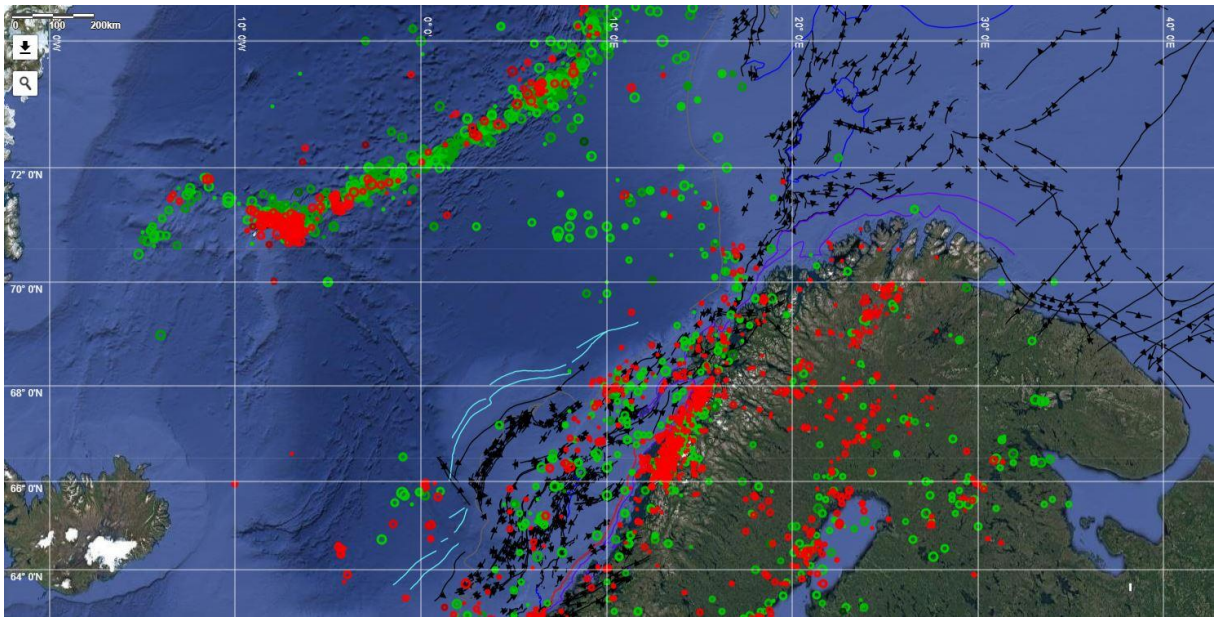

Figure 34: Final seismicity catalogue covering the periods before (green circles) and after 1980 (red circles) for Northern Norway (M>3). Faults shown in black are from Norwegian Petroleum Directorate database.

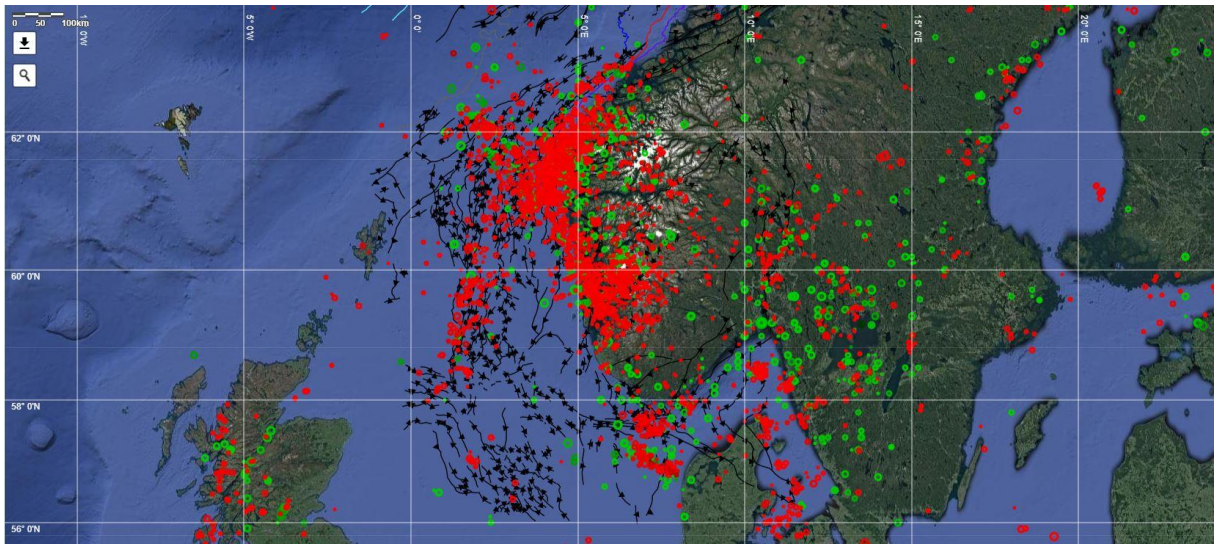

Figure 35: Final seismicity catalogue covering the periods before (green circles) and after 1980 (red circles) for Southern Norway (M>3). Faults shown in black are from Norwegian Petroleum Directorate database.

Steps done to compile seismic catalogue can be summarized and represented in Figure 36.

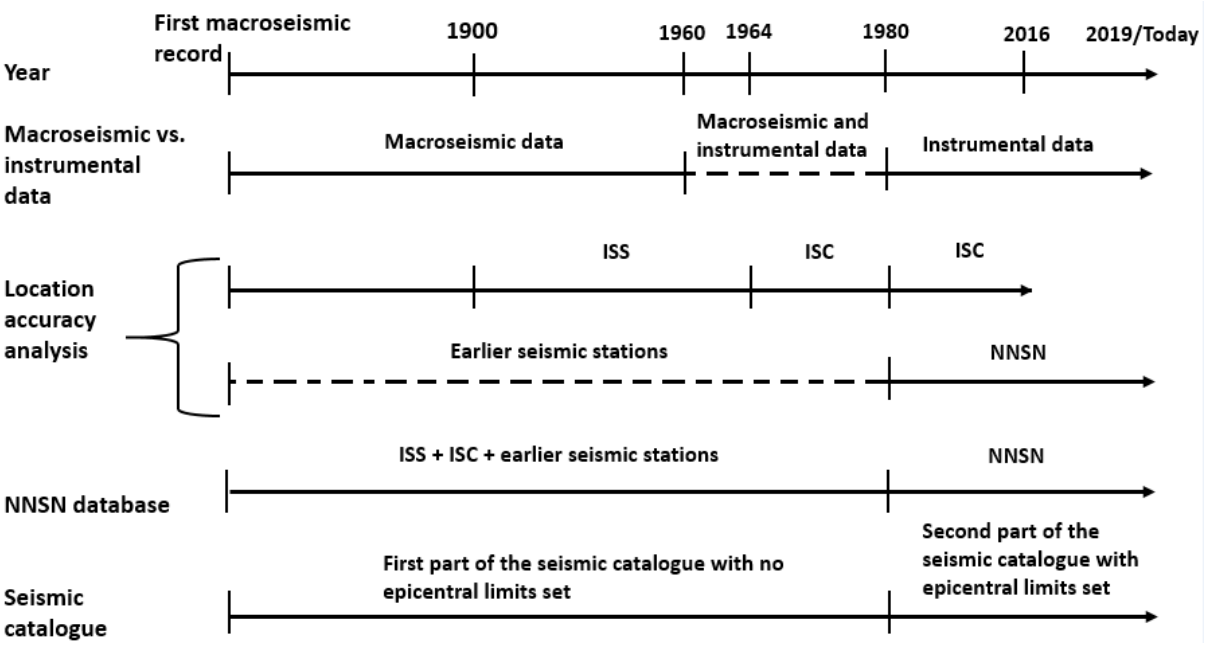

Figure 36: Representation of research made in the chapter Seismological data, and steps done to compile seismic catalogue.

1. Line – **Year** represents critical years influenced the development of the way seismic records were gathered, stored and rebuilt in Norway.
2. Line – **Macroseismic vs. instrumental data** represents the development from macroseismic to instrumental data. This section introduces background information necessary for overview of seismic records and their development in Norway. Based on this, one can make first division with critical years marking transitions from macroseismic to macroseismic and instrumental data in 1960; and from macroseismic and instrumental to instrumental data in 1980.
3. Lines – **Location accuracy analysis** represent two databases, in particular NNSN and ISC. First line introduces the development of ISC database, in particularly it shows the first seismic records were gathered by ISS starting form 1900's and only in 1964 ISC came into existence. The second line shows the development of NNSN that before 1980's mainly consisted of seismic records collected by early seismic stations. These seismic data were merged together constituting the base for NNSN. Therefore, there are two chains of events happening at the same time and hence two sets of data available. In that sense, the main aim of the section was to argue that the NNSN – local database, has all significant events ISC has.
4. Line – **NNSN database** introduces a choice made in favor of NNSN database. Critical date 1980's marks the onset of the time when NNSN consisted mostly of seismic data collected by the Norwegian seismic stations/networks. Based on this information, NNSN seismic data was divided in two. Seismic data before 1980's considered to be less accurate and reliable in comparison to the seismic data coming after 1980's.
5. Line – **Seismic catalogue** introduces the compiled seismic catalogue. The catalogue consists of two parts – the first part consists of seismic data with no epicentral error limits set before 1980's whereas the second part is made of seismic data with epicentral error limits set. After a number of tests made, it was seen that epicentral error limit of 0 – 20 km gives the best agreement between quality and quantity of the data.

5.4.3 Earthquake relocations for western Norway

The issue of accurate earthquake location has drawn attention of many scientist. There were studies done to investigate and test methods that enable to improve and locate seismic events more precisely. The intention of the following section is to introduce without going into details one of such methods – double-difference relocation method used in a work "Evaluation of seismicity in the area between the Troll field and the Øygarden fault" done by Tjåland and Ottemöller (2018). In this method earthquakes located relative to each other instead of being located one at a time. This enables to reduce the effect of velocity heterogeneities and arrival times of seismic waves (Waldhauser and Ellsworth, 2000). This is achieved by using differential travel-times derived from waveform cross-correlation. The results from this study, a catalogue of relocated earthquakes, will be lately used (chapter discussion) to determine reactivation potential of a fault using the method established (chapter 3 – Methodology). Afterwards, results obtained using seismic catalogue compiled in the thesis (chapter 5) and a catalogue of relocated earthquakes from Tjåland and Ottemöller (2018) studies will be compared. This will show whether relocated earthquakes help to set better correlation between fault and seismicity nearby it and hence whether better estimation of reactivation potential of a fault can be done. If it is the case and its effect is significant enough so that it can lead to different results, then the method would be highly recommended to apply to other Norwegian and adjacent areas to estimate reactivation potential of the faults. If it is not the case and results do not change much, then the criteria used to compile seismic catalogue in the following thesis can be applied to other similar to Norway, low-seismicity, regions.

5.4.4 Magnitude scales

Magnitude can be calculated using different scales depending on the distance to the earthquake and the type of instruments used. These different scales are partly a result of the historical development of magnitude scales in seismology. The main scales are Local Magnitude (M_L), Coda Magnitude (M_c), Body Wave Magnitude (m_b), Surface Wave Magnitude (M_s) and Moment Magnitude (M_w).

- M_L suits for events of magnitudes not larger than 6.0 – 7.0 and distances not larger than 1500 km; It is also the first magnitude scale defined (for California local earthquakes); and consequently all other magnitude scales are linked to M_L. It is measured from the maximum amplitude on a Wood-Anderson seismogram (Havskov and Ottemöller, 2010).
- M_c suits for events of magnitudes not large than 5.0 and distances not larger than 1500 km; It is measured from the duration of the earthquake signal (Havskov and Ottemöller, 2010).
- m_b suits for teleseismic events of magnitude no more than 7 and distances 20˚ - 100˚; It is measured from the P-wave amplitude at a period of around 1 s (Havskov and Ottemöller, 2010).
- M_s suits for teleseismic events of magnitudes not larger than 8.0 and distances 20˚ - 160˚; It is measured from the surface wave amplitude at a period of around 20 s (Havskov and Ottemöller, 2010).
- M_w suits for events of any magnitude and at any distance (Havskov and Ottemöller, 2010). It is calculated from the seismic moment.

Each magnitude scale has its own advantages and disadvantages that are thoroughly described in New Manual of Seismological Observatory Practice (NMSOP) (Bormann, 2002) and works done by Bormann and Saul (2008); Bormann and Saul (2009); Bormann et al. (2009). The main issue related to magnitude scales, except the M_w, is magnitude saturation. This means that when magnitude is high enough (the maximum value depends on magnitude scale), one cannot observe magnitude change since it reached its maximum threshold and now behaves constantly. M_L is the one that saturates first, around 6.5. The only magnitude scale that is not saturated is M_w. That is because it is calculated using seismic moment M_0 that is a "direct measure of the tectonic size and therefore does not saturate" (Havskov and Ottemöller, 2010). Consequently, M_w is used as a reference magnitude scale necessary for the comparison and the control of other magnitude scales behavior.

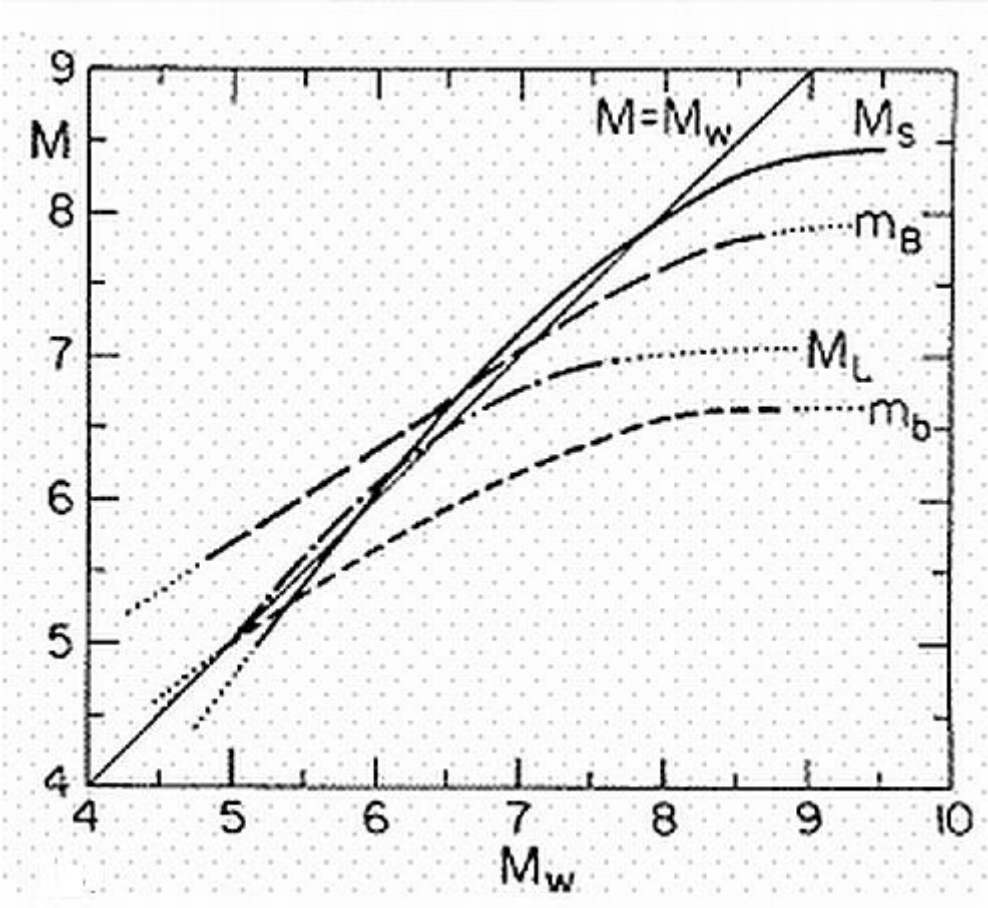

Figure 37: Comparison of moment magnitude scale to other magnitude scales (Modified picture from Kanamori, 1983).

As can be seen from Figure 37, for most of the magnitude scales there is a good agreement between the different scales for low and moderate magnitudes. A common practice in earthquake hazard assessment and when dealing with magnitudes of various magnitude types is to convert magnitude to one type to make the data homogeneous. However, since Norway experiences low to intermediate seismicity and the seismic catalogue that was compiled contains events within the magnitudes not larger than 6.1, this means there would not be significant difference in magnitudes when they are provided by different magnitude scales. Therefore, no attempts to make magnitude conversion will be made since seismic events in Norway are in the region where all magnitudes are in a good agreement with each other. For large significant events in Norway and adjacent offshore areas magnitude type and its exact magnitude value will be checked in the literature.

Magnitudes in the following work will be used to sort out significant seismic events (in the following study seismic events of magnitude equal to 3 and large will be considered) from the compiled seismic catalogue. Also, magnitude will be used to find out seismogenic potential of the active faults. This will be done by determining if the fault length matches the maximum magnitude of the earthquakes associated with the fault. In a case when seismic events characterized by significant magnitudes are lack, the maximum possible magnitude will be calculated using Wells and Coppersmith (1994) magnitude-length relations. After which calculated magnitude value will be assigned to the fault.

5.4.5 Focal mechanisms

The focal mechanisms contained in the NNSN database were not systematically updated with the newly revised fault plane solutions. Therefore, the fault plane solution for Norway and adjacent areas being in the prime area will be collected from several reliable sources and compiled in one catalogue. The most recent works done to revise the fault plane solutions are

- "Evaluation of seismicity in the Northern North Sea" by Tjåland and Ottemöller (2018)
- "Revision of fault plane solutions in the University of Bergen (UiB) seismic database, 1959 – 2001" by Sørensen (2002)
- Focal mechanisms prepared for NGU report 2018.010 "Neotectonics in Nordland – implications for petroleum exploration (NEONOR2)" by Michálek (2018).
- NNSN was searched from 2002 to 2019 for solution with more than 10 polarities and not included in the above.

For the Northern North Sea there are two sources of fault plane solutions available, one from the work done by Sørensen (2002) and the other one done by Tjåland and Ottemöller (2018), and hence one has to make a judgment which one to use. Since the work done by Tjåland and Ottemöller (2018) is the latest version of the revised fault plane solutions, it is the one that will be used for the analyses of the Northern North Sea. The total number of fault plane solutions from this work is 39 and they cover the area enclosed in latitude (59.1 – 62.6) ˚N and longitude (1.5 – 6.3) ˚E. The fault plane solutions for this area constitute the first part of the compiled catalogue. Remaining prime area is now searched for the solution in NNSN from 1959 to 2001. The total number of fault plane solutions for the remaining prime area is 88 and they are taken from the work done by Sørensen (2002) for the period 1959 – 2001 as they were found in the NNSN database. Fault plane solutions for this area constitute the second part of the compiled catalogue. The third part constituting the catalogue consists of fault plane solutions gathered for Lofoten area for the time period from 2014.01.09 to 2016.11.15 by Michálek (2018). The total number of fault plane solutions for this area is 82. The fourth part constituting the catalogue consists of 3 fault plane solutions from the NNSN database that was not present in any of the abovementioned work. They were revised. Consequently, compiled seismic catalogue with the fault plane solution data consists of 212 fault plane solutions.

5.5 Catalogue completeness

When the final catalogue is compiled, one can make quantitative statistics of the data constituting the catalogue. This enables to get an overall feeling of the data, its type and distribution over the time

periods. Parameters that will be investigated and, in particular are important for the study, are frequency of seismic events in time and types of magnitude and their distribution over time. Statistics on these parameters enables to discuss changes happened over time, the way it influences the data quality and quantity that is characteristic/typical for the specific time interval. Consequently, conclusions regarding each parameter and its variation or non-variation over the time period will be regarded. Such statistics provides deeper insight into the data one deal with, its structure and help to reach concrete conclusions based not only on qualitative analysis but also supported quantitatively.

5.5.1 Frequency of seismic events in time

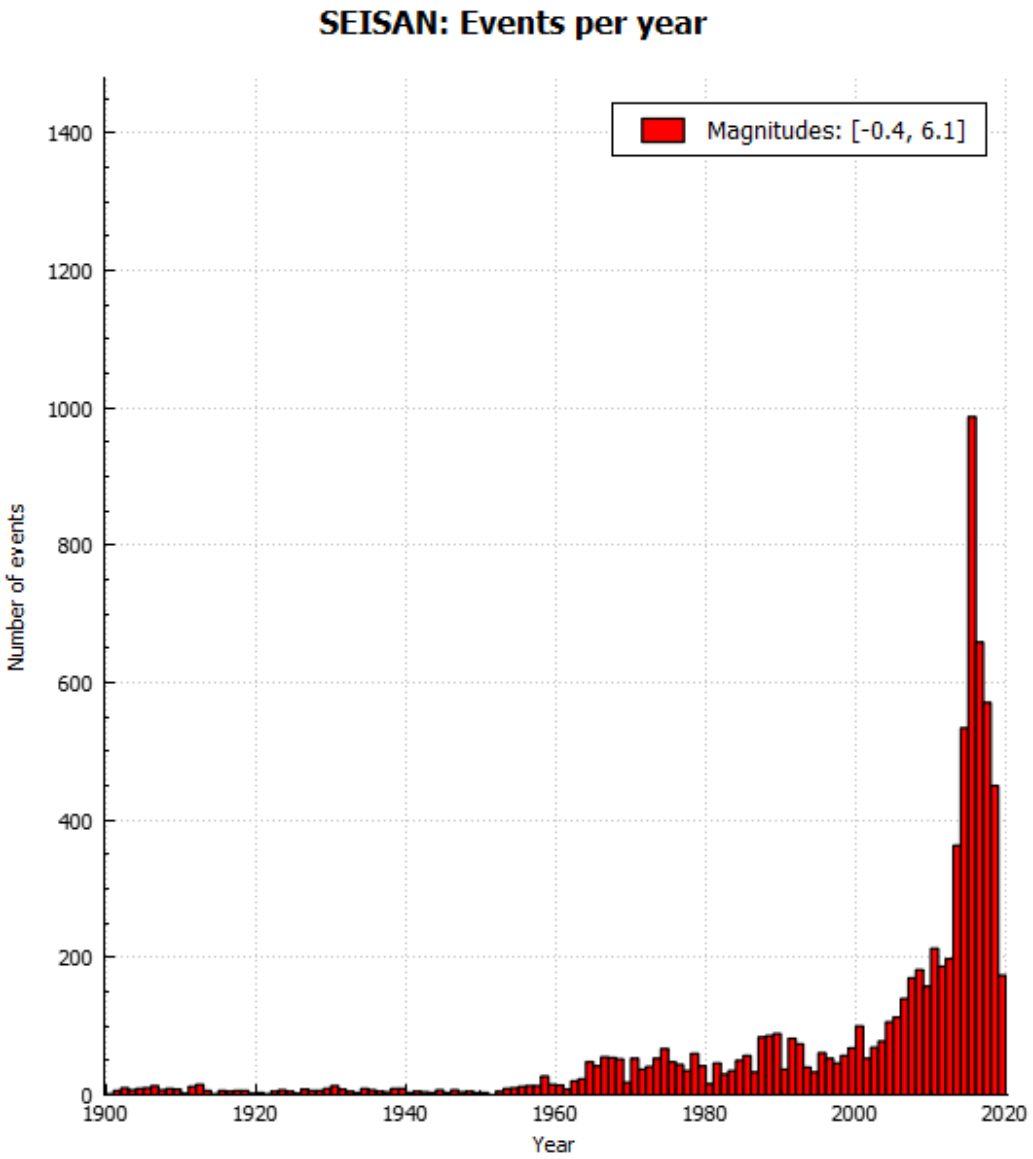

Figure 38: Frequency of seismic events in time.

Figure 38 shows statistics of seismic events in Norway recorded each year starting from 1900 and onwards. As it is seen from this figure, one can distinguish three major periods. The first one starts from 1900's and lasts until 1960's. Number of seismic events recorded for this time period is relatively small. As it can be seen from this figure, no more than 25 seismic records of magnitude equal to 3.0

and larger were recorded each year. That is explained by macroseismic records that were collected in Norway and as a result gives that poor statistics for the time period 1900 – 1964. The second period starts from 1960's and continues until 1980's. The number of seismic events recorded of magnitude equal 3.0 and larger in comparison with the first period is twice large. As it can be seen from the Figure 38, average number of earthquakes recorded each year is approximately 50. That is explained by the appearance of instrumental data from 1960's that positively influenced the statistics of recorded seismic events and increase it twice. The third period begins from 1980's and onwards shows the highest number of seismic events recorded each year. In comparison with the first two periods the number of seismic events recorded increased dramatically, in particular, this sharp increase can be seen from 2000's. As can be seen from the Figure 38, number of earthquakes detected increases each year starting from 100, 200, 350, 550 and goes until almost 1000 seismic events recorded. That is explained by the rapid development of seismic stations in Norway and its adjacent areas and rapid development of instrumental data.

5.5.2 Magnitude vs. time

When performing search using select and not specifying the desired scale of magnitude the output will be with no, one or several magnitude scales available. While building seismic catalogue, no magnitude specification was set meaning that one ends up with all available magnitude scales for seismic events. Statistics made for main magnitude types constituting the compiled seismic catalogue enables to reveal magnitude scale tendencies over the time period considered.

Moment magnitude – M_w

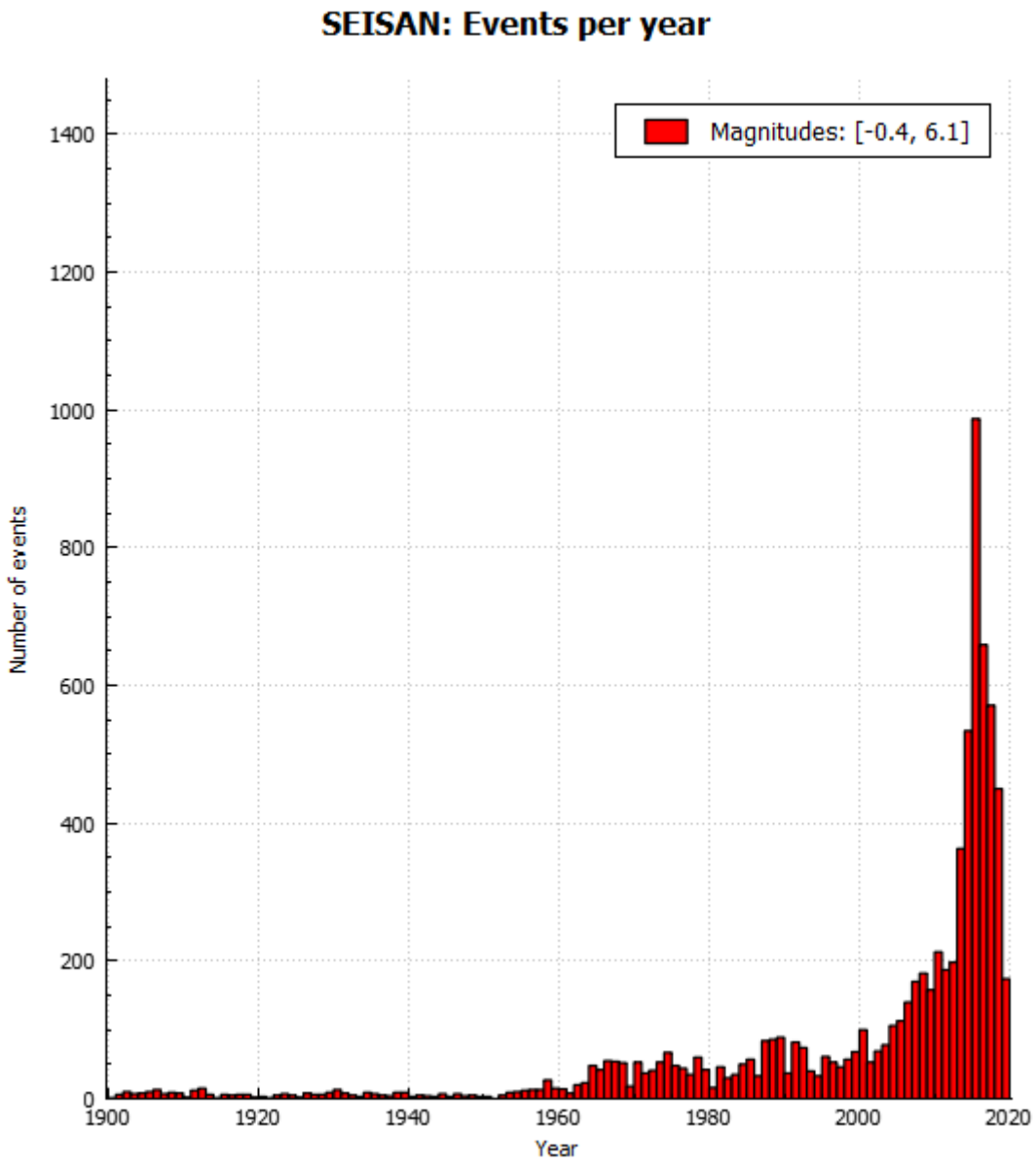

Figure 39: Moment magnitude vs. number of events recorded per year.

From Figure 39 it is seen that the moment magnitude in Norway was calculated starting from 1900 and onwards. According to the statistics represented on the plot, M_w had relatively constant poor statistics from 1900 to 1960 with the average number of events calculated per year not exceeding 20. For the time period from 1960 to 1980's number of events calculated each year for the M_w magnitude scale increased trice. Starting from 1980's to 2014 M_w had sharp positive statistics growth.

Local magnitude – M_L

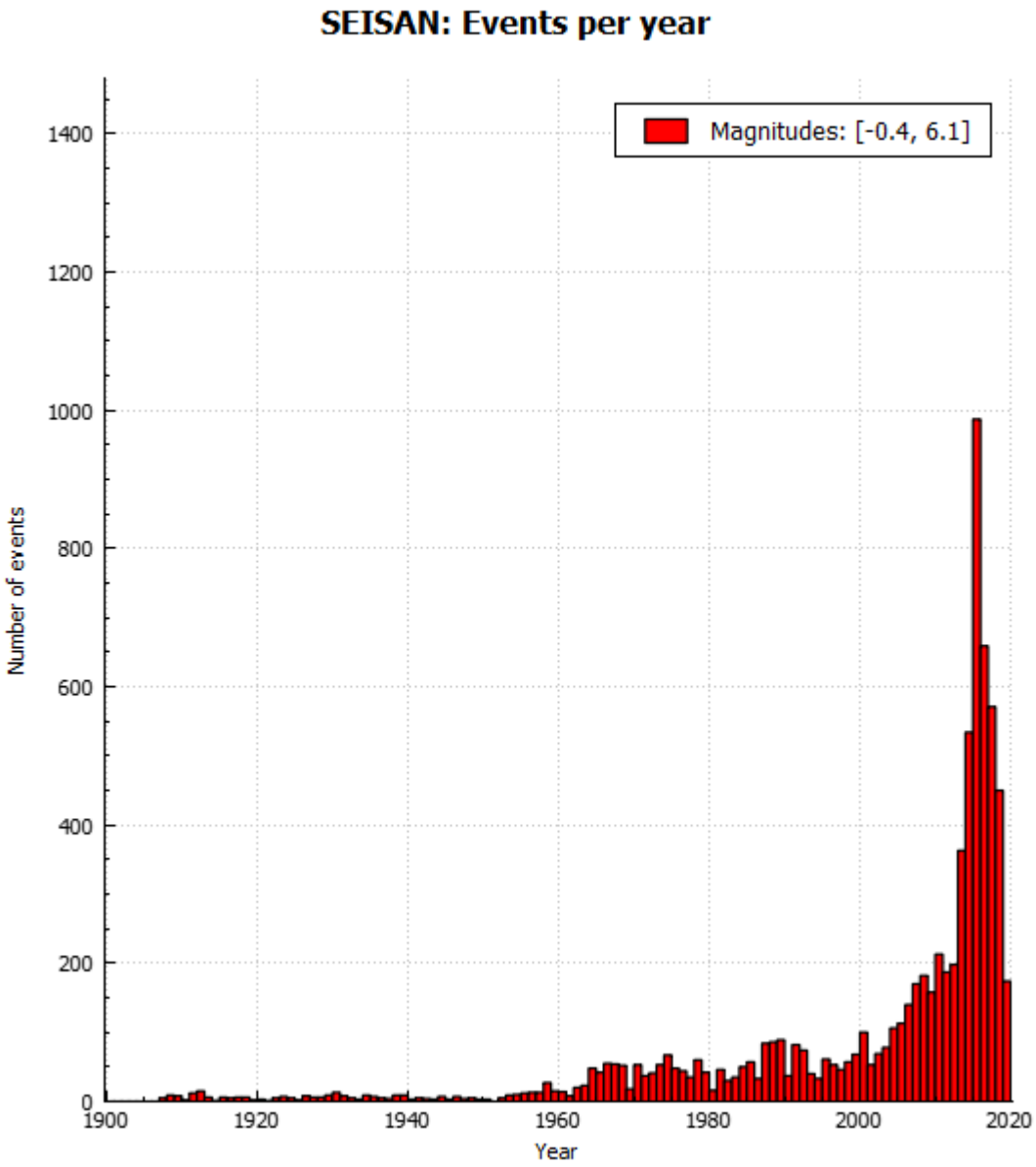

Figure 40: Local magnitude vs. number of events recorded per year.

As can be seen from Figure 40, local magnitudes in Norway was recorded starting from 1907 and onwards. One can trace similar trends to the ones observed for moment magnitude for the periods 1900 – 1960, 1960 – 1980 and 1980 – onwards.

Coda magnitude – M_c

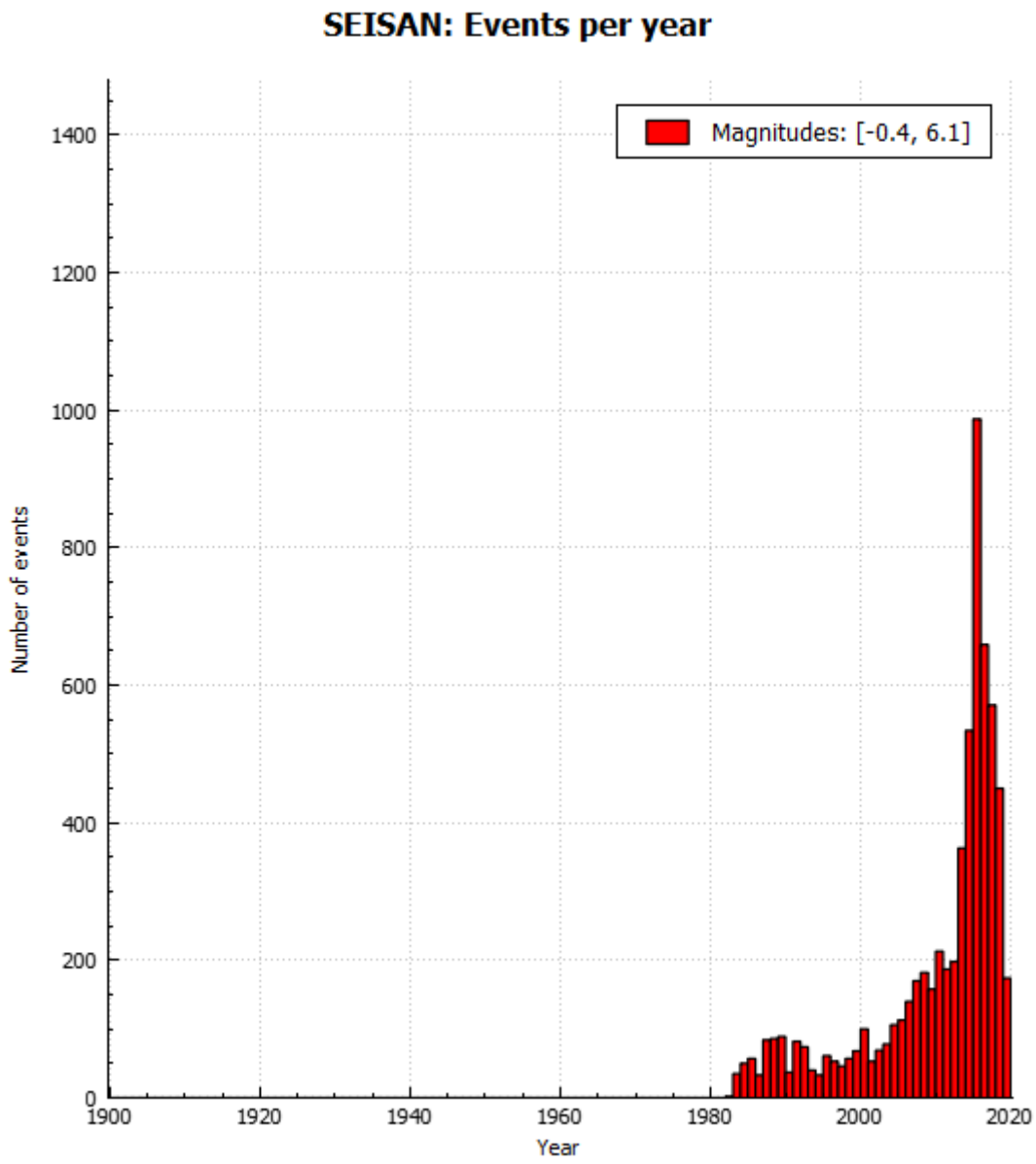

Figure 41: Coda magnitude vs. number of events recorded per year.

Coda magnitude records in Norway appeared starting from 1980's and onwards (Figure 41). Period from 1980's until the present time is characterized by the same trend observed for moment magnitude.

Body wave magnitude – m_b

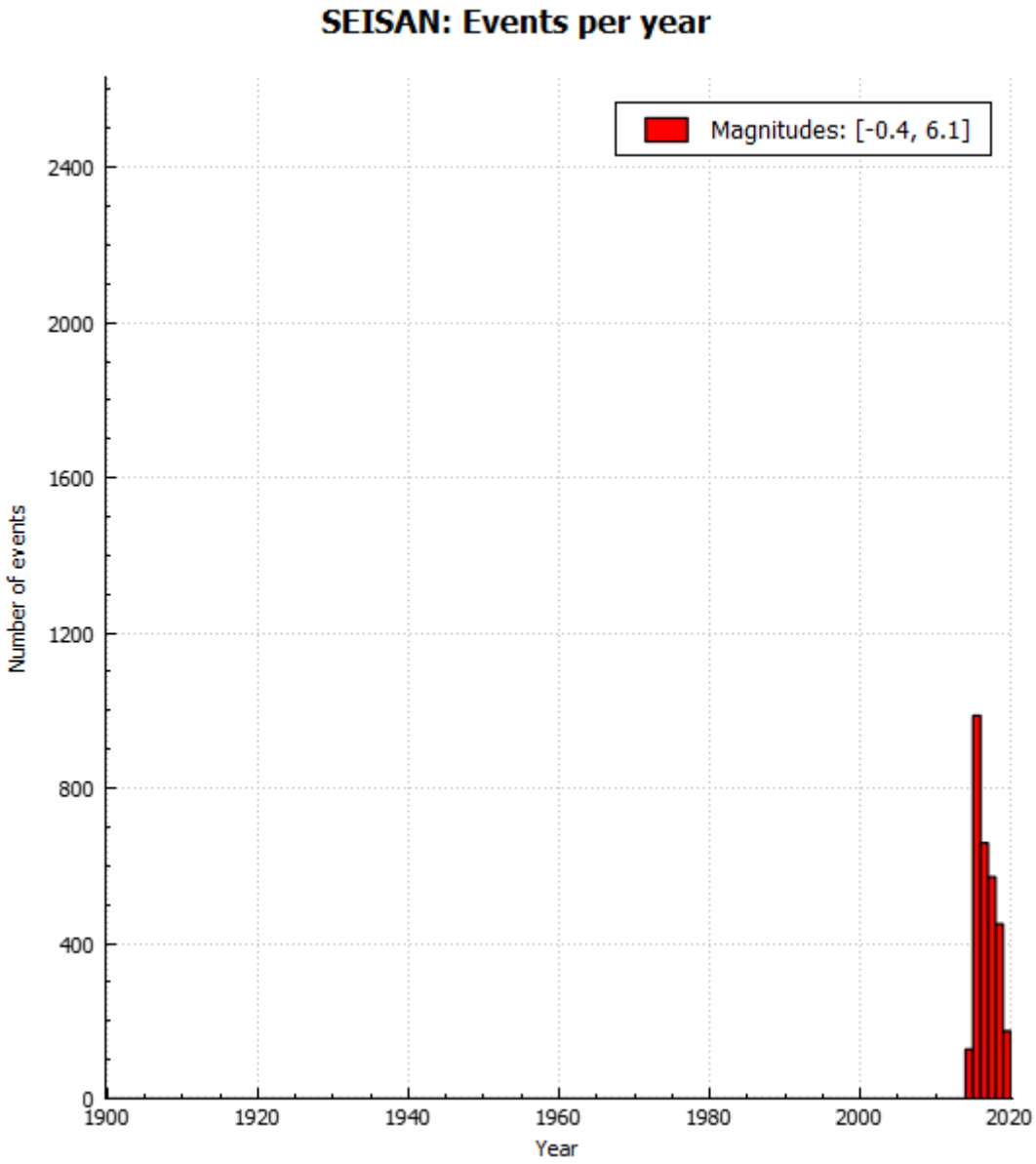

Figure 42: Body wave magnitude vs. number of events recorded per year.

Body wave magnitude in Norway is relatively recent magnitude scale, as can be seen from Figure 42, this appeared starting from 2015 and continues until the present time. From this figure it is seen the sharp increase in number of events recorded each year. The highest number of events recorded is equal to approximately 1000 in a year 2015.

Surface Wave magnitude – M_s

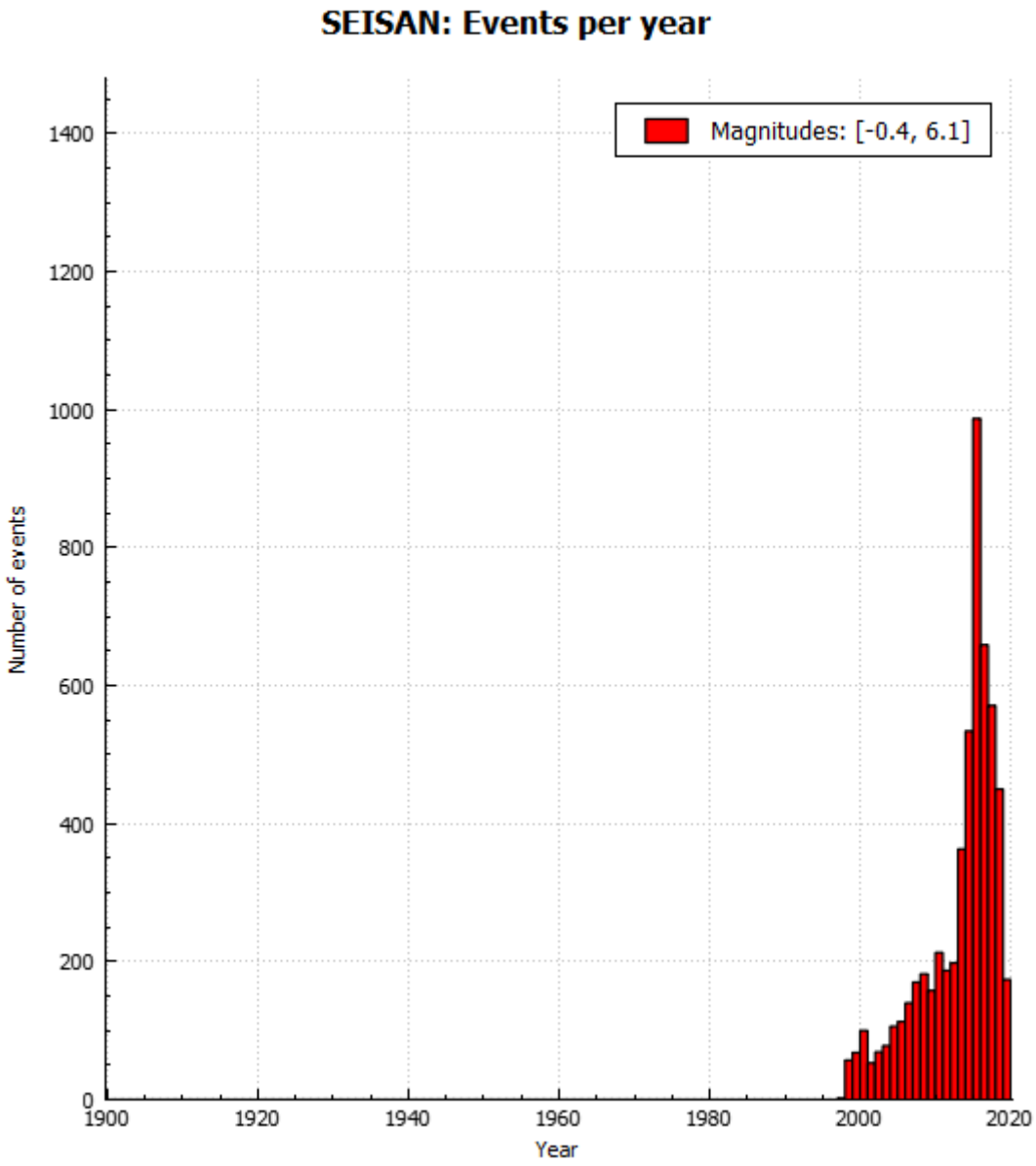

Figure 43: Surface wave magnitude vs, number of events recorded per year.

Surface wave magnitude records in Norway started being recorded from 2000's and continues onwards. This positive trend of sharp increase of seismic events being recorded each year is shown in Figure 43.

Main magnitude scales constituting seismic catalogue are summarized in Table 13.

Table 13: Main magnitude scales constituting seismic catalogue.

Magnitude scale	Time span
M_w	1900 – onwards
M_L	1907 – onwards
M_c	1980's – onwards
m_b	2015 – onwards
M_s	2000's – onwards

5.6 Zonation

Based on tectonostratigraphy, geological, seismological and geophysical data six zones have been established. These are

- **North Sea – Zone-01**

North Sea is a shallow intracratonic basin formed during Triassic-Cretaceous rifting, mostly accommodates shallow intra-platform sedimentary basins, platforms and basin flank zones. Major geological structures lying in the North Sea are Central, Viking and Horn grabens. Large-scale faults, fault zones and complexes are listed in Table 14 that comes at the end of this section. Level of seismicity in the Northern North Sea is very high and, on the contrary, very low in the Southern North Sea.

- **Onshore Southern Norway – Zone-02**

Onshore southern Norway is mostly made of undisturbed Precambrian basement rocks, Precambrian basement, sedimentary and metamorphic rocks influenced by Caledonian episodes, Permian extrusive and plutonic rocks in the Oslo area and Devonian sedimentary rocks. Major geological structures are Caledonian thrust belts, Oslo graben and detachment Devonian structures. Large-scale faults, fault zones and complexes are listed in Table 14 that comes at the end of this section. Level of seismicity is high.

- **Norwegian Sea – Zone-03**

Norwegian Sea is a deep sedimentary basin formed during Cretaceous-Paleocene rifting, mostly accommodates deep sedimentary basins along with platform areas, highs, Cenozoic domes and magmatic crust. Major geological structures lying in the Norwegian Sea are Møre and Vøring basins, Trøndelag platform, Møre and Vøring marginal highs, Lofoten-Vesterålen shelf and slope. Large-scale faults, fault zones and complexes are listed in Table 14 that comes at the end of this section. Level of seismicity is high.

- **Onshore Mid Norway – Zone-04**

Onshore Mid Norway is mostly made of metamorphic, magmatic and Precambrian basement rocks influenced by Caledonian episodes. Major geological structures are Caledonian thrust belts. Large-scale faults, fault zones and complexes are listed in Table 14 that comes at the end of this section. Level of seismicity is low in the southern part and very high in the northern part due to earthquakes swarms.

- **Barents Continental Shelf – Zone-05**

Barents continental shelf is a sediment-covered intracratonic basin formed during Jurassic-Tertiary rifting followed by later uplift. Barents continental shelf mostly accommodates deep sedimentary basins along with highs and platforms. Major geological structures are Harstad, Troms and Bjørnøya basins, Vestbakken volcanic province. Large-scale faults, fault zones and complexes are listed in Table 14 that comes at the end of this section. Level of seismicity is very low.

- **Onshore Northern Norway – Zone-06**

Onshore northern Norway is mostly made of thrust nappes of late Proterozoic origin influenced by Caledonian episodes, undisturbed Precambrian basement and partly metamorphic and magmatic units effected by Caledonian episodes. Major geological structure is Caledonian thrust belts. Level of seismicity is low except the eastern part (Stuoragurra fault and Mierujavri-Sværholt shear zone).

Compilation of faults, fault zones and complexes and assigned to them zones are summarized in Table 14.

Table 14: Six zones established and faults, fault zones and complexes that belong to them.

Onshore Faults/Fault Zones	Offshore Faults/Fault Zones
	Sorgenfrei-Tornquist Fault
	Fjerritslev Fault Zone
	Central Graben Eastern Boundary Fault
	Central Graben Western Boundary Fault
	Øygarden Fault Zone
	Viking Graben Eastern Boundary Fault
	Viking Graben Western Boundary Fault
	Horn Graben Eastern Boundary Fault
	Horn Graben Western Boundary Fault
Oslo Graben Eastern boundary Fault	
Oslo Graben Western boundary Fault	
Skagerrak Graben Eastern boundary Fault	
Skagerrak Graben Western boundary Fault	
Fedafjord Fault	
Porsgrunn-Kristiansand Fault	
Mandal-Ustaoset Fault Zone	
Stord-Bømlo-Karmøy Fault Zone	
Røldal Shear Zone	
Hardangerfjord Shear Zone	
Lærdal-Gjende Fault Complex	
Bergen Arc Shear Zone	
Solund Detachment Fault	
Kvamshesten Detachment Fault	
Håsteinen Detachment Fault	
Hornelen Detachment Fault	
	Fles Fault Complex
	Vesterdjupet Fault Zone
	Helland-Hansen Arch Eastern Boundary Fault
	Klakk Fault Complex
	Ytreholmen Fault Zone
	Revfallet Fault Complex
	Faeroe-Shetland Escarpment
	East Jan Mayen Fracture Zone
	Vøring Plateau Escarpment
	Lofoten-Vesterålen Margin
	Utrøst Ridge NW Boundary Fault
	Bremstein – Vingleia Fault Complex
Møre-Trøndelag Fault Zone	
Nesna Shear Zone	
Værangfjord-Nordfjord Fault	
Meloyfjord Fault	
Meloy-Glomtfjorden Fault	
Skjærstadfjord Fault	
Sagfjord Shear Zone	
	Senja Fracture Zone
	Troms-Finnmark Fault Complex
	Ringvassøy-Loppa Fault Complex
	Bjørnøyrenna Fault Complex
	Leirdjupet fault
	Hornsund Fault Zone
Vestfjorden-Vanna Fault	
Kvaløysletta-Straumhella Fault	
Vargsund Fault	
Mierujavri-Sværholt Shear Zone	
Stuoragurra Fault	
Trollfjorden-Komagelva Fault Zone	

6 Results and interpretation

6.1 North Sea

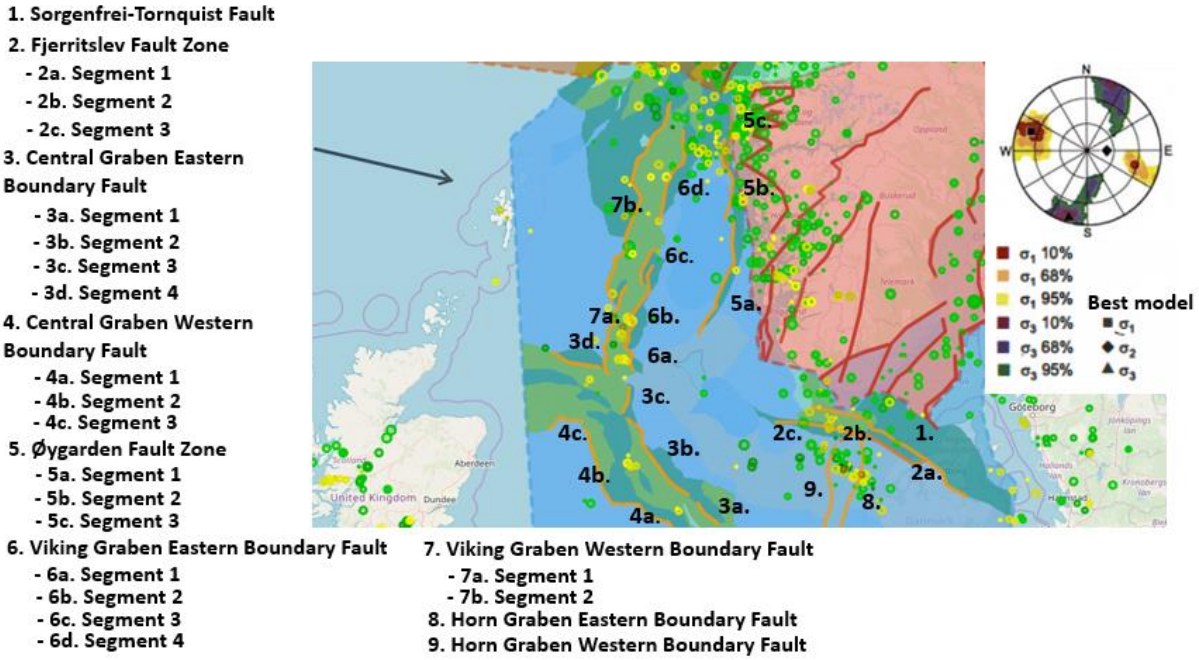

Figure 44: North Sea Zone is represented by light blue color. Faults and segments in the North Sea chosen for the analysis are represented with the orange color. Seismicity from 1980 onwards represented by yellow circles whereas seismicity for the period preceding 1980 represented with the green circles. The size of a circle is proportional to the magnitude of the event. Circle at the right upper corner represents stress model generated as a result from the inversion of earthquake focal mechanism solutions. The yellow, green and red areas represent 95%, 68% and 10% confidence limits respectively (Hicks et al., 2000).

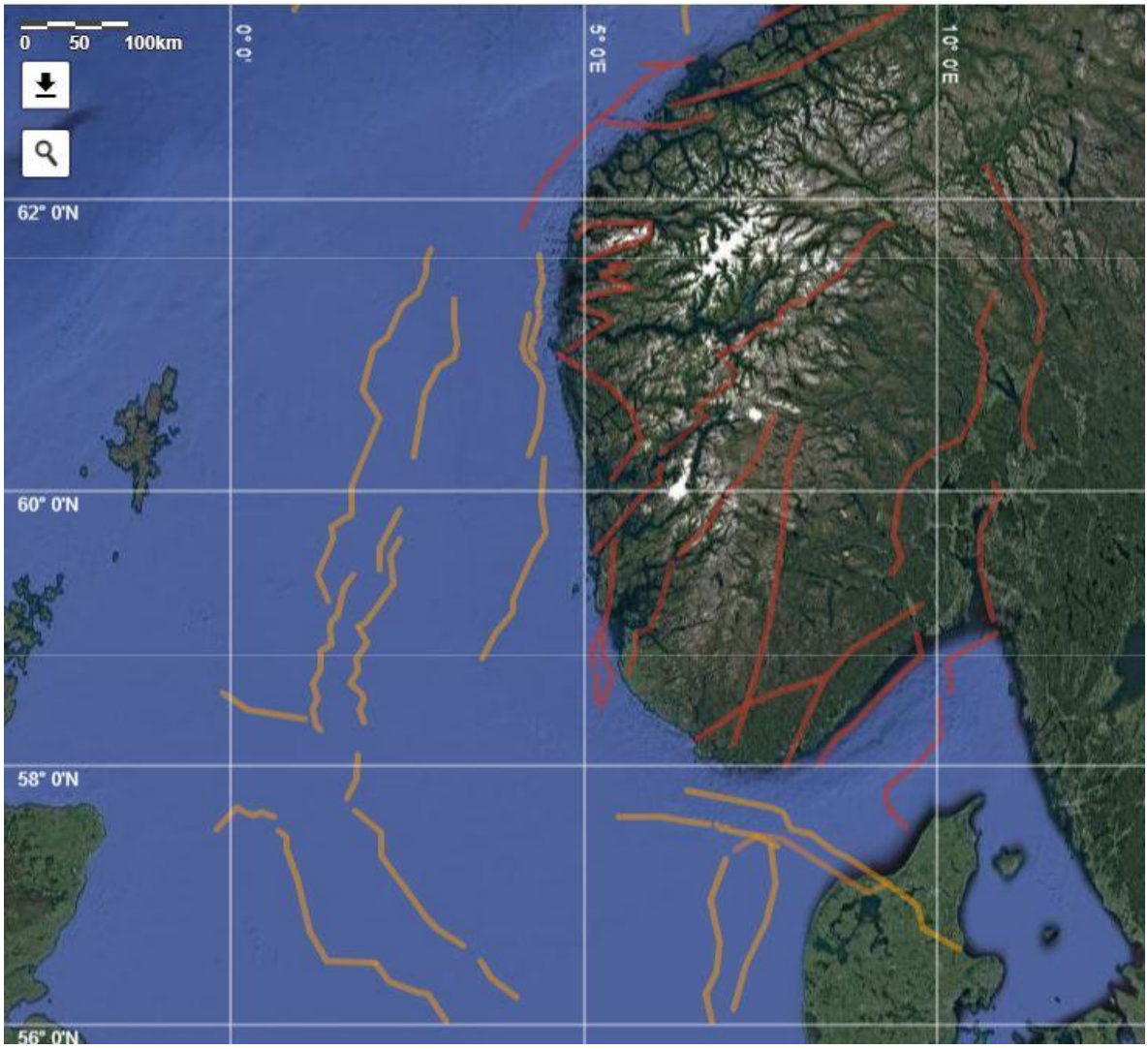

Figure 45: Location of the significant faults in the North Sea.

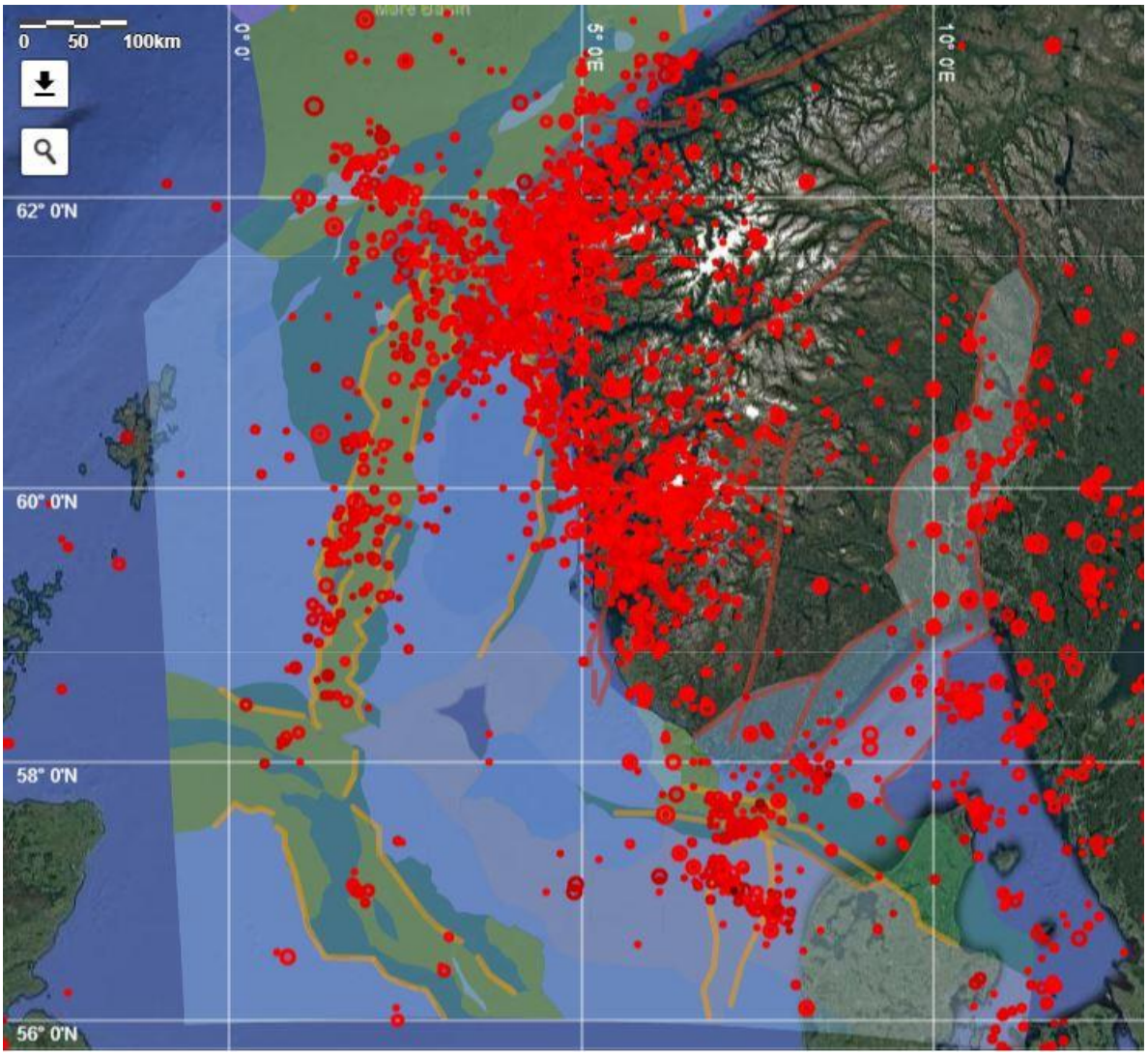

Figure 46: Location of the significant faults in the North Sea, shown together with the main structural elements (in color-shaded areas) from NPD and the seismicity (since 1980) from NNSN (red circles).

In total seven faults and two fault zones have been analyzed, with 22 segments. Distribution of these faults in the North Sea is as follows (see Figures 44, 45 and 46):

- Two fault zones, Sorgenfrei-Tornquist fault and Fjerritslev fault zones, with the WNW-ESE strike cut across Kattegat Sea, northern Denmark and Skagerrak area.
- Two faults bounding Central Graben with dominant NW-SE strike located in the central North Sea. These are the Central Graben eastern boundary and the Central Graben western boundary faults.
- Two faults bounding Viking Graben with NNE-SSW strike are nearly parallel to the western coast of mainland Norway. These are the Viking Graben eastern boundary and the Viking Graben western boundary faults.
- Two faults bounding Horn Graben with NNE-SSW strike are nearly parallel to the western coast of Denmark.
- Øygarden fault zone with WNW strike runs parallel to the western coast of mainland Norway.

Table 15: Geological data for the North Sea zone. Abbreviation *Surf. P. of the W.* in the column *Fault Dimensions* stands for surface projection of the width.

Fault ID	Fault Name	Segment ID	Seg. Name	Fault location				Fault dimesions			Fault orientation			Max possible	References
				End point-1		End point-2		Length	Surf. P. of the W.	Width	Strike	Dip	Slip	Magnitude	
				Lat	Lon	Lat	Lon	km	km	km					
Z-01-F01	Sorgenfrei-Tornquist Fault	Z-01-F01-S01	Seg-01	56,6078	10,3271	57,8184	6,4599	285,00	5,00	29,00	WNW-ESE	80 °SW	dextral strike-slip	7,9	Ramberg et al., 2007
Z-01-F02	Fjerritslev Fault Zone	Z-01-F02-S01	Seg-01	57,0817	9,2779	57,3733	7,1081	146,00	5,00	29,00	WNW-ESE	80 °NW	dextral strike-slip	7,6	Ramberg et al., 2007
		Z-01-F02-S02	Seg-02	57,3792	7,7563	57,5479	6,8664	58,00	5,00	29,00	WNW-ESE	80 °NW	dextral strike-slip	7,1	Faleide et al, 2010
		Z-01-F02-S03	Seg-03	57,5538	6,7895	57,6083	5,4684	80,00	5,00	29,00	WNW-ESE	80 °NW	dextral strike-slip	7,3	Faleide et al, 2010
Z-01-F03	Central Graben Eastern B. F.	Z-01-F03-S01	Seg-01	56,2487	4,0465	56,5013	3,5211	44,00	10,00	29,00	NW-SE	70 °SW	normal	7,0	Ramberg et al., 2007
		Z-01-F03-S02	Seg-02	56,6228	3,2794	57,6577	1,7578	153,00	10,00	29,00	NW-SE	70° SW	normal	7,7	Faleide et al, 2010
		Z-01-F03-S03	Seg-03	57,7448	1,6644	58,0907	1,7935	39,00	9,00	26,00	N-S	70° W	normal	7,0	Faleide et al, 2010
		Z-01-F03-S04	Seg-04	58,3405	1,0437	58,5419	-0,1647	75,00	9,00	26,00	WNW-ESE	70° S	normal	7,3	Faleide et al, 2010
Z-01-F04	Central Graben Western B. F.	Z-01-F04-S01	Seg-01	56,0091	3,0541	56,4843	2,0599	86,00	10,00	29,00	NW-SE	70 ° NE	normal	7,4	Ramberg et al., 2007
		Z-01-F04-S02	Seg-02	56,4881	2,0462	57,4956	0,6591	166,00	10,00	29,00	NNW-SSE	70 °NE	normal	7,8	Faleide et al, 2010
		Z-01-F04-S03	Seg-03	57,6069	0,6372	57,5126	-0,2087	58,00	10,00	29,00	WNW-ESE	70 °NE	normal	7,2	Faleide et al, 2010
Z-01-F05	Øygarden Fault Zone	Z-01-F05-S01	Seg-01	58,7908	3,5156	60,2458	4,4384	175,00	10,00	29,00	NNE-SSW	70°WNW	normal	7,8	Ramberg et al., 2007
		Z-01-F05-S02	Seg-02	60,2445	4,2077	61,2197	4,2242	115,00	9,00	26,00	NNE-SSW	70°WNW	normal	7,6	Faleide et al, 2010
		Z-01-F05-S03	Seg-03	60,9083	4,2956	61,6401	4,3560	85,00	9,00	26,00	NNE-SSW	70°WNW	normal	7,4	Faleide et al, 2010
Z-01-F06	Viking Graben Eastern B. F.	Z-01-F06-S01	Seg-01	58,3204	1,8566	59,0135	1,0810	92,00	10,00	29,00	NNE-SSW	70° WNW	normal	7,4	Ramberg et al., 2007
		Z-01-F06-S02	Seg-02	59,0310	1,8017	59,6634	2,3826	83,00	9,00	26,00	NNE-SSW	70° WNW	normal	7,4	Faleide et al, 2010
		Z-01-F06-S03	Seg-03	59,4363	2,1203	59,8639	2,3840	53,00	9,00	26,00	NNE-SSW	70° WNW	normal	7,1	Faleide et al, 2010
		Z-01-F06-S04	Seg-04	60,2472	2,5817	61,3518	3,1475	141,00	8,00	23,00	NNE-SSW	70° WNW	normal	7,7	Faleide et al, 2010
Z-01-F07	Viking Graben Western B. F.	Z-01-F07-S01	Seg-01	58,2617	1,2744	59,3938	1,7303	140,00	10,00	29,00	NNE-SSW	70° ESE	normal	7,7	Ramberg et al., 2007
		Z-01-F07-S02	Seg-02	59,1837	1,4062	61,6748	2,8234	311,00	9,00	26,00	NNE-SSW	70° ESE	normal	8,2	Faleide et al, 2010
Z-01-F08	Horn Graben Eastern B. F.	Z-01-F08-S01	Seg-01	56,1012	7,0532	57,4027	7,6245	150,00	10,00	29,00	NNE-SSW	70°WNW	normal	7,7	Ramberg et al., 2007
Z-01-F09	Horn Graben Western B. F.	Z-01-F09-S01	Seg-01	55,9534	6,8005	57,3015	7,0092	157,00	10,00	29,00	NNE-SSW	70°ESE	normal	7,8	Ramberg et al., 2007

Table 16: Seismological data for the North Sea zone.

Fault ID	Fault Name	Segment ID	Seg. Name	#earthquakes	Max observed magnitude		Focal mechanism					Regional stress tensor						D. to Moho
					Historical	Instrumental	Nodal Plane 1			Nodal plane 2			Sigma 1		Sigma 2		Sigma 3		
					Before 1980	After 1980	Strike	Dip	Rake	Quality	Strike	Dip	Rake	Azimuth	Plunge	Azimuth	Plunge	Azimuth	Plunge	
Z-01-F01	Sorgenfrei-Tornquist Fault	Z-01-F01-S01	Seg-01	5	4,0	3,6	NA	NA	NA	NA	NA	NA	NA	NA	NA	NA	NA	NA	NA	30,00
Z-01-F02	Fjerritslev Fault Zone	Z-01-F02-S01	Seg-01	2	3,0	3,1	NA	NA	NA	NA	NA	NA	NA	NA	NA	NA	NA	NA	NA	30,00
		Z-01-F02-S02	Seg-02	4	NA	4,2	NA	NA	NA	NA	NA	NA	NA	NA	NA	NA	NA	NA	NA	30,00
		Z-01-F02-S03	Seg-03	5	4,5	4,2	NA	NA	NA	NA	NA	NA	NA	NA	NA	NA	NA	NA	NA	30,00
Z-01-F03	Central Graben Eastern B. F.	Z-01-F03-S01	Seg-01	0	NA	NA	NA	NA	NA	NA	NA	NA	NA	NA	NA	NA	NA	NA	NA	27,50
		Z-01-F03-S02	Seg-02	0	NA	NA	NA	NA	NA	NA	NA	NA	NA	NA	NA	NA	NA	NA	NA	27,50
		Z-01-F03-S03	Seg-03	0	NA	NA	NA	NA	NA	NA	NA	NA	NA	NA	NA	NA	NA	NA	NA	25,00
		Z-01-F03-S04	Seg-04	1	3,0	NA	NA	NA	NA	NA	NA	NA	NA	NA	NA	NA	NA	NA	NA	25,00
Z-01-F04	Central Graben Western B. F.	Z-01-F04-S01	Seg-01	0	NA	NA	NA	NA	NA	NA	NA	NA	NA	NA	NA	NA	NA	NA	NA	27,50
		Z-01-F04-S02	Seg-02	0	NA	NA	NA	NA	NA	NA	NA	NA	NA	NA	NA	NA	NA	NA	NA	27,50
		Z-01-F04-S03	Seg-03	1	NA	3,3	NA	NA	NA	NA	NA	NA	NA	NA	NA	NA	NA	NA	NA	27,50
Z-01-F05	Øygarden Fault Zone	Z-01-F05-S01	Seg-01	4	4,5	3,0	125,5000	82,5000	-156,3000	B	32,2200	66,5200	-8,1800	289	21	90	68	196	7	27,50
							112,1000	62,2000	-48,6000	C	229,9800	48,4300	-141,4400	289	21	90	68	196	7	27,50
							111,9000	62,0000	-49,5000	NA	230,7000	47,8200	-140,6900	289	21	90	68	196	7	27,50
		Z-01-F05-S02	Seg-02	12	3,8	3,7	122,1400	81,4600	-34,0700	NA	217,87	56,3600	-169,7200	289	21	90	68	196	7	25,00
							173,9000	52,9000	65,5000	B	30,9700	43,4700	118,7400	289	21	90	68	196	7	25,00
		Z-01-F05-S03	Seg-03	15	4,3	3,6	150,0000	70,0000	90,0000	B	330,0000	20,0000	90,0000	289	21	90	68	196	7	25,00
							75,4000	52,8000	16,0000	D	335,5600	77,3200	141,7000	289	21	90	68	196	7	25,00
							184,5000	60,6000	78,4000	B	27,1900	31,4100	109,6400	289	21	90	68	196	7	25,00
							150,0000	10,0000	90,0000	D	330,0000	80,0000	90,0000	289	21	90	68	196	7	25,00
Z-01-F06	Viking Graben Eastern B. F.	Z-01-F06-S01	Seg-01	10	3,0	4,7	122,1400	81,4600	-34,0700	NA	217,87	56,3600	-169,7200	289	21	90	68	196	7	27,50
							158,0000	56,0000	-11,0000	C	254,2000	80,9000	-145,5100	289	21	90	68	196	7	27,50
		Z-01-F06-S02	Seg-02	0	NA	NA	NA	NA	NA	NA	NA	NA	NA	289	21	90	68	196	7	25,00
		Z-01-F06-S03	Seg-03	0	NA	NA	NA	NA	NA	NA	NA	NA	NA	289	21	90	68	196	7	25,00
		Z-01-F06-S04	Seg-04	7	4,5	3,9	118,9000	68,4000	-134,1000	B	8,1000	48,1100	-29,6400	289	21	90	68	196	7	22,50
							319,6000	84,4000	-7,1000	C	50,3000	82,9300	-174,3600	289	21	90	68	196	7	22,50
							123,2000	28,0000	-43,2000	D	252,8600	71,2500	-111,1900	289	21	90	68	196	7	22,50
Z-01-F07	Viking Graben Western B. F.	Z-01-F07-S01	Seg-01	7	3,6	3,9	NA	NA	NA	NA	NA	NA	NA	289	21	90	68	196	7	27,50
		Z-01-F07-S02	Seg-02	11	5,3	3,5	326,9100	56,1700	-22,7600	NA	70,0600	71,2500	-143,9900	289	21	90	68	196	7	25,00
							51,4000	67,6000	117,9000	C	177,1400	35,2100	47,3700	289	21	90	68	196	7	25,00
							333,5000	68,5300	-13,1200	NA	68,3800	77,8000	-158,0100	289	21	90	68	196	7	25,00
Z-01-F08	Horn Graben Eastern B. F.	Z-01-F08-S01	Seg-01	16	5,1	4,7	NA	NA	NA	NA	NA	NA	NA	NA	NA	NA	NA	NA	NA	27,50
Z-01-F09	Horn Graben Western B. F.	Z-01-F09-S01	Seg-01	5	4,4	NA	NA	NA	NA	NA	NA	NA	NA	NA	NA	NA	NA	NA	NA	27,50

All faults analyzed in the area, except the Sorgenfrei-Tornquist fault and Fjerritslev fault zones, have relatively steep dip angles, originated primarily as extensional structures (Table 15). Faults bounding the Viking, Central and Horn grabens, dip usually towards the basin. Eastern boundary graben faults dip towards the west, whereas faults along the western boundary of grabens dip towards the east, with some minor variation. As seen from Table 15, dominant mechanism is normal faulting that correlates well with the graben structures in the area. There is also strike-slip faulting associated with Sorgenfrei-Tornquist fault and Fjerritslev fault zones.

The longest fault segment in the area is of 311 km and is part of the Viking Graben western boundary fault. The shortest fault segment in the area is 39 km and is part of the Central Graben eastern boundary fault. Other segments vary in length. Based on the length of the fault segments, the largest possible earthquake magnitude is assigned for each of these segments using Wells and Coppersmith's (1994) empirical relation. The maximum possible earthquake magnitudes at each segment of the faults vary between 7.0 and 8.2 (Table 15).

Northern North Sea is a complex area which experiences an influence of anomalous elevation differences in the southern Norway. This is explained by Scandinavian mountains that generate gravitational stresses in the adjacent offshore basins that may be the reason of 90˚ stress rotation detected from the Norwegian margin to the northern North Sea (Fejerskov and Lindholm, 2000). This correlates well with the studies done by Hicks et al. (2000) where out of 34 earthquake focal mechanism solutions for the northern North Sea eight were 90˚ rotated reflecting 90˚ stress rotation. Consequently, three stress models for the northern North Sea have been prepared. The first stress model represents inversion results for nonrotated 26 focal mechanisms showing WNW-ESE oriented sigma 1 and SSW-NNE oriented sigma 3. The second stress model represents inversion results for the eight rotated focal mechanisms showing NNE-SSW oriented sigma 1 and WNW-ESE oriented sigma 3. The third model represents composite results for all 34 (rotated and nonrotated) focal mechanisms showing WSW-ENE oriented sigma 1 and NNW-SSE oriented sigma 3. Referring to Bungum et al. (1991), the first stress model is compatible with the expected direction of the continental ridge-push force in this study area and hence one will rely on it and use it when estimating seismogenic potential of the faults and fault zones in the Northern North Sea. In that case with given WNW-ESE oriented sigma 1 and SSW-NNE oriented sigma 3 the expected faulting mechanism in the area is reverse to oblique-reverse. For the Southern North Sea there is not enough data available to get a stress model indicating orientation of sigma 1 and sigma3. However, there is borehole breakouts data that gives orientation of the maximum horizontal stress, that is ESE-WNW (Hicks et al., 2000).

Each fault and its individual segments are analyzed separately (Table 16). In the case where there are only few earthquakes associated with a segment and no focal mechanisms available, we consider these segments to be not seismogenic. Those fault segments that have significant number of earthquakes where there is focal mechanism available, we make further interpretation of their seismogenic potential. These are explained below.

Sorgenfrei-Tornquist fault zone: It consists of one segment for which several criteria described in chapter 3 (Methodology), are not fulfilled and therefore for this fault zone reactivation potential is considered "not possible".

Fjerritslev fault zone: It consists of three segments for which several criteria described in chapter 3 (Methodology), are not fulfilled and therefore for this fault zone reactivation potential is considered "not possible".

Central Graben eastern boundary fault: It consists of four segments for which several criteria described in chapter 3 (Methodology), are not fulfilled and therefore for this fault reactivation potential is considered “not possible”.

Central Graben western boundary fault: It consists of three segments for which several criteria described in chapter 3 (Methodology), are not fulfilled and therefore for this fault reactivation potential is considered “not possible”.

Øygarden fault zone: It consists of three segments and for two of them only one of the criteria described in chapter 3 (Methodology) is not fulfilled and therefore further interpretation is required.

Segment 1: The first segment has three focal mechanisms and only one is of trustworthy B quality indicating oblique-normal slip along one of the nodal planes concordant with the orientation of the fault segment. The remaining two focal mechanisms have similar solutions although one of them has quality C and there is no quality information available for the last one. Considering the segment is NNE-SSW oriented whereas sigma 1 is WNW-ESE oriented and sigma 3 is SSW-NNE oriented, the reactivation of a segment in normal faulting would be difficult. Two interpretations of focal mechanism showing oblique-normal faulting are possible. The first one is that it is associated with rotated focal mechanism solutions which inversion gives NNE-SSW oriented sigma 1 and WNW-ESE oriented sigma 3. In that case expected faulting is normal to strike-slip. The second is strike variation in the northern part of the segment that is interpreted as being small transverse structure with magnitudes less than 3 corresponding to lengths less than ½ km. Such variation along a complex fault segment extending 175 km is assumed to be natural. Earthquakes distributed along both favorable for reactivation WNW dipping segment’s side and unfavorable ESE side. Analyzing all information gathered for the segment it is interpreted that for this segment potential of being reactivated is possible.

Segment 2: The second segment has two focal mechanisms and one of them is of good B quality indicating oblique-reverse slip along one of the nodal planes concordant with the orientation of the fault segment. The remaining focal mechanism is without quality information available and indicates oblique-normal slip. With given NNE-SSW orientation of a segment and WNW-ESE oriented sigma 1 and SSW-NNE oriented sigma 3, the reactivation of the segment in oblique-normal faulting would be difficult. Two interpretations of focal mechanism showing oblique-normal faulting are possible. The first one is that it is associated with rotated focal mechanism solutions which inversion gives NNE-SSW oriented sigma 1 and WNW-ESE oriented sigma 3. In that case expected faulting is normal to strike-slip. The second is minor strike variations that can be interpreted as being small transverse structure with magnitudes less than 3.8 corresponding to lengths less than 1 km. Such variation along a complex fault extending 115 km is assumed to be natural. Earthquakes distributed along both favorable for reactivation WNW dipping segment’s side and unfavorable ESE side. Analyzing all information gathered for the segment it is interpreted that for this segment potential of being reactivated is possible.

Segment 3: The third segment has four focal mechanisms, two of which are of B quality whereas remaining are of poor D quality. All focal mechanisms are consistent and show reverse to oblique-reverse slip along one of the nodal planes concordant with the orientation of the fault segment. With given NNE-SSW orientation of the segment and WNW-ESE oriented sigma 1 and SSW-NNE oriented sigma 3, the reactivation of the segment in reverse to oblique-reverse faulting is expected. In addition, all four earthquakes with focal mechanisms available lie along favorable for reactivation WNW dipping segment’s side. Analyzing all information gathered for the segment it is interpreted that for this segment potential of being reactivated is probable.

Viking Graben eastern boundary fault: It consists of four segments. For segments 2 and 3 several criteria described in chapter 3 (Methodology), are not fulfilled and therefore for these segments reactivation potential is considered "not possible". For segment 1 and 4 only one of the criteria described in chapter 3 (Methodology), is not fulfilled and hence further interpretation is required.

Segment 1: There are two focal mechanisms available, one of which does not have quality information whereas another one is of poor C quality. Focal mechanisms are consistent showing oblique-normal slip along one of the nodal planes concordant with the orientation of the fault segment. With given NNE-SSW orientation of the segment and WNW-ESE oriented sigma 1 and SSW-NNE oriented sigma 3, the reactivation of the segment in oblique-normal faulting would be difficult. Two interpretations of focal mechanism showing oblique-normal faulting are possible. The first one is that it is associated with rotated focal mechanism solutions which inversion gives NNE-SSW oriented sigma 1 and WNW-ESE oriented sigma 3. In that case expected faulting is normal to strike-slip. The second is minor strike variations that can be interpreted as being small transverse structures of magnitudes less than 4.7 corresponding to lengths less 2.2 km. Such variation along 92 km segment is assumed to be natural. Earthquakes predominantly lie along WNW favorable for reactivation dipping segment's side. Analyzing all information gathered for the segment it is interpreted that for this segment potential of being reactivated is possible.

Segment 4: There are three focal mechanisms available of B, C and D quality. All focal mechanisms are consistent showing oblique-normal faulting. With given NNE-SSW orientation of a segment 4 and WNW-ESE oriented sigma 1 and SSW-NNE oriented sigma 3, the reactivation of the segment in oblique-normal faulting would be difficult. Two interpretations of focal mechanism showing oblique-normal faulting are possible. The first one is that it is associated with rotated focal mechanism solutions which inversion gives NNE-SSW oriented sigma 1 and WNW-ESE oriented sigma 3. In that case expected faulting is normal to strike-slip. The second is minor strike variations that can be interpreted as being small transverse structures with magnitude less than 3,6 corresponding to the lengths less than 0,6 km. Such variation along 141 km segment is assumed to be natural. Earthquakes predominantly lie along WNW favorable for reactivation dipping segment's side. Analyzing all information gathered for the segment it is interpreted that for this segment potential of being reactivated is possible.

Viking Graben western boundary fault: It consists of two segments. For segment 1 several criteria described in chapter 3 (Methodology), are not fulfilled and therefore for this segment reactivation potential is considered "not possible". For segment 2 only one of the criteria described in chapter 3 (Methodology) is not fulfilled and therefore further interpretation is required.

Segment 2: There are three focal mechanisms two of which do not have quality information available whereas another one is of quality C showing oblique-reverse faulting. Focal mechanisms without quality present indicate oblique-normal faulting. With given NNE-SSW orientation of the segment and WNW-ESE oriented sigma 1 and SSW-NNE oriented sigma 3, the reactivation of the segment in oblique-normal faulting would be difficult. Two interpretations of focal mechanism showing oblique-normal faulting are possible. The first one is that it is associated with rotated focal mechanism solutions which inversion gives NNE-SSW oriented sigma 1 and WNW-ESE oriented sigma 3. In that case expected faulting is normal to strike-slip. The second is minor steps along the segment that show opposite to the main strike. This can be the reason of transverse structures along 311 km segment with magnitudes less than 5.3 corresponding to lengths less than 4 km. In addition, earthquakes with focal mechanisms analyzed locate along favorable for reactivation ESE dipping segment's side. Analyzing all information gathered for the segment it is interpreted that for this segment potential of being reactivated is possible.

Horn Graben eastern boundary fault: It consists of one segment for which several criteria described in chapter 3 (Methodology), are not fulfilled and therefore for this fault reactivation potential is considered “not possible”.

Horn Graben western boundary fault: It consists of one segment for which several criteria described in chapter 3 (Methodology), are not fulfilled and therefore for this fault reactivation potential is considered “not possible”.

Table 17: Interpreted results for the North Sea zone.

Fault/Fault Zone	Potential of being reactivated			
	Almost certain	Probable	Possible	Not possible
Sorgenfrei-Tornquist Fault				v
Fjerritslev Fault Zone				v
Central Graben Eastern Boundary Fault				v
Central Graben Western Boundary Fault				v
Øygarden Fault Zone (Segment 1)			v	
Øygarden Fault Zone (Segment 2)			v	
Øygarden Fault Zone (Segment 3)		v		
Viking Graben Eastern Boundary Fault (Segment 1)			v	
Viking Graben Eastern Boundary Fault (Segment 2)				v
Viking Graben Eastern Boundary Fault (Segment 3)				v
Viking Graben Eastern Boundary Fault (Segment 4)			v	
Viking Graben Western Boundary Fault (Segment 1)				v
Viking Graben Western Boundary Fault (Segment 2)			v	
Horn Graben Eastern Boundary Fault				v
Horn Graben Western Boundary Fault				v

Summarizing interpretations made for the North Sea zone, one can distinguish between faults for which potential of being reactivated is probable, possible and not possible (Table 17). It was interpreted that for majority of the segments potential of being reactivated is not possible. For few segments potential of being reactivated was estimated to be possible. Only for Øygarden fault – segment 3 potential of being reactivated was estimated to be probable and hence this special case will be represented with figure (Figure 47).

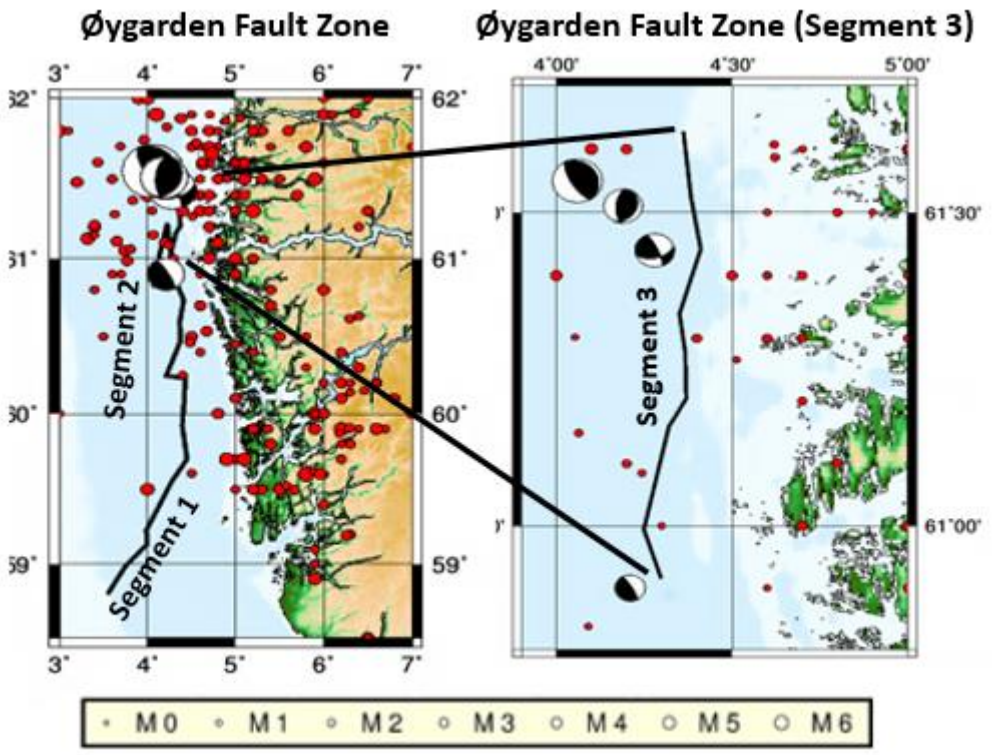

Figure 47: Left: Øygarden Fault Zone. Right: Øygarden Fault Zone (Segment 3) is represented by a solid black line. Seismicity in the area nearby is represented by red circles. The size of a circle is proportional to the magnitude of the event. Focal mechanisms represented in the form of "beach balls".

6.2 Onshore Southern Norway

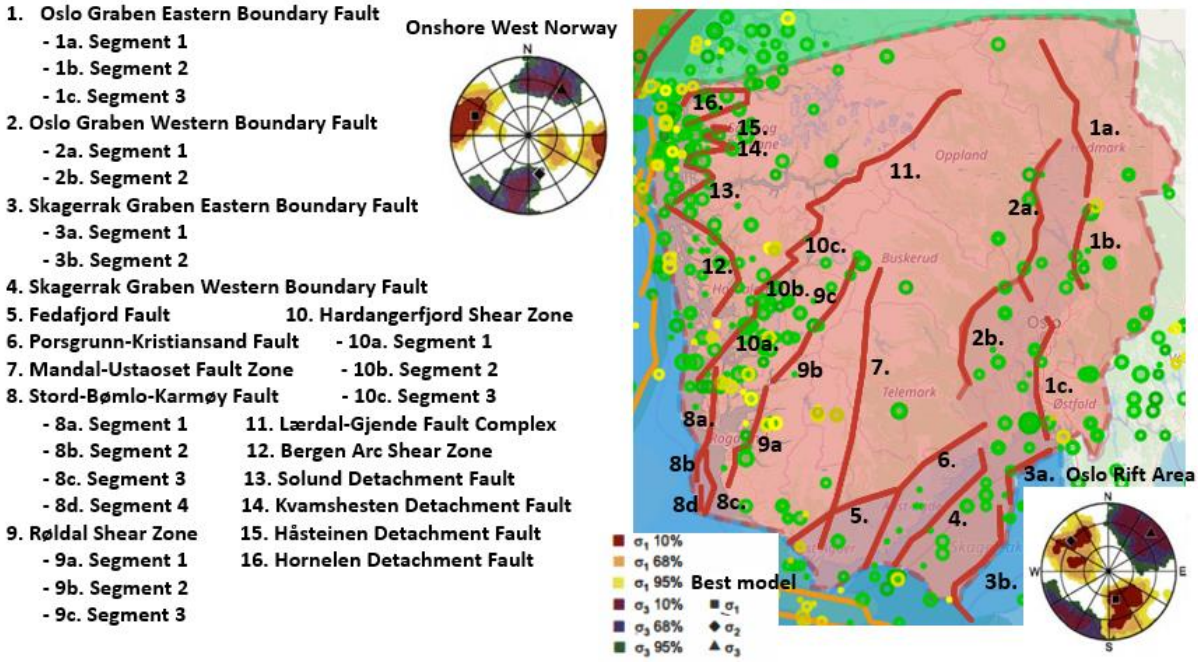

Figure 48: Onshore Southern Norway Zone is represented by light red color. Faults and segments chosen for the analysis are represented with the red color. Seismicity from 1980 onwards represented by yellow circles whereas seismicity for the period preceding 1980 represented with the green circles. The size of a circle is proportional to the magnitude of the event. Circles at the corners (right lower and left upper) represent stress model generated as a result from the inversion of earthquake focal mechanism solutions. The yellow, green and red areas represent 95%, 68% and 10% confidence limits, respectively (Hicks et al., 2000).

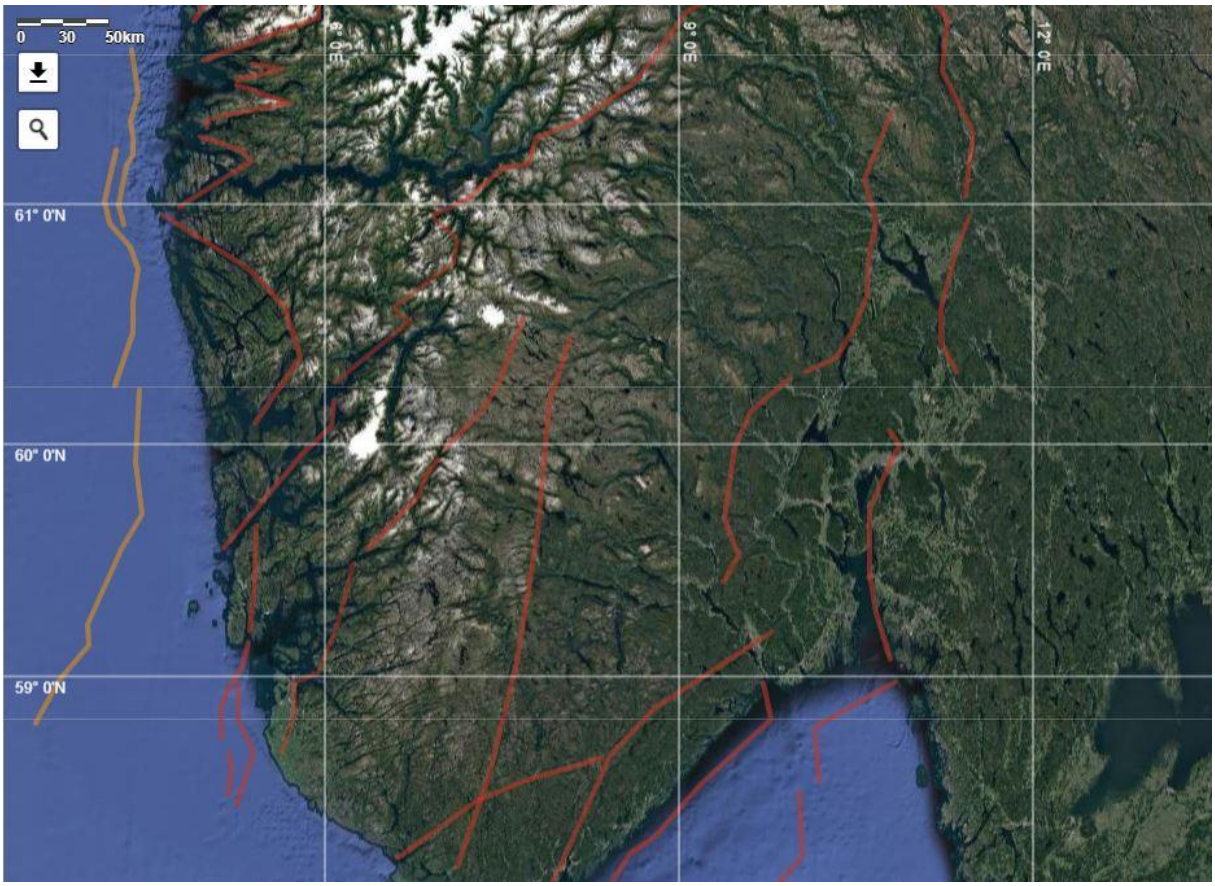

Figure 49: Location of the significant faults in Southern Norway.

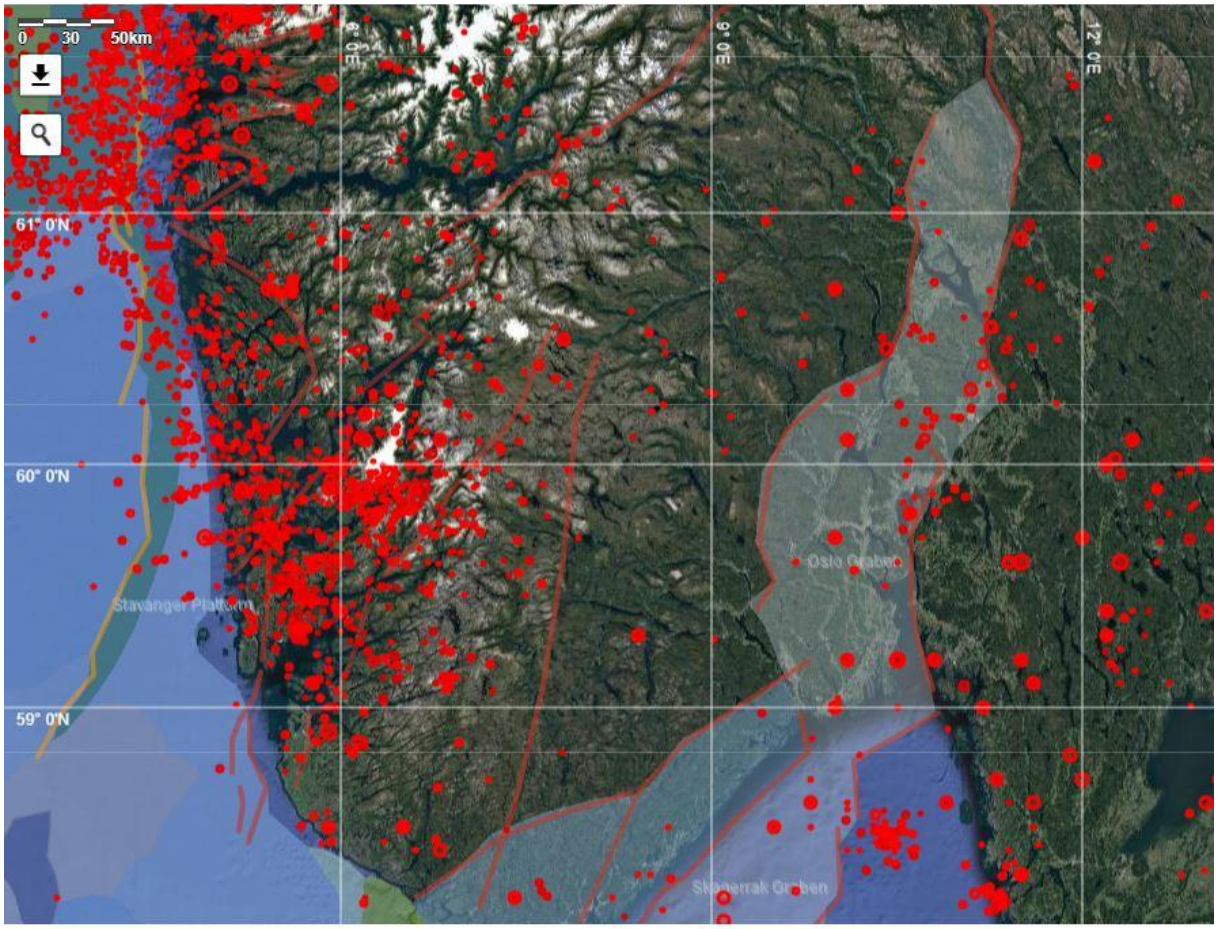

Figure 50: Location of the significant faults in Southern Norway, shown together with the main structural elements (in color-shaded areas) from NPD and the seismicity (since 1980) from NNSN (red circles).

In total ten faults, five fault zones and one fault complex have been analyzed, with 27 segments. Distribution of these faults along onshore southern Norway is as follows (see Figures 48, 49 and 50):

- Two faults bounding Oslo graben with NNW-SSE strike located at the eastern mainland Norway. These are the Oslo Graben eastern boundary and the Oslo Graben western boundary faults.
- Two faults bounding Skagerrak Graben, that is considered to be offshore continuation of the Oslo graben structure, with NW-SE strike situated at the Skagerrak area and are nearly parallel to the eastern coast of mainland Norway. These are Skagerrak Graben eastern boundary fault and Skagerrak Graben western boundary fault.
- Faults located at the southern tip of mainland Norway are Fedafjord fault with ENE-WSW strike, NE-SW oriented Porsgrunn-Kristiansand fault that are nearly parallel to the eastern coast of Norway and NNE-SSW oriented Mandal-Ustaoset fault zone that separates Telemarkia into the Telemark sector to the east and the Hardangervidda sector to the west (Sigmond, 1985).
- N-S oriented fault zone, Stord-Bømlo-Karmøy, located at the southwestern part of mainland Norway and is nearly parallel to the southwestern Norwegian coast.
- Shear faults stretched along southwestern part of mainland Norway that are related to the formation of Caledonides. These are Røldal and Hardangerfjord shear zones with NNE-SSW and NE-SW strikes respectively. NE-SW oriented fault complex, Lærdal-Gjende, that follows the same trend as Hardangerfjord shear zone (Fossen et al., 2005).

- Four arc structures located at the western coast of mainland Norway. These are Bergen Arc Shear Zone, Devonian Solund, Kvamshesten, Håsteinen and Hornelen detachment faults.

Table 18: Geological data for the Onshore Southern Norway zone. Abbreviation *Surf. P. of the W.* in the column *Fault Dimensions* stands for surface projection of the width.

Fault ID	Fault Name	Segment ID	Seg. Name	Fault location				Fault dimesions			Fault orientation			Max possible	References
				End point-1		End point-2		Length	Surf. P. of the W	Width	Strike	Dip	Slip	Magnitude	
				Lat	Lon	Lat	Lon	km	km	km					
Z-02-F01	Oslo Graben Eastern B. F.	Z-02-F01-S01	Seg-01	61,0199	11,4257	62,2265	10,6567	150,00	14,00	41,00	NNW-SSE	70 ° WSW	normal	7,7	Ramberg et al., 2007
		Z-02-F01-S02	Seg-02	60,3037	11,3708	60,9529	11,4601	77,00	14,00	41,00	N-S	70 ° W	normal	7,4	Ramberg et al., 2007
		Z-02-F01-S03	Seg-03	59,0557	10,7775	60,0526	10,7336	125,00	11,00	32,00	N-S	70 ° W	normal	7,6	Ramberg et al., 2007
Z-02-F02	Oslo Graben Western B. F.	Z-02-F02-S01	Seg-01	60,1900	10,5468	60,8759	10,7006	137,00	12,00	35,00	NNW-SSE	70°ESE	normal	7,7	Ramberg et al., 2007
		Z-02-F02-S02	Seg-02	59,5217	9,5690	60,3096	9,9426	110,00	12,00	35,00	NNW-SSE	70°ESE	normal	7,6	Ramberg et al., 2007
Z-02-F03	Skagerrak Graben Eastern B. F.	Z-02-F03-S01	Seg-01	58,5328	10,1678	58,9832	10,8380	72,00	9,00	26,00	NE-SW	70 °NW	normal	7,3	Ramberg et al., 2007
		Z-02-F03-S02	Seg-02	57,5267	9,5416	58,5045	10,0085	134,00	10,00	29,00	NE-SW	70 ° NW	normal	7,7	Ramberg et al., 2007
Z-02-F04	Skagerrak Graben Western B. F.	Z-02-F04-S01	Seg-01	57,9696	8,3111	58,9584	9,7064	150,00	12,00	35,00	NE-SW	70°SE	normal	7,7	Ramberg et al., 2007
Z-02-F05	Fedafjord Fault	Z-02-F05-S01	Seg-01	58,1788	6,5890	58,6438	8,3496	116,00	0,00	35,00	ENE-WSW	90°	dextral strike-slip	7,5	Holtedahl, 1988
Z-02-F06	Porsgrunn-Kristiansand Fault	Z-02-F06-S01	Seg-01	58,0011	7,8222	59,2036	9,7833	179,00	56,00	65,00	NE-SW	30 °SE	thrust	7,7	Lie et al., 1993
Z-02-F07	Mandal-Ustaoset Fault Zone	Z-02-F07-S01	Seg-01	58,1596	7,1136	60,4414	8,0749	270,00	13,00	38,00	N-S	70°E	reverse	8,0	Gabrielsen et al., 2002
Z-02-F08	Stord-Bømlo-Karmøy Fault Zone	Z-02-F08-S01	Seg-01	59,1956	5,3503	59,6594	5,4327	53,00	19,00	38,00	N-S	60°W	reverse	7,1	Pettenati et al., 2005
		Z-02-F08-S02	Seg-02	58,6992	5,0976	59,1531	5,3448	54,00	17,00	34,00	N-S	60°W	reverse	7,1	Pettenati et al., 2005
		Z-02-F08-S03	Seg-03	58,4210	5,2239	58,9665	5,2624	64,00	17,00	34,00	N-S	60°W	reverse	7,2	Pettenati et al., 2005
		Z-02-F08-S04	Seg-04	58,4616	5,1663	58,6637	5,1828	24,00	16,00	32,00	N-S	60°W	reverse	6,7	Pettenati et al., 2005
Z-02-F09	Rødal Shear Zone	Z-02-F09-S01	Seg-01	58,6471	5,6359	59,5001	6,2402	105,00	56,00	65,00	NNE-SSW	30°WNW	thrust	7,5	Fossen et al., 2005
		Z-02-F09-S02	Seg-02	59,9314	6,9515	59,5339	6,3528	56,00	65,00	75,00	NNE-SSW	30°WNW	thrust	7,1	Fossen et al., 2005
		Z-02-F09-S03	Seg-03	59,9757	7,0092	60,5320	7,6904	74,00	65,00	75,00	NNE-SSW	30°WNW	thrust	7,3	Fossen et al., 2005
Z-02-F10	Hardangerfjord Fault Zone	Z-02-F10-S01	Seg-01	59,5198	5,1416	60,2083	6,0809	100,00	56,00	65,00	NE-SW	30°NW	thrust	7,4	Fossen et al., 2005
		Z-02-F10-S02	Seg-02	60,2578	6,0644	60,5618	6,5753	54,00	56,00	65,00	NE-SW	30°NW	thrust	7,1	Fossen et al., 2005
		Z-02-F10-S03	Seg-03	60,5702	6,5588	60,9460	6,9049	61,00	56,00	65,00	NE-SW	30°NW	thrust	7,2	Fossen et al., 2005
Z-02-F11	Lærdal-Gjende Fault Complex	Z-02-F11-S01	Seg-01	60,9558	6,8774	61,8449	9,4152	174,00	61,00	70,00	NE-SW	30°NW	normal	7,8	Fossen et al., 2005
Z-02-F12	Bergen Arc Shear Zone	Z-02-F12-S01	Seg-01	60,0747	5,3338	60,9565	4,6032	139,00	NA	NA	arc	tward-dip	thrust	7,6	Fossen et al., 2005
Z-02-F13	Solund Detachment Fault	Z-02-F14-S01	Seg-01	60,9834	4,7433	61,2687	4,9328	67,00	NA	NA	arc	tward-dip	normal	7,3	Séguret et al., 1989
Z-02-F14	Kvamshesten Detachment Fault	Z-02-F15-S01	Seg-01	61,3144	4,9768	61,4858	5,2418	66,00	NA	NA	arc	tward-dip	normal	7,3	Séguret et al., 1989
Z-02-F15	Håsteinen Detachment Fault	Z-02-F16-S01	Seg-01	61,4962	5,2157	61,5656	5,3558	39,00	NA	NA	arc	tward-dip	normal	7,0	Séguret et al., 1989
Z-02-F16	Hornelen Detachment Fault	Z-02-F17-S01	Seg-01	61,5848	4,8779	61,7387	4,8779	128,00	NA	NA	arc	tward-dip	normal	7,6	Séguret et al., 1989

Table 19: Seismological data for the Onshore Southern Norway zone (Part 1).

Fault ID	Fault Name	Segment ID	Seg. Name	# earthquakes	Max observed magnitude		Focal mechanism				Nodal plane 2			Regional stress tensor						D. to Moho
					Historical	Instrumental	Nodal Plane 1			Quality				Sigma 1		Sigma 2		Sigma 3		
					Before 1980	After 1980	Strike	Dip	Rake		Strike	Dip	Rake	Azimuth	Plunge	Azimuth	Plunge	Azimuth	Plunge	
Z-02-F01	Oslo Graben Eastern B. F.	Z-02-F01-S01	Seg-01	0	NA	NA	NA	NA	NA	NA	NA	NA	NA	166	55	309	29	49	17	37,50
		Z-02-F01-S02	Seg-02	6	4,3	3,8	158,2000	87,9000	-14,8000	B	248,7500	75,2100	-177,8300	166	55	309	29	49	17	37,50
							3,7000	49,9000	78,2000	A	201,6700	41,5200	103,6500	166	55	309	29	49	17	37,50
							117,1000	64,0000	34,4000	A	10,3900	59,4800	149,4100	166	55	309	29	49	17	37,50
							359,9000	70,3000	-96,7000	D	199,1100	20,7700	-71,9500	166	55	309	29	49	17	37,50
							108,2000	79,1000	106,0000	B	231,6000	19,2800	34,9400	166	55	309	29	49	17	37,50
							218,6000	51,2000	-76,3000	B	17,3400	40,7900	-106,4100	166	55	309	29	49	17	37,50
							189,2000	68,3000	63,1000	B	63,1200	34,0400	138,6700	166	55	309	29	49	17	37,50
							166,8000	65,8000	-46,1000	B	279,8700	48,9100	-147,0500	166	55	309	29	49	17	37,50
							180,1000	74,2000	-21,2000	D	276,1300	69,6400	-163,1200	166	55	309	29	49	17	37,50
							154,8000	75,1000	35,0000	B	54,5900	56,3400	162,0100	166	55	309	29	49	17	37,50
		Z-02-F01-S03	Seg-03	6	3,9	3,6	118,9000	68,4000	-134,1000	B	8,1000	48,1100	-29,6400	166	55	309	29	49	17	30,00
							203,1000	70,5000	-36,3000	C	306,0800	56,0800	-156,2800	166	55	309	29	49	17	30,00
Z-02-F02	Oslo Graben Western B. F.	Z-02-F02-S01	Seg-01	3	3,7	NA	9,7000	59,8000	-70,9000	A	155,1600	35,2400	-119,3500	166	55	309	29	49	17	32,50
							359,8000	70,3000	-96,7000	D	199,0100	20,7700	-71,9500	166	55	309	29	49	17	32,50
							351,5000	76,5000	-74,7000	B	121,9800	20,3000	-137,7000	166	55	309	29	49	17	32,50
		Z-02-F02-S02	Seg-02	3	3,7	NA	50,5000	64,3000	123,4000	C	173,8300	41,2100	41,1600	166	55	309	29	49	17	32,50
Z-02-F03	Skagerrak Graben Eastern B. F.	Z-02-F03-S01	Seg-01	3	3,3	NA	NA	NA	NA	NA	NA	NA	NA	166	55	309	29	49	17	25,00
		Z-02-F03-S02	Seg-02	2	3,0	NA	NA	NA	NA	NA	NA	NA	NA	166	55	309	29	49	17	27,50
Z-02-F04	Skagerrak Graben Western B. F.	Z-02-F04-S01	Seg-01	8	4,3	NA	152,9000	81,4000	-55,6000	C	255,2200	35,3300	-165,0100	NA	NA	NA	NA	NA	NA	32,50
Z-02-F05	Fedafjord Fault	Z-02-F05-S01	Seg-01	3	4,2	3,1	NA	NA	NA	NA	NA	NA	NA	290	28	164	48	37	29	35,00
Z-02-F06	Porsgrunn-Kristiansand Fault	Z-02-F06-S01	Seg-01	0	NA	NA	NA	NA	NA	NA	NA	NA	NA	290	28	164	48	37	29	32,50
Z-02-F07	Mandal-Ustaoset Fault Zone	Z-02-F07-S01	Seg-01	5	4,2	3,7	NA	NA	NA	NA	NA	NA	NA	290	28	164	48	37	29	35,00
Z-02-F08	Stord-Bømlo-Karmøy Fault Zone	Z-02-F08-S01	Seg-01	6	4,5	3,6	333,0000	40,0000	58,0000	NA	192,2000	56,9700	113,9700	290	28	164	48	37	29	32,50
							136,0000	67,0000	-125,0000	NA	16,8400	41,0600	-36,5000	290	28	164	48	37	29	32,50
		Z-02-F08-S02	Seg-02	0	NA	NA	35,0000	52,0000	150,0000	NA	144,5700	66,8000	42,0600	290	28	164	48	37	29	30,00
		Z-02-F08-S03	Seg-03	0	NA	NA	NA	NA	NA	NA	NA	NA	NA	290	28	164	48	37	29	30,00
		Z-02-F08-S04	Seg-04	0	NA	NA	NA	NA	NA	NA	NA	NA	NA	290	28	164	48	37	29	27,50

Table 20: Seismological data for the Onshore Southern Norway zone (Part 2).

Fault ID	Fault Name	Segment ID	Seg. Name	# earthquakes	Max observed magnitude		Focal mechanism							Regional stress tensor						D. to Moho
					Historical	Instrumental	Nodal Plane 1			Quality	Nodal plane 2			Sigma 1		Sigma 2		Sigma 3		
					Before 1980	After 1980	Strike	Dip	Rake		Strike	Dip	Rake	Azimuth	Plunge	Azimuth	Plunge	Azimuth	Plunge	
Z-02-F09	Røldal Shear Zone	Z-02-F09-S01	Seg-01	7	4,5	3,7	NA	NA	NA	NA	NA	NA	NA	290	28	164	48	37	29	32,50
		Z-02-F09-S02	Seg-02	8	4,4	4,2	159,8000	86,5000	-7,8000	C	250,2800	82,2100	-176,4700	290	28	164	48	37	29	37,50
							323,7000	62,2000	-40,0000	B	75,0700	55,3500	-145,4600	290	28	164	48	37	29	37,50
							246,0000	74,8000	-131,8000	NA	139,6600	44,0000	-22,1800	290	28	164	48	37	29	37,50
							86,6000	75,1000	153,6000	C	183,8700	64,5500	16,5400	290	28	164	48	37	29	37,50
		Z-02-F09-S03	Seg-03	2	3,0	NA	309,7000	80,8000	-3,6000	B	40,2800	86,4500	-170,7800	290	28	164	48	37	29	37,50
							326,9100	56,1700	-22,7600	NA	70,0600	71,2500	-143,9900	290	28	164	48	37	29	37,50
Z-02-F10	Hardangerfjord Fault Zone	Z-02-F10-S01	Seg-01	17	4,9	3,6	191,9000	57,0000	114,0000	A	332,6300	39,9900	57,9400	290	28	164	48	37	29	32,50
							230,0400	71,2500	-68,8300	NA	359,7300	27,9900	-136,7700	290	28	164	48	37	29	32,50
							110,0000	5,0000	0,0000	NA	20,0000	90,0000	95,0000	290	28	164	48	37	29	32,50
							312,4000	65,4000	-32,8000	B	57,4200	60,4900	-151,4200	290	28	164	48	37	29	32,50
							115,7000	36,0000	31,2000	C	359,6000	72,2700	121,8600	290	28	164	48	37	29	32,50
							340,3000	44,0000	22,1000	C	234,0200	74,8500	131,8200	290	28	164	48	37	29	32,50
		Z-02-F10-S02	Seg-02	8	3,9	3,3	150,4000	85,0000	-85,0000	D	285,2900	7,0700	-134,8900	290	28	164	48	37	29	32,50
							134,2000	64,2000	56,4000	C	116,4200	49,7200	35,0700	290	28	164	48	37	29	32,50
		Z-02-F10-S03	Seg-03	1	NA	3,2	139,2900	75,4800	39,8600	B	37,4700	51,6500	161,3600	290	28	164	48	37	29	32,50
Z-02-F11	Lærdal-Gjende Fault Complex	Z-02-F11-S01	Seg-01	1	3,5	NA	NA	NA	NA	NA	NA	NA	NA	290	28	164	48	37	29	35,00
Z-02-F12	Bergen Arc Shear Zone	Z-02-F12-S01	Seg-01	10	4,1	NA	115,7000	36,0000	31,2000	C	62,1700	320,7200	-150,6400	290	28	164	48	37	29	32,50
							116,1000	35,5000	30,6000	D	0,3900	72,8100	121,5500	290	28	164	48	37	29	32,50
							327,9000	73,8000	-44,1000	C	73,0300	48,0700	-157,9700	290	28	164	48	37	29	32,50
							134,2000	64,2000	56,4000	C	10,9700	41,4200	138,8600	290	28	164	48	37	29	32,50
							340,3000	44,0000	22,1000	C	234,0200	74,8500	131,8200	290	28	164	48	37	29	32,50
							116,3200	80,3400	-2,6100	NA	206,7600	87,4300	-170,3300	290	28	164	48	37	29	32,50
Z-02-F13	Solund Detachment Fault	Z-02-F13-S01	Seg-01	12	4,9	NA	NA	NA	NA	NA	NA	NA	NA	290	28	164	48	37	29	27,50
Z-02-F14	Kvamshesten Detachment Fault	Z-02-F14-S01	Seg-01	8	4,9	NA	NA	NA	NA	NA	NA	NA	NA	290	28	164	48	37	29	27,50
Z-02-F15	Håsteinen Detachment Fault	Z-02-F15-S01	Seg-01	10	4,8	NA	NA	NA	NA	NA	NA	NA	NA	290	28	164	48	37	29	27,50
Z-02-F16	Hornelen Detachment Fault	Z-02-F16-S01	Seg-01	17	4,8	3,6	23,9000	70,0000	-78,4000	B	172,9300	23,0000	-118,9200	290	28	164	48	37	29	27,50
							192,5000	51,9000	70,7000	C	42,0800	42,0400	112,8600	290	28	164	48	37	29	27,50
							23,6000	70,3000	-79,4000	NA	174,5600	22,2700	-117,1900	290	28	164	48	37	29	20,00

Dip of the faults, locating onshore southern Norway, varies (Table 18). Shear structures tend to have shallow dip angle that is equal to 30˚ whereas faults bounding Oslo and Skagerrak grabens show steep dip angle that is equal to 70˚. There is also fault, Fedafjord fault, that has dip of 90˚ and hence shows pure strike-slip movement along it. Porsgrunn-Kristiansand fault is a thrust structure and therefore has shallow 30˚ angle whereas Mandal-Ustaoset fault zone that divides basement in two parts is a reverse fault that has steep 70˚ dip angle. Stord-Bømlo-Karmøy fault zone is a reverse structure showing steep dip angle that is equal to 60˚ whereas Lærdal-Gjende fault complex that follows the same trend as Hardangerfjord shear zone has shallow 30˚ dip. There are also arc structures in the area whose dip changes significantly along the arc extent. Dip direction of the faults, fault complex and zones change along the area as well. Faults bounding grabens that are located at the eastern part of the mainland Norway generally dip towards the basin. That is, faults bounding graben from the eastern side usually dip towards the west whereas faults bounding western side of the graben towards the east. All faults located at the western side of the mainland Norway, except Stord-Bømlo-Karmøy fault zone and Lærdal-Gjende fault complex, are related to different modes of Caledonides episodes and hence show dominant westward dip (Table 18).

The longest fault segment in the area is of 270 km that corresponds to the full extent of the Mandal-Ustaoset fault zone. The shortest fault segment is of 39 km that corresponds to the full extent of the Håsteinen detachment arc-shaped fault. Based on the length of the fault segment the maximum possible magnitude using Well and Coppersmith (1994) empirical relationship has been assigned to each segment. The maximum possible magnitudes for the fault segments in the area vary between 7.0 and 8.0 (Table 18).

Onshore Southern Norway is a complex area for which there have been prepared two stress models (Tables 19; 20). The first was prepared based on stress inversion of earthquake focal mechanism solutions from the Oslo rift area. This stress model shows sigma 1 is NW-SE oriented whereas sigma 3 is NE-SW oriented (Hicks et al., 2000). Referring to Hicks et al. (2000) interpretations of inversion results for the Oslo rift area the expected faulting mechanism for shallow events (<15 km) is normal to strike-slip whereas for deep earthquakes (> 15 km) is reverse. The same observation was also made by Olesen et al. (2013) who stated that in the Oslo region focal mechanisms of shallow (< 13 km) earthquakes are associated with normal and strike-slip faulting whereas focal mechanisms for deeper events with reverse faulting. That is well demonstrated and can be reviewed in Figure 7. The second stress model was prepared based on stress inversion of earthquake focal mechanism solutions from the onshore west Norway. Referring to this stress model, sigma 1 is WNW-ESE oriented whereas sigma 3 is NE-SW oriented (Hicks et al., 2000). The same as for the Oslo rift area normal faulting is associated with shallow earthquakes whereas reverse faulting with deep seismic events (Figure 7). The main focus of the following thesis is to study seismogenic faults that rupture the entire crust and penetrate to the Moho depth. Therefore, only reverse faulting that is related to deep seismic events will be used when estimating seismogenic potential of faults/segments of being reactivated.

Oslo Graben eastern boundary fault: It consists of three segments. For segment 1 several criteria described in chapter 3 (Methodology), are not fulfilled and therefore for this segment reactivation potential is considered “not possible”. For segments 2 and 3 only one of the criteria described in chapter 3 (Methodology) is not fulfilled and therefore further interpretation is required.

Segment 2: There are ten focal mechanism of A, B and D qualities available showing both oblique-reverse and oblique-normal faulting. Focal mechanisms showing oblique-reverse faulting are only of good, trustworthy A (2 focal mechanisms) and B (3 focal mechanisms) qualities whereas the ones showing oblique-normal faulting are of B (3 focal mechanisms) and D (2 focal mechanisms) quality. With given N-S orientation of the segment 2 and NW-SE oriented sigma 1 and NE-SW oriented sigma

3, the reactivation of a segment in oblique-normal faulting would be difficult. Two interpretations of focal mechanism showing oblique-normal faulting are possible. The first one is that it is related to shallow seismicity. The second is minor strike variations that can be interpreted as being small transverse structure with magnitudes less than 4.3 corresponding to lengths less than 1.3 km. Such variation along a fault extending 77 km is assumed to be natural. Earthquakes distributed along favorable for reactivation western dipping segment's side and along unfavorable eastern side. Analyzing all information gathered for the fault segment it is interpreted that potential of being reactivated for this segment is possible.

Segment 3: There are two focal mechanisms available of B and C qualities, both show oblique-normal faulting. With given N-S orientation of the segment 3 and NW-SE oriented sigma 1 and NE-SW oriented sigma 3, the reactivation of the segment in oblique-normal faulting would be difficult. Two interpretations of focal mechanism showing oblique-normal faulting are possible. The first one is that it is related to shallow seismicity. The second is minor strike variations that can be interpreted as being small transverse structure with magnitudes less than 3.9 corresponding to lengths less than 0.8 km. Such variation along a fault extending 125 km is assumed to be natural. Earthquakes distributed along favorable for reactivation western dipping segment's side and along unfavorable eastern side. Analyzing all information gathered for the fault segment it is interpreted that potential for this segment of being reactivated is not possible.

Oslo Graben western boundary fault: It consists of two segments and for all of them only one of the criteria described in chapter 3 (Methodology) is not fulfilled and hence further interpretation is required.

Segment 1: There are three focal mechanisms available of A, B and D qualities and all are consistent in showing oblique-normal faulting. With given NNW-SSE orientation of a segment and NW-SE oriented sigma 1 and NE-SW oriented sigma 3, the reactivation of the segment in oblique-normal faulting would be difficult. Two interpretations of focal mechanism showing oblique-normal faulting are possible. The first one is that it is related to shallow seismicity. The second is minor strike variations that can be interpreted as being small transverse structure with magnitudes less than 3.7 corresponding to lengths less than 0.7 km. Such variation along a fault extending 137 km is assumed to be natural. Seismic events with focal mechanisms are dispersed, locate both at the western and eastern sides along the fault segment. Analyzing all information gathered for the segment it is interpreted that potential for this segment of being reactivated is not possible.

Segment 2: There is one focal mechanism of poor C quality showing oblique-reverse faulting. This faulting mechanism is compatible with NNW-SSE oriented segment and NW-SE oriented sigma 1 and NE-SW oriented sigma 3. There is not much seismicity in the area, the only three earthquakes near the segment locate along favorable for reactivation ESE dipping segment's side. Analyzing all information gathered for the segment it is interpreted that potential for this segment of being reactivated is possible.

Skagerrak Graben eastern boundary fault: It consists of two segments for which several criteria described in chapter 3 (Methodology), are not fulfilled and therefore for this fault reactivation potential is considered "not possible".

Skagerrak Graben western boundary fault: It consists of one segment for which only one criteria described in chapter 3 (Methodology), is not fulfilled and therefore further interpretation is required. The focal mechanism shows oblique-normal faulting. With given NE-SW orientation of the fault and NW-SE oriented sigma 1 and NE-SW oriented sigma 3, the reactivation of the fault in oblique-normal faulting would be difficult. Two interpretations of focal mechanism showing oblique-normal faulting

are possible. The first one is that it is related to shallow seismicity. The second is minor strike variations that can be interpreted as being small transverse structure with magnitudes less than 4.3 corresponding to lengths less than 1.3 km. Such variation along a fault extending 150 km is assumed to be natural. Majority of earthquakes nearby the fault locate at the favorable for the reactivation SE dipping segment's side. Analyzing all information gathered for the fault it is interpreted that potential for this fault of being reactivated is not possible.

Fedafjord fault: It consists of one segment for which several criteria described in chapter 3 (Methodology), are not fulfilled and therefore for this fault reactivation potential is considered "not possible".

Porsgrunn-Kristiansand fault: It consists of one segment for which several criteria described in chapter 3 (Methodology), are not fulfilled and therefore for this fault reactivation potential is considered "not possible".

Mandal-Ustaoset fault zone: It consists of one segment for which several criteria described in chapter 3 (Methodology), are not fulfilled and therefore for this fault zone reactivation potential is considered "not possible".

Stord-Bømlo-Karmøy fault zone: It consists of four segments. For segments 1 and 2 only one criterion described in chapter 3 (Methodology), is not fulfilled and hence further interpretation is required. For segment 3 and 4 several criteria described in chapter 3 (Methodology), are not fulfilled and therefore for these segments reactivation potential is considered "not possible".

Segment 1: There are two focal mechanisms available and for none of them there is no quality information given. One focal mechanism shows oblique-reverse faulting whereas the other oblique-normal faulting. With given N-S orientation of a segment and WNW-ESE oriented sigma 1 and NE-SW oriented sigma 3, the reactivation of the segment in oblique-normal faulting would be difficult. Two interpretations of focal mechanism showing oblique-normal faulting are possible. The first one is that it is related to shallow seismicity. The second is minor strike variations that can be interpreted as being small transverse structure with magnitudes less than 4.5 corresponding to lengths less than 1.5 km. Such variation along a fault extending 53 km is assumed to be natural. Earthquake distributed along both favorable for reactivation western dipping segment's side and unfavorable eastern side. Since there are only two focal mechanisms without quality, showing opposite faulting along the segment the potential for this segment of being reactivated is interpreted to be possible.

Segment 2: There is one focal mechanism available without quality information provided. The focal mechanism shows oblique-reverse faulting. This faulting mechanism is compatible with N-S orientation of the segment and WNW-ESE oriented sigma 1 and NE-SW oriented sigma 3. However, there is not much seismicity in the area and hence it is interpreted that for this segment potential of being reactivated is possible.

Røldal shear zone: It consists of three segments. For segment 1 several criteria described in chapter 3 (Methodology), are not fulfilled and therefore for this segment reactivation potential is considered "not possible". For segments 2 and 3 only one criterion described in chapter 3 (Methodology), is not fulfilled and hence further interpretation is required.

Segment 2: There are four focal mechanisms available, for one of them there is no quality information given whereas for the remaining three quality is B and C. Three focal mechanisms show oblique-normal faulting whereas the remaining one reverse faulting. With given NNE-SSW orientation of the segment and WNW-ESE oriented sigma 1 and NE-SW oriented sigma 3, the reactivation of the segment in

oblique-normal faulting would be difficult. Two interpretations of focal mechanism showing oblique-normal faulting are possible. The first one is that it is related to shallow seismicity. The second is minor strike variations that can be interpreted as being small transverse structure with magnitudes less than 4.4 corresponding to lengths less than 1.4 km. Such variation along a fault extending 56 km is assumed to be natural. Majority of earthquakes nearby the segment locate at the favorable for reactivation WNW dipping segment's side. Analyzing all information gathered for the fault segment it is interpreted that for this segment reactivation potential is possible.

Segment 3: There are two focal mechanisms available one of which is of B quality whereas for another one information about the quality is not given. Focal mechanisms are consistent showing oblique-normal faulting. With given NNE-SSW orientation of the segment and WNW-ESE oriented sigma 1 and NE-SW oriented sigma 3, the reactivation of the segment in oblique-normal faulting would be difficult. Two interpretations of focal mechanism showing oblique-normal faulting are possible. The first one is that it is related to shallow seismicity. The second is minor strike variations that can be interpreted as being small transverse structure with magnitudes less than 3.0 corresponding to lengths less than 0.3 km. Such variation along a fault extending 74 km is assumed to be natural. Earthquakes almost equally distributed along WNW favorable for reactivation segment's dipping side and unfavorable ESE side. Analyzing all information gathered for the fault segment it is interpreted that for this segment reactivation potential is not possible.

Hardangerfjord shear zone: It consists of three segments for which only one criterion described in chapter 3 (Methodology), is not fulfilled and hence further interpretation is required.

Segment 1: There are six focal mechanisms available. For two of them there is no quality information given whereas the remaining four are of A, B and C qualities. Three focal mechanisms of A and C qualities show oblique-reverse faulting. Two focal mechanisms one of which does not have information about the quality, and another is of quality B show oblique-normal faulting. With given NE-SW orientation of the segment and WNW-ESE oriented sigma 1 and NE-SW oriented sigma 3, the reactivation of the segment in oblique-normal faulting would be difficult. Two interpretations of focal mechanism showing oblique-normal faulting are possible. The first one is that it is related to shallow seismicity. The second is minor strike variations that can be interpreted as being small transverse structure with magnitudes less than 4.9 corresponding to lengths less than 2.5 km. Such variation along a fault extending 100 km is assumed to be natural. The remaining focal mechanism without quality information shows pure left-lateral strike-slip faulting. This focal mechanism can be related to shallow seismicity or being small transverse structure reflecting strike variation along the fault extent. Earthquakes distributed both along NW favorable for reactivation segment's dipping side and unfavorable SE side. Analyzing all information gathered for the segment it is interpreted that for this segment potential of being reactivated is possible.

Segment 2: There are two focal mechanism available, one of which is of D quality showing oblique-normal faulting whereas another one is of C quality showing oblique-reverse faulting. With given NE-SW orientation of the segment and WNW-ESE oriented sigma 1 and NE-SW oriented sigma 3, the reactivation of the segment in oblique-normal faulting would be difficult. Two interpretations of focal mechanism showing oblique-normal faulting are possible. The first one is that it is related to shallow seismicity. The second is minor strike variations that can be interpreted as being small transverse structure with magnitudes less than 3.9 corresponding to lengths less than 0.8 km. Such variation along a fault extending 54 km is assumed to be natural. Majority of earthquakes nearby the fault segment locate at the favorable for reactivation northwestern segment's dipping side. Analyzing all information gathered for the segment it is interpreted that for this segment potential of being reactivated is possible.

Segment 3: There is one focal mechanism of B quality showing oblique-reverse faulting. This faulting mechanism is compatible with NE-SW oriented segment and WNW-ESE oriented sigma 1 and NE-SW oriented sigma 3. However, there is not much seismic activity nearby this segment, there is only one earthquake of magnitude 3.2. Analyzing all information gathered for the segment it is interpreted that for this segment potential of being reactivated is possible.

Lærdal-Gjende fault complex: It consists of one segment for which several criteria described in chapter 3 (Methodology), are not fulfilled and therefore for this fault complex reactivation potential is considered “not possible”.

Bergen Arc shear zone: It consists of one segment for which only one criterion described in chapter 3 (Methodology), is not fulfilled and hence further interpretation is required. There are six focal mechanisms of C and D qualities available. Four focal mechanisms show oblique-reverse faulting whereas the remaining two oblique-normal faulting. Two interpretations of focal mechanism showing oblique-normal faulting are possible. The first one is that it is related to shallow seismicity. The second is fault geometry. Since the fault is arched its strike varies significantly along the fault extent and hence this can lead to the formation of small transverse structures with magnitudes less than 4.1 corresponding to lengths less than 1.5 km. Such variation along a complex fault extending 139 km is assumed to be natural. Earthquakes locate at both sides (inside and outside) the arc. Analyzing all information gathered for the fault it is interpreted that potential for Bergen Arc shea zone of being reactivated is possible.

Solund detachment fault: It consists of one segment for which several criteria described in chapter 3 (Methodology), are not fulfilled and therefore for this fault reactivation potential is considered “not possible”.

Kvamshesten detachment fault: It consists of one segment for which several criteria described in chapter 3 (Methodology), are not fulfilled and therefore for this fault reactivation potential is considered “not possible”.

Håsteinen detachment fault: It consists of one segment for which several criteria described in chapter 3 (Methodology), are not fulfilled and therefore for this fault reactivation potential is considered “not possible”.

Hornelen detachment fault: It consists of one segment for which only one criterion described in chapter 3 (Methodology), is not fulfilled and hence further interpretation is required. There are three focal mechanisms available. Two focal mechanisms one of which is of B quality whereas another one is without quality information show oblique-normal faulting. Considering the fault is arched meaning its strike varies significantly along the fault extent focal mechanisms showing oblique-normal faulting are interpreted as being small transverse structures with magnitudes less than 4.8 corresponding to lengths less than 2.5 km. Such variation along a complex fault segment extending 128 km is natural. Another interpretation is shallow seismicity that is associated with oblique-normal faulting. The third focal mechanism is of C quality and shows oblique-reverse faulting that is compatible with WNW-ESE oriented sigma 1 and NE-SW oriented sigma 3. Earthquakes locate at both sides (inside and outside) the arc. Analyzing all information gathered for the fault it is interpreted that for Hornelen detachment fault potential of being reactivated is possible.

Table 21: Interpreted results for Onshore Southern Norway zone.

Fault/Fault zone/Fault complex	Potential of being reactivated			
	Almost certain	Probable	Possible	Not possible
Oslo Graben Eastern boundary Fault (Segment 1)				v
Oslo Graben Eastern boundary Fault (Segment 2)			v	
Oslo Graben Eastern boundary Fault (Segment 3)				v
Oslo Graben Western boundary Fault (Segment 1)				v
Oslo Graben Western boundary Fault (Segment 2)			v	
Skagerrak Graben Eastern boundary Fault (Segment 1)				v
Skagerrak Graben Eastern boundary Fault (Segment 2)				v
Skagerrak Graben Western boundary Fault				v
Fedafjord fault				v
Porsgrunn-Kristiansand fault				v
Mandal-Ustaoset fault zone				v
Stord-Bømlo-Karmøy fault zone (Segment 1)			v	
Stord-Bømlo-Karmøy fault zone (Segment 2)			v	
Stord-Bømlo-Karmøy fault zone (Segment 3)				v
Stord-Bømlo-Karmøy fault zone (Segment 4)				v
Røldal shear zone (Segment 1)				v
Røldal shear zone (Segment 2)			v	
Røldal shear zone (Segment 3)				v
Hardangerfjord shear zone (Segment 1)			v	
Hardangerfjord shear zone (Segment 2)			v	
Hardangerfjord shear zone (Segment 3)			v	
Lærdal-Gjende Fault Complex				v
Bergen Arc Shear Zone			v	
Solund Detachment Fault				v
Kvamshesten Detachment Fault				v
Håsteinen Detachment Fault				v
Hornelen Detachment Fault			v	

Summarizing interpretations made for the onshore southern Norway zone, one can distinguish between faults for which potential of being reactivated is possible and not possible (Table 21). It was interpreted that for the majority of segments potential of being reactivated is not possible. For several segments potential of being reactivated is possible.

6.3 Norwegian Sea

1. Fles Fault Complex
   - 1a. Segment 1
   - 1b. Segment 2
   - 1c. Segment 3
   - 1d. Segment 4
2. Vesterdjupet Fault Zone
3. Helland-Hansen Arch Eastern Boundary Fault
4. Klakk Fault Complex
   - 4a. Segment 1
   - 4b. Segment 2
5. Ytreholmen Fault Zone
6. Revfallet Fault Complex
7. Faeroe-Shetland Escarpment
8. East Jan Mayen Fracture Zone
   - 8a. Segment 1
   - 8b. Segment 2
9. Vøring Plateau Escarpment
10. Lofoten-Vesterålen Margin
11. Utrøst Ridge NW Boundary Fault
12. Bremstein – Vingleia Fault Complex

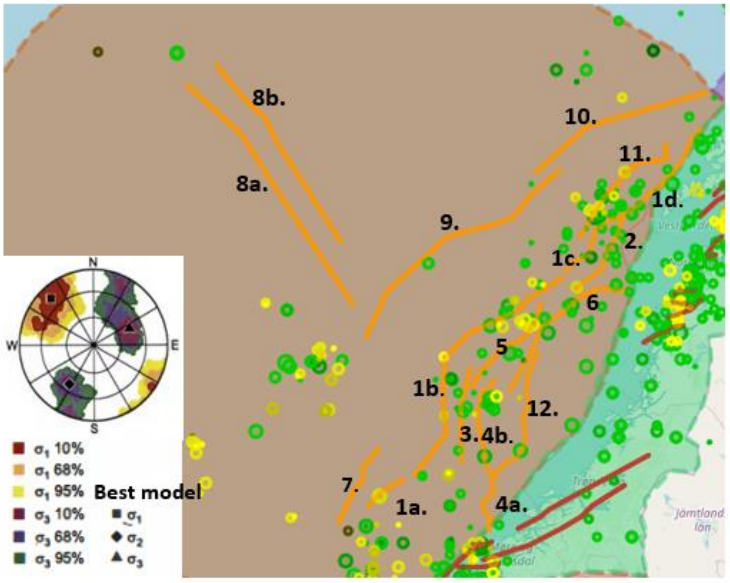

Figure 51: Norwegian Sea Zone is represented by light red color. Faults and segments in the Norwegian Sea chosen for the analysis are represented with the orange color. Seismicity from 1980 onwards represented by yellow circles whereas seismicity for the period preceding 1980 represented with the green circles. The size of a circle is proportional to the magnitude of the event. Circle at the left lower corner represents stress model generated as a result from the inversion of earthquake focal mechanism solutions. The yellow, green and red areas represent 95%, 68% and 10% confidence limits respectively (Hicks et al., 2000).

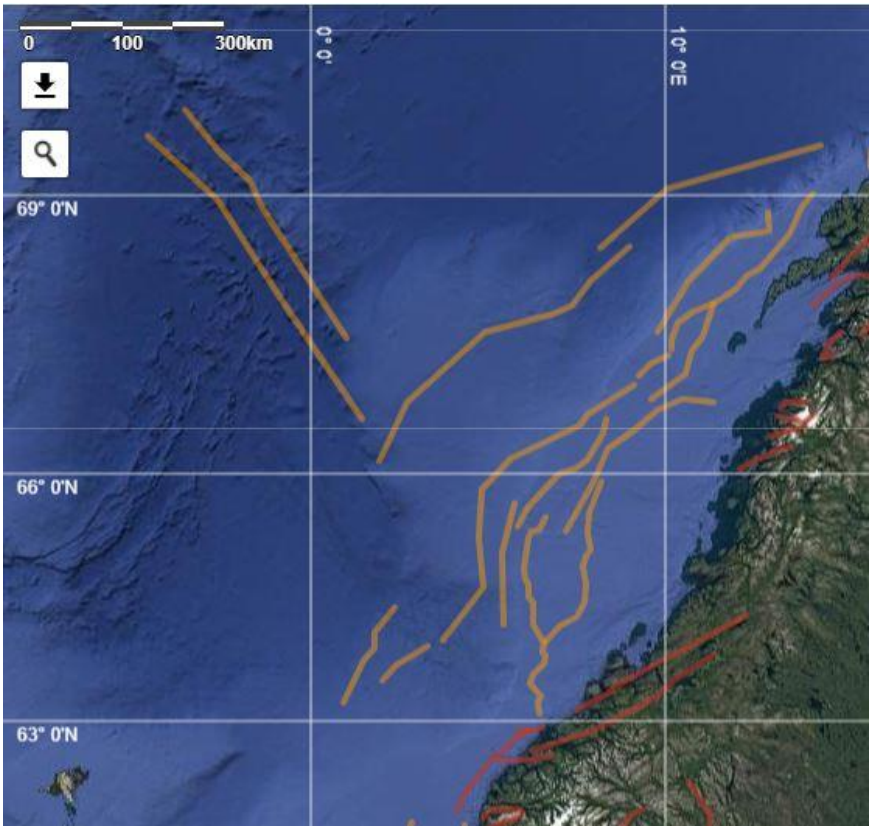

Figure 52: Location of the significant faults in the Norwegian Sea.

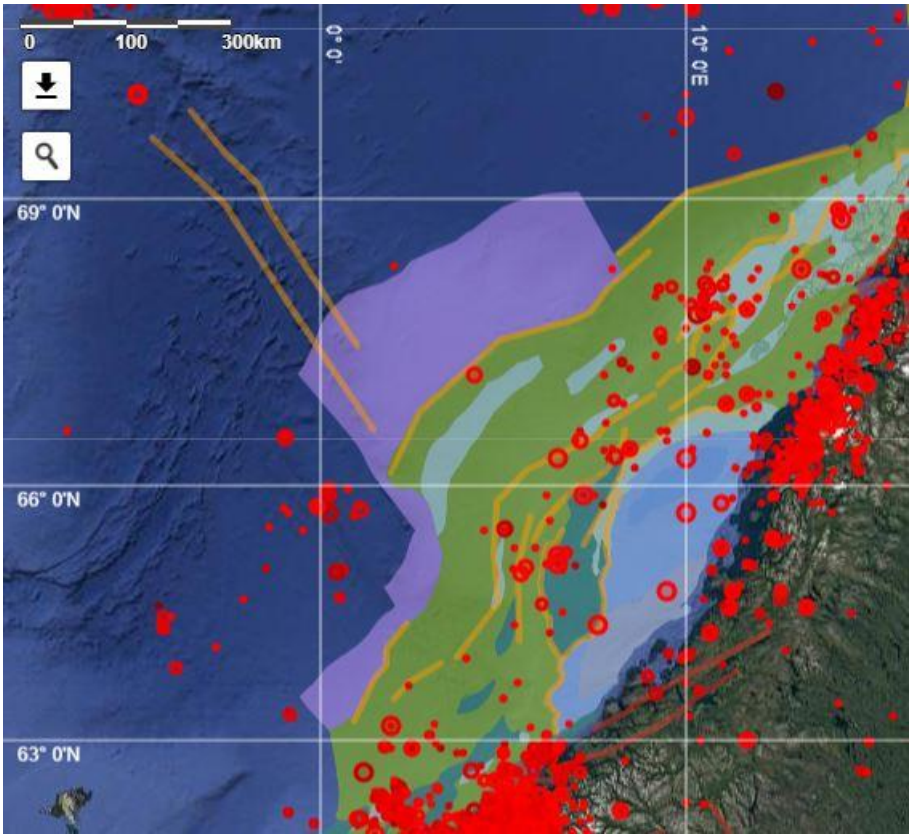

Figure 53: Location of the significant faults in the Norwegian Sea, shown together with the main structural elements (in color-shaded areas) from NPD and the seismicity (since 1980) from NNSN (red circles).

In total two faults, three faults zones, four fault complexes, two escarpments and one continental margin have been analyzed, with 17 segments. Distribution of these faults in the Norwegian Sea is as follows (see Figures 51, 52 and 53):

- Majority of the faults analyzed have NE-SW strike and are nearly parallel to the central coast of mainland Norway. These are Fles fault complex, Vesterdjupet fault zone, Ytreholmen fault zone, Revfallet fault complex, Vøring Plateau Escarpment, Utrøst Ridge NW Boundary Fault and Bremstein-Vingleia fault complex.
- N-S oriented faults that are diagonal to the central coast of mainland Norway. These are Helland-Hansen arch eastern boundary fault and Klakk fault complex.
- NW-SE oriented east Jan Mayen fracture zone that is perpendicular to the central coast of mainland Norway.
- NNE-SSW oriented Faeroe-Shetland escarpment and ENE-WSW oriented Lofoten-Vesterålen margin that are oblique-parallel to the central coast of mainland Norway.

Table 22: Geological data for the Norwegian Sea zone. Abbreviation *Surf. P. of the W.* in the column *Fault Dimensions* stands for surface projection of the width.

Fault ID	Fault Name	Segment ID	Seg. Name	Fault location				Fault dimesions			Fault orientation			Max possible	References
				End point-1		End point-2		Length	Surf. P. of the W	Width	Strike	Dip	Slip	Magnitude	
				Lat	Lon	Lat	Lon	km	km	km					
Z-03-F01	Fles Fault Complex	Z-03-F01-S01	Seg-01	63,4939	1,9171	63,9441	3,2739	83,00	8,00	23,00	NE-SW	70°NW	normal	7,4	He, 2015
		Z-03-F01-S02	Seg-02	63,9650	3,6694	67,0163	9,0527	464,00	8,00	23,00	NE-SW	70°NW	normal	8,4	He, 2015
		Z-03-F01-S03	Seg-03	67,1012	9,2175	67,3221	10,1184	45,00	9,00	26,00	NE-SW	70°NW	normal	7,0	He, 2015
		Z-03-F01-S04	Seg-04	67,3683	10,1733	69,0174	14,1394	257,00	9,00	26,00	NE-SW	70°NW	normal	8,0	He, 2015
Z-03-F02	Vesterdjupet Fault Zone	Z-03-F02-S01	Seg-01	66,7950	9,5581	68,6803	13,3593	265,00	8,00	23,00	NE-SW	70°NW	normal	8,1	He, 2015
Z-03-F03	Helland-Hansen Arch Eastern B. F.	Z-03-F03-S01	Seg-01	64,1711	5,2624	65,7017	5,8227	180,00	7,00	20,00	N-S	70°W	normal	7,8	He, 2015
Z-03-F04	Klakk Fault Complex	Z-03-F04-S01	Seg-01	63,0587	6,4270	64,2088	6,2402	150,00	10,00	29,00	N-S	70°W	normal	7,7	He, 2015
		Z-03-F04-S02	Seg-02	64,2529	6,2731	65,4943	6,6577	149,00	10,00	29,00	NNE-SSW	70°WNW	normal	7,7	He, 2015
Z-03-F05	Ytreholmen Fault Zone	Z-03-F05-S01	Seg-01	65,3655	5,7678	66,6131	8,3605	196,00	10,00	29,00	NE-SW	70°NW	normal	7,9	He, 2015
Z-03-F06	Revfallet Fault Complex	Z-03-F06-S01	Seg-01	65,3015	7,1740	66,8047	11,4038	275,00	6,00	18,00	NE-SW	70°NW	normal	8,1	He, 2015
Z-03-F07	Faeroe-Shetland Escarpment	Z-03-F07-S01	Seg-01	63,2273	0,7141	64,4247	2,4169	164,00	4,00	12,00	NNE-SSW	70°WNW	normal	7,8	He, 2015
Z-03-F08	East Jan Mayen Fracture Zone	Z-03-F08-S01	Seg-01	66,6212	1,4611	69,6039	-4,6362	428,00	0,00	15,00	NW-SE	90°	sinistral strike-slip	8,1	He, 2015
		Z-03-F08-S02	Seg-02	67,4869	1,0546	69,8818	-3,6474	327,00	0,00	19,00	NW-SE	90°	sinistral strike-slip	8,0	He, 2015
Z-03-F09	Vøring Plateau Escarpment	Z-03-F09-S01	Seg-01	66,0854	1,7358	68,4936	9,0966	420,00	5,00	15,00	NE-SW	70°NW	normal	8,3	He, 2015
Z-03-F10	Lofoten-Vesterålen Margin	Z-03-F10-S01	Seg-01	68,4777	8,1518	69,5176	14,4360	280,00	10,00	29,00	ENE-WSW	70°NNW	normal	8,1	He, 2015
Z-03-F11	Utrøst Ridge NW B. F.	Z-03-F11-S01	Seg-01	67,5568	9,6679	68,8621	12,8759	221,00	8,00	23,00	NE-SW	70°NW	normal	8,0	He, 2015
Z-03-F12	Bremstein – Vingleia Fault Compl	Z-03-F12-S01	Seg-01	63,9940	6,6137	65,9016	8,2397	249,00	9,00	26,00	NE-SW	70°NW	normal	8,0	He, 2015

Table 23: Seismological data for the Norwegian Sea zone.

Fault ID	Fault Name	Segment ID	Seg. Name	# earthquakes	Max observed magnitude		Focal mechanism				Nodal plane 2			Regional stress tensor						D. to Moho
					Historical	Instrumental	Nodal Plane 1			Quality				Sigma 1		Sigma 2		Sigma 3		
					Before 1980	After 1980	Strike	Dip	Rake		Strike	Dip	Rake	Azimuth	Plunge	Azimuth	Plunge	Azimuth	Plunge	
Z-03-F01	Fles Fault Complex	Z-03-F01-S01	Seg-01	2	NA	5,3	176,3000	51,3000	74,8000	B	19,7900	41,1400	108,1200	317	17	213	39	66	46	22,50
		Z-03-F01-S02	Seg-02	18	4,8	3,6	349,3000	60,4000	-17,6000	NA	88,2100	74,7600	-149,2100	317	17	213	39	66	46	22,50
							340,1000	60,0000	-59,9000	D	110,8800	41,4800	-130,9800	317	17	213	39	66	46	22,50
							61,7000	86,2000	40,0000	B	328,5200	50,1100	175,0400	317	17	213	39	66	46	22,50
							247,2000	61,8000	101,2000	C	44,4700	30,1700	70,0900	317	17	213	39	66	46	22,50
							340,1000	60,0000	-59,9000	D	110,8800	41,4800	-130,9800	317	17	213	39	66	46	22,50
							180,0000	0,0000	-97,9800	D	187,9800	90,0000	90,0000	317	17	213	39	66	46	25,00
		Z-03-F01-S03	Seg-03	1	3,0	NA	NA	NA	NA	NA	NA	NA	NA	317	17	213	39	66	46	25,00
		Z-03-F01-S04	Seg-04	10	4,6	3,6	52,5000	71,2000	-111,8000	B	283,3400	28,4800	-42,5100	317	17	213	39	66	46	25,00
Z-03-F02	Vesterdjupet Fault Zone	Z-03-F02-S01	Seg-01	7	4,3	3,5	28,4300	42,0600	31,1100	D	274,3000	69,7500	127,6900	317	17	213	39	66	46	22,50
							251,9800	15,7900	71,3000	D	91,3400	75,0600	95,1800	317	17	213	39	66	46	22,50
							315,9000	28,7000	-64,4000	D	107,2600	64,3400	-103,3100	317	17	213	39	66	46	22,50
							216,3000	47,5000	99,0000	B	23,1100	43,2600	80,3100	317	17	213	39	66	46	20,00
Z-03-F03	Helland-Hansen Arch Eastern B. F.	Z-03-F03-S01	Seg-01	6	4,3	NA	340,1000	60,0000	-59,9000	D	110,8800	41,4800	-130,9800	317	17	213	39	66	46	20,00
							16,9000	62,0000	-49,5000	C	135,7000	47,8200	-140,6900	317	17	213	39	66	46	22,50
Z-03-F04	Klakk Fault Complex	Z-03-F04-S01	Seg-01	0	NA	NA	NA	NA	NA	NA	NA	NA	NA	317	17	213	39	66	46	27,50
		Z-03-F04-S02	Seg-02	3	5,0	NA	NA	NA	NA	NA	NA	NA	NA	317	17	213	39	66	46	27,50
Z-03-F05	Ytreholmen Fault Zone	Z-03-F05-S01	Seg-01	11	5,0	4,4	179,6000	83,6000	-7,8000	D	270,4700	82,2500	-173,5400	317	17	213	39	66	46	27,50
Z-03-F06	Revfallet Fault Complex	Z-03-F06-S01	Seg-01	7	5,3	NA	NA	NA	NA	NA	NA	NA	NA	317	17	213	39	66	46	17,50
Z-03-F07	Faeroe-Shetland Escarpment	Z-03-F07-S01	Seg-01	1	3,1	NA	NA	NA	NA	NA	NA	NA	NA	NA	NA	NA	NA	NA	NA	12,00
Z-03-F08	East Jan Mayen Fracture Zone	Z-03-F08-S01	Seg-01	NA	NA	NA	NA	NA	NA	NA	NA	NA	NA	NA	NA	NA	NA	NA	NA	15,00
		Z-03-F08-S02	Seg-02	NA	NA	NA	NA	NA	NA	NA	NA	NA	NA	317	17	213	39	66	46	19,00
Z-03-F09	Vøring Plateau Escarpment	Z-03-F09-S01	Seg-01	1	4,0	NA	NA	NA	NA	NA	NA	NA	NA	NA	NA	NA	NA	NA	NA	15,00
Z-03-F10	Lofoten-Vesterålen Margin	Z-03-F10-S01	Seg-01	2	3,0	3,4	178,4000	80,2000	45,2000	C	78,6700	45,6400	166,2300	17	32	172	55	279	12	27,5
Z-03-F11	Utrøst Ridge NW B. F.	Z-03-F11-S01	Seg-01	11	4,6	3,6	52,5000	71,2000	-111,8000	B	283,3400	28,4800	-42,5100	17	32	172	55	279	12	22,5
							78,1000	56,5000	-126,3000	C	311,1800	47,7700	-48,1900	17	32	172	55	279	12	22,5
							24,8000	74,8000	-60,0000	C	139,2200	33,3100	-151,4800	17	32	172	55	279	12	22,5
							180,0000	0,0000	-97,9800	D	187,9800	90,0000	90,0000	17	32	172	55	279	12	22,5
							80,2600	85,0000	79,9600	D	324,0500	11,2000	153,3500	17	32	172	55	279	12	22,5
Z-03-F12	Bremstein – Vingleia Fault Compl	Z-03-F12-S01	Seg-01	1	5,0	NA	NA	NA	NA	NA	NA	NA	NA	17	32	172	55	279	12	25,0

All faults, except East Jan Mayen fracture zone, have steep dip angle that is equal to 70˚ (Table 22). East Jan Mayen fracture zone is a pure left-lateral strike-slip fault that has vertical dip angle equal to 90˚. All faults with a steep 70˚ angle mainly dip towards the basins' side, Møre and Vøring, that is towards the west with some slight variations. That is explained by several extensional episodes during late Devonian-Paleocene periods that led to the formation of Møre and Vøring basins, and sea-floor spreading in the North Atlantic that has started in the earliest Eocene (Norwegian Petroleum Directorate, 2019). Dominant mechanism is normal faulting that is as well explained by basin structures and extensional episode in the area (Table 22).

The longest fault segment in the area is of 464 km and is a part of Flex fault complex. There are also other two segments that stretched over large area. These are segments of east Jan Mayen fracture zone that is of 428 km and Vøring plateau escarpment that is of 420 km. The shortest fault segment is of 45 km and is a part of Flex fault complex. Other segments vary in length. Based on the length of the fault segments largest possible earthquake magnitude is assigned for each of these segments using Wells and Coppersmith's (1994) empirical relation. The maximum possible earthquake magnitudes at each segment of the faults vary between 7.0 and 8.4 (Table 22).

For the Norwegian Sea one stress model has been prepared based on stress inversion of earthquake focal mechanism solutions from offshore Mid Norway (Table 23). This stress model shows sigma 1 is NW-SE oriented whereas sigma 3 is ENE-WSW oriented (Hicks et al., 2000). Both these axes are almost horizontal and hence indicate reverse to oblique-reverse faulting regime.

Fles Fault Complex: It consists of four segments. For segments 1, 2 and 4 only one criterion described in chapter 3 (Methodology), is not fulfilled and hence further interpretation is required. For segment 3 several criteria described in chapter 3 (Methodology), are not fulfilled and hence for this segment reactivation potential is considered "not possible".

Segment 1: There is one focal mechanism of B quality that shows oblique-reverse faulting. This faulting mechanism is compatible with NE-SW oriented segment and NW-SE oriented sigma 1 and ENE-WSW oriented sigma 3. However, there is not much seismicity in the area nearby the segment. Analyzing all data gathered for the segment it is interpreted that for this segment potential of being reactivated is possible.

Segment 2: There are six focal mechanisms of various qualities indicating different types of faulting. Four focal mechanisms for one of which there is no quality information, and three remaining that are of D quality show oblique-normal faulting. Other two focal mechanisms of B and C qualities show oblique-reverse faulting. With given NE-SW orientation of the segment and NW-SE oriented sigma 1 and ENE-WSW oriented sigma 3, the reactivation of the segment in oblique-normal faulting would be difficult. Focal mechanisms showing oblique-normal faulting can only be interpreted as being small transverse structures with magnitudes less than 4.8 corresponding to lengths less than 2.2 km. Such variation along a fault segment extending 464 km is assumed to be natural. Earthquake distributed along both favorable for reactivation NW segment's dipping side and unfavorable SE side. Analyzing all data gathered for the segment it is interpreted that for this segment potential of being reactivated is possible.

Segment 4: There is one focal mechanism of B quality showing oblique-normal faulting. With given NE-SE orientation of the segment and NW-SE oriented sigma 1 and ENE-WSW oriented sigma 3 reactivation of the segment in oblique-normal faulting would be difficult. Focal mechanism showing oblique-normal faulting is interpreted as being small transverse structure with magnitudes less than 4.6 corresponding to lengths less than 1.8 km. Such variation along a fault segment extending 257 km

is assumed to be natural. Analyzing all information gathered for the segment it is interpreted that for this segment potential of being reactivated is not possible.

Vesterdjupet fault zone: It consists of one segment for which only one criterion described in chapter 3 (Methodology), is not fulfilled and hence further interpretation is required. There are four focal mechanisms of B and D qualities available. Three focal mechanisms (two of D and one of B quality) show oblique-reverse faulting that is compatible with NE-SW orientation of the fault and NW-SE oriented sigma 1 and ENE-WSW oriented sigma 3. Remaining focal mechanism is of D quality and show oblique-normal faulting. Considering the fault has slight variations in strike the focal mechanism showing oblique-normal faulting can be only interpreted as being small transverse structure with magnitudes less than 4.3 corresponding to length less than 1.2 km. Such variation along a complex fault extending 265 km is natural. Earthquakes distributed along the NW favorable for reactivation segment's dipping side and SE unfavorable side. Analyzing all information gathered for the fault zone it is interpreted that for this fault zone potential of being reactivated is possible.

Helland-Hansen Arch eastern boundary fault: It consists of one segment for which only one criterion described in chapter 3 (Methodology), is not fulfilled and hence further interpretation is required. There are two focal mechanisms available. Focal mechanisms are of D and C qualities and both show oblique-normal faulting. With given N-S orientation of the fault and NW-SE oriented sigma 1 and ENE-WSW oriented sigma 3, the reactivation of a fault in oblique-normal faulting would be difficult. Focal mechanisms showing oblique-normal faulting are interpreted as being small transverse structures with magnitudes less than 4.3 corresponding to lengths less than 1.3 km. Such variation along a fault segment extending 180 km is assumed to be natural. Earthquakes distributed both on the eastern (unfavorable for reactivation) and western (favorable for reactivation) sides. Analyzing all information gathered for the fault it is interpreted that for this fault potential of being reactivated is not possible.

Klakk fault complex: It consists of two segments for which several criteria described in chapter 3 (Methodology), are not fulfilled and hence for this segment reactivation potential is considered "not possible".

Ytreholmen fault zone: It consists of one segment for which only one criterion described in chapter 3 (Methodology), is not fulfilled and hence further interpretation is required. There is one focal mechanism available. The focal mechanism is of D quality showing oblique-normal faulting. With given NE-SW orientation of the fault and NW-SE orientated sigma 1 and ENE-WSW oriented sigma 3, the reactivation of a fault in oblique-normal faulting would be difficult. Majority of earthquakes around the fault locate at the favorable for reactivation northwestern segment's dipping side. Analyzing all information gathered for the fault zone it is interpreted that for this fault zone potential of being reactivated is not possible.

Revfallet fault complex: It consists of one segment for which several criteria described in chapter 3 (Methodology), are not fulfilled and hence for this fault complex reactivation potential is considered "not possible".

Faeroe-Shetland escarpment: It consists of one segment for which several criteria described in chapter 3 (Methodology), are not fulfilled and hence for this escarpment reactivation potential is considered "not possible".

East Jan Mayen fracture zone: It consists of two segments for which several criteria described in chapter 3 (Methodology), are not fulfilled and hence for these segments reactivation potential is considered "not possible".

Vøring plateau escarpment: It consists of one segment for which several criteria described in chapter 3 (Methodology), are not fulfilled and hence for this escarpment reactivation potential is considered "not possible".

Lofoten-Vesterålen margin: It consists of one segment for which only one criterion described in chapter 3 (Methodology), is not fulfilled and hence further interpretation is required. There is one focal mechanism available. Focal mechanism is of C quality showing oblique-reverse faulting. This faulting mechanism is compatible with ENE-WSW orientation of the segment and NW-SE oriented sigma 1 and ENE-WSW oriented sigma 3. There are only two earthquakes observed near the margin, one of which locates at the NNW of the margin side that is favorable for reactivation whereas another one locates at the opposite unfavorable side. Analyzing all information gathered for the margin one interprets that for this margin seismogenic potential of being reactivated is possible.

Utrøst Ridge NW boundary fault: It consists of one segment for which only one criterion described in chapter 3 (Methodology), is not fulfilled and hence further interpretation is required. There are five focal mechanisms available. Four focal mechanisms of B, C and D qualities show oblique-normal faulting whereas remaining one is of D quality and show oblique-reverse faulting. With given NE-SW orientation of a fault and NW-SE oriented sigma 1 and ENE-WSW oriented sigma 3, the reactivation of a fault in oblique-normal faulting would be difficult. Focal mechanisms showing oblique-normal faulting can only be interpreted as being small transverse structures with magnitudes less than 4.6 corresponding to length less than 1,8 km. Such variation along a fault extending 221 km is natural. Earthquakes locate on both favorable for reactivation northwestern side and along unfavorable southeastern side. Analyzing all information gathered for the fault it is interpreted that potential for this fault of being reactivated is possible.

Bremstein – Vingleia fault complex: It consists of one segment for which several criteria described in chapter 3 (Methodology), are not fulfilled and hence for this segment reactivation potential is considered "not possible".

Table 24: Interpreted results for the Norwegian Sea zone.

Fault/Fault zone/Fault complex	Potential of being reactivated			
	Almost certain	Probable	Possible	Not possible
Fles Fault Complex (Segment 1)			v	
Fles Fault Complex (Segment 2)			v	
Fles Fault Complex (Segment 3)				v
Fles Fault Complex (Segment 4)				v
Vesterdjupet Fault Zone			v	
Helland-Hansen Arch Eastern Boundary Fault				v
Klakk Fault Complex				v
Ytreholmen Fault Zone				v
Revfallet Fault Complex				v
Faeroe-Shetland Escarpment				v
East Jan Mayen Fracture Zone				v
Vøring Plateau Escarpment				v
Lofoten-Vesterålen Margin			v	
Utrøst Ridge NW Boundary Fault			v	
Bremstein – Vingleia Fault Complex				v

Summarizing interpretations made for the Norwegian Sea zone, one can distinguish between faults for which potential of being reactivated is possible and not possible (Table 24). It was interpreted that for the majority of the segments potential of being reactivated is not possible. For several segments potential of being reactivated is possible.

6.4 Onshore Mid Norway

1. Møre-Trøndelag Fault Zone
   - 1a. Segment 1
   - 1b. Segment 2
   - 1c. Segment 3
   - 1d. Segment 4
   - 1e. Segment 5
2. Nesna Shear Zone
3. Værangfjord-Nordfjord Fault
4. Meloyfjord Fault
5. Meloy-Glomtfjorden Fault
6. Skjærstadfjord Fault
7. Sagfjord Shear Zone

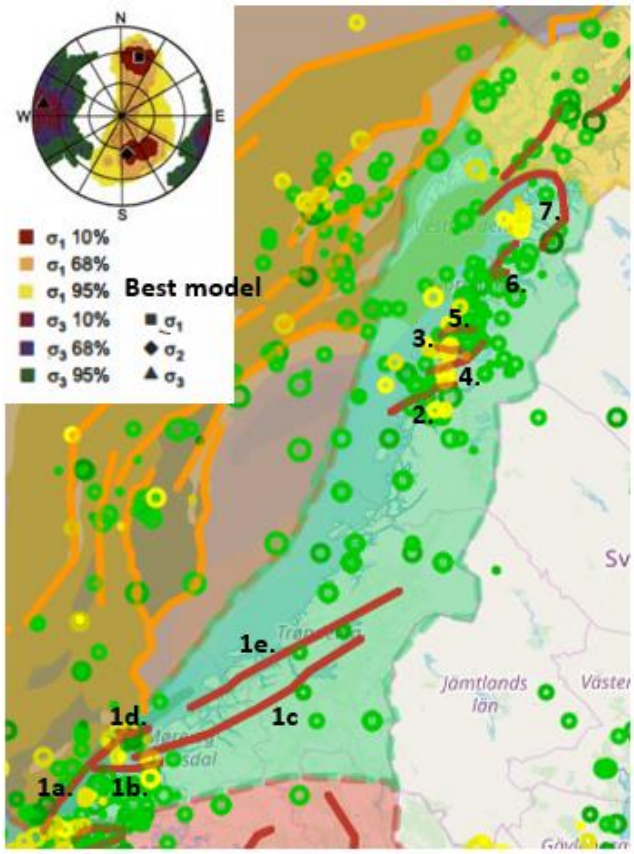

Figure 54: Onshore Mid Norway is represented by light green color. Faults and segments along Onshore Mid Norway chosen for the analysis are represented with the red color. Seismicity from 1980 onwards represented by yellow circles whereas seismicity for the period preceding 1980 represented with the green circles. The size of a circle is proportional to the magnitude of the event. Circle at the left upper corner represents stress model generated as a result from the inversion of earthquake focal mechanism solutions. The yellow, green and red areas represent 95%, 68% and 10% confidence limits respectively (Hicks et al., 2000).

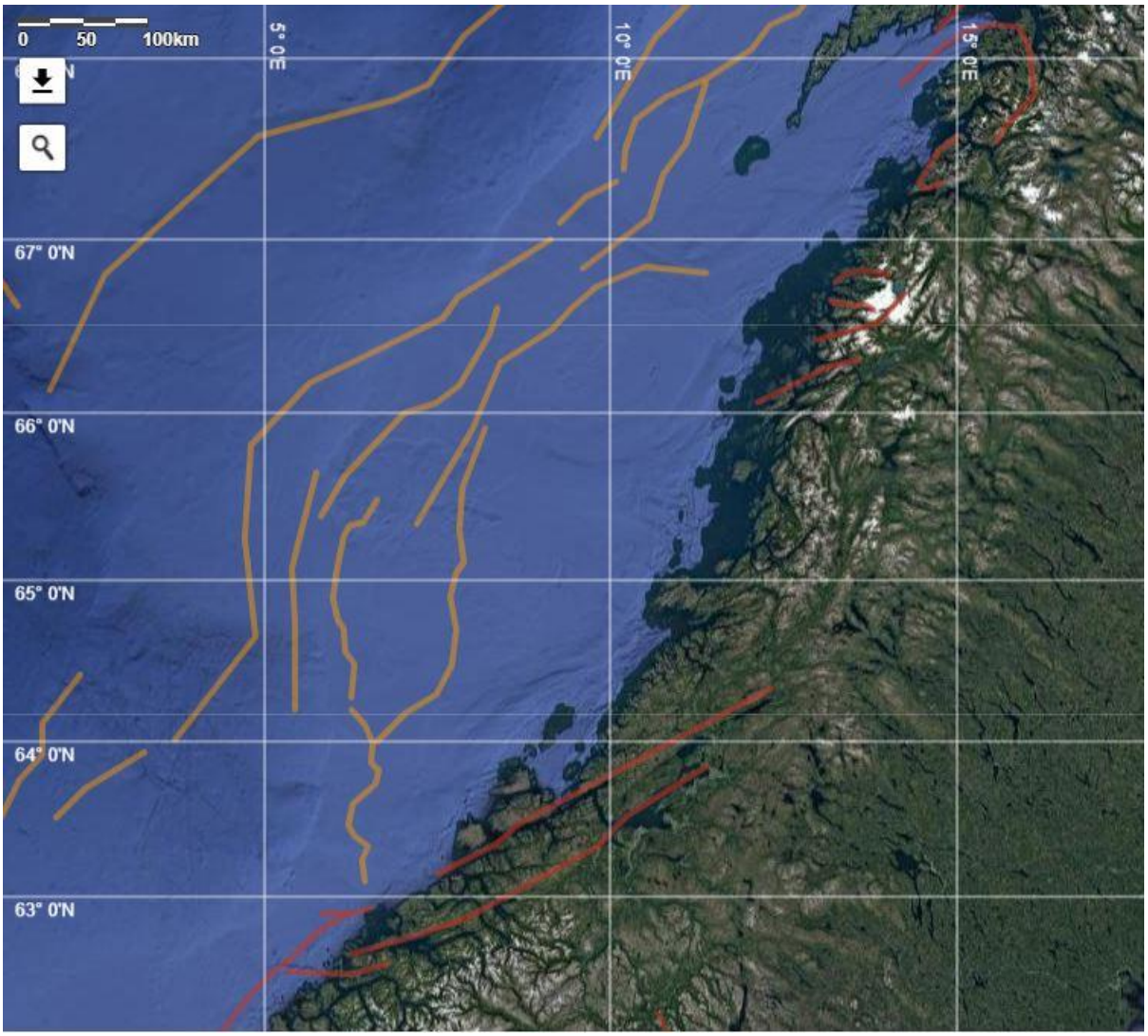

Figure 55: Location of the significant faults in Mid-Norway.

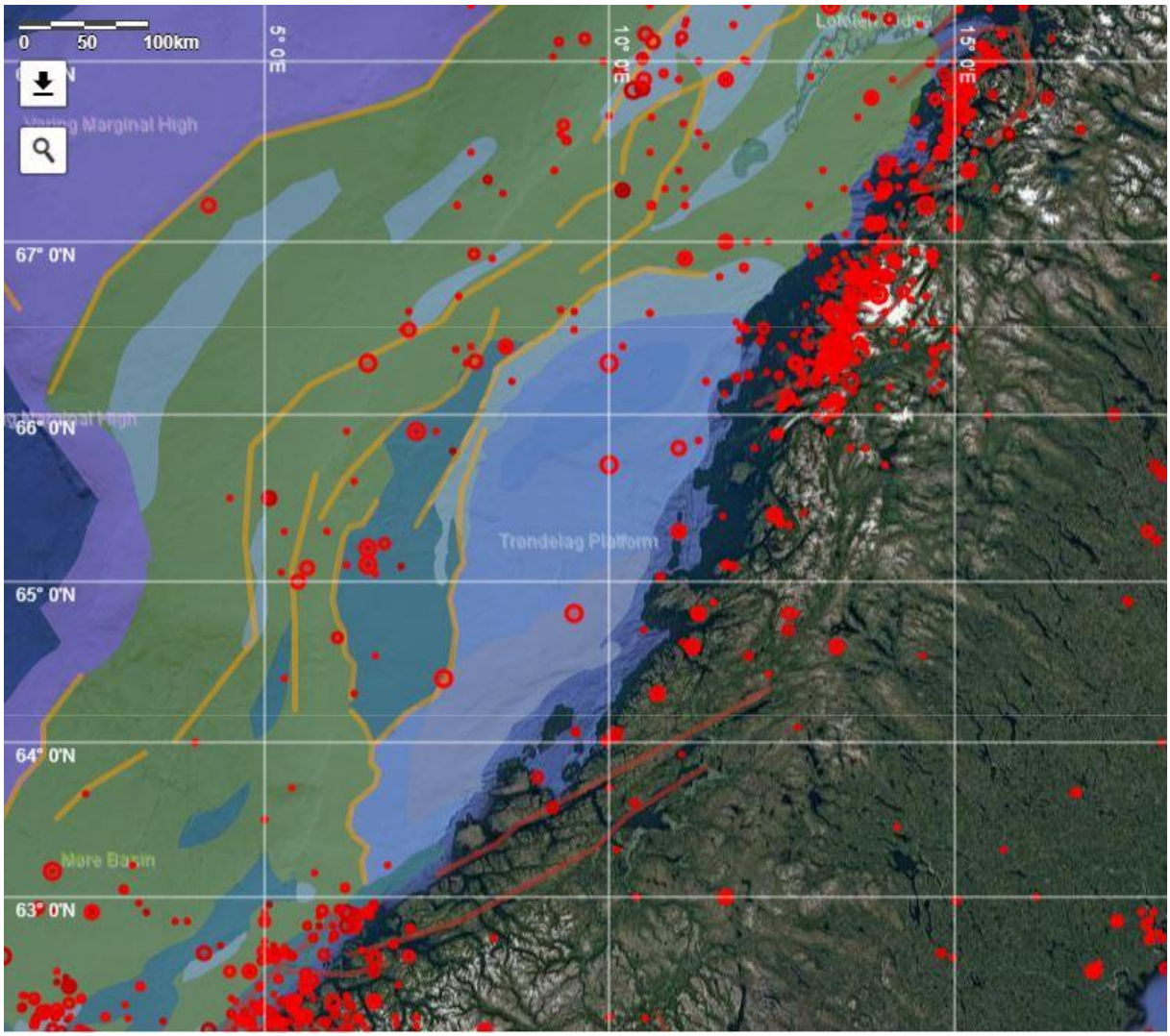

Figure 56: Location of the significant faults shown in Mid-Norway, together with the main structural elements (in color-shaded areas) from NPD and the seismicity (since 1980) from NNSN (red circles).

In total four faults and three fault zones have been analyzed. Distribution of these faults along onshore Mid Norway is as follows (see Figures 54, 55 and 56):

- Møre-Trøndelag fault zone with dominant NE-SW orientation diagonally cuts central part of mainland Norway.
- Two faults and one fault zone with NE-SW orientation diagonally cut northern part of mainland Norway. These are Nesna shear zone, Meløyfjord and Skjærstadfjord fault. There is also one fault zone that has the same NE-SW orientation and appears in the form of an arch that crops out at the northern mainland Norway. This is Sagfjord shear zone.
- Two faults with E-W strike cut northern mainland Norway in nearly perpendicular way. These are Værangfjord-Nordfjord and Meløy-Glomtfjorden faults.

Table 25: Geological data for the Onshore Mid Norway zone. Abbreviation *Surf. P. of the W.* in the column *Fault Dimensions* stands for surface projection of the width.

Fault ID	Fault Name	Segment ID	Seg. Name	Fault location				Fault dimesions			Fault orientation			Max possible	References
				End point-1		End point-2		Length	Surf. P. of the W	Width	Strike	Dip	Slip	Magnitude	
				Lat	Lon	Lat	Lon	km	km	km					
Z-04-F01	Møre-Trøndelag Fault Zone	Z-04-F01-S01	Seg-01	61,8063	4,1281	62,8814	6,1866	163,00	5,00	15,00	NE-SW	80°NW	dextral strike-slip	7,6	Gabrielsen et al., 2002
			Seg-02	62,4991	5,3009	62,5498	6,8334	80,00	-	32,50	ENE-WSW	90°	dextral strike-slip	7,3	Gabrielsen et al., 2002
			Seg-03	62,6079	6,2072	63,8480	11,4147	300,00	-	27,50	NE-SW	90°	dextral strike-slip	7,9	Gabrielsen et al., 2002
			Seg-04	62,8811	5,8529	62,9249	6,5451	37,00	-	30,00	ENE-WSW	90°	dextral strike-slip	6,9	Gabrielsen et al., 2002
			Seg-05	63,1437	7,4761	64,3302	12,3321	277,00	-	32,50	NE-SW	90°	dextral strike-slip	7,9	Gabrielsen et al., 2002
Z-04-F02	Nesna Shear Zone	Z-04-F02-S01	Seg-01	66,0438	12,0849	66,3146	13,6230	79,00	56,00	65,00	NE-SW	30° NW	thrust	7,3	Janutyte et al., 2017
Z-04-F03	Værangfjord-Nordfjord Fault	Z-04-F03-S01	Seg-01	66,6549	13,1753	66,6037	13,8070	31,00	NA	NA	E-W	NA	NA	6,8	This work
Z-04-F04	Meløyfjord Fault	Z-04-F04-S01	Seg-01	66,4264	12,9803	66,6844	14,2410	65,00	NA	NA	NE-SW	NA	NA	7,2	This work
Z-04-F05	Meløy-Glomtfjorden Fault	Z-04-F05-S01	Seg-01	66,7537	13,2302	66,8035	14,0103	36,00	NA	NA	E-W	NA	NA	6,9	This work
Z-04-F06	Skjerstadfjord Fault	Z-04-F06-S01	Seg-01	67,3160	14,7711	67,5795	15,0128	58,00	NA	NA	NE-SW	NA	NA	7,1	This work
Z-04-F07	Sagfjord Shear Zone	Z-04-F07-S01	Seg-01	67,8538	14,1613	67,5410	15,5676	161,00	61,00	70,00	NE-SW	30° NW	thrust	7,7	Ramberg et al., 2007

Table 26: Seismological data for the Onshore Mid Norway zone (Part 1).

Fault ID	Fault Name	Segment ID	Seg. Name	# earthquakes	Max observed magnitude		Focal mechanism							Regional stress tensor						D. to Moho
					Historical	Instrumental	Nodal Plane 1			Quality	Nodal plane 2			Sigma 1		Sigma 2		Sigma 3		
					Before 1980	After 1980	Strike	Dip	Rake		Strike	Dip	Rake	Azimuth	Plunge	Azimuth	Plunge	Azimuth	Plunge	
Z-04-F01	Møre-Trøndelag Fault Zone	Z-04-F01-S01	Seg-01	18	5,2	3,8	321,4000	62,0000	-67,1000	B	99,4200	35,5700	-126,2000	17	32	172	55	279	12	27,5
							184,5000	60,6000	78,4000	B	27,9000	31,4100	109,6400	17	32	172	55	279	12	27,5
							319,6000	84,4000	-7,1000	C	50,3000	82,9300	-174,3600	17	32	172	55	279	12	27,50
			Seg-02	5	4,1	3,9	192,5000	51,9000	70,7000	C	42,0800	42,0400	112,8600	17	32	172	55	279	12	32,50
			Seg-03	5	3,2	3,8	NA	NA	NA	NA	NA	NA	NA	17	32	172	55	279	12	27,50
			Seg-04	6	4,7	3,6	NA	NA	NA	NA	NA	NA	NA	17	32	172	55	279	12	30,00
			Seg-05	2	3,2	NA	NA	NA	NA	NA	NA	NA	NA	17	32	172	55	279	12	32,50
Z-04-F02	Nesna Shear Zone	Z-04-F02-S01	Seg-01	12	4,9	3,9	80,2600	85,0800	79,9600	D	324,4100	11,1700	153,7200	17	32	172	55	279	12	32,50
							124,0100	24,8100	51,9200	D	344,8100	70,7100	105,9100	17	32	172	55	279	12	32,50
							260,0000	30,0000	-90,0000	D	80,0000	60,0000	-90,0000	17	32	172	55	279	12	32,50
							174,7200	20,5100	60,2900	C	26,0700	72,2800	100,5000	17	32	172	55	279	12	32,50
							13,2400	45,0300	-64,1000	A	158,7500	50,4700	-113,6200	17	32	172	55	279	12	32,50
Z-04-F03	Værangfjord-Nordfjord Fault	Z-04-F03-S01	Seg-01	10	3,0	3,4	262,8600	84,0300	-83,9700	B	37,4200	8,4800	-135,1300	17	32	172	55	279	12	32,50
							40,7600	66,7600	-74,7300	B	186,0800	27,5700	-121,5200	17	32	172	55	279	12	32,50
							211,9100	10,0000	-90,0000	B	31,9100	80,0000	-90,0000	17	32	172	55	279	12	32,50
							308,1000	28,0700	-85,7500	C	123,2900	62,0100	-92,2600	17	32	172	55	279	12	32,50
							209,9200	16,0000	-90,0000	C	29,9200	74,0000	-90,0000	17	32	172	55	279	12	32,50
							13,9000	74,1600	-81,6800	B	165,7200	17,8400	-117,0200	17	32	172	55	279	12	32,50
							39,5600	58,7800	-75,9300	B	193,7500	33,9500	-111,8600	17	32	172	55	279	12	32,50
							40,7600	66,7600	-74,7300	B	186,0800	27,5700	-121,5200	17	32	172	55	279	12	32,50
							337,5200	48,4400	-30,7900	C	89,0900	67,4800	-134,1000	17	32	172	55	279	12	32,50
							224,0600	74,0100	87,9200	B	51,5700	16,1200	97,2200	17	32	172	55	279	12	32,50

Table 27: Seismological data for the Onshore Mid Norway zone (Part 2).

Fault ID	Fault Name	Segment ID	Seg. Name	#earthquakes	Max observed magnitude		Focal mechanism					Nodal plane 2		Regional stress tensor						D. to Moho
					Historical	Instrumental	Nodal Plane 1			Quality				Sigma 1		Sigma 2		Sigma 3		
					Before 1980	After 1980	Strike	Dip	Rake		Strike	Dip	Rake	Azimuth	Plunge	Azimuth	Plunge	Azimuth	Plunge	
Z-04-F04	Meløyfjord Fault	Z-04-F04-S01	Seg-01	15	4,5	3,9	1,2000	64,2000	56,4000	B	237,9700	41,4200	138,8600	17	32	172	55	279	12	32,50
							158,2000	81,1000	-141,5000	B	61,1800	52,0500	-11,3200	17	32	172	55	279	12	32,50
							218,4300	8,9400	-63,3200	B	11,4700	82,0200	-94,0400	17	32	172	55	279	12	32,50
							251,9800	15,7900	71,3200	D	91,3400	75,0600	95,1800	17	32	172	55	279	12	32,50
							213,4000	75,1000	-153,6000	B	116,1300	64,5500	-16,5400	17	32	172	55	279	12	32,50
							240,5800	76,5700	29,3200	C	143,1500	61,5600	164,6800	17	32	172	55	279	12	32,50
Z-04-F05	Meløy-Glomtfjorden Fault	Z-04-F05-S01	Seg-01	18	3,3	3,4	195,9600	42,0600	50,8900	D	63,5600	58,6800	119,6500	17	32	172	55	279	12	32,50
							7,4800	52,4100	-28,7600	C	115,9900	67,5900	-138,7100	17	32	172	55	279	12	32,50
							187,4800	20,1000	-84,1700	C	1,2700	70,0100	-92,1300	17	32	172	55	279	12	32,50
							75,4000	52,8000	16,0000	D	335,5600	77,3200	141,7000	17	32	172	55	279	12	32,50
							187,4800	20,1000	-84,1700	C	1,2700	70,0100	-92,1300	17	32	172	55	279	12	32,50
							355,0000	24,0600	64,7900	B	202,2700	68,3500	100,7700	17	32	172	55	279	12	35,00
Z-04-F06	Skjærstadfjord Fault	Z-04-F06-S01	Seg-01	11	4,6	3,2	43,1900	51,4700	-37,3700	B	158,6300	61,6500	-134,9400	17	32	172	55	279	12	35,00
							40,4000	29,0300	-73,3300	C	201,5000	62,3000	-99,0500	17	32	172	55	279	12	35,00
							229,0900	84,0600	81,9600	B	102,8600	9,9800	143,3500	17	32	172	55	279	12	35,00
							203,1000	70,5000	-36,3000	C	306,8800	56,0800	-156,2800	17	32	172	55	279	12	35,00
Z-04-F07	Sagfjord Shear Zone	Z-04-F07-S01	Seg-01	6	3,6	3,5	40,4000	29,0300	-73,3300	C	201,1400	62,3000	-99,0500	17	32	172	55	279	12	35,00
							355,0300	9,9900	-52,9400	C	137,5500	82,0400	-96,0600	17	32	172	55	279	12	35,00
							31,3900	80,0200	85,9400	C	233,6600	10,7700	111,9200	17	32	172	55	279	12	35,00

Dip of the faults, locating onshore Mid Norway, varies (Table 25). Shear structures formed during Caledonian episodes tend to have shallow dip angle that is equal to 30˚. Møre-Trøndelag fault zone is a pure dextral strike-slip structure that has vertical dip equal to 90 ˚. However, there is one segment that demonstrates oblique-slip where dip angle is equal to 80 ˚. There are also four faults that have been extracted from NGU open-file maps "Berggrunn raster" at a scale 1:250,000 (Norwegian Geological Survey, 2019). These faults are Værangfjord-Nordfjord, Meløyfjord, Meløy-Glomtfjorden and Skjærstadfjord faults. The faults are named based on the structures they cut, fjords. No studies on these faults have been reported in the literature and hence there is no dip and slip information available. Therefore, such parameters as width and surface projection of the width could not been calculated. That is as well reflected in Table 25. There are two types of faulting mechanisms in the study area. These are dextral strike-slip faulting associated with Møre-Trøndelag fault zone and thrust faulting associated with shear Caledonian structures, Nesna and Sagfjord shear zones (Table 25).

The longest fault segment in the area is of 300 km and is a part of the Møre-Trøndelag fault zone. The shortest fault segment in the area is of 31 km and is a part of Værangfjord-Nordfjord fault. Other segments vary in length. Based on the length of a fault segments the largest possible earthquake magnitude is assigned for each of these segments using Well and Coppersmith's (1994) empirical relation. The maximum possible earthquake magnitudes at each segment of the faults vary between 7.9 and 6.8 (Table 25).

For the Onshore Mid Norway one stress model has been prepared based on stress inversion of earthquake focal mechanism solutions from onshore Mid Norway (Tables 26, 27). This stress model shows sigma 1 is NNE-SSW oriented whereas sigma 3 is WNW-ESE oriented (Hicks et al., 2000). Such orientation of sigma 1 and sigma 3 indicate normal to strike-slip faulting regime.

Møre-Trøndelag fault zone: It consists of five segments. For segments 1 and 2 only one criterion described in chapter 3 (Methodology), is not fulfilled and hence further interpretation is required. For segments 3,4 and 5 several criteria described in chapter 3 (Methodology), are not fulfilled and hence for these segments reactivation potential is considered "not possible".

Segment 1: There are three focal mechanisms of B and C qualities showing different types of faulting. Two focal mechanisms one of which is of B and another one is of C quality show oblique-normal faulting whereas the remaining one is of C quality and shows oblique-reverse faulting. With given NE-SW orientation of the segment and NNE-SSW oriented sigma 1 and WNW-ESE oriented sigma 3, the reactivation of the segment in oblique-reverse faulting would be difficult. Focal mechanism showing oblique-reverse faulting can only be interpreted as being small transverse structure with magnitudes less than 5.2 corresponding to lengths 2.6 km. Such variation along a segment extending 163 km and showing minor strike variations is natural. Earthquake distributed along favorable for reactivation segment's dipping northwestern side and along unfavorable southeastern side. Analyzing all information gathered for the segment it is interpreted that for this segment potential of being reactivated is possible.

Segment 2: There is one focal mechanism of C quality showing oblique-reverse faulting. With given ENE-WSW orientation of the segment and NNE-SSW oriented sigma 1 and WNW-ESE oriented sigma 3, the reactivation of the segment in oblique-reverse faulting would be difficult. Focal mechanism showing oblique-reverse faulting can only be interpreted as being small transverse structure with magnitudes less than 4.1 corresponding to lengths less than ½ km. Such variations for the fault segment extending 80 km and showing minor strike variations is natural. Majority of earthquakes locate at the southeastern unfavorable for reactivation side. Analyzing all information gathered for the segment it is interpreted that for this segment potential of being reactivated is not possible.

Nesna shear zone: It consists of one segment for which only one criterion described in chapter 3 (Methodology), is not fulfilled and hence further interpretation is required. There are five focal mechanisms available. Three focal mechanisms two of which are of D quality and the remaining one is of C quality show oblique-reverse faulting. The remaining two focal mechanisms one of which is of A quality showing oblique-normal faulting whereas another one is of D quality showing pure normal faulting. With given NE-SW orientation of the fault and NNE-SSW oriented sigma 1 and WNW-ESE oriented sigma 3, the reactivation of the fault in oblique-reverse faulting would be difficult. This can be explained by the mixture of focal mechanisms observed in northern Norway. Several studies performed to study seismic activity in northern Norway indicate normal faulting mechanism to be dominant for the onshore northern area. For the transition coastal area prevailing focal mechanisms are normal and strike-slip whereas for the northern offshore area these are reverse and oblique-reverse (Olesen et al., 2018). According to Olesen et al. (2018), Nesna shear zone has earthquake swarms located north of it where it possibly changes direction and migrates offshore. Therefore, complex faulting mechanisms are natural feature that is observed in the area nearby the fault. Analyzing all information gathered for the fault it is interpreted that for this fault potential of being reactivated is possible.

Værangfjord-Nordfjord fault: It consists of one segment for which only one criterion described in chapter 3 (Methodology), is not fulfilled and hence further interpretation is required. There are ten focal mechanism available. Seven focal mechanisms of predominantly B quality show oblique-normal faulting whereas two focal mechanism of B and C qualities show pure normal faulting. Only one focal mechanism of B quality shows oblique-reverse faulting. With given E-W orientation of a fault and NNE-SSW oriented sigma 1 and WNW-ESE oriented sigma 3, the reactivation of the fault in oblique-reverse faulting would be difficult. Værangfjord-Nordfjord fault locates onshore with its minor part extending into offshore realm can be an explanation of a single focal mechanism showing oblique-reverse faulting that as was described by Olesen et al. (2018) typical offshore faulting mechanisms for northern Norway. All other focal mechanisms showing oblique-normal and normal faulting correlates well with investigations done by Olesen et al. (2018); Atakan et al. (1994); Bungum and Husebye (1979). Their studies show that earthquakes swarms occurred in Meløy in 1978-1979 and Steigen in 1992 led to sequence of normal- and oblique-normal faulting earthquakes propagating along N-S. Analyzing all information gathered for the fault it is interpreted that for this fault potential of being reactivated is possible.

Meløyfjord fault: It consists of one segment for which only one criterion described in chapter 3 (Methodology), is not fulfilled and hence further interpretation is required. There are six focal mechanisms available. Three focal mechanisms of B quality show oblique-normal faulting whereas three remaining focal mechanisms of B, C and D qualities show oblique-reverse faulting. With given NE-SW orientation of a fault and NNE-SSW oriented sigma 1 and WNW-ESE oriented sigma 3, the reactivation of the fault in oblique-reverse faulting would be difficult. The focal mechanisms showing oblique-reverse faulting can be explained by the location of Meløyfjord fault that lies both onshore and in transition coastal area that as was mentioned by Olesen et al. (2018) has complex faulting network. In addition, there is minor strike variation along the fault extent that can also be the reason of normal-faulting: in the southern part the fault is of ENE-WSW strike whereas the remaining dominant part is of NNE-SSW strike. Analyzing all gathered information for the fault it is interpreted that for this fault potential of being reactivates is possible.

Meløy-Glomtfjorden fault: It consists of one segment for which only one criterion described in chapter 3 (Methodology), is not fulfilled and hence further interpretation is required. There are six focal mechanisms available. Three focal mechanisms of C quality show oblique-normal faulting whereas

three remaining of D and B qualities show oblique-reverse faulting. With given E-W orientation of the fault and NNE-SSW oriented sigma 1 and WNW-ESE oriented sigma 3, the reactivation of the fault in oblique-reverse faulting would be difficult. The focal mechanisms showing oblique-reverse faulting can be explained by the location of Meløy-Glomtfjorden fault whose large part lies in the transition onshore-offshore coastal area that is characterized by complex faulting mechanisms. In addition, some minor strike variations along the fault extent are present that can also be the reason of complex faulting network nearby the fault. Other focal mechanisms showing oblique-normal faulting correlate well with the expected faulting regime caused by local flexural uplift-the force that triggered earthquake swarms around Meløy and Steigen area in 1978-1979 and 1992 respectively. Analyzing all information gathered for the fault it is interpreted that for this fault potential of being reactivated is possible.

Skjærstadfjord fault: It consists of one segment for which only one criterion described in chapter 3 (Methodology), is not fulfilled and hence further interpretation is required. There are four focal mechanisms available. Three focal mechanisms of B and C qualities show oblique-normal faulting whereas the remaining one is of B quality and shows oblique-reverse faulting. With given NE-SW orientation of the fault and NNE-SSW oriented sigma 1 and WNW-ESE oriented sigma 3, the reactivation of the fault in oblique-reverse faulting would be difficult. Focal mechanisms showing oblique-reverse faulting can be explained by the location of Skjærstadfjord fault that lies in the transition coastal area associated with complex faulting network and has minor strike variation related to its slightly bended northern part. Other three focal mechanisms showing oblique-normal faulting correlate well with the expected extensional faulting caused by local flexural uplift as was concluded by Gradmann et al. (2018). Analyzing all information gathered for the fault it is interpreted that for this fault potential of being reactivated is possible.

Sagfjord shear zone: It consists of one segment for which only one criterion described in chapter 3 (Methodology), is not fulfilled and hence further interpretation is required. There are three focal mechanisms available. Two focal mechanisms are of C quality and show oblique-normal faulting whereas the remaining one is of C quality showing oblique-reverse faulting. With given NE-SW orientation of the fault and NNE-SSW oriented sigma 1 and WNW-ESE oriented sigma 3, the reactivation of the fault in oblique-reverse faulting would be difficult. The focal mechanism showing oblique-reverse faulting can be explained by complex arched nature of the fault that shows strike variations. In addition, Sagfjord shear zone is stretched over the onshore, transition coastal area and offshore realm. Its eastern part lies onshore, arched part in transition coastal area whereas western part locates offshore. Referring to Olesen et al. (2018), normal faulting is the dominant onshore faulting mechanism, normal to strike-slip is associated with transitional coastal zone whereas complex mixed faulting network was mostly registered offshore. Considering Sagfjord shear zone is a complex fault extending over 161 km such variations in faulting mechanisms are assumed to be natural. Analyzing all information gathered for the fault it is interpreted that for this fault potential of being reactivated is possible.

Table 28: Interpreted results for the Onshore Mid Norway zone.

Fault/Fault zone/Fault complex	Potential of being reactivated			
	Almost certain	Probable	Possible	Not possible
Møre-Trøndelag Fault Zone (Segment 1)			v	
Møre-Trøndelag Fault Zone (Segment 2)				v
Møre-Trøndelag Fault Zone (Segment 3)				v
Møre-Trøndelag Fault Zone (Segment 4)				v
Møre-Trøndelag Fault Zone (Segment 5)				v
Nesna Shear Zone			v	
Værangfjord-Nordfjord Fault			v	
Meløyfjord Fault			v	
Meløy-Glomtfjorden Fault			v	
Skjærstadfjord Fault			v	
Sagfjord Shear Zone			v	

Summarizing interpretations made for the onshore Mid Norway zone, one can distinguish between faults for which potential of being reactivated is possible and not possible (Table 28). It was interpreted that for the majority of the segments potential of being reactivated is possible. For few segments potential of being reactivated is not possible.

6.5 Barents Continental shelf

1. Senja Fracture Zone
2. Troms-Finnmark Fault Complex
   - 2a. Segment 1
   - 2b. Segment 2
3. Ringvassøy-Loppa Fault Complex
   - 3a. Segment 1
   - 3b. Segment 2
   - 3c. Segment 3
4. Bjørnøyrenna Fault Complex
5. Leirdjupet fault
6. Hornsund Fault Zone
   - 6a. Segment 1
   - 6b. Segment 2
   - 6c. Segment 3
   - 6d. Segment 4

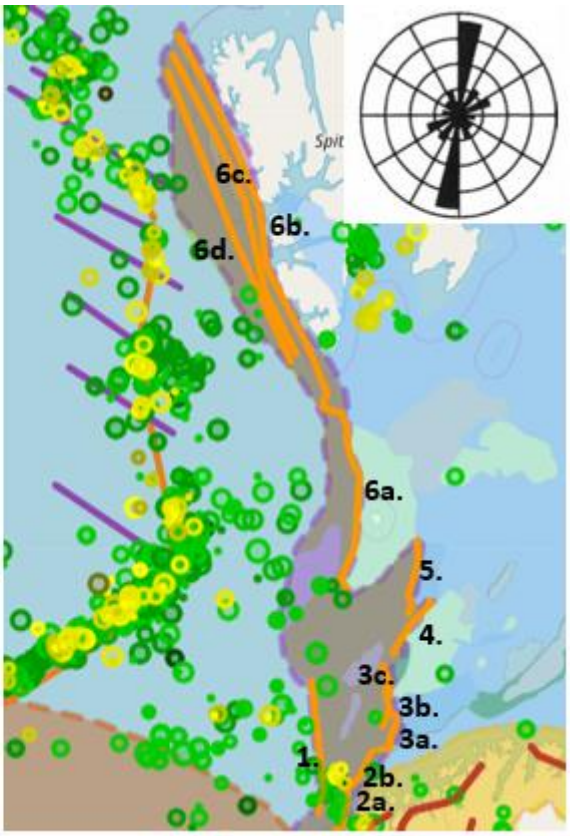

Figure 57: Barents Continental Shelf is represented by light purple color. Faults and segments along Barents Continental Shelf chosen for the analysis are represented with the orange color. Seismicity from 1980 onwards represented by yellow circles whereas seismicity for the period preceding 1980 represented with the green circles. The size of a circle is proportional to the magnitude of the event. Circle at the right upper corner represents directions of maximum horizontal compressive stress.

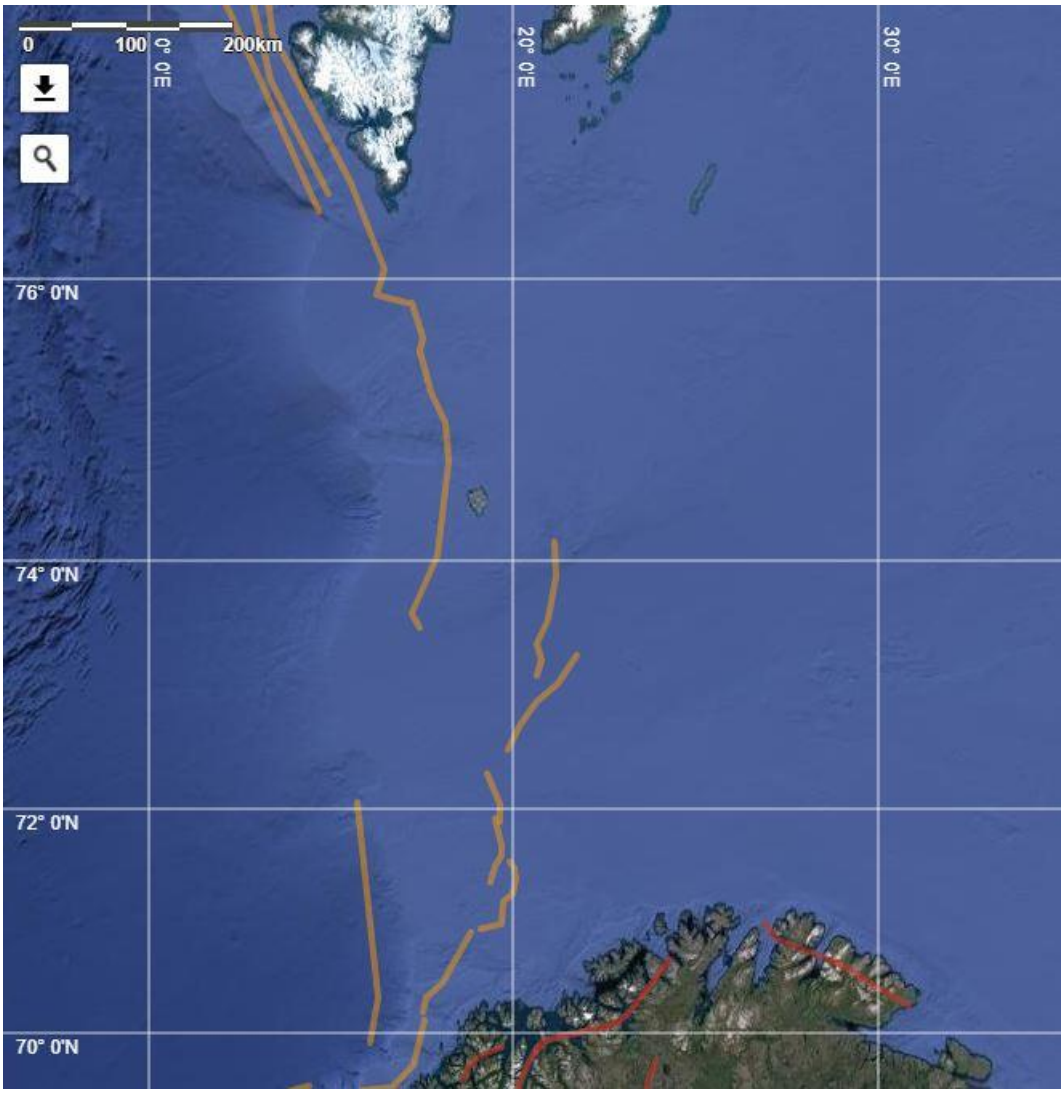

Figure 58: Location of the significant faults along the Barents Sea continental shelf.

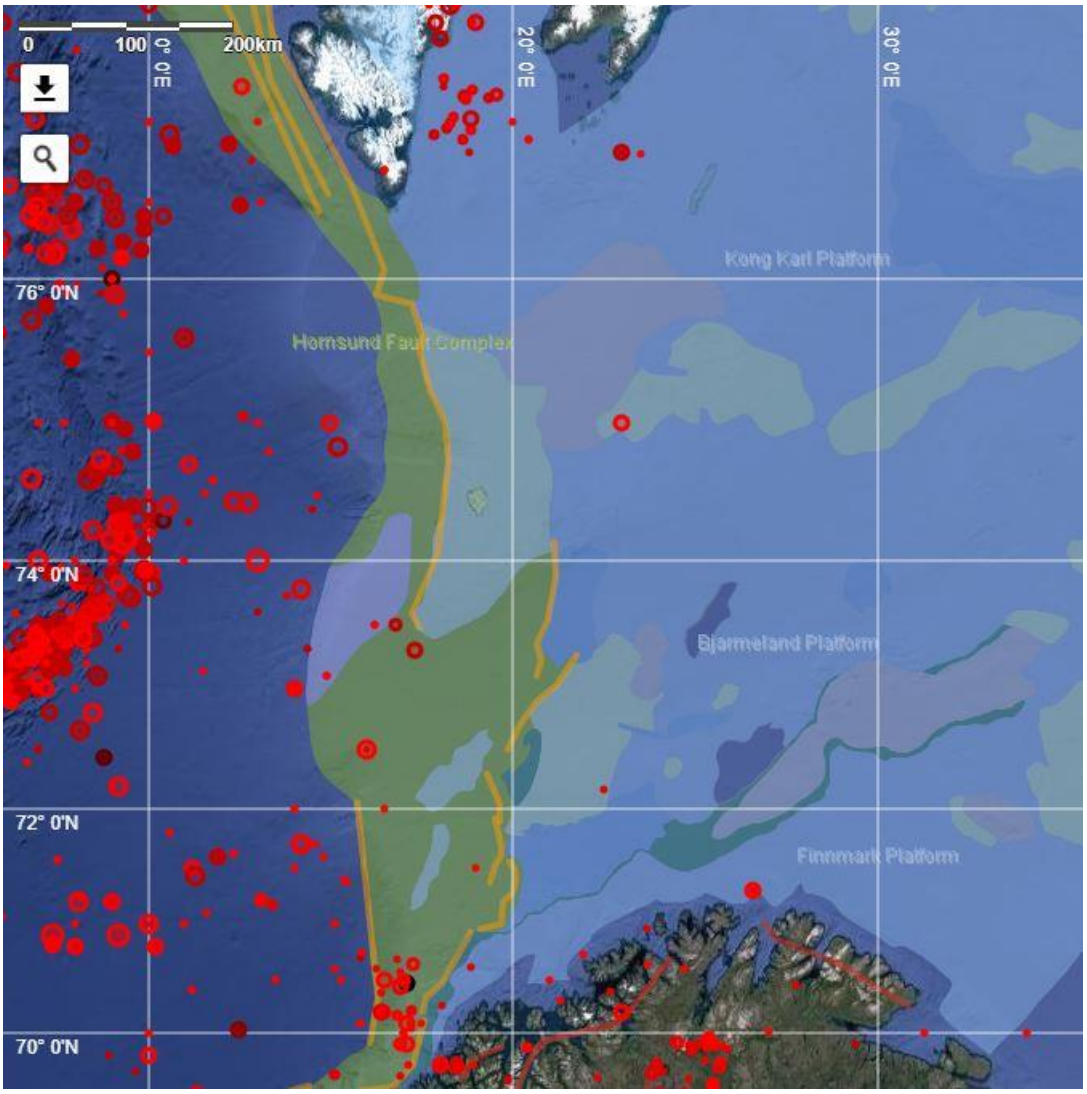

Figure 59: Location of the significant faults shown along the Barents Sea continental shelf, together with the main structural elements (color-shaded areas) from NPD and the seismicity (since 1980) from NNSN (red circles).

In total four fault complexes and two fault zones have been analyzed. Distribution of fault complexes and fault zones is as follows (see Figures 57, 58 and 59):

- There are two fault zones, one fault complex and one fault that are N-S oriented and stretches along eastern and western margins of the Barents continental shelf repeating its shape. These are Senja fracture zone that lies along southwestern margin of the Barents continental shelf, Ringvassøy-Loppa and Bjørnøyrenna fault complexes along Mid-eastern margin of Barents continental shelf and Hornsund fault zone, in particularly its first segment, along northeastern margin of the Barents continental shelf.
- There is also other fault and remaining segments of Hornsund fault zone that stretches along margins of Barents continental shelf showing slightly different strike. These are NNE-SSW oriented segment 1 and NE-SW oriented segment 2 constituting Troms-Finnmark fault complex, NE-SW oriented Leirdjupet fault and NNW-SSE oriented segments 2, 3 and 4 constituting Hornsund fault zone.

Table 29: Geological data for the Barents Continental Shelf zone. Abbreviation *Surf. P. of the W.* in the column *Fault Dimensions* stands for surface projection of the width.

Fault ID	Fault Name	Segment ID	Seg. Name	Fault location				Fault dimesions			Fault orientation			Max possible	References
				End point-1		End point-2		Length	Surf. P. of the W	Width	Strike	Dip	Slip	Magnitude	
				Lat	Lon	Lat	Lon	km	km	km					
Z-05-F01	Senja Fracture Zone	Z-05-F01-S01	Seg-01	69,8756	15,9960	72,0599	15,7324	247,00	10,00	29,00	N-S	70°W	normal	8,0	Ramberg et al., 2007
Z-05-F02	Troms-Finnmark Fault Complex	Z-05-F02-S01	Seg-01	69,2466	15,6665	70,1167	17,5451	146,00	11,00	32,00	NNE-SSW	70°NW	normal	7,7	Ramberg et al., 2007
		Z-05-F02-S02	Seg-02	70,1678	17,4737	70,9431	18,9349	105,00	11,00	32,00	NE-SW	70°NW	normal	7,5	Ramberg et al., 2007
Z-05-F03	Ringvassøy-Loppa Fault Complex	Z-05-F03-S01	Seg-01	70,9429	19,0997	71,5472	19,8522	92,00	11,00	32,00	N-S	70°W	normal	7,5	Ramberg et al., 2007
		Z-05-F03-S02	Seg-02	71,3667	19,3139	71,9308	19,4897	70,00	11,00	32,00	N-S	70°W	normal	7,3	Ramberg et al., 2007
		Z-05-F03-S03	Seg-03	71,8814	19,6490	72,2972	19,2919	54,00	11,00	32,00	N-S	70°W	normal	7,1	Ramberg et al., 2007
Z-05-F04	Bjørnøyrenna Fault Complex	Z-05-F04-S01	Seg-01	72,4868	19,7753	73,2574	21,7529	107,00	11,00	32,00	NE-SW	70°NW	normal	7,5	Ramberg et al., 2007
Z-05-F05	Leirdjupet fault	Z-05-F05-S01	Seg-01	73,0849	20,6542	74,1404	21,1102	129,00	9,00	26,00	N-S	70°E	normal	7,6	Ramberg et al., 2007
Z-05-F06	Hornsund Fault Zone	Z-05-F06-S01	Seg-01	73,4580	17,4023	75,8315	17,2375	282,00	9,00	26,00	N-S	70°WSW	normal	8,1	Ramberg et al., 2007
		Z-05-F06-S02	Seg-02	75,8364	17,0837	79,8387	8,8549	504,00	8,00	23,00	NNW-SSE	70°WSW	normal	8,4	Ramberg et al., 2007
		Z-05-F06-S03	Seg-03	76,5144	14,8535	79,6828	8,5913	383,00	8,00	23,00	NNW-SSE	70°WSW	normal	8,3	Ramberg et al., 2007
		Z-05-F06-S04	Seg-04	76,4310	14,6118	79,5232	8,1738	375,00	11,00	32,00	NNW-SSE	70°WSW	normal	8,3	Ramberg et al., 2007

Table 30: Seismological data for the Barents Continental Shelf zone.

Fault ID	Fault Name	Segment ID	Seg. Name	# earthquakes	Max observed magnitude		Focal mechanism							Regional stress tensor						D. to Moho
					Historical	Instrumental	Nodal Plane 1			Quality	Nodal plane 2			Sigma 1		Sigma 2		Sigma 3		
					Before 1980	After 1980	Strike	Dip	Rake		Strike	Dip	Rake	Azimuth	Plunge	Azimuth	Plunge	Azimuth	Plunge	
Z-05-F01	Senja Fracture Zone	Z-05-F01-S01	Seg-01	7	4,7	3,4	NA	NA	NA	NA	NA	NA	NA	NA	NA	NA	NA	NA	NA	27,50
Z-05-F02	Troms-Finnmark Fault Complex	Z-05-F02-S01	Seg-01	5	3,8	NA	NA	NA	NA	NA	NA	NA	NA	NA	NA	NA	NA	NA	NA	30,00
		Z-05-F02-S02	Seg-02	2	3,9	3,2	NA	NA	NA	NA	NA	NA	NA	NA	NA	NA	NA	NA	NA	30,00
Z-05-F03	Ringvassøy-Loppa Fault Complex	Z-05-F03-S01	Seg-01	0	NA	NA	NA	NA	NA	NA	NA	NA	NA	NA	NA	NA	NA	NA	NA	30,00
		Z-05-F03-S02	Seg-02	1	3,0	NA	NA	NA	NA	NA	NA	NA	NA	NA	NA	NA	NA	NA	NA	30,00
		Z-05-F03-S03	Seg-03	0	NA	NA	NA	NA	NA	NA	NA	NA	NA	NA	NA	NA	NA	NA	NA	30,00
Z-05-F04	Bjørnøyrenna Fault Complex	Z-05-F04-S01	Seg-01	0	NA	NA	NA	NA	NA	NA	NA	NA	NA	NA	NA	NA	NA	NA	NA	30,00
Z-05-F05	Leirdjupet fault	Z-05-F05-S01	Seg-01	0	NA	NA	NA	NA	NA	NA	NA	NA	NA	NA	NA	NA	NA	NA	NA	25,00
Z-05-F06	Hornsund Fault Zone	Z-05-F06-S01	Seg-01	2	3,8	NA	NA	NA	NA	NA	NA	NA	NA	NA	NA	NA	NA	NA	NA	25,00
		Z-05-F06-S02	Seg-02	0	NA	NA	NA	NA	NA	NA	NA	NA	NA	NA	NA	NA	NA	NA	NA	22,50
		Z-05-F06-S03	Seg-03	0	NA	NA	NA	NA	NA	NA	NA	NA	NA	NA	NA	NA	NA	NA	NA	22,50
		Z-05-F06-S04	Seg-04	2	4,4	NA	NA	NA	NA	NA	NA	NA	NA	NA	NA	NA	NA	NA	NA	25,00

Dip of all fault complexes and fault zones studied along Barents continental shelf area is mostly steep and equal to 70˚ (Table 29). Most of the fault segments occupying eastern margin of the Barents continental shelf dip towards the west, with some slight variations, that is towards the dip Cretaceous basin. Senja fracture zone extending along western margin of continental Barents shelf as well dips towards the west. The only fault that dips towards the east is the Leirdjupet fault that bounds Fingerdjupet sub-basin from its the western side (Dahlberg, 2014). Dominant mechanism is normal faulting that correlates well with basin and sub-basin structures in the area (Table 29).

The longest fault segment in the area is of 504 km and is a part of the Hornsund fault zone. The shortest fault segment is of 54 km and is a part of Ringvassøy-Loppa fault complex. Other segments vary in length. Based on the length of the fault segments, largest possible earthquake magnitude is assigned for each of these segments using Wells and Coppersmith's (1994) empirical relation. The maximum possible earthquake magnitudes at each segment of the faults vary between 8.4 and 7.1 (Table 29).

There is not enough data available that helps to reveal stress tensor in the area, in particular the exact orientation of the principal stress axes (Sigma 1, Sigma 2 and Sigma 3) (Table 30). However, there is borehole breakouts data available that gives orientation of the maximum horizontal stress, that is N-S.

Senja fracture zone: It consists of one segment for which several criteria described in chapter 3 (Methodology), are not fulfilled and therefore for this fracture zone reactivation potential is considered "not possible".

Troms-Finnmark fault complex: It consists of two segments for which several criteria described in chapter 3 (Methodology), are not fulfilled and therefore for this fault complex reactivation potential is considered "not possible".

Ringvassøy-Loppa fault complex: It consists of three segments for which several criteria described in chapter 3 (Methodology), are not fulfilled and therefore for this fault complex reactivation potential is considered "not possible".

Bjørnøyrenna fault complex: It consists of one segment for which several criteria described in chapter 3 (Methodology), are not fulfilled and therefore for this fault complex reactivation potential is considered "not possible".

Leirdjupet fault: It consists of one segment for which several criteria described in chapter 3 (Methodology), are not fulfilled and therefore for this fault reactivation potential is considered "not possible".

Hornsund fault zone: It consists of four segments for which several criteria described in chapter 3 (Methodology), are not fulfilled and therefore for this fault zone reactivation potential is considered "not possible".

Table 31: Interpreted results for the Barents Continental Shelf zone.

Fault/Fault zone/Fault complex	Potential of being reactivated			
	Almost certain	Probable	Possible	Not possible
Senja Fracture Zone				v
Troms-Finnmark Fault Complex (Segment 1)				v
Troms-Finnmark Fault Complex (Segment 2)				v
Ringvassøy-Loppa Fault Complex (Segment 1)				v
Ringvassøy-Loppa Fault Complex (Segment 2)				v
Ringvassøy-Loppa Fault Complex (Segment 3)				v
Bjørnøyrenna Fault Complex				v
Leirdjupet fault				v
Hornsund Fault Zone (Segment 1)				v
Hornsund Fault Zone (Segment 2)				v
Hornsund Fault Zone (Segment 3)				v
Hornsund Fault Zone (Segment 4)				v

Summarizing interpretations made for the Barents continental shelf zone, it is interpreted that for all faults, fault zones and complexes potential of being reactivated is not possible (Table 31).

6.6 Onshore Northern Norway

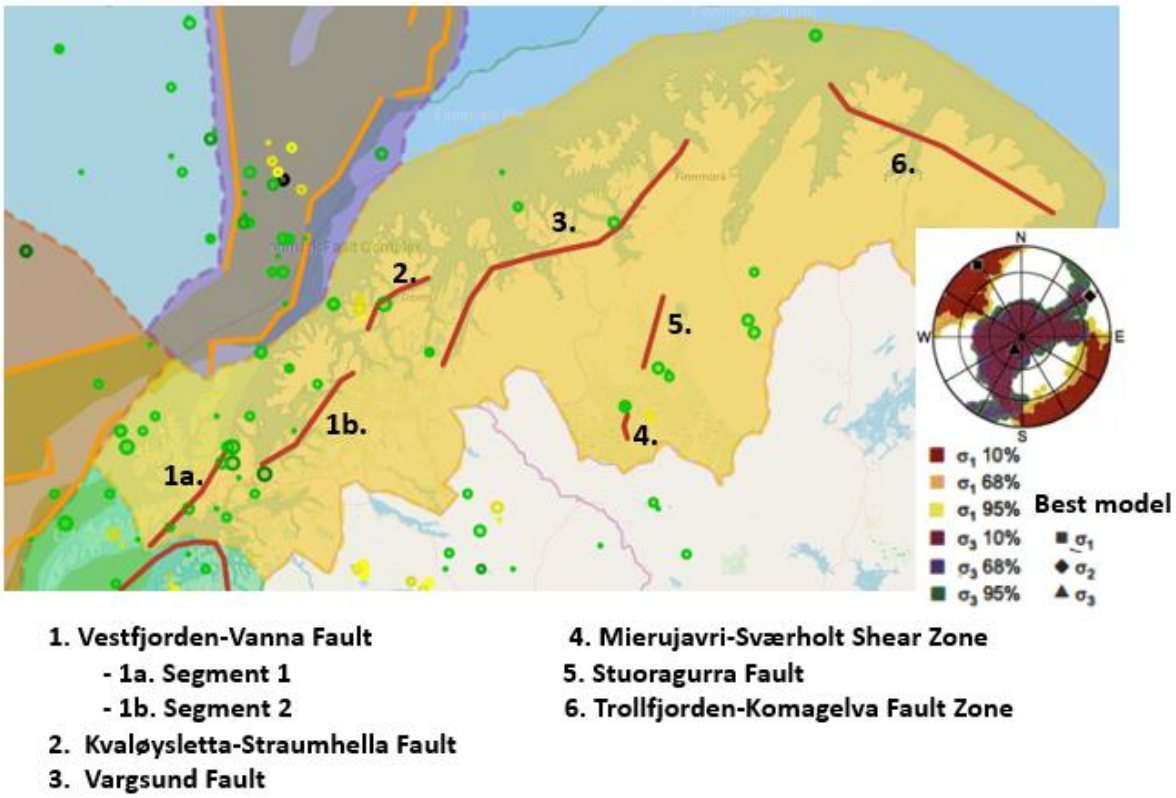

Figure 60: Onshore Northern Norway (Troms and Finnmark areas) is represented by light yellow color. Faults and segments along Onshore Northern Norway chosen for the analysis are represented with the red color. Seismicity from 1980 onwards represented by yellow circles whereas seismicity for the period preceding 1980 represented with the green circles. The size of a circle is proportional to the magnitude of the event. Circle at the right lower corner represents stress model generated as a result from the inversion of earthquake focal mechanism solutions. The yellow, green and red areas represent 95%, 68% and 10% confidence limits, respectively (Hicks et al., 2000).

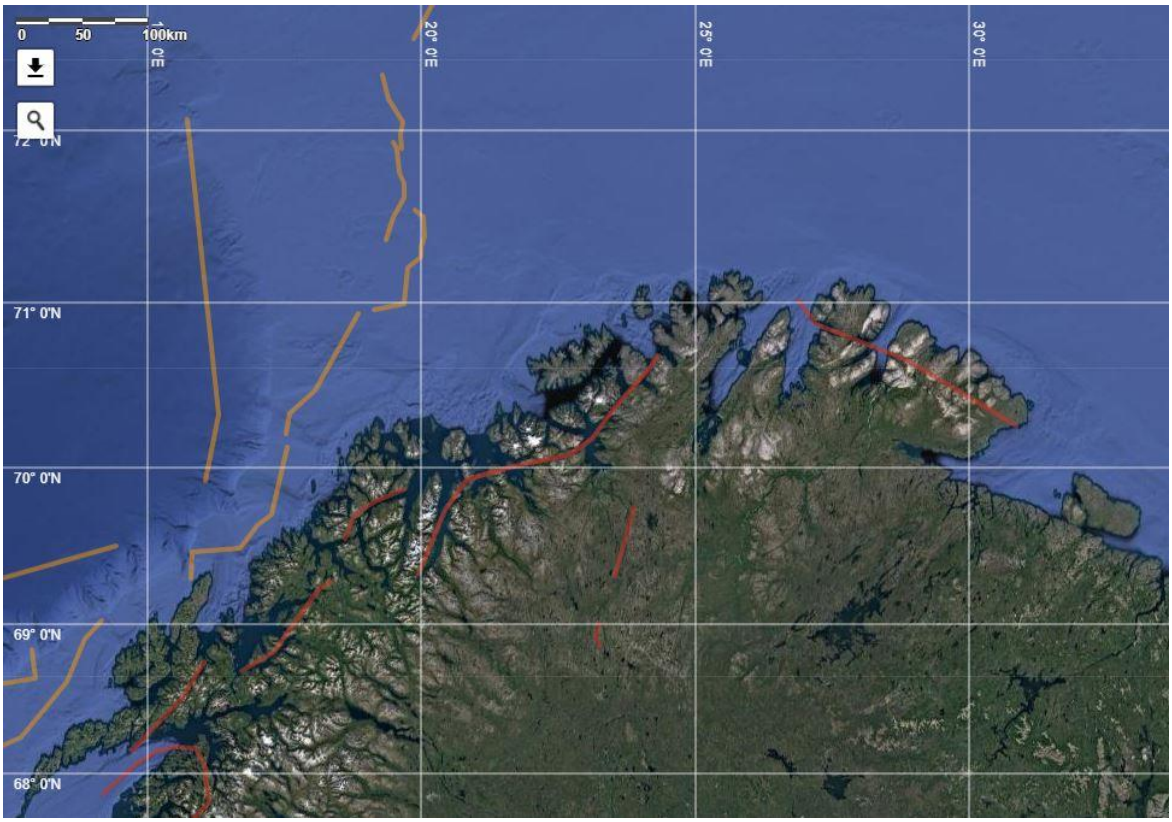

Figure 61: Location of the significant faults on mainland Northern Norway (Troms and Finnmark areas).

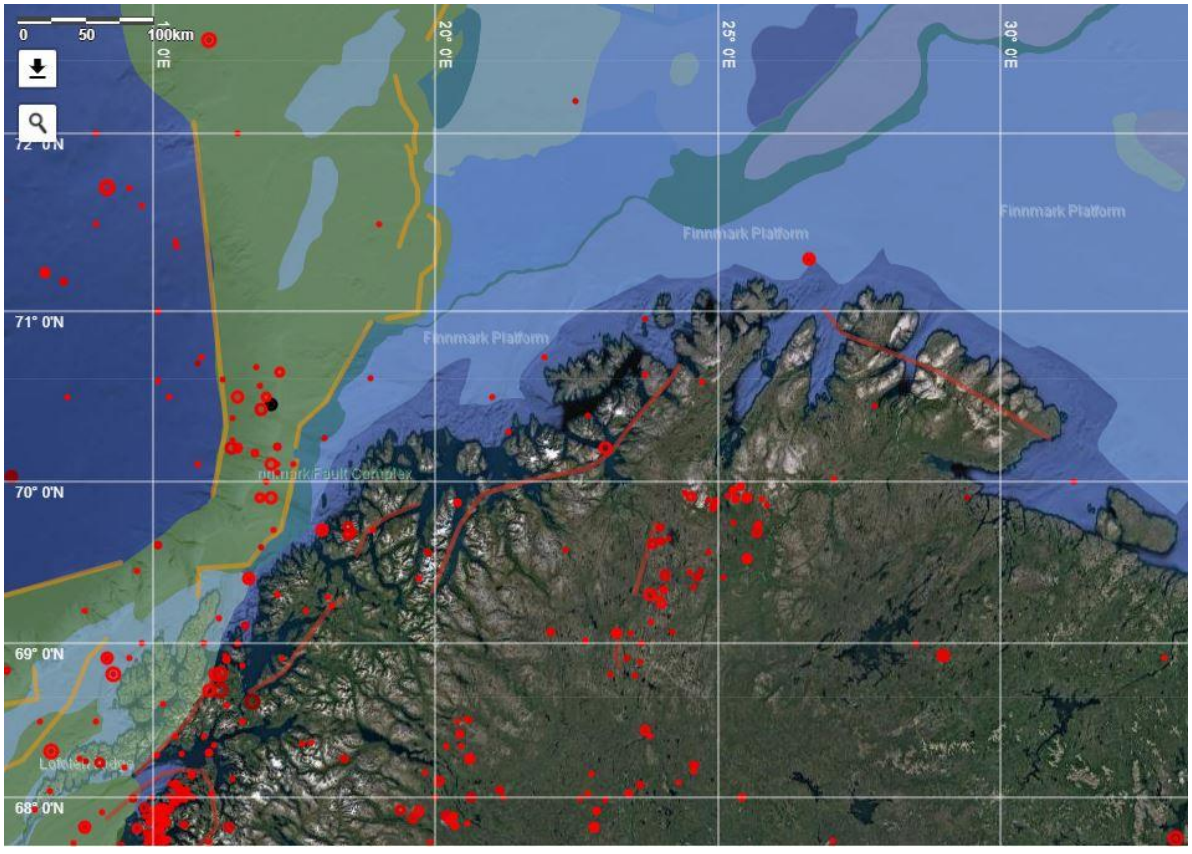

Figure 62: Location of the significant faults shown on mainland Northern Norway (Troms and Finnmark areas), together with the main structural elements (color-shaded areas) from NPD and the seismicity (since 1980) from NNSN (red circles).

In total four faults and two fault zones have been analyzed. Distribution of faults and fault zones is as follows (see Figures 60, 61 and 62):

- Majority of the faults are NE-SW oriented and stretches along northwestern mainland Norway in a nearly parallel or sub-parallel to this orientation. These are Vestfjorden-Vanna fault, Kvaløysletta-Straumhella fault and Vargsund fault.
- Two other fault zones have the same NE-SW oriented strike further to east south of Alta. These are the Stuoragurra fault and the Mierujavri-Sværholt shear zone.
- The NW-SE oriented fault zone, Trollfjorden-Komagelva fault zone, cuts across the Varanger peninsula almost parallel to the northernmost mainland Norway.

Table 32: Geological data for the Onshore Northern Norway zone. Abbreviation *Surf. P. of the W.* in the column *Fault Dimensions* stands for surface projection of the width.

Fault ID	Fault Name	Segment ID	Seg. Name	Fault location				Fault dimesions			Fault orientation			Max possible	References
				End point-1		End point-2		Length	Surf. P. of the W	Width	Strike	Dip	Slip	Magnitude	
				Lat	Lon	Lat	Lon	km	km	km					
Z-06-F01	Vestfjorden-Vanna Fault	Z-06-F01-S01	Seg-01	68,1615	14,6557	68,7826	16,0839	91,00	12,00	35,00	NE-SW	70°SE	sinistral-oblique normal	7,4	Gabrielsen et al., 2002
		Z-06-F01-S02	Seg-02	68,6649	16,6003	69,2645	18,4790	100,00	13,00	38,00	NE-SW	70°SE	sinistral-oblique normal	7,4	Gabrielsen et al., 2002
Z-06-F02	Kvaløysletta-Straumhella Fault	Z-06-F02-S01	Seg-01	69,5489	18,6328	69,8577	19,6655	57,00	15,00	41,00	NE-SW	70°SE	oblique-dextral normal	7,1	Gabrielsen et al., 2002
Z-06-F03	Vargsund Fault	Z-06-F03-S01	Seg-01	69,2862	19,8632	70,6851	24,2797	247,00	34,00	53,00	NE-SW	50°NW	normal-oblique dextral	7,9	Roberts et al., 2005
Z-06-F04	Mierujavri-Sværholt Shear Zone	Z-06-F04-S01	Seg-01	68,8388	23,2690	69,0032	23,2360	22,00	69,00	80,00	NE-SW	30°SE	reverse fault	6,6	Olesen et al., 1990
Z-06-F05	Stuoragurra Fault	Z-06-F05-S01	Seg-01	69,2902	23,5217	69,7441	23,8842	80,00	74,00	85,00	NE-SW	30°SE	reverse fault	7,3	Olesen, 1988
Z-06-F06	Trollfjorden-Komagelva Fault Zone	Z-06-F06-S01	Seg-01	71,0209	26,8725	70,2520	30,8825	174,00	0,00	42,50	NW-SE	90°	dextral strike-slip	7,7	Herrevold et al., 2009

Table 33: Seismological data for the Onshore Northern Norway zone.

Fault ID	Fault Name	Segment ID	Seg. Name	# earthquakes	Max observed magnitude		Focal mechanism							Regional stress tensor						D. to Moho
					Historical	Instrumental	Nodal Plane 1			Quality	Nodal plane 2			Sigma 1		Sigma 2		Sigma 3		
					Before 1980	After 1980	Strike	Dip	Rake		Strike	Dip	Rake	Azimuth	Plunge	Azimuth	Plunge	Azimuth	Plunge	
Z-06-F01	Vestfjorden-Vanna Fault	Z-06-F01-S01	Seg-01	6	4,9	NA	166,6500	37,1600	62,8500	B	19,4100	57,4900	109,0800	17	32	172	55	279	12	32,50
		Z-06-F01-S02	Seg-02	2	4,5	NA	NA	NA	NA	NA	NA	NA	NA	NA	NA	NA	NA	NA	NA	35,00
Z-06-F02	Kvaløysletta-Straumhella Fault	Z-06-F02-S01	Seg-01	3	4,7	3,6	NA	NA	NA	NA	NA	NA	NA	328	7	60	12	210	76	40,00
Z-06-F03	Vargsund Fault	Z-06-F03-S01	Seg-01	2	4,4	NA	NA	NA	NA	NA	NA	NA	NA	328	7	60	12	210	76	40,00
Z-06-F04	Mierujavri-Sværholt Shear Zone	Z-06-F04-S01	Seg-01	2	4,0	3,0	270,0000	90,0000	-180,0000	D	0,0000	90,0000	0,0000	328	7	60	12	210	76	40,00
Z-06-F05	Stuoragurra Fault	Z-06-F05-S01	Seg-01	2	3,8	NA	173,9000	52,9000	65,5000	B	30,9700	43,4700	118,7400	328	7	60	12	210	76	42,50
							170,6000	52,3000	63,6000	C	29,6700	44,8700	119,9100	328	7	60	12	210	76	42,50
							309,7800	40,3700	-80,7100	NA	117,6600	50,2700	-97,8100	328	7	60	12	210	76	42,50
Z-06-F06	Trollfjorden-Komagelva Fault Zon	Z-06-F06-S01	Seg-01	0	NA	NA	NA	NA	NA	NA	NA	NA	NA	NA	NA	NA	NA	NA	NA	42,50

Dip of the faults and fault zones varies significantly. Two faults dip towards the SE and have steep deep angle that is equal to 70˚ (Table 32). These are Vestfjorden-Vanna and Kvaløysletta-Straumhella faults. There is one shear structure, Mierujavri-Sværholt shear zone, that dips to the SE and is of 30˚ shallow angle that is typical for shear structures. Another fault showing shallow 30˚ angle and dipping to the SE is Stuoragurra fault. There is also moderately 50˚ NW dipping fault, Vargsund fault. In addition, there is a fault zone, Trollfjorden-Komagelva, that has a pure vertical dipping angle. Faulting mechanisms in the area are complex. Faulting mechanisms showing only one type of faulting are reverse and dextral strike-slip that are associated with Mierujavri-Sværholt shear zone, Stuoragurra fault and Trollfjorden-Komagelva fault zone respectively. All the remaining faults are characterized by the mixture of whether dextral or sinistral strike-slip and normal or oblique slip faulting (Table 32).

The longest fault segment in the area is of 247 km that is Vargsund fault. The shortest fault segment in the area is of 22 km that is Mierujavri-Sværholt shear zone. Other segments vary in length. Based on the length of a fault segments the largest possible earthquake magnitude is assigned for each of these segments using Well and Coppersmith's (1994) empirical relation. The maximum possible earthquake magnitudes at each segment of the faults vary between 6.6 and 7.9 (Table 32).

There is not enough data available that helps to reveal stress tensor in the whole area, in particular the exact orientation of the principal stress axes (Sigma 1, Sigma 2 and Sigma 3) (Table 33). However, there is stress model prepared for Finnmark area based on stress inversion of earthquake focal mechanism solutions from Finnmark (Table 33). This stress model shows sigma 1 is NNW-SSE oriented whereas sigma 3 is SSW-NNE oriented (Hicks et al., 2000). Both these axes are nearly horizontal and hence indicate reverse faulting regime. Referring to Fejerskov and Lindholm (2000), one can state that the remaining northern mainland Norway displays N-S oriented maximum horizontal stress.

Vestfjorden-Vanna fault: It consists of two segments. For segment 1 only one criterion described in chapter 3 (Methodology), is not fulfilled and therefore further interpretation is required. For segment 2 several criteria described in chapter 3 (Methodology), are not fulfilled and therefore for this fault reactivation potential is considered "not possible".

Segment 1: There is one focal mechanism of B quality showing oblique-reverse faulting. This segment lies in the area which according to zonation made by Hicks et al. (2000) belongs to onshore Mid Norway and hence have NNE-SSW oriented sigma 1 and WNW-ESE oriented sigma 3. Therefore, the expected faulting mechanism for this segment is normal to strike-slip. With given NE-SW orientation of the segment and NNE-SSW oriented sigma 1 and WNW-ESE oriented sigma 3, the reactivation of this segment in oblique-reverse faulting would be difficult. The focal mechanism showing oblique-reverse faulting can be explained by the close location of a fault segment to the northern offshore area that as was described by Olesen et al. (2018) displays complex faulting network. Earthquakes predominantly distributed along the southeastern favorable for reactivation segment's dipping side. Analyzing all information gathered for the segment it is interpreted that for this segment potential of being reactivated is possible.

Kvaløysletta-Straumhella fault: It consists of one segment for which several criteria described in chapter 3 (Methodology), are not fulfilled and therefore for this fault reactivation potential is considered "not possible".

Vargsund fault: It consists of one segment for which several criteria described in chapter 3 (Methodology), are not fulfilled and therefore for this fault reactivation potential is considered "not possible".

Mierujavri-Sværholt shear zone: It consists of one segment for which only one criterion described in chapter 3 (Methodology), is not fulfilled and hence further interpretation is required. There is one focal mechanism of D quality that shows normal-oblique dextral faulting. With given NE-SW orientation of the fault and NNW-SSE oriented sigma 1 and SSW-NNE oriented sigma 3, the reactivation of the fault in normal-oblique dextral faulting would be difficult. The focal mechanism showing this type of faulting can be explained by contaminations of other stress generating mechanisms, for example N-S oriented maximum horizontal stress acting in the northernmost Norway. There are only two earthquakes nearby the fault that locate on both favorable for reactivation SE segment's dipping side and unfavorable NW side. Analyzing all information gathered for the fault it is interpreted that for this fault potential of being reactivated is possible.

Stuoragurra fault: It consists of one segment for which only one criterion described in chapter 3 (Methodology), is not fulfilled and therefore further interpretation is required. There are three focal mechanisms available. Two focal mechanisms one of which is of B quality whereas another one is of C quality show oblique-reverse faulting. The remaining focal mechanism shows oblique-normal faulting, however, there is no information about its quality. With given NE-SW orientation of the fault and NNW-SSE oriented sigma 1 and NNE-SSW oriented sigma 3, the reactivation of the fault in oblique-reverse as is the case for the two earthquakes with quality B and one quality C, is possible. However, the reactivation potential based on the last focal mechanism in oblique-normal faulting (which is for the remaining focal mechanism with no quality assessment) would be difficult. Assuming that the focal mechanism that shows oblique-normal faulting is true, it can be explained by the possible effects of other stress generating mechanisms, for example N-S oriented maximum horizontal stress acting in the northernmost Norway. Earthquakes predominantly locate at the segment's southeastern dipping side and are therefore compatible with the geometry of the fault.

The special case for the Stuoragurra Fault is that it has a continuous fault scarp visible in the morphology for 7 km and is studied in detail using paleoseismological and other geophysical methods (Olesen, 1988; Olesen et al., 1992a; Dehls et al., 2002). Existence of a continuous fault scarp in the post-glacial landscape is a manifestation of a significant earthquake rupture in itself. Its possible age is found to be soon after the last deglaciation and hence is within Holocene. However, considering that the stress conditions leading to large surface rupturing post-glacial faulting in the area (including the well-studied examples in both Northern Sweden and Finland – e.g. Suasselkä (Kujansuu, 1964), Pärvie (Lundqvist and Lagerbäck, 1976), Lainio–Suijavaara (Lagerbäck, 1978)) due to isostatic rebound of the crust due to deglaciation, need not be the same stress conditions that exist today. Having both a clear post-glacial large earthquake as well as occurrence of earthquakes since 1980, with at least two consistent focal mechanisms, the reactivation potential for this fault is considered "probable".

Analyzing all information gathered for the fault it is interpreted that for this fault potential of being reactivated is probable.

Trollfjorden-Komagelva fault zone: It consists of one segment for which several criteria described in chapter 3 (Methodology), are not fulfilled and therefore for this fault zone reactivation potential is considered "not possible".

Table 34: Interpreted results for the Onshore Northern Norway zone.

Fault/Fault zone/Fault complex	Potential of being reactivated			
	Almost certain	Probable	Possible	Not possible
Vestfjorden-Vanna Fault (Segment 1)			v	
Vestfjorden-Vanna Fault (Segment 2)				v
Kvaløysletta-Straumhella Fault				v
Vargsund Fault				v
Mierujavri-Sværholt Shear Zone			v	
Stuoragurra Fault		v		
Trollfjorden-Komagelva Fault Zone				v

Summarizing interpretations made for the onshore northern Norway zone, one can distinguish between faults for which potential of being reactivated is probable, possible and not possible (Table 34). It was interpreted that for the majority of the segments potential of being reactivated is not possible. For few segments potential of being reactivated is possible. Only for Stuoragurra fault potential of being reactivated was estimated to be probable and hence this special case is represented with figure (Figure 63).

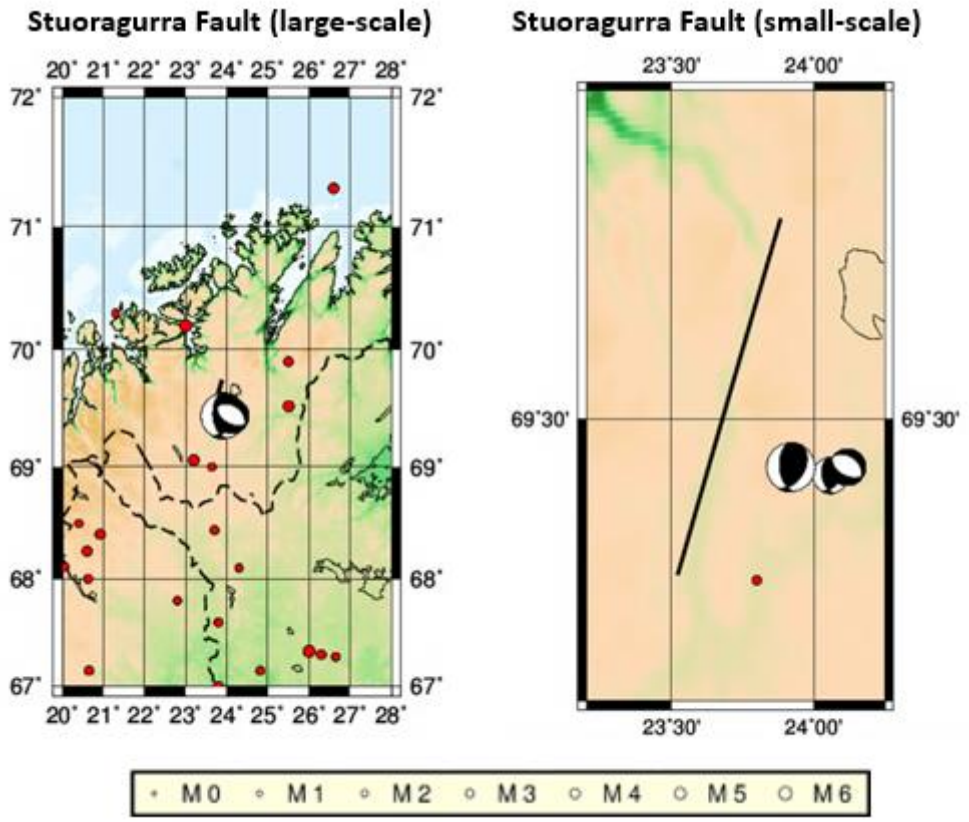

Figure 63: Left: Stuoragurra Fault at a large-scale. Right: Stuoragurra Fault (at a small-scale) is represented by a solid black line. Seismicity in the area nearby is represented by red circles. The size of a circle is proportional to the magnitude of the event. Focal mechanisms represented in the form of "beach balls".

7 Discussion

A good knowledge and critical assessment of uncertainties related to geological, geophysical and seismological data along with stress models play an important part in understanding the seismotectonics of any region. Estimation of such uncertainties is an integral part of the research conducted in this thesis and hence each individual subject is addressed and discussed in more detail in the following sections.

7.1 Uncertainties in geological data

Each individual offshore and several onshore faults/segments were visualized based on the data extracted from Norwegian Petroleum Directorate (Norwegian Petroleum Directorate, 2019) using the D-Map software (D-Map, 2019). Majority of the onshore faults, segments were also visualized using D-Map software, but their locations were extracted mostly from the scientific literature and from Norwegian Geological Survey (Norwegian Geological Survey, 2019). Such data collection and further interpretation and selection of significant faults can lead to uncertainties in several fault parameters. Among them are uncertainties in length, strike, dip, slip, width and surface projection of the width.

Uncertainties in fault segmentation and length

Firstly, each individual fault was assumed to represent only one segment in a case when there was no visible disturbance or disruptions along its extent and if strike variations were not drastic. Otherwise, faults, fault zones or complexes were segmented, such that each individual segment showing a distinct feature could be studied in more detail. Offshore and few onshore faults were segmented based on the NPD data if (after being visualized) significant disruptions in their orientation are observed. However, it was not the case for the onshore faults. As mentioned earlier in the text, onshore faults were depicted based on the way these are represented in the scientific literature, usually as one solid line. In this case no disruptions are seen and usually no information regarding the fault being segmented or not is reported. In such uncertain instances, faults were segmented based on the observed significant strike variations along the fault extent. The fault zone with the largest number of segments is Møre-Trøndelag fault zone. It was segmented into five segments three of which were NE-SW oriented whereas the remaining two ENE-WSW.

Length of a fault segment directly depends on a how accurate fault was depicted and segmented. Therefore, uncertainties in fault representation and segmentation directly leads to uncertainties in lengths measured.

Uncertainties in strike

Strike is one of the parameters describing fault orientation relative to North measured along the horizontal plane. When measuring strike of a fault segment, the original orientation of faults and segments from NPD shown on the map were assumed to be correct. Several onshore faults, especially the ones along onshore Mid Norway, were drawn based on the way these are depicted in the scientific literature. This could cause slight distortion and dislocation of the faults drawn. In addition, despite minor strike variations along extensive fault segments, only dominant strike was specified as an average. Furthermore, there were several distinct cases of significant strike variations were substantially and continuously bending. In such cases, instead of specifying orientation of the fault, the complete shape of the fault was given. Examples for this are Bergen arc shear zone and Devonian detachment faults in western Norway (Solund, Kvamshesten, Håsteinen and Hornelen faults).

Uncertainties in dip

Dip is one of the parameters describing inclination of the fault plane relative to the horizontal plane. Firstly, dip of the offshore faults was mainly specified based on the available seismic cross-sections presented in the scientific literature. Seismic profiles are usually vertically and horizontally exaggerated, especially for steep dipping faults and complex geological structures, that leads to inevitable structural and geometrical distortion that influenced accuracy of dip specified. The range of dip uncertainties read from the seismic cross-sections is estimated to be in a range of ± 20˚. Secondly, dip of the onshore faults was mostly taken from the scientific literature. In several instances various scientific papers/articles provide slightly different records of the dip that also lead to uncertainties in a dip in a range of ± 20˚. One such example is Stuoragurra fault. Referring to Roberts (1991), the fault dips 30˚ to the SE while according to Olesen et al. (1991) there are two possibilities for the change in the course of the fault. The first one suggests the dip of the fault at the uppermost (10 m) subsurface is around 50˚ whereas when it reaches depth of 25 – 40 m it is around 30˚. The second model assumes that dip of the fault does not change with depth and it is in the range of 50 – 60˚. Since it was concluded that the first model was more likely to be the solution and since the main goal of the thesis is to study seismogenic potential meaning cutting through the whole crust to the Moho, the value of 30˚ was used and specified. Thirdly, it was assumed that dip of the shear structures formed during Caledonian episodes, representing low-angle thrust faulting, is relatively low around 30˚ whereas dip of the faults bounding grabens is steeper around 70˚. Fourthly, dip of the complex arched structures could be hardly given precisely, and hence only direction of the dip was specified. Fifthly, faults that were extracted from NGU open-file maps "Berggrunn raster" at a scale 1:250,000 (Norwegian Geological Survey, 2019.) have not been reported in the literature and hence there is no dip information available.

Uncertainties in slip vector

Sense of slip along the faults was mostly taken from the literature and from seismic cross-sections for offshore faults. Slip vector and slip-angle is in general difficult, unless it is specifically assessed in the literature or obtained from the available focal mechanisms. Therefore, uncertainties in the fault plane caused by uncertainties in strike and dip combined with uncertainties in stress tensor lead to uncertainties in the calculated slip vectors.

Uncertainties in Moho depth

Exact value of depth to Moho was read using the available Moho map (Figure 10, Ebbing and Olesen (2010)). Each value corresponds to a distinct color code. In many cases fault segments stretch over longer distances where the value of depth to Moho changes. In such cases, the value of depth to Moho corresponding to the longest part of the segment was read and specified. This leads to uncertainties in depth to Moho equal to one contour interval (scale division), that is 2.5 km.

Uncertainties in surface projection of the width

Surface projection of the width is calculated as described in chapter 3 (Methodology) using two fault parameters. These are dip of the fault and depth to Moho. As mentioned, dip of the fault has error limit of ± 20˚. Depth to Moho also changes over the fault extent and has uncertainty in a range of 2.5 km. Therefore, uncertainties in dip and depth to Moho directly lead to uncertainties in computed surface projection of the width. For arc-shaped faults surface projection of the width was affected by its complex structure and difficulties finding dip angle.

Uncertainties in width of the fault

Width of the fault is calculated as described in chapter 3 (Methodology) using two fault parameters. These are surface projection of the width and dip of the fault. As mentioned, dip of the fault has an error limit of ± 20˚ and computed value of surface projection of the width also has slight uncertainties in its confidence limit. Therefore, uncertainties in parameters used to compute the third parameter, that is width of the fault, will also lead to uncertainties of its computed value. For arc-shaped faults surface projection of the width was not calculated and the width of the fault could not be computed.

Uncertainties in maximum possible magnitude

Maximum possible magnitude was calculated using empirical Wells and Coppersmith (1994) relation. Each calculated magnitude has its uncertainty. In cases of uncertain or complex slip (for example, Vestfjorden-Vanna fault – sinistral-oblique normal slip, Kvaløysletta-Straumhella fault – oblique-dextral normal slip and Vargsund fault – normal-oblique dextral slip) magnitude was calculated using magnitude-length relationship for all rupture types. This gives uncertainty of ± 0.28. Other length-magnitude relationship gives uncertainty of ± 0.28, 0.28 and 0.34 for strike-slip, reverse and normal ruptures respectively. Additionally, the uncertainties in the length of the faults or segments naturally affect the resulting magnitude obtained from the empirical relations.

Uncertainties in maximum possible length

Wells and Coppersmith (1994) empirical magnitude-length relationship was also used to calculate/estimate lengths various magnitudes can affect. This was done many times when interpreting results and showing that some of the focal mechanisms that are not compatible with the orientation of the principal stress axes can only be interpreted as being small transverse structures. The assumptions were made based on the lengths computed. Referring to Wells and Coppersmith (1994), each computed length has its uncertainty depending on the type of rupture. Uncertainties on logarithm of the length are ± 0.22, 0.23, 0.20, and 0.21 for all rupture types, strike-slip, reverse and normal ruptures, respectively.

It was found that, for example that

- magnitude of 5.3 corresponds to length 4 km (Viking graben western boundary fault – segment 2). Length of the segment is 311 km;
- magnitude of 5.2 corresponds to length 2.6 km (Møre-Trøndelag fault zone – segment 1). Length of the segment is 163 km;
- magnitude of 4.9 corresponds to length 2.5 km (Hardangerfjord shear zone – segment 1). Length of the segment is 100 km;
- magnitude of 4.8 corresponds to length 2.5 km (Hornelen detachment fault). Length of the segment is 128 km;
- magnitude of 4.8 corresponds to length 2.2 km (Fles fault complex – segment 2). Length of the segment is 464 km.

Considering only small part of the fault or a segment could be associated to the given magnitudes, it was assumed that these are small transverse structures that mostly reflect minor strike variations.

Regarding uncertainties related to magnitude, it is important to discuss the magnitude of Stuoragurra fault which was calculated using two different approaches. Referring to Dehls et al. (2000), Stuoragurra fault extends 80 km and have a single-vertical displacement. This implies that the fault was produced by a tectonic event of a magnitude 7.3 (based on comparison with analogous data from recent active fault zones) computed using empirical Wells and Coppersmith (1994) magnitude-length relationship.

On the other hand, Bungum and Lindholm (1997) assumed the fault was created by a single seismic event of magnitude 7.7. The moment magnitude was computed using seismic moment that in turn was calculated using length and displacement of the fault gathered from Muir Wood (1993). Despite magnitudes do no match, both conclusions were supported by two additional trenches dug 3 km north of Masi in 1999 (Dehls et al., 2000).

Uncertainties in stress models

Stress models generated by Hicks et al. (2002) also show some degree of uncertainty that are discussed in the following sub-sections divided into larger geographical areas.

Northern North Sea

Northern North Sea is a complex area experiencing high level of seismic activity. As mentioned earlier, three stress models were generated for this area. Stress model generated based on 34 both rotated (8) and nonrotated (26) earthquake focal mechanism solutions have relatively large area covered by confidence limit. This is explained by large scatter of the input data. Stress model generated for nonrotated and rotated earthquake focal mechanisms (the ones interpretation of the result is based on) have well-defined sigma 1 and sigma 3 axes. However, referring to the inversion results represented in Figure 13, there are some minor areas covered by confidence limit meaning that some uncertainties are still present.

Orientation of the maximum horizontal stress is given by a weak trend and hence uncertain. This is explained by scattered in situ data from borehole breakouts (Hicks et al., 2002). In addition, WNW-ESE orientation of the maximum horizontal compression determined by Hicks et al. (2002) is also compatible with earlier studies done by Fejerskov et al. (2000) and recent studies by Simonsen (2018).

Southern North Sea

Southern North Sea is an area experiencing low level of seismic activity. As was mentioned earlier, due to lack of focal mechanism solutions necessary to perform stress inversion, no stress model was generated for this area. However, based on the scattered in situ data from borehole breakouts weak trend indicating orientation of maximum horizontal stress was specified (Figure 12; Hicks et al., 2002).

Onshore West Norway

Onshore West Norway experiences high level of seismic activity. Stress model was generated based on 15 available earthquake focal mechanism solutions. Stress inversion results show well-defined sigma 1 axis, and sigma 2 and 3 axes which confidence limit covers relatively large area and hence indicating relatively large uncertainty, Figure 13 (Hicks et al., 2002).

Orientation of the maximum horizontal stress is based on near random distribution of the in situ data (overcoring measurements) and hence has some degree of uncertainty (Hicks et al., 2002). In addition, WNW-ESE orientation of the maximum horizontal compression determined by Hicks et al. (2002) is also compatible with earlier studies done by Fejerskov et al. (2000) and recent studies by Simonsen (2018). Also, both Hicks et al. (2002) and Simonsen (2018) recognize depth to be an important parameter that influences the orientation of the maximum horizontal compression in the area.

Oslo Rift Area

Oslo rift area experiences intermediate level of seismic activity. Stress model based on 20 earthquakes focal mechanisms available for the area was generated. Stress inversion results show that confidence limit indicating location of sigma 1 covers relatively large area, so that best model for sigma 2 axis

locates in the confidence limit of sigma 1 axis. Orientation of sigma 3 principal axis is also very uncertain that is proven by confidence limit covering large area, Figure 13 (Hicks et al., 2002).

There was neither enough in situ measurements nor good quality of overcoring measurements to determine accurate orientation of the maximum horizontal stress in the area. However, it is assumed that orientation of the maximum horizontal compression is similar to the onshore West Norway (Hicks et al., 2002). In addition, WNW-ESE orientation of the maximum horizontal compression determined by Hicks et al. (2002) is also compatible with earlier studies done by Fejerskov et al. (2000) and recent studies by Simonsen (2018). Depth is still an important parameter in the area that may have effect on type of faulting mechanism.

Onshore Mid Norway

Onshore Mid Norway experiences high level of seismic activity at its northern part and low seismic activity at its southern part. One stress model was generated based on 15 available earthquake focal mechanism solutions. Inversion results show well-defined sigma 3 axis whereas sigma 1 and sigma 2 are less certain and appear to interchange, Figure 13 (Hicks et al., 2002).

Orientation of the maximum horizontal stress is based on scattered in situ data (overcoring measurements) and hence has some degree of uncertainty (Hicks et al., 2002). Orientation of the maximum horizontal stress in the area given by Hicks et al. (2002) is slightly different compared to findings by Fejerskov et al. (2000) and Simonsen (2018). Hicks et al. (2002) determined that compressional stress is centered around N-S orientation. Referring to Fejerskov et al. (2000), orientation of the maximum horizontal stress is mostly WNW-ESE whereas, according to Simonsen (2018), it is depth dependent. At the depths of 5-50 km it is WNW-ESE that correlates well with the ridge-push force whereas at shallow depths (25-700 m) this trend disappears. Despite, orientation of the maximum horizontal stress determined by Hicks et al. (2002) slightly differ from other studies, Simonsen (2018) indicated that onshore data is relatively scattered in comparison to the one from offshore. This makes it difficult to determine orientation of the maximum horizontal stress explicitly and hence increase level of uncertainty.

Offshore Mid Norway

Offshore Mid Norway experiences high level of seismic activity. Stress model was generated based on 14 earthquake focal mechanism solutions. Inversion results show well-defined sigma 1 axis whereas it is not the case for sigma 2 and 3 axes. These appear to be more uncertain, Figure 13 (Hicks et al., 2002).

Orientation of the maximum horizontal stress is based on few in situ measurements that appear to be quite consistent and compatible with the expected direction of the ridge-push force. (Hicks et al., 2002). In addition, NW-SE orientation of the maximum horizontal compression determined by Hicks et al. (2002) is also nearly compatible with earlier studies done by Fejerskov et al. (2000) and recent studies by Simonsen (2018) showing orientation of the maximum horizontal stress is WNW-ESE.

Finnmark

Finnmark experiences low level of seismic activity. Stress model was generated based on 5 earthquake focal mechanism solutions. Despite data is scattered due to small amount of earthquake focal mechanism solutions, inversion results still show orientation of principal stress axes, yet with large uncertainty. As for sigma 1, confidence limit of 95 % covers the entire northwestern quadrant and

hence orientation of the axis is uncertain, Figure 13 (Hicks et al., 2002). Sigma 3 is also uncertain that can be proven by and clearly seen from the confidence limit occupying large area, Figure 13.

Orientation of the maximum horizontal stress is very uncertain due to scarce data. However, it appears to be compatible with the expected direction of horizontal compression from the Mid-Atlantic spreading ridge (Hicks et al., 2002). In addition, NW-SE orientation of the maximum horizontal compression determined by Hicks et al. (2002) is also compatible with earlier studies done by Fejerskov et al. (2000) and recent studies by Simonsen (2018).

Western Barents Sea

Western Barents Sea experiences very low level of seismic activity. As was mentioned earlier, due to lack of focal mechanism solutions necessary to perform stress inversion, no stress model was generated for this area. However, based on the scattered in situ data from 17 borehole breakouts trend indicating orientation of maximum horizontal stress was specified (Figure 12; Hicks et al., 2002). In addition, N-S orientation of the maximum horizontal compression determined by Hicks et al. (2002) is also compatible with earlier studies done by Fejerskov et al. (2000) and recent studies by Simonsen (2018) showing orientation of the maximum horizontal stress is N-S to NNW-SSE.

7.2 Uncertainties in seismological data

There are two datasets constituting the final catalogue (Figures 33, 34 and 35). The dataset representing seismic events before 1980's is colored in green whereas dataset for seismic events after 1980's onwards is colored in red. Seismic events before and at a year 1980 are used to show historical seismic records taking place at a certain time before the year 1981. However, one cannot rely on them when correlating seismicity with the faults since most of them are based on felt reports and questioners and hence have large location errors. Therefore, in order to correlate seismicity with the faults only seismic events recorded starting from the year 1980 onwards was used. However, historical records were considered when estimating seismogenic potential of each individual fault/segment. Earthquake records from the year 1980 onwards in the compiled seismic catalogue are of various magnitude values, starting from -0.4 to 6.1. All these seismic records were brought on maps (maps are given in the chapter 6 – Results and Interpretations) to trace significant seismicity trends, in particularly seismicity alignments with the faults. However, low magnitude seismic events (lower than magnitude 3.0) are uncertain and usually have larger location errors than seismic events of intermediate and large magnitudes. Therefore, only seismic records with magnitude equal to 3.0 and larger were considered when correlating seismicity with the faults.

Earthquake location accuracy

Seismic catalogue has been compiled as it was described in chapter 5 (Seismological Data). After several tests were performed, epicentral error limit showing best agreement between quality and quantity of the data was chosen, "0 – 20 km". The conclusions reached using this seismic catalogue are summarized in Tables 16, 19, 20, 23, 26, 27, 30 and 33.

Additionally, the effect of the improved location accuracy in the North Sea area is tested using the recently finished work by Tjåland and Ottemöller (2018). In doing this, the same criteria applied in the methodology section is adopted this time using the earthquake catalogue of relocated events from this study. The resulting interpretations with regard to the reactivation potential of faults and

segments were compared to those that were obtained previously based on the compiled catalogue as explained in the results chapter. In the following, the results of this comparison are presented.

As was mentioned in chapter 5 (Seismological data), the method established to determine reactivation potential of a fault is used for several faults lying in the North Sea zone and few faults from the zone 2 – onshore southern Norway. This is done using catalogue of seismic events extracted from the studies done by Tjåland and Ottemöller (2018). Double-difference relocation method used to improve location of earthquakes significantly reduce number of seismic events in the area as they could not been linked to other seismic events. Despite seismicity in the area became less diffuse and some earthquakes clustering became more evident, the general seismicity was still scattered and no apparent correlation with the faults could be made. The result of double-difference relocation can be reviewed in Figure 64.

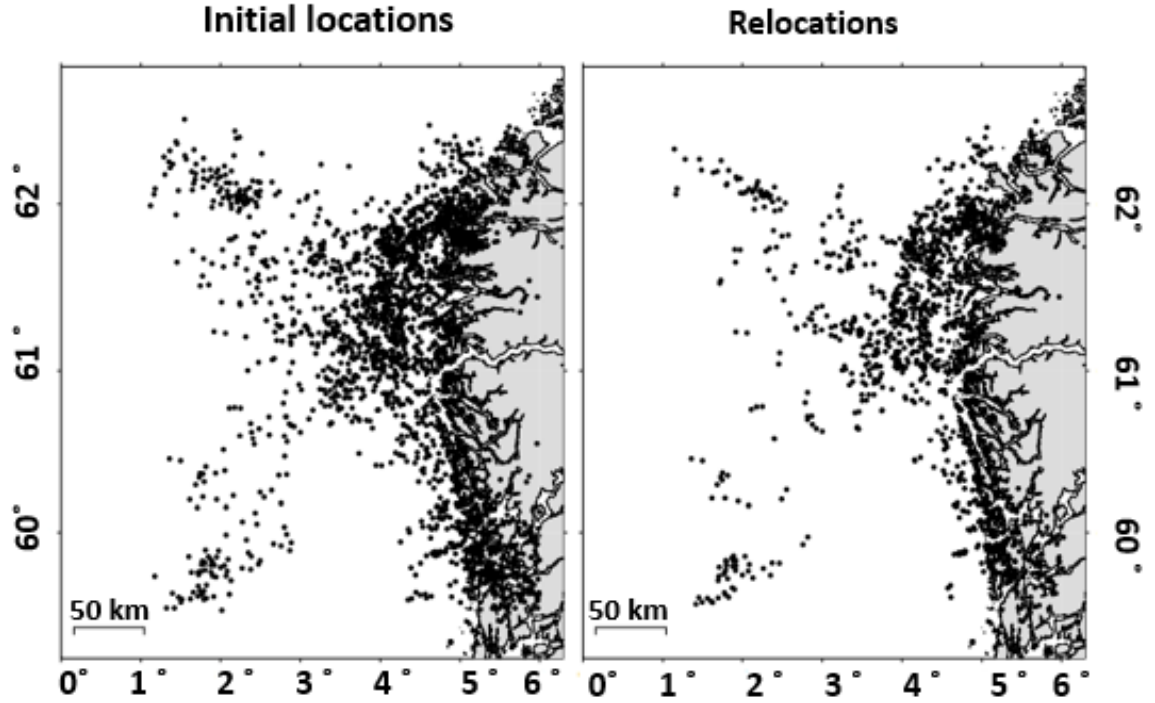

Figure 64: Relocation results. Left: before relocations have been made. Right: after relocations have been made. The earthquake catalogue used cover period from January 1990 to July 2018. Modified picture (Tjåland and Ottemöller, 2018).

Catalogue of relocated earthquakes will be applied to estimate reactivation potential of the faults lying only within the area of relocated seismic events. These are Øygarden fault zone, Viking graben eastern and western boundary faults, Stord-Bømlo-Karmøy fault zone, Hardangerfjord fault zone, Bergen arc shear zone, Solund detachment fault, Kvamshesten detachment fault, Håsteinen detachment fault and Hornelen detachment fault.

Fault parameters (fault location, dimension, orientation and maximum possible magnitude) collected for the faults and its segments remain the same as neither new segmentations nor fault relocations were made. Fault parameters can be reviewed in Tables 15, 18, 22, 25, 29 and 32. Focal mechanisms as well remain the same since for the following thesis fault plane solutions for Norway and adjacent areas was collected from several reliable and revised sources (these are listed and described in chapter 5 – Seismological data). One of such sources was the work done by Tjåland and Ottemöller (2018), meaning that revised and improved focal mechanisms from their studies were already used when estimating reactivation potential of the faults. Focal mechanism data can be reviewed in Tables 16, 19,

20, 23, 26, 27, 30 and 33. The only parameter that will be checked is the number of earthquakes located nearby each fault/segment. This will help to check whether better alignment of relocated seismic events with the faults/segments can change results when estimating reactivation potential of the fault. This is especially crucial for the cases when only one focal mechanism, that is compatible with the orientation of the fault and stress tensor, is available. This is exactly the case for Stord-Bømlo-Karmøy fault zone (segment 2) and Hardangerfjord fault zone (segment 3) that was interpreted to have possible reactivation potential due to low level of seismic activity in the area nearby. Only significant events of magnitude 3 or larger will be considered when correlating faults and seismic events nearby.

In order to perform pure comparison only events covering period January 1990 – July 2018 will be extracted from the catalogue used in the thesis and then compared with the ones relocated using double-difference method.

Table 35: Comparison between earthquake locations from the thesis and relocated by Tjåland and Ottemöller (2018).

Fault/fault zone	# Segment	# Earthquakes (from the thesis)	# Relocated earthquakes	Results
Øygarden fault zone	1	1	1	No change
	2	4	2	No change
	3	5	2	No change
Viking graben eastern boundary fault	1	0	0	No change
	2	0	0	No change
	3	1	0	No change
	4	3	1	No change
Viking graben western boundary fault	1	2	0	No change
	2	7	7	No change
Stord-Bømlo-Karmøy fault zone	1	3	1	No change
	2	0	0	No change
	3	0	0	No change
	4	0	0	No change
Hardangerfjord fault zone	1	1	1	No change
	2	2	0	No change
	3	1	0	No change
Bergen arc shear zone	1	3	1	No change
Solund detachment fault	1	0	0	No change
Kvamshesten detachment fault	1	2	0	No change
Håsteinen detachment fault	1	0	0	No change
Hornelen detachment fault	1	1	1	No change

Results of comparison (Table 35):

1) Double-difference method gives definitely improved locations and hence correlation of seismic events that can be related to the faults/segments expected to be more reliable. Better linkage between the faults/segments and earthquakes around them enables to perform more accurate analysis.
2) In the applied criteria, the location accuracy is considered important. Using the relocated earthquakes in the criteria did not change the results and interpretations made for the faults (Stord-Bømlo-Karmøy fault zone (segment 2) and Hardangerfjord fault zone (segment 3)) for

which seismicity in the area was a critical factor to decide on whether reactivation potential is possible or probable. This indicates that the choice of epicentral error limit (0 – 20 km), indeed, enables to correlate faults and seismic events in the area nearby.

3) The comparison of the results and interpretations, using the relocated earthquakes and those included in the catalogue compiled in this thesis, did not change (faults for which reactivation potential was interpreted to be "not possible", "possible" and "probable" stays the same).
4) In the future, relocation of earthquakes with more advanced methods can be done in the remaining zones, which may improve the correlations between the seismicity and the faults. The adopted methodology, however, seems to be robust enough to identify the most significant faults that may have a potential for reactivation.

Concluding remark: Relocation method works well and can be used for areas experiencing low level of seismic activity, such as Norway.

7.3 Discussion of the results

North Sea

Results obtained for the North Sea correlate well with the earlier studies done by Bungum et al. (1991); Hicks et al. (2000); Simonsen (2018); and Olesen et al. (2013). Firstly, one fault zone – Øygarden Fault Complex, for which reactivation potential was interpreted to be probable was identified. This correlates well with the Northern North Sea being one of the most seismically active areas in Norway. Secondly, due to complex stress mode in the area two faulting mechanisms, normal to strike-slip (for shallow foci events) and dominant reverse to oblique-reverse (for deep foci events), are expected. Indeed, as was specified in Table 16, focal mechanisms showing both of them were identified. Thirdly, based on the complex stress regime in the area and focal mechanisms showing opposite slip it is expected that for most faults/segments lying in the Northern North Sea reactivation potential would be possible rather than probable. In fact, as was summarized in Table 17, for most faults/segments lying in the Northern North Sea reactivation potential was interpreted to be possible.

Onshore Southern Norway

Results obtained for the Onshore Southern Norway correlate with the earlier studies done by Bungum et al. (1991); Hicks et al. (2000); Fejerskov and Lindholm (2000); Simonsen (2018); and Olesen et al. (2013). Onshore Southern Norway is a complex area. Firstly, this is due to complex arched structures, in particularly Bergen arc shear zone and Devonian detachment faults stretching along Onshore West Norway. Secondly, this is due to complex stress modes in the Oslo rift zone where for the events with shallow foci expected faulting mechanisms is normal to strike-slip whereas for the events with deep foci it is reverse. Despite level of seismic activity in the area is high to intermediate for most of the faults/segments, the reactivation potential is interpreted to be not possible and only for few possible. This is mostly due to complex structures and various stress modes causing different faulting in the area. That is also supported by focal mechanisms identified and specified in Tables 19 and 20, that show all types (reverse, normal, strike-slip and oblique-slip) of faulting mechanisms in the area. Summarizing, points discussed for the Onshore Southern Norway it is assumed that combination of all factors (geological structures, stress modes, foci depth) makes it difficult to interpret reactivation potential of a fault/segment in one or another slip mode.

Norwegian Sea

Results obtained for the Norwegian Sea correlate well with the earlier studies done by Bungum et al. (1991); Byrkjeland et al. (2000); Hicks et al. (2000); Fejerskov and Lindholm (2000); Simonsen (2018); and Olesen et al. (2013). Firstly, most prominent belt of seismicity in the area goes through the eastern part of the Vøring basin and stretches in a nearly parallel manner to the continental shelf. What is interesting and correlates very well with the previous studies is that only for the faults/segments lying within this area and also Lofoten-Vesterålen margin, the reactivation potential was interpreted to be possible. Secondly, focal mechanisms identified and specified in Table 23 for the seismically active belt, show mostly two types of slip. These are oblique-reverse and oblique-normal faulting. This is compatible with various stress generating mechanisms acting in the Vøring and Møre basins. These are first order continental ridge-push force, regional continent-ocean boundary density contrast, sediment deposition since Jurassic, the effect of glacial erosion (post-glacial rebound which is dominant in coastal regions) and local basement relief. Thirdly, for all other faults/segments stretching to the east and west from seismically active belt, reactivation potential was interpreted to be not possible. Indeed, Møre and Vøring Marginal Highs are assumed to be of anomalous aseismic nature, mostly due to combination of locally induced stresses that decrease or in several cases counteract ridge-push force (Byrkjeland et al., 2000). For faults/segments enclosing Trøndelag platform reactivation potential was interpreted to be not possible that is compatible with the Trøndelag platform being aseismic or experiencing very low level of seismic activity.

Onshore Mid Norway

Results obtained for the Onshore Mid Norway correlate well with the earlier studies done by Bungum and Husebye (1979); Bungum et al. (1991); Atakan et al. (1994); Hicks et al. (2000); Gradmann et al. (2018); and Olesen et al. (2018). Firstly, for faults and fault zones locating at the Troms and Nordland areas reactivation potential was estimated to be possible. This is compatible with high level of seismic activity related to flexural uplift that causes earthquake swarms in the area, two of well-known occurred in Meløy and Steigen areas in 1978-1979 and 1992 respectively. Secondly, focal mechanisms specified in Tables 26 and 27, showing oblique-normal, normal, and oblique-reverse slip are compatible with the complex faulting network in Nordland area. Referring to Olesen et al. (2018) normal faulting mechanism is dominant for the onshore northern area. For the transition coastal area prevailing focal mechanisms are normal and strike-slip whereas for the northern offshore area these are reverse and oblique-reverse. Considering faults and fault zones stretch along nearshore area focal mechanisms showing various slip assumed to be natural and expected.

Barents Continental Shelf

Results obtained for the Barents Continental Shelf correlate well with the earlier studies done by Bungum et al. (1991); Byrkjeland et al. (2000); Hicks et al. (2000); Fejerskov and Lindholm (2000); Simonsen (2018); and Olesen et al. (2013). For all faults, fault zones and complexes, the reactivation potential was estimated to be not possible. This correlates well with the Barents Continental shelf experiencing very low level of seismic activity. That in turn is compatible with a weak ridge-push force acting on a thinned, strong crust of the Barents Continental Shelf where destructive interference with tensile stresses is expected (Fiedler and Faleide, 1996). In addition, since Barents Continental Shelf is far away from seismic stations there is no focal mechanisms available. This is also specified in Table 30.

Onshore Northern Norway

Results obtained for the Onshore Northern Norway (Troms and Finnmark areas) correlate well with the earlier studies done by Bungum et al. (1991); Olesen (1988); Tolgensbakk and Sollid (1988); Hicks et al. (2000); and Olesen et al. (2013). Firstly, for most faults lying within Finnmark area reactivation potential was interpreted to be not possible (Table 34). This correlates with Finnmark being an area experiencing low level of seismic activity. This is also true for dextral strike-slip Trollfjorden-Komagelva fault zone. However, for the faults and fault zones lying at the central and eastern part of the Onshore Northern Norway level of seismic activity is higher. This is compatible with Mierujavri-Sværholt shear zone for which reactivation potential was interpreted to be possible and confirmed neotectonic Stuoragurra fault for which reactivation potential was interpreted to be probable (Table 34).

7.4 Discussion of the criteria

Identifying reactivation potential of faults, fault zones or complexes for an area lying within SCR, such as Norway, and hence experiencing low level of seismic activity is not an easy task. Criteria established for identifying reactivation potential of faults in seismically active regions, such as Mediterranean and Alpine belt are thus not applicable to areas of low seismicity. Therefore, there was a need to develop a method and selection criteria that can be used for such purposes. The aim of this subsection is to compare criteria used to determine seismogenic potential of faults lying within seismically active regions with the ones developed in this thesis to estimate seismogenic potential for faults within SCR. Greece is a seismically active area that performs systematic analysis of significant faults and reports its data to EDSF. Therefore, its criteria and most significant points used to estimate seismogenic potential of faults will be compared to criteria used in the thesis.

Criteria used by Greece (Sboras et al., 2011; McCalpin, 1996; Pavlides et al., 2007; Caputo et al., 2003) includes three major steps. These are explained below and for each step the criteria used in Greece are compared to the ones adopted in this thesis and further discussed.

- The first step was to classify faults into six established groups (detailed description of each group is in Sboras et al. (2011)):
    - Seismic faults;
    - Holocene active faults;
    - Late Quaternary active faults;
    - Quaternary active faults;
    - Capable faults of uncertain age;
    - Faults of uncertain activity.

Since Greece is an area with high seismicity level, there are no difficulties related with classifying faults into six groups. However, since Norway experiences low level of seismic activity such differentiation of faults would be difficult. There is no well-documented evidence or facts for majority of faults that allow to assert readers that one or another fault is either seismic or active. Therefore, onshore and offshore faults compiled in the thesis were split into six zones (detailed description of zones can be found in the last section of chapter 5) bearing similar tectonostratigraphic, geological, geophysical and seismic characteristics.

- The second step is to apply criteria to evaluate seismogenic potential of a fault
    - Collect geological and morphological features;

These include morphotectonic features such as fault scarps, tilted Quaternary sediments and triangular facets that can give clues related to the latest reactivation of tectonic structures. In that sense palaeoseismological data and its careful analysis is very important. Since Norway experiences low level of seismic activity there are not many morphological features listed, that can be either observed in the field or found in the literature. Until now there is only one well-studied and documented neotectonic Stuoragurra fault that has a visible continuous fault scarp of approximately seven meters (Olesen, 1988; Olesen et al., 1992a; Dehls et al., 2002). Palaeoseismological and geophysical methods used to study Stuoragurra fault revealed that continuous fault scarp found in post-glacial landscape is a manifestation of a significant earthquake rupture. The age of the fault is considered to be soon after the last deglaciation and hence is within Holocene. Another fault extending 2.5 km that also has a fault scarp is a Berill fault. The fault scarp observed is too short to be considered to be related to a significant earthquake. Based on empirical relations between fault length and magnitude (Wells and Coppersmith, 1994), the corresponding magnitude for the Berill fault scarp would be $M < 6$. In such a case the expected depth dimension of the fault would be shallow (less than 2.5 km) to be considered as a crustal scale fault and hence cannot be classified as a significant fault. Therefore, it was not taken for the studies in this thesis. In addition, there have not been enough studies done and information gathered to reveal its nature, in particular whether it is neotectonic or not. However, it should be mentioned that Olesen et al. (2013) mentions that the Berill fault could be triggered by adjacent large-magnitude earthquake and hence is assumed to be probably neotectonic.

- Study seismic activity (important to differentiate between historical and instrumental earthquakes);

This point correlates very well with what have been done in the thesis (chapter 5 – seismological data). Careful choice of database was performed. Historical and instrumental seismic records were analyzed using ISC and NNSN databases and thorough comparison of both was performed. The choice was made in favor of NNSN database since it was found to be complete and reliable for both historical and instrumental periods. However, since historical data was mostly based on felt reports and questionnaires only significant seismic events of magnitude equal to 3 or larger were used to compile seismic catalogue. For these earthquakes ($M > 3$) instrumental seismic records are considered trustworthy, as they are recorded by several seismic stations in the region and hence assumed to have sufficiently reliable accuracy in the source parameters. Nevertheless, stricter conditions were applied to the data selection process (this is described in detail in chapter 5 – seismological data). Consequently, compiled seismic catalogue consisted of two parts. Seismic records before 1980's with no epicentral error limit set constituted the first part of the seismic catalogue whereas instrumental data from 1980's onwards with epicentral error limits set constituted the second part of the seismic catalogue. After a number of tests made, it was seen that the best agreement between quality and quantity of the data was reached when using 0 – 20 km epicentral error limit.

- Collect data from geophysical survey

Geophysical survey may include such methodological approaches as electrical resistivity tomography, high-resolution seismic profiles or ground-penetrating radar. Data gathered may give important information that can be further used to characterize faults. In this thesis only seismic profiles extracted from the literature were used to collect necessary geological information related to fault orientation and kinematics.

- Consider regional geodynamic setting

Checking whether orientation of the fault is compatible with the orientation of the active stress field in broad area or not is one of the most important parameters that used to estimate reactivation

potential of a fault. However, referring to Sboras et al. (2011) this approach can be misleading in areas where combination of several stresses is observed. Indeed, it can be difficult for areas experiencing high seismic activity, but it works very well for passive continental margin setting, experiencing low level of seismic activity such as Norway, where dominant horizontal compressional stress is related to the ridge-push force oriented NW-SE originating from the mid-oceanic ridge in the North Atlantic (i.e. Kolbeinsey, Mohns and Knipovich ridges). This horizontal compressional stress corresponds roughly to the largest principal stress axis sigma 1. However, local variations exist where sigma 1 orientation is rotated more in the E-W orientation along the Western Norway coastal region and is rotated more vertical along the coast of the Northern Norway, giving rise to normal faulting mechanisms along the Nordland coast.

- The third step is data parametrization

Before being submitted to EDSF collected data should be analyzed, filtered and parametrized.

In this thesis the reactivation potential was interpreted to be probable only for two faults. These are the Øygarden fault zone (Segment 3) and the Stuoragurra fault. Accordingly, only data related to these structures will be submitted to EDSF. In EDSF, data need to be subdivided into general and parametric information. General information requires:

- Region;
- Code;
- Name;
- Compiler(s);
- Contributor(s);
- Time source information was created/updated.

General information for the two selected faults (Øygarden and Stuoragurra) can be submitted without any difficulties since all of it was systematically recorded (Table 36).

Parametric information requires:

- Min. Depth (km);
- Max. Depth (km);
- Strike (Deg.);
- Dip (Deg.);
- Rake (Deg.);
- Slip Rate (mm/y);
- Max Magnitude (M_W)

All parametric information except Min. and Max. Depth and Slip Rate will be submitted to EDSF since it was systematically recorded. The depth issue was discussed in detail in chapter 5 – Seismological data. Since Norway experiences low level of seismic activity, slip rates are relatively low and uncertain and hence was not recorded and specified in none of Tables 15, 18, 22, 25, 29 and 32. Quality keys (Q-keys) for other parametric information for this study are as follows:

- Strike (Deg.) – OD (original data);
- Dip (Deg.) – LD (literature data);
- Rake (Deg.) – LD (literature data);
- Max Magnitude (M_W) – ER (empirical relationship).

For the Øygarden Fault Complex and the Stuoragurra Fault, required parametric information is given in Tables 37 and 38.

Table 36: General information about Øygarden Fault Zone and Stuoragurra Fault.

General Information		
Fault	**Øygarden Fault Zone**	**Stuoragurra Fault**
Region	North Sea	Onshore Northern Norway
Code	Z-01-F05	Z-06-F05
Name	Norway	Norway
Compiler(s)	Smirnova (1), Atakan (1)	Smirnova (1), Atakan (1)
Contributor(s)	Smirnova (1), Atakan (1), Ramberg et al. (2007)	Smirnova (1), Atakan (1), Olesen (1988)
Created	01.06.2019	01.06.2019
Updated	-	-
Affiliations		
1) Department of Earth Science; University of Bergen; Allégaten 41, N-5007 Bergen		

Table 37: Parametric information about Øygarden Fault Zone.

Parametric Information			
	Parameter	**Qual.**	**Evidence**
Min Depth (km)	-	-	-
Max Depth (km)	-	-	-
Strike (deg)	NNE-SSW	OD	Based on structural and geological data from various authors
Dip (deg)	70˚WNW	LD	Based on structural and geological data from various authors
Rake (deg)	normal	LD	Inferred from regional geological and seismological data
Slip Rate (mm/y)	-		-
Max Magnitude (M_W)	7,8	ER	Inferred from fault characteristics and seismological considerations
Q-keys	LD = Literature Data; OD = Original Data; ER = Empirical Relationship		

[1]

Table 38: Parametric information about Stuoragurra Fault.

Parametric Information			
	Parameter	**Qual.**	**Evidence**
Min Depth (km)	-	-	-
Max Depth (km)	-	-	-
Strike (deg)	NE-SW	OD	Based on structural and geological data from various authors
Dip (deg)	30˚SE	LD	Based on structural and geological data from various authors
Rake (deg)	reverse	LD	Inferred from regional geological and seismological data
Slip Rate (mm/y)	-		-
Max Magnitude (M_W)	7,3	ER	Inferred from fault characteristics and seismological considerations
Q-keys	LD = Literature Data; OD = Original Data; ER = Empirical Relationship		

[2]

[1] Strike and slip of the fault are not given in angles (deg) but rather orientation and sense of slip are specified which reflects the level of uncertainties.
[2] Strike and slip of the fault are not given in angles (deg) but rather orientation and sense of slip are specified which reflects the level of uncertainties.

8 Conclusions

In this chapter based on the reactivation potential presented in the results chapter, “seismogenic potential” of the faults are classified as:

- Probably seismogenic
- Possibly seismogenic
- Not seismogenic

The reactivation potential of the Øygarden Fault Complex (3rd and northernmost segment) was assigned “probable” because all observations satisfied the applied criteria shown in the methodology chapter. There is, however, no large earthquakes (M>5) recorded during the instrumental or historical periods and no palaeoseismological analysis is conducted to find out if the fault was activated by large earthquakes during the Holocene. For this reason, the Øygarden Fault Complex is classified as “probably seismogenic”.

The reactivation potential of the Stuoragurra Fault on the other hand was assigned “probable” because all observations satisfied the applied criteria shown in the methodology chapter, with the only exception of having one focal mechanism not compatible with the current stress tensor orientation. However, the Stuoragurra fault is the only fault that shows a clear and continuous fault scarp in the morphology in the post-glacial landscape and was demonstrated to be active during the Holocene, based on the paleoseismological and geophysical analyses (Olesen, 1988; Olesen et al.,1992a; Dehls et al., 2002). Such a continuous fault scarp in the morphology together with paleoseismological and geophysical evidence, indicates clearly that there has been large (M>6) earthquake(s) that have occurred along this fault after the de-glaciation due to the isostatic-rebound combined with the NW-SE oriented horizontal compression due to the ridge-push. As such this fault could be classified as “seismogenic”. However, the current stress conditions may not necessarily be the same as was the case when these large earthquakes occurred in northern Norway, northern Sweden and northern Finland. Because of this, the Stuoragurra fault is classified as “probably seismogenic”.

Based on the analysis of the reactivation potential of the significant faults in the six zones that are presented in the results chapter, only two faults were found “**probably seismogenic**”. These are the Øygarden Fault Complex in the North Sea and the Stuoragurra Fault in Finnmark (mainland Northern Norway). In addition, 18 faults were found “**possibly seismogenic**”, based on the applied criteria. Remaining 36 faults are considered “**not-seismogenic**”.

Detailed information about the two faults that are classified as “probably seismogenic” will be submitted to the European Database of Seismogenic Faults (EDSF).

9 Future recommendations

- Magnitude unification

It was demonstrated that for most of the magnitude scales there is a good agreement between the different scales for low and moderate magnitudes. Therefore, no attempts to make magnitude conversion was made. However, when dealing with magnitudes of various types the common practice is to convert magnitude to one type to make the data homogeneous. This is therefore recommended in future studies.

- Study Svalbard and Barents Sea

Svalbard and Barents Sea areas were not included in the present study due to the scope of this thesis. Therefore, these two remaining areas are recommended to be included in future studies.

- Perform detailed deep study of individual fault(s)/segment(s)

In this thesis faults, fault zones and complexes were studied on a large-scale. Therefore, detailed and deep analysis of, for example, faults for which seismogenic potential of being reactivated was interpreted to be probable is recommended. In addition, complex structures such as Bergen Arc shear zone and Devonian detachment faults are of interest as well and can be studied in more detail.

- Applicability of the criteria and the method developed in this thesis on other similar regions

The method and the criteria developed in this thesis should be tested in other similar tectonic regions. A benchmarking study can be performed to test the applicability of this method in Stable Continental Regions (SCR) and other slowly deforming areas.

10 References

Anda, E., Blikra, L. H., & Braathen, A. (2002). The Berill Fault-first evidence of neotectonic faulting in southern Norway. *Norwegian Journal of Geology/Norsk Geologisk Forening*, *82*(3).

Andersen, T. B. (1998). Extensional tectonics in the Caledonides of southern Norway, an overview. *Tectonophysics*, *285*(3-4), 333-351.

Annual report for the Norwegian National Seismic Network. (2018). Internal Report. *Department of Earth Science, University of Bergen*, March 2019.

Atakan, K., Lindholm, C. D., & Havskov, J. (1994). Earthquake swarm in Steigen, northern Norway: an unusual example of intraplate seismicity. *Terra Nova*, *6*(2), 180-194.

Baarli, G. B., Johnson, M. E., & Antoshkina, A. I. (2003). Silurian stratigraphy and paleogeography of Baltica. *New York State Museum Bulletin*, 493, 3-34.

Bakun, W. H., & Hopper, M. G. (2004). *Catalog of significant historical earthquakes in the central United States*. US Department of the Interior, US Geological Survey.

Bormann, P. (2002). *New manual of seismological observatory practice: NMSOP* (No. 550.34 NEW). International Association of Seismology and Physics of the Earth Interior.

Bormann, P., & Saul, J. (2008). The new IASPEI standard broadband magnitude m B. *Seismological Research Letters*, *79*(5), 698-705.

Bormann, P., Liu, R., Xu, Z., Ren, K., Zhang, L., & Wendt, S. (2009). First application of the new IASPEI teleseismic magnitude standards to data of the China National Seismographic Network. *Bulletin of the Seismological Society of America*, *99*(3), 1868-1891.

Bormann, P., & Saul, J. (2009). Earthquake magnitude. *Encyclopedia of complexity and systems science*, 2473-2496.

Braathen, A., Nordgulen, Ø., Osmundsen, P. T., Andersen, T. B., Solli, A., & Roberts, D. (2000). Devonian, orogen-parallel, opposed extension in the Central Norwegian Caledonides. *Geology*, *28*(7), 615-618.

Bungum, H., Hokland, B. K., Husebye, E. S., & Ringdal, F. (1979). An exceptional intraplate earthquake sequence in Meløy, Northern Norway. *Nature*, *280*(5717), 32.

Bungum, H., & Husebye, E. S. (1979). The Meløy, northern Norway, earthquake sequence—a unique intraplate phenomenon. *Norsk geologisk tidsskrift*, *59*(2), 189-193.

Bungum, H., Alsaker, A., Kvamme, L. B., & Hansen, R. A. (1991). Seismicity and seismotectonics of Norway and nearby continental shelf areas. *Journal of Geophysical Research: Solid Earth*, *96*(B2), 2249-2265.

Bungum, H., & Lindholm, C. (1997). Seismo-and neotectonics in Finnmark, Kola and the southern Barents Sea, part 2: Seismological analysis and seismotectonics. *Tectonophysics*, *270*(1-2), 15-28.

Bungum, H., Lindholm, C., & Faleide, J. I. (2005). Postglacial seismicity offshore mid-Norway with emphasis on spatio-temporal–magnitudal variations. *Marine and Petroleum Geology*, *22*(1-2), 137-148.

Byrkjeland, U., Bungum, H., & Eldholm, O. (2000). Seismotectonics of the Norwegian continental margin. *Journal of Geophysical Research: Solid Earth*, *105*(B3), 6221-6236.

Båth, M. (1979). *Introduction to Seismology*. Birkhäuser Basel.

Caputo, R., Piscitelli, S., Oliveto, A., Rizzo, E., & Lapenna, V. (2003). The use of electrical resistivity tomographies in active tectonics: examples from the Tyrnavos Basin, Greece. *Journal of Geodynamics*, *36*(1-2), 19-35.

Cocks, L. R. M., & Torsvik, T. H. (2005). Baltica from the late Precambrian to mid-Palaeozoic times: the gain and loss of a terrane's identity. *Earth-Science Reviews*, *72*(1-2), 39-66.

Dahlberg, M. E. (2014). *Structural and stratigraphical evolution of the Fingerdjupet Subbasin, SW*

Barents Sea (Master's thesis).
Dehls, J. F., Olesen, O., Olsen, L., & Blikra, L. H. (2000). Neotectonic faulting in northern Norway; the Stuoragurra and Nordmannvikdalen postglacial faults. *Quaternary science reviews*, *19*(14-15), 1447-1460.
Dehls, J. F., Basilico, M., & Colesanti, C. (2002). Ground deformation monitoring in the Ranafjord area of Norway by means of the permanent scatterers technique. In *IEEE International Geoscience and Remote Sensing Symposium* (Vol. 1, pp. 203-207). IEEE.
D-Map. (2019). D-Map, Userfriendly GIS. Retrieved 25 May, 2019, from: https://dmap.no/
Earthquake track. (2019). Biggest Earthquakes Near Norway. Retrieved 1 June, 2019, from: https://earthquaketrack.com/p/norway/biggest
Ebbing, J., & Olesen, O. (2010). New compilation of top basement and basement thickness for the Norwegian continental shelf reveals the segmentation of the passive margin system. In *Geological Society, London, Petroleum Geology Conference series* (Vol. 7, No. 1, pp. 885-897). Geological Society of London.
European Database for Seismogenic Faults. (2019). Retrieved 25 May, 2019, from: http://diss.rm.ingv.it/share-edsf/
European Plate Observing System. (2019). Retrieved 25 May, 2019, from: www.epos-ip.org
Faleide, J. I., Bjørlykke, K., & Gabrielsen, R. H. (2010). Geology of the Norwegian continental shelf. In *Petroleum Geoscience* (pp. 467-499). Springer, Berlin, Heidelberg.
Fejerskov, M., & Lindholm, C. (2000). Crustal stress in and around Norway: an evaluation of stress-generating mechanisms. *Geological Society, London, Special Publications*, *167*(1), 451-467.
Fejerskov, M., Lindholm, C., Myrvang, A., & Bungum, H. (2000). Crustal stress in and around Norway: a compliation of in situ stress observations. *Geological Society, London, Special Publications*, *167*(1), 441-449.
Fiedler, A., & Faleide, J. I. (1996). Cenozoic sedimentation along the southwestern Barents Sea margin in relation to uplift and erosion of the shelf. *Global and Planetary Change*, *12*(1-4), 75-93.
Fjeldskaar, W., Lindholm, C., Dehls, J. F., & Fjeldskaar, I. (2000). Postglacial uplift, neotectonics and seismicity in Fennoscandia. *Quaternary Science Reviews*, *19*(14-15), 1413-1422.
Fossen, H., & Hurich, C. A. (2005). The Hardangerfjord Shear Zone in SW Norway and the North Sea: a large-scale low-angle shear zone in the Caledonian crust. *Journal of the Geological Society*, *162*(4), 675-687.
Funck, T., Geissler, W. H., Kimbell, G. S., Gradmann, S., Erlendsson, Ö., McDermott, K., & Petersen, U. K. (2017). Moho and basement depth in the NE Atlantic Ocean based on seismic refraction data and receiver functions. *Geological Society, London, Special Publications*, *447*(1), 207-231.
Gabrielsen, R. H. (1989). Reactivation of faults on the Norwegian continental shelf and its implications for earthquake occurrence. In *Earthquakes at North-Atlantic Passive Margins: Neotectonics and Postglacial Rebound* (pp. 67-90). Springer, Dordrecht.
Gabrielsen, R. H., Braathen, A., Dehls, J., & Roberts, D. (2002). Tectonic lineaments of Norway. *Norsk Geologisk Tidsskrift*, *82*(3), 153-174.
Gee, D. G. (1975). A tectonic model for the central part of the Scandinavian Caledonides. *American Journal of Science*, *275*(A), 468-515.
Gomberg, J., & Schweig, E. (2003). Earthquake hazard in the heart of the homeland. *US Geological Survey*. Fact Sheet FS-131-02.
Gradmann, S., Olesen, O., Keiding, M., & Maystrenko, Y. (2018). Chapter 9: The regional 3D stress field of Nordland, Northern Norway – Insights from numerical modeling prepared for Norges Geologiske Undersøkelse (NGU) report 2018.010 Neotectonics in Nordland – implications for petroleum exploration (NEONOR2). *Norges Geologiske Undersøkelse (NGU)*, September 2018.
Havskov, J., & Ottemöller, L. (2010). *Routine Data Processing in Earthquake Seismology – with Sample*

Data, Exercises and Software. Springer, Dordrecht.
Herrevold, T., Gabrielsen, R. H., & Roberts, D. (2009). Structural geology of the southeastern part of the Trollfjorden-Komagelva Fault Zone, Varanger Peninsula, Finnmark, North Norway. *Norwegian Journal of Geology/Norsk Geologisk Forening*, *89*(4).
Hicks, E. C., Bungum, H., & Lindholm, C. D. (1996). Crustal stresses in Norway and surrounding areas as derived from earthquake focal mechanism solutions and in-situ stress measurements. *Cand. Scient., University of Oslo*.
Hicks, E. C., Bungum, H., & Lindholm, C. D. (2000). Stress inversion of earthquake focal mechanism solutions from onshore and offshore Norway. *Norsk Geologisk Tidsskrift*, *80*(4), 235-250.
Holtedahl, H. (1988). Bedrock geology and Quaternary sediments in the Lista basin, S. Norway. *Norsk geologisk tidsskrift*, *68*, 1-20.
Husebye, E. S. (2005). Comments on the Lurøy 1819 earthquake controversy. *Norwegian Journal of Geology/Norsk Geologisk Forening*, *85*(3).
International Seismological Centre. (2019a). Retrieved 19 May, 2019, from: http://www.isc.ac.uk/
International Seismological Centre. (2019b). Rebuild of the ISC Bulletin. Retrieved 19 May, 2019, from: http://www.isc.ac.uk/projects/rebuild/
Janutyte, I., Lindholm, C., & Olesen, O. (2017). Relation between seismicity and tectonic structures offshore and onshore Nordland, northern Norway. *Norwegian Journal of Geology/Norsk Geologisk Forening*, *97*(3).
Johnston, A. C., & Kanter, L. R. (1990). Earthquakes in stable continental crust. *Scientific American, 262*(3), 68-75.
Kanamori, H. (1983). Magnitude scale and quantification of earthquakes. *Tectonophysics*, *93*(3-4), 185-199.
Kujansuu, R. (1964). Nuorista siirroksista Lapissa. *Summary: recent faults in Lapland. Geologi*, *16*(3-4), 30-36.
Lagerbäck, R. (1978). Neotectonic structures in northern Sweden. *Geologiska Föreningen i Stockholm Förhandlingar*, *100*(3), 263-269.
Lie, J. E., & Husebye, E. S. (1994). Simple-shear deformation of the Skagerrak lithosphere during the formation of the Oslo Rift. *Tectonophysics*, *232*(1-4), 133-141.
Lundqvist, J., & Lagerbäck, R. (1976). The Pärve Fault: a late-glacial fault in the Precambrian of Swedish Lapland. *Geologiska Föreningen i Stockholm Förhandlingar*, *98*(1), 45-51.
McCalpin, J. P. (1996). Paleoseismology, 588 pp. *Academic Press, San Diego, California.*
Michálek, J. (2018). Chapter 4.1: Focal mechanisms prepared for Norges Geologiske Undersøkelse (NGU) report 2018.010 Neotectonics in Nordland – implications for petroleum exploration (NEONOR2). *Norges Geologiske Undersøkelse (NGU)*, September 2018.
Michelsen, O., & Nielsen, L. H. (1993). Structural development of the Fennoscandian border zone, offshore Denmark. *Marine and petroleum geology*, *10*(2), 124-134.
Mogensen, T. E., & Korstgård, J. A. (2003). Triassic and Jurassic transtension along part of the Sorgenfrei-Tornquist Zone, in the Danish Kattegat: In: Ineson, JR & Surlyk, F.(eds): The Jurassic of Denmark and Greenland. *Review of Survey Activities*, *1*, 439-458.
Muir Wood, R., & Woo, G. (1987). The historical seismicity of the Norwegian continental shelf. *ELOCS (Earthquake Loading on the Norwegian Continental Shelf) Report*, 2-1.
Muir Wood, R. (1993). A review of the seismotectonics of Sweden. *Swedish Nuclear Fuel and Waste Management Co.(SKB) Technical Report 93*, *13*, 225.
Myrvang, A. M. (1996). Kompendium Bergmekanikk. *Norwegian University of Science and Technology, department of Geology and Mineral Resources, Trondheim*.
NORSAR & NGI. (1998). Seismic zonation of Norway. *NORSAR Report 629*.
Norwegian Geological Survey (2019). Retrieved 19 May, 2019, from: www.ngu.no

Norwegian National Seismic Network (2019). Earthquakes. Retrieved 19 May, 2019, from: www.skjelv.no

Norwegian Petroleum Directorate (2019). Retrieved 19 May, 2019, from: https://www.npd.no/en/

Olesen, O. (1988). The Stuoragurra Fault, evidence of neotectonics in the Precambrian of Finnmark, northern Norway. *Norsk Geologisk Tidsskrift*, *68*(2), 107-118.

Olesen, O., Roberts, D., Henkel, H., Lile, O. B., & Torsvik, T. H. (1990). Aeromagnetic and gravimetric interpretation of regional structural features in the Caledonides of West Finnmark and North Troms, northern Norway. *Norges geologiske undersøkelse 419*, 1-24.

Olesen, O., Henkel, H., Lile, O. B., Mauring, E., & Rønning, J. S. (1991). Detailed geophysical investigations of the Stuoragurra postglacial fault, Finnmark, northern Norway. Norges Geologiske Undersøkelse (NGU) report 90.160. *Norges Geologiske Undersøkelse (NGU)*, March 1991.

Olesen, O., Henkel, H., Lile, O. B., Mauring, E., & Rønning, J. S. (1992a). Geophysical investigations of the Stuoragurra postglacial fault, Finnmark, northern Norway. *Journal of Applied Geophysics*, *29*(2), 95-118.

Olesen, O., Henkel, H., Lile, O. B., Mauring, E., Rønning, J. S., & Torsvik, T. H. (1992b). Neotectonics in the Precambrian of Finnmark, northern Norway. *Norsk Geologisk Tidsskrift*, *72*(3), 301-306.

Olesen, O., Torsvik, T. H., & Tveten, E. (1997). Basement structure of the continental margin in the Lofoten-Lopphavet area, northern Norway: constraints from potential field data, on-land structural mapping and palaeomagnetic data. *Oceanographic Literature Review*, *12*(44), 1478.

Olesen, O., Brönner, M., Ebbing, J., Gellein, J., Gernigon, L., Koziel, J., ... & Solheim, D. (2010). New aeromagnetic and gravity compilations from Norway and adjacent areas: methods and applications. In *Geological Society, London, Petroleum Geology Conference series* (Vol. 7, No. 1, pp. 559-586). Geological Society of London.

Olesen, O., Bungum, H., Dehls, J., Lindholm, C., Pascal, C., & Roberts, D. (2013). Neotectonics, seismicity and contemporary stress field in Norway–mechanisms and implications. *Quaternary Geology of Norway, Geological Survey of Norway Special Publication*, *13*, 145-174.

Olesen, O., Janutyte, I., Michálek, J., Keiding, M., Lindholm, C., ..., Rodenay, S. (2018). Neotectonics in Nordland – implications for petroleum exploration (NEONOR2). Norges Geologiske Undersøkelse (NGU) report 2018.010. *Norges Geologiske Undersøkelse (NGU)*, September 2018.

Pavlides, S., Valkaniotis, S., & Chatzipetros, A. (2007). Seismically capable faults in Greece and their use in seismic hazard assessment. In *Proc. 4th Int. Conf. Earthquake Geotech. Eng., Thessaloniki, Greece, paper* (No. 1609).

Pettenati, F., Sirovich, L., Bungum, H., & Schweitzer, J. (2005). Source inversion of regional intensity patterns of five earthquakes from south-western Norway. *Boll Geofis Teor Appl*, *46*, 111-134.

Qing He (2015). *Structural analysis of the Klakk Fault Complex, offshore mid-Norway* (Master's thesis).

Ramberg, I. B., Bryhni, I., & Nøttvedt, A. (2007). *Landet blir til: Norges geologi*. Norsk geologisk forening.

Roberts, D. (1991). A contemporary small-scale thrust-fault near Lebesly, Finnmark. *Norsk Geologisk Tidsskrift*, *71*(2), 117-120.

Roberts, D. A. V. I. D., & Lippard, S. J. (2005). Inferred Mesozoic faulting in Finnmark: current status and offshore links. *Norges geologiske undersøkelse Bulletin*, *443*(55-60).

Sboras, S., Pavlides, S., Caputo, R., Chatzipetros, A., Michailidou, A., Valkaniotis, S., & Papathanasiou, G. (2011). Improving the resolution of seismic hazard estimates for critical facilities: the Database of Greek crustal seismogenic sources in the frame of the SHARE project. *Proceedings of the 30 Convegno Nazionale GNGTS*, *1417*.

Seguret, M., Seranne, M., Chauvet, A., & Brunel, A. (1989). Collapse basin: A new type of extensional

sedimentary basin from the Devonian of Norway. *Geology*, *17*(2), 127-130.

SEISAN Earthquake Analysis Software for Windows, Solaris, Linux & Macosx. (2018). Editors: Ottemöller, L., Voss, P., & Havskov, J. *Department of Earth Science, University of Bergen & Geological Survey of Denmark and Greenland*.

Seismo Group. (2011). Data available at the Norwegian National Earthquake Data Base at Department of Earth Science. Internal Report. *Department of Earth Science, University of Bergen*, May 2011.

Sellevoll, M. A., & Sundvor, E. (2001). *Jordskjelvstasjonen: institutt for den faste jords fysikk gjennom ett århundrede*. Universitet i Bergen.

Sigmond, E. M. (1985). The Mandal—Ustaoset Line, A Newly Discovered Major Fault Zone in South Norway. In: *The Deep Proterozoic Crust in the North Atlantic Provinces* (pp. 323-331). Springer, Dordrecht.

Simonsen, A. L. L. (2018). *Updated Norwegian In Situ Rock Stress Database* (Master's thesis, NTNU).

Soh, I., Chang, C., Lee, J., Hong, T. K., & Park, E. S. (2018). Tectonic stress orientations and magnitudes, and friction of faults, deduced from earthquake focal mechanism inversions over the Korean Peninsula. *Geophysical Journal International*, *213*(2), 1360-1373.

Starmer, I. C. (1993). The Sveconorwegian Orogeny in Southern Norway, relative to deep crustal structures and events in the North Atlantic Proterozoic supercontinent. *Norsk Geologisk Tidsskrift*, *73*(2), 109-132.

Surlyk, F. (1980). Denmark, Finland, Sweden, Norway. In: *Geology of the European countries*, 1–50. Graham and Trotman, London.

Sørensen, M.B. (2002). Revision of fault plane solutions in the University of Bergen (UiB) seismic database, 1959 – 2001. Norwegian National Seismic Network – Technical Report No. 10. *Institute of Solid Earth Physics, University of Bergen*, October 2002.

Tjåland, N., & Ottemöller, L. (2018). Evaluation of seismicity in the area between the Troll field and the Øygarden Fault. Internal Report. *Department of Earth Science, University of Bergen*, September 2018, 21p.

Tolgensbakk, J., & Sollid, J. L. (1988). Kåfjord, kvartærgeologi og geomorfologi 1: 50 000, 1634 II: Geografisk Institutt. *Universitetet i Oslo*.

Torsvik, T. H., & Cocks, L. R. M. (2005). Norway in space and time: A Centennial cavalcade. *Norwegian Journal of Geology/Norsk Geologisk Forening*, *85*.

Torsvik, T. H., & Rehnström, E. F. (2003). The Tornquist Sea and Baltica–Avalonia docking. *Tectonophysics*, *362*(1-4), 67-82.

Waldhauser, F., & Ellsworth, W. L. (2000). A double-difference earthquake location algorithm: Method and application to the northern Hayward fault, California. *Bulletin of the Seismological Society of America, 90*(6), 1353-1368.

Wells, D. L., & Coppersmith, K. J. (1994). New empirical relationships among magnitude, rupture length, rupture width, rupture area, and surface displacement. *Bulletin of the seismological Society of America*, *84*(4), 974-1002.

Ziegler, W. H., Doery, R., & Scott, J. (1986). Tectonic habitat of Norwegian oil and gas. *Habitat of Hydrocarbons on the Norwegian Continental Shelf*, 3-19.

11 Appendix

Data used and results obtained in this thesis are available at

ftp://ftp.geo.uib.no/pub/seismo/REPORTS/THESIS/PREVIOUS THESIS / and are listed below.

Results:

- Complete results table (Excel-arc), with short explanation text in READ-ME file.
- D-Map project file with a READ-ME file explaining how to reconstruct the project data in D-Map software (https://dmap.no) and how to download the coordinates of the zones and faults digitally.
- GMT scripts.

Data used:

- International Seismological Centre (ISC). Retrieved from: http://www.isc.ac.uk/
- Norwegian Geological Survey (NGU). Retrieved from: www.ngu.no
- Norwegian National Seismic Network (NNSN). Retrieved from: www.skjelv.no
- Norwegian Petroleum Directorate (NPD). Retrieved from: https://www.npd.no/en/